ELASTIC ANALYSIS OF LOAD DISTRIBUTION IN WIDE-FACED SPUR GEARS

by

J. H. STEWARD

A thesis submitted to
the University of Newcastle upon Tyne
for
the Degree of Doctor of Philosophy

January 1989

ABSTRACT

The load distribution across the contact line(s) of spur gears is essential for the gear designer to be able to accurately stress gears for a given application.

Existing gear standards (eg BS 436, AGMA 218 DIN 3990) use a thin slice (2D) model of the meshing gear teeth to estimate the contact line load distribution. This approach clearly fails to model properly teeth subjected to mal-distributed loads, since the buttressing effect of adjacent tooth sections tends to flatten the load distribution. Non-linear tooth modifications such as crowning and some forms of lead correction are also inadequately modelled.

This thesis sets out the theory for a 3D elastic model of wide-faced spur gears that has been implemented on a micro-computer. The required 3D contact line influence coefficients for standard form zero modification spur gears with 18 to 100 teeth have been determined by Finite Element analysis. These theoretical values have been compared with results from experiments carried out on a complete large module (18.0mm) wide-faced spur gear. The effect of the various elemental gear errors (eg pitch, profile, lead) and profile modifications have been investigated using the 3D computer model; the results compared with results predicted by the existing gear design standards.

The existing gear standards use 2D tooth compliance values up to 50% less than those obtained in this work, largely due to inadequate modelling of the gear body compliance, which is most significant in gear wheels. Comparison of 3D tooth compliance values shows a large discrepancy between author's results again due to inadequate modelling of the gear body.

------oOo------

ACKNOWLEDGEMENTS

I would like to thank the following people for their continued help in this project; Mr D A Hofmann, Director of Design Unit, University of Newcastle upon Tyne, for setting up the SERC research project that forms the basis of this thesis as well as for his technical assistance; my tutor, Mr J A Pennell for his enthusiastic and highly constructive technical guidance throughout the project; Mr C Woodford of The University Computing Department for his invaluable help in the use of the University mainframe facilities; the remaining members of Design Unit, especially Mr M E Norman for his expertise in the use of micro-computers and finally many thanks to Mrs J Maclean for her meticulous and prompt typing of the thesis.

DECLARATION

This thesis consists of the original work of the author except where specific reference is made to the work of others, and has not been previously submitted for any other degree or qualification.

******

CONTENTS

APPENDICES

2.1 Program SPURDIST for the Elastic Analysis of Spur Gears

2.1.3 Calculation of Loading Diameter, dy, and Initial Tooth Clearance, ct, Outside Theoretical Phase of Mesh

2.3.2 Surface Co-ordinates of a Spur Gear with Addendum Modification

2.3.4 Plots of F.E. Net Tooth Centre-Line Deflection Results

2.4.2 Optimising Routine for Curve Fitting of F.E. Tooth Deflection Data

3.8.4 Test Gear Tooth Root Strain Gauge Results and Calculated Stresses

******

CHAPTER 1

INTRODUCTION

1.1 Background

The design of gears of appropriate size and reliability for a particular application requires a method for predicting both the surface stresses between the meshing gear teeth and the bending stresses in the tooth root. These are relatively easily determined once the load distribution across the contact line of the meshing gear teeth is known.

The methods of analysis currently used in practical gear design are usually based on one of the modern gear rating standards such as BS[B3], ISO[I5], DIN[D3], AGMA[A8]. In these analyses, the contact and bending stresses are first calculated for idealised "perfect " gears (without errors of any form). The values so calculated are then modified (for "real" gears) by introducing various load distribution factors to allow for the effect of inaccurate manufacturing and alignment errors. All adopt a fundamentally similar approach to calculating contact and root bending stress and so BS 436:PART 3:1986 will be looked at as an example.

The mechanism for pitting failure is not fully understood, so that a rigorous failure analysis is not possible. However, Hertzian contact stress σ_H is an adequate criterion for comparing surface fatigue strength. The contact stress is calculated by considering the mating gear tooth surfaces as equivalent to two elastic cylindrical bodies in contact with an elliptical pressure distribution first treated by Hertz in 1895[H8]. Using the notation shown in Fig. 1.1 the contact stress at the reference diameter for a pair of perfect gears is given by:

$$\sigma_{H0} = -\sqrt{\frac{E w}{2\pi(1-\nu^2)}}\ \sqrt{\frac{1}{D_1}+\frac{1}{D_2}} \qquad (1.1)$$

or $$\sigma_{HO} = -\sqrt{\frac{F_t}{d_1 b}\,\frac{u+1}{u}}\; Z_H Z_\varepsilon Z_\epsilon \qquad (1.2)$$

Where the three Z factors respectively take account of tooth geometry; elastic material properties and transverse contact ratio, which determines how the load is shared between adjacent teeth in mesh. The length of contact line varies continuously through the mesh cycle in helical gears and, due to elastic interaction between the teeth, the load is not distributed uniformly along the line of contact. It is a largely empirical factor which is intended to allow for these effects.

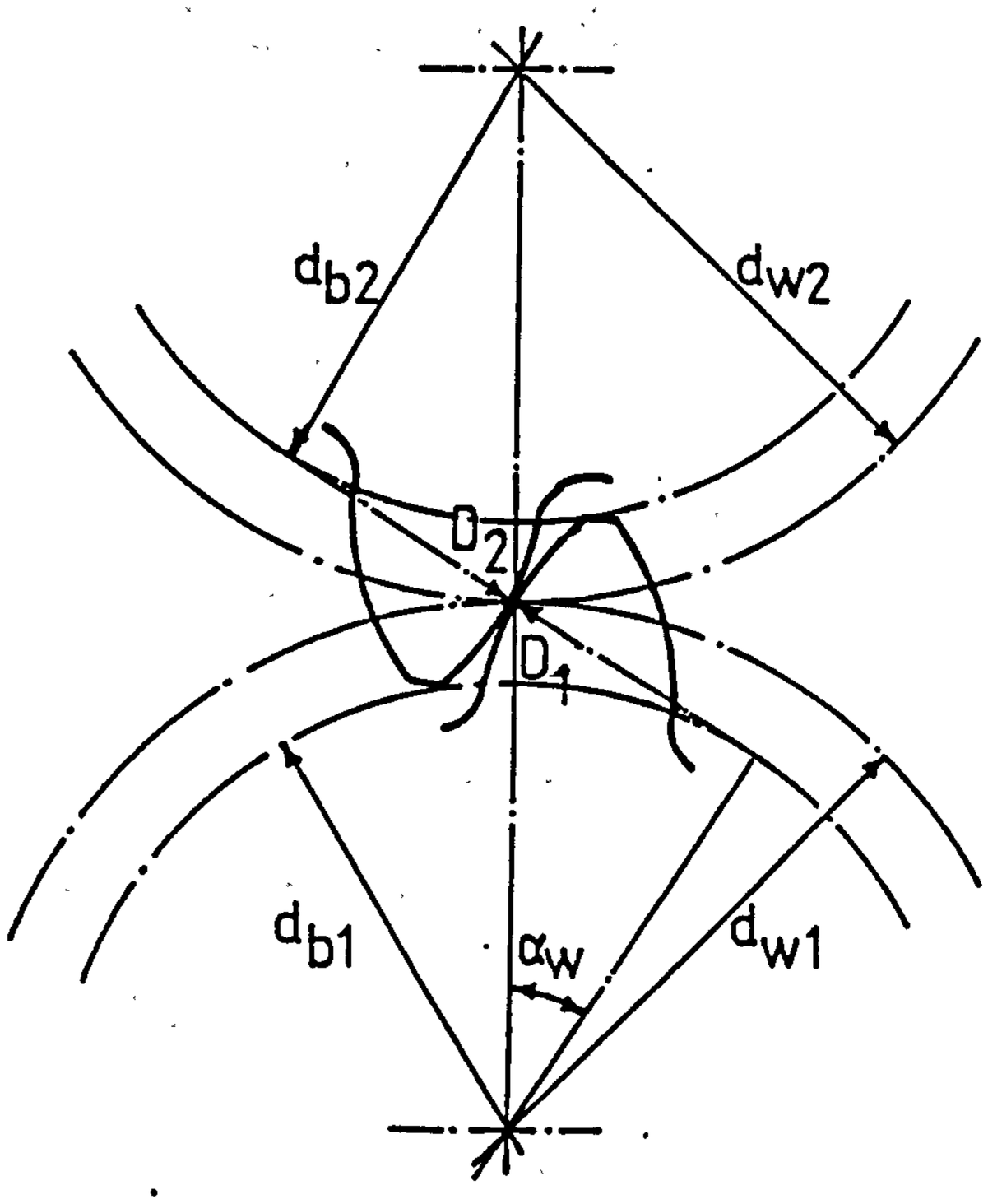

Fig. 1.1 Notation for Contact Stress: BS 436

In BS 436 the nominal root bending stress is calculated at the outermost point of single tooth contact, treating the gear tooth as a simple cantilever in bending subjected to the tangential component of the tooth load. The critical section at the tooth root is assumed to be defined by the 30° tangent as shown in Fig 1.2. There are also shear and compressive loads on the tooth root, but these are of secondary importance and in BS 436 are allowed for in the stress concentration factor. Using the notation shown in Fig. 1.2 the nominal bending stress for the cantilever at the critical section is given by:

$$\sigma_F = \frac{b F_t \cos \alpha_{en} h_f}{b S_{FN}^2 \cos \alpha} \qquad (1.3)$$

whence, introducing a stress concentration factor Ys, the peak notch stress at the 30° tangent is given by:

$$\sigma_F = \frac{F_t}{b\, m_n} Y_F Y_S \qquad (1.4)$$

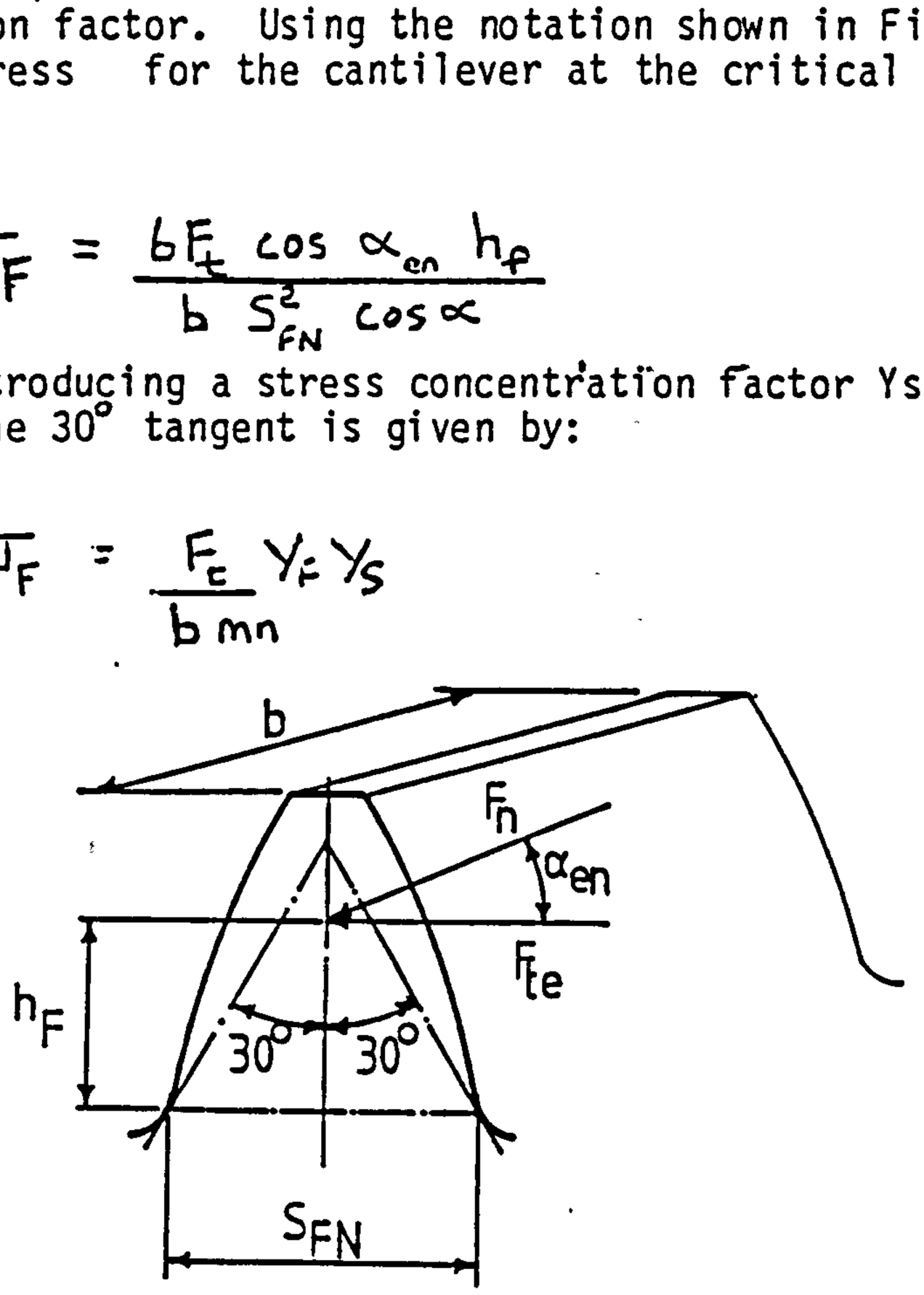

Fig. 1.2 Notation for Bending Stress: BS 436

The values of stress concentration factor, Ys, are based on strain gauge measurments on a large number of tooth forms by Hirt [H9], Finite Element analysis and "exact" solutions of the 2D elasticity problem by conformal mapping [C1]. Earlier analyses of this problem were based on a somewhat different analysis of tooth bending proposed by Lewis[L1]. Stress concentration factors applied to the nominal bending stress were based on photo-elastic experiments such as those reported by Dolan and Broghammer [D4], and Heywood[H10]. These methods have now been shown to considerably underestimate the peak tooth root stresses for perfect gears.

Now consider the stressing of "real" gears. BS 436 corrects the nominal contact stresses for perfect gears by introducing various load factors to allow for the effect of non-uniform torques, gear errors and misalignments. The contact stress is then given by:

$$\sigma_H = \sigma_{H0} \sqrt{KA \cdot KV \cdot K_{H\beta} \cdot K_{H\alpha}} \qquad (1.5)$$

The application factor, KA, takes account of external dynamic loads superimposed on the mean applied load; the dynamic factor, KV, allows for of internal dynamic loads generated by the relative vibration of the two meshing gears. This work is concerned only with the slow-speed "static" stress analysis of gears subjected to known external loading, for which KA = KV = 1 by definition. Calculation of KA and KV for other situations will not be considered. The face load factor, $K_{H\beta}$ accounts for the increase in contact stress due to unequal tooth loading accross the tooth face, (see Fig. 1.3). Its magnitude depends on the initial total tooth misalignment and the mesh stiffness. The transverse load factor, $K_{H\alpha}$ accounts for load sharing between adjacent teeth during multi-mesh contact, and depends primarily on the pitch/profile errors and mesh stiffness.

It is these two load distribution factors that are the prime concern of this project, either separately or combined into one static load factor, KLoad, where KLoad is the ratio of peak to nominal static load. It is not the intention to provide an alternative to the existing BS 436 gear stressing standard but to improve the modelling of the load distribution and provide more accurate peak static load

input data. The remaining parts of the standard are still applicable and together provide a more comprehensive analysis of spur gears.

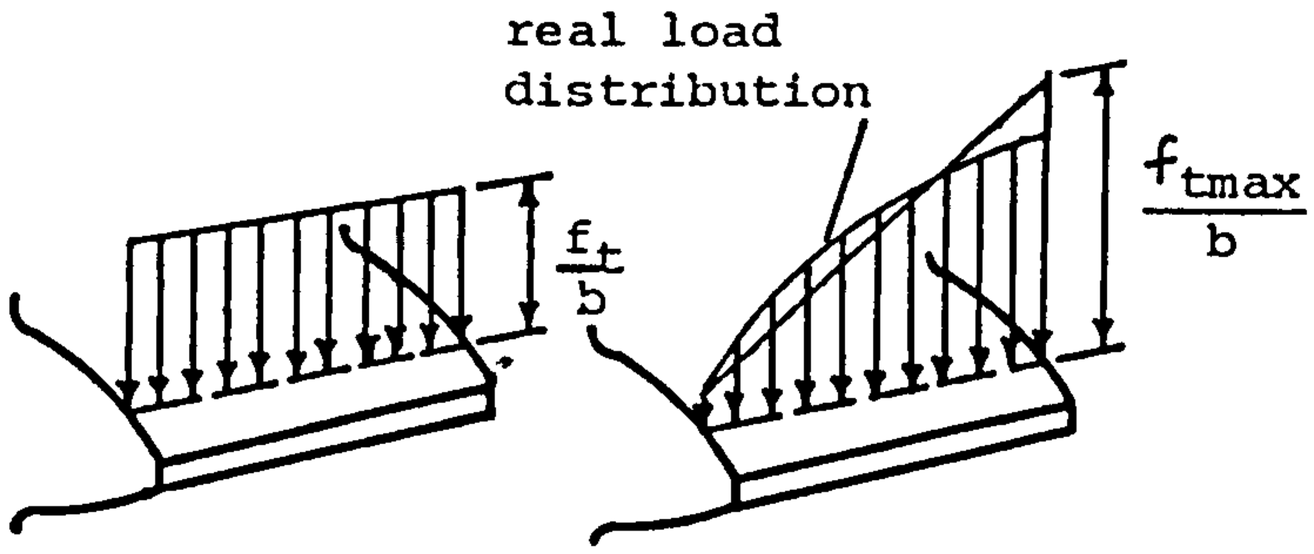

Fig. 1.3 Mal-distribution of Load in Real Gears

In this work the static contact stress will be determined by using equation (1.1); and the bending stress by using equation (1.4) as in BS436. However, the corrections for "real" gears will NOT be calculated by the BS436 method.

The gear meshing models used in all the gear standards used to

predict the load distribution factor $K_{H\beta}$ consider the gear teeth as a series of thin slices that deflect indpendently. A linearly varying load distribution across the face is assumed to predict the load distribution $K_{H\beta}$.

The mesh stiffness values used are based on two-dimensional analysis of gear teeth carried out by Winter & Podlesnik [W12] based on equations originally developed by Weber and Banaschek [W4 - W7].

Corrected value for the root bending stress are calculated in a similar way by writing:

$$\sigma_F = \sigma_{F0} KA \cdot KV \cdot K_{F\beta} \cdot K_{F\alpha} \qquad (1.6)$$

where KA and KV are the application factors and dynamic factors previously defined. $K_{F\beta}$ and $K_{F\alpha}$, the longtitudinal and transverse load distribution factors, allow like $K_{H\beta}$ and $K_{H\alpha}$ for the effects of non-uniform torques, gear errors and misalignments. The contact loads at the most heavily loaded section of the tooth are actually supported bu root bending stresses over a finite width of the tooth flank on each side of the critical section. Some "averaging" of the contact load distribution is thus apparent in the distribution of bending stress, so that $K_{F\beta} < K_{H\beta}$. BS436 assumes that $K_{F\alpha} = K_{H\alpha}$ based on work by Jaramillo[J1] and Wellauer[W8,W9] discussed below.

Limitations of BS436 and Other Existing Gear Design Standards

1. The thin slice model assumed in BS436 clearly fails to model teeth subjected to mal-distributed loads. The resultant buttressing effect of adjacent tooth sections tends to flatten the thin slice 2D distribution.

2. The linear 2D model is incapable of accurately modelling non-linear tooth modifications eg crowning and non linear lead correction (now readily available to the gear designer with CNC hobbing at his disposal).

3. The stiffness values employed in the 2D analyses are generally too great due to inaccurate modelling of the gear body compliance.

4. The face and transverse loads distribution factors $K_{H\alpha}$ and $K_{H\beta}$ are assumed multiplicative but there is no evidence to suggest that their effects are independent.

Several attempts have been made to overcome these shortcommings. The elastic deflection of each tooth at any point along the contact line actually depends on the loads at ALL the other points (not as assumed in this "slice model" which is only valid for the contact compliance). It is thus possible (with the use of a computer) to determine the contact load distribution by solving a system of near linear equations of compatibility of deformation for points along the contact lines of engaging gear teeth in which the deflection at any point is obtained by integrating the the effects of loads applied anywhere along the contact line and also, to a much lesser extent, on the adjacent meshing teeth.

Since the teeth are such a complex geometrical shape, no simple analytical solution has so far been developed for the contact line compliance of any given set of gear teeth. Several approximations have consequently been suggested for modelling the tooth compliance, generally involving splitting the total deflection into (assumed independent) deflections. The influence coefficients of the contact line have previously been split up into Hertzian or local contact deflections, bending/shear of the gear tooth, deflections of the gear bodies, and finally, deflections of the shafts, bearings, casings etc.

In 1949 Weber [W4 - W7] obtained expressions for the tooth contact deflection by integrating the two dimensional stress function equations derived by Hertz. Tooth deflections were obtained by equating the strain energy due to the applied bending moment, shear force and normal force to the work of deformation. The gear body considered by modelling it as a semi-infinite plane loaded by the tooth root bending moment, shear force and normal force, again by using a strain energy method.

Kagawa[K1] put forward a theory for calculating the gear tooth

compliance based on the formulae for a beam on an elastic foundation modified by a torsional compliance along the tooth facewidth. This provided a basis for several models developed in the 1960's.

In 1963 Hayashi and Sayama[H2] measured the bending deflections of a 240mm wide, 8.0mm module rack tooth. The experimental results were correlated with deflection equations for a thin cantilever plate similar to those developed by Kagawa [K1]. This work was continued by Umezawa [U1 - U8] who developed a finite difference solution for tapered rack shaped cantilever plates. Local contact deflections were calculated from a 'point' load. Deflections of the gear body were not included in the analysis, and consequently the tooth compliance was underestimated.

Schmidt [S1,S2] used equations of the same form as Weber and Banaschek's tooth stiffness formulae (derived from Kagawa's formulae) to obtain the combined stiffness of the meshing pinion and wheel. The equation constants were slightly modified to allow for the additional flexibility of the wheel only. This at least acknowledged that the wheel has a significantly greater flexibility than the pinion. However, the additional compliance was still based on the Weber/Banaschek semi-infinite plane assumption for the gear wheel body and was thus inaccurate. The contact deflections were treated as a two-dimensional Hertzian compliance.

Tobe[T4], treated a helical gear as a rack shaped plate encastre at the root. The deflections were determined by Finite Element analysis. The deformation of the root was again based on an analysis of forces and moments applied to a half space. The contact deflections were approximated by using Lundberg's empirical formulae [L5].

Conry and Seirig [C3,C4] defined the flexibility of the tooth as a torsional and bending compliance by considering it a cantilever plate. The increased compliance near each end of the gear teeth was taken into account by using the mirror or moment image law[J1]. The data obtained from Jaramillo[J1] for an infinitely long plate was used as a basis for the plate model. It can be shown that under uniform load the ends of the teeth then behave as though the tooth were infinitely wide, i.e. the tooth stiffness is over estimated. Deflection of the

gear body has been completely neglected.

Vedmar [V3] used three dimensional finite elements to model tooth bending compliance. Only approximately two modules of the rim was included in the finite element mesh effectively ignoring the gear body deflection. Contact deflections were again dealt with two-dimensionally using Hertz formulae. Vedmar also performed a 3D contact analysis to show that for gears with a "reasonable" load distribution, the errors involved in using the 2D contact deflection formula are small.

Finally, several authors have published work in which the contact compliance for spur gears is based on the conformed mapping of the gear profile projecting from a half plane (e.g. Cardou [C1]). No-one appears to have mapped the half plane into a complete gear to model correctly the gear body deformation.

As shown by this brief survey, several authors have already developed 3D elastic models of spur gears based on the contact line stiffness of the meshing gear teeth, (see Section 2.1). However, the accuracy of these models depends directly on the accuracy of the stiffness coefficients used and no-one appears to have modelled correctly the contact line stiffness. The tooth centre-line deflection has been found to include a significant 'disc' rotation, (the gear body component). For gear wheels this increases the tooth centre-line deflection by 125%. In view of this it is essential to model the gear body deformation correctly and the semi-infinite plane assumption is not valid.

Objectives of the Work:

1. Develop and verify experimentally a 3D stiffness model for spur gear teeth. Of particular importance were:

    a. Verify that the commonly adopted method of seperating the contact/"bending"/gear body components of contact line deflection is sufficiently accurate.

    b. Verify that the Hertz solution for the contact deflection of

an elastic half space is valid for a gear tooth surface especially at the tip and root.

c. Examine the magnitude and effects of gear body deformation.

2. Incorporate 1. into a 3D mesh capable of:

a. Analysing multi-tooth contact at all phases of mesh including when teeth are not in contact until under load and are elastically deformed (outside the kinematically defined phase of mesh).

b. Correctly take account of arbitrary tooth and gear misalignments (pitch, profile, lead error; profile modifications).

3. Develop and implement 1. and 2. on a micro-computer. The program is to be more easily used as an improved analysis of load distribution than existing gear design standards and also operate as a stand alone gear load distribution analysis program.

4. Investigate and report the shortcommings of the existing gear design standards (BS, DIN, ISO, AGMA).

In order to properly represent the gear body distortion, the author has found it necessary to model the complete gear, including the adjacent shaft, during the Finite Element Analysis, (Section 2.3). Separate 2D studies have shown that the analytical solution for the contact compliance, (Section 2.2), is a valid approximation to the compression between the tooth surface and centre-line.

A test rig has been constructed to load an 18 tooth pinion and the F.E./analytical gear modelling of contact line deflections and root stressing validated (see Chapter 3).

The stiffness data has been incorporated in a micro-computer elastic analysis program for spur gears, and Chapter 5 reports an investigation, using this program, into the effect of manufacturing errors and profile modifications on face and transverse load distribution. The results are compared with predictions based on the

BS, ISO and DIN standards which are shown to over-estimate gear tooth stiffness by upto 100% for large numbers of teeth (z = 100).

*****

1.2 Notation

A[i]	Weighting coefficient at the 'i'th gauss integration point
B	Offset of tool tip origin from tool axis
Ca	Height of tip relief
Cb	Height of end relief
Cc	Height of crowning
C[1..7]	Coefficients for curve fitting tooth centre-line deflection
CF[1..4]	Coefficients for curve fitting the 'Master curve' deflection
CG[1..3]	Coefficients for curve fitting the 'end effect' deflection
D	Contact surface diameter
E	Youngs Modulus (209 E3 N/mm2 for steel)
F(z')	Centre-line deflection 'master curve' function
Fn	Total tooth force along base tangent
Ft	Tangential tooth force acting along reference diameter
Fte	Tangential tooth force at OPSTC
$F_{\beta y}$	Equivalent mesh misalignment
G(z,zF)	Bending deflection end effect function
K(z,zF)	Contact line deflection influence function
KA	BS436 application factor
KD	Relative (contact) surface diameter of curvature
$K_{H\alpha}$ $K_{F\alpha}$	Transverse load distribution factors
$K_{H\beta}$ $K_{F\beta}$	Face load distribution factors
KLoad	Ratio of peak specific load to nominal specific load
KV	BS436 dynamic factor
Ktb[z,zF]	Tooth bending deflection influence function
Ktc[z]	Tooth contact compliance influence function
K_{σ}	Tooth root stress influence function
S_{FN}	BS 436 normal tooth chord thickness at critical section
X	X coordinate
Y	Y coordinate
YF	BS 436 Form factor
YS	BS 436 stress correction factor
Y_{α}	Running in allowance
Z	Z coordinate
ZB	Pinion single contact factor
Z_E	BS 436 elasticity factor
Z_H	BS 436 zone factor
Z_{β}	BS 436 helix angle factor
Z_{ε}	BS 436 contact ratio factor

a	Centre distance
b	Facewidth
bcal	Calculated equivalent facewidth
beff	Effective facewidth
c	Constant to account for 'disc' rotation component of tooth centre-line deflection
ct	Initial, zero load, tooth seperation
c'	Single tooth stiffness (BS, ISO, DIN)
c'r	Relative single tooth stiffness
c_γ	Mesh stiffness
da	Tip diameter
db	Base diameter
ds	Shaft diameter
dy	Meshing diameter
dyp2	Pinion tip diameter relative to the wheel axis
e	Angle used in tooth clearance calculations (Appendix 2.1.3)
ff	BS436:Pt.2:1970 profile error; DIN 3962 profile error
fp	Pitch error
fpe	Adjacent pitch error
$f_{H\alpha}$	Profile angle error
ft	Transmission error
g	Length of path of contact
h	Depth below tooth surface (for calculating contact deflection)
hao	Tool addendum
hF	BS 436 bending moment arm for root stress calculation
l	Length of path of contact from base normal, test rig loading anvil length
lc	Length of end relief
ls	Length of path of contact to start of engagement
ly	Length of path of contact to mesh diameter dy
mn	Normal module
po	Peak Hertzian contact pressure
r	Radius
rb	Base radius
rao	Tool tip radius
rf	Radius on a given fillet trochoid
s	Tooth thickness at reference diameter
sy	Tooth thickness at diameter dy

u	Gear ratio
x	Addendum modification coefficient
z	Number of teeth, Axial coordinate of tooth deflection
zF	Axial coordinate of applied point (Gauss) load
z'	|z - zF|

α	Pressure angle
α_{en}	Pressure angle at outer point of single tooth contact
α_w	Working pressure angle
δ	Contact line deflection
δ_{AB}	Loading anvil compression
δ_A	Adjacent tooth surface deflection
δ_e	Tooth surface deviations from the theoretical involute
δ_p	Surface deflection of an elastic half space due to an applied point load
δ_{tb}	Tooth centre-line deflection relative to the bearing supports
δ_{tc}	Tooth surface deflection relative to the tooth centre-line
δ_s	Tooth centre-line deflection due calculated 'shaft' deflection
ε	Equivalent angular separation of teeth at end of engagement
	Contact ratio
θ	Angle between mesh point and line joining centres (polar coordinate of trochoid)
θ_f	Vectorial angle of fillet form (Appendix 2.3.2)
θ_t	Vectorial angle of point trochoid form (Appendix 2.3.2)
λ	Angle between tooth centre-line and radial line through meshing point
ν	Poissons ratio (0.3 for steel)
σ	Stress
σ_{HO}	Contact stress at reference diameter for perfect gears
σ_H	Contact stress at reference diameter for real gears
σ_a	Surface fillet (30°) stress normal to the gear axis
σ_F	Tooth root stress
σ_{Fe}	Tooth root (or 'bending') stress due to a load applied at the OPSTC
σ_o	Axial fillet (30°) stress parallel to the gear axis
$\sigma_{1,2}$	Principal stress
τ	Angular pitch
ϕ	Phase angle relative to the pinion base normal
ϕ_E	Phase angle at the theoretical end of engagement
ϕ_S	Phase angle at the theoretical start of engagement
ψ_t	Angle between tantent to trochoid and radius vector (Appendix 2.3.2)
ψ_y	Distance of mesh point above the reference diameter
ω	Specific tooth load, angle between tooth centre-line and a line joining the two gear axes

w_{bm}	Nominal specific tooth load
Δ	Interval of facewidth for two point Gauss integration
$\Delta\varphi$	Estimate of pinion rotation out of mesh at which no tooth contact occurs
∇	Gradient vector

additional Subscripts

a	Tip diameter
b	Base diameter
f	Root diameter
y	Meshing point
A	Start of mesh, adjacent tooth
E	End of mesh
'	Non-dimensional

Abbreviations

DTC	Double tooth contact
EN	Engineering number for material specification
F.E.	Finite element
B.E	Boundary element
HV	Hardness, Vickers
IPSTC	Inner point of single tooth contact
LVDT	Linearly variable differential transformer
LOA	Line of action
LOC	Line of contact
OPSTC	Outer point of single tooth contact
SAP	Start of active profile
STC	Single tooth contact
mu	Microns (1.0E-6 metres)
2D	Two dimensional
3D	Three dimensional

*****

CHAPTER 2

MATHEMATICAL MODELLING OF THE MESHING CONDITIONS BETWEEN SPUR GEARS

2.1 A Three Dimensional Elastic Model of Spur Gears

2.1.1 Elementary Theory of Tooth Meshing

The load distribution between a pair of meshing gear teeth is dependent on the initial misalignment of the engaging teeth and the stiffness of the contact line (The theory about to be presented here can be extended to apply to multi-tooth contact of spur, helical, bevel and worm gears). Consider the engagement of a single pair of parallel-axis gears. Contact between the two teeth will occur over a narrow band lying approximatly in the common base tangent plane with a width of order mn/30. This plane intersects the tooth flanks in straight line known as the line of contact (LOC). For the time being we will assume that the tooth load is distributed along the LOC with intensity w(zF) per unit length, where zF is the axial coordinate as shown in Fig. 2.1. The elemental force dF(zF)at zF will, for an elastic solid, cause an elemental deflection $\delta(z)$ at point z on the contact line (eqn 2.1). The arbitrary load intensity w(zF) will give rise to deflections $\delta(z)$ at point z on the contact line (Fig. 2.1).

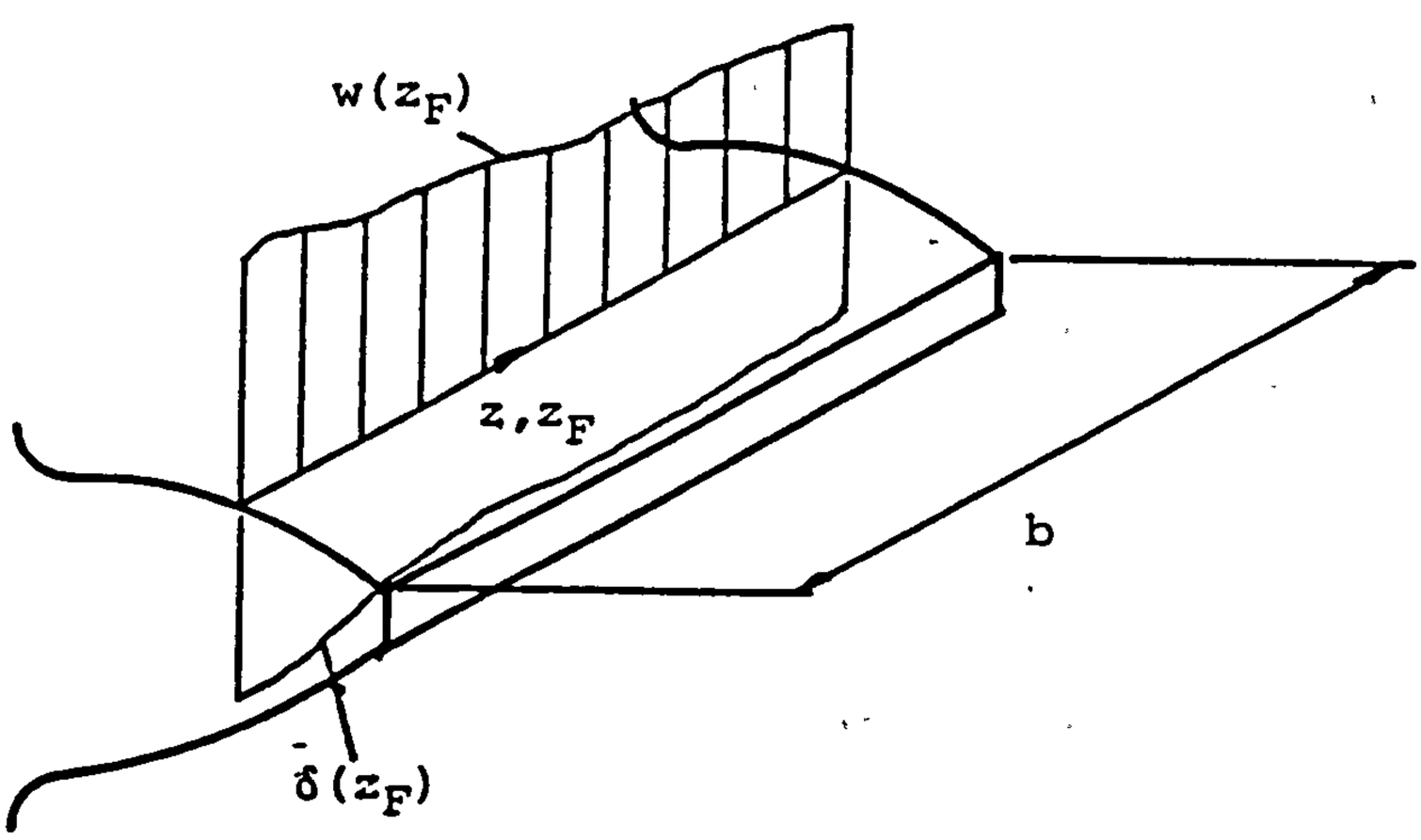

Fig. 2.1 Force Acting Along a Contact Line

$$\delta = \int_0^b K(z,zF)\,\omega(zF)\,dz \qquad (2.1)$$

where K(z,zF) is an influence function. By Maxwell's reciprocal theorem we must also have:

$$K(z,zF) = K(zF,z) \qquad (2.2)$$

Integration along the contact line also gives the total applied force:

$$F_n = \int_0^b \omega(zF)\,dz \qquad (2.3)$$

Now consider the overall displacement of the tooth contact line from its perfectly manufactured, unloaded position. This comprises of the following components:

Load dependent deviations:

δ_{tc} : Local deformation of the tooth surface relative to the tooth centre-line of tooth. This will be referred to as the contact deflection.

δ_{tb} : Deflection of tooth centre-line along the base tangent relative to the bearing support centres excluding calculated shaft bending, torsion and bending deflections.

Non load dependent deviations:

δ_e : Tooth surface deviations from the theoretical involute profile along base tangent, positive deviations add material to the tooth flank.

δ_s : Deflections of the tooth centre-line along the base tangent

due to 'rigid' shaft bending, torsion, shear deformations. Shaft deflections only vary slightly with change in load distribution and so can be considered independent of load distribution to a first approximation.

ct : Initial gap between perfect teeth due to being outside of the theoretical phase of engagement. This is important only in multi-tooth engagement but has been included here for completeness.

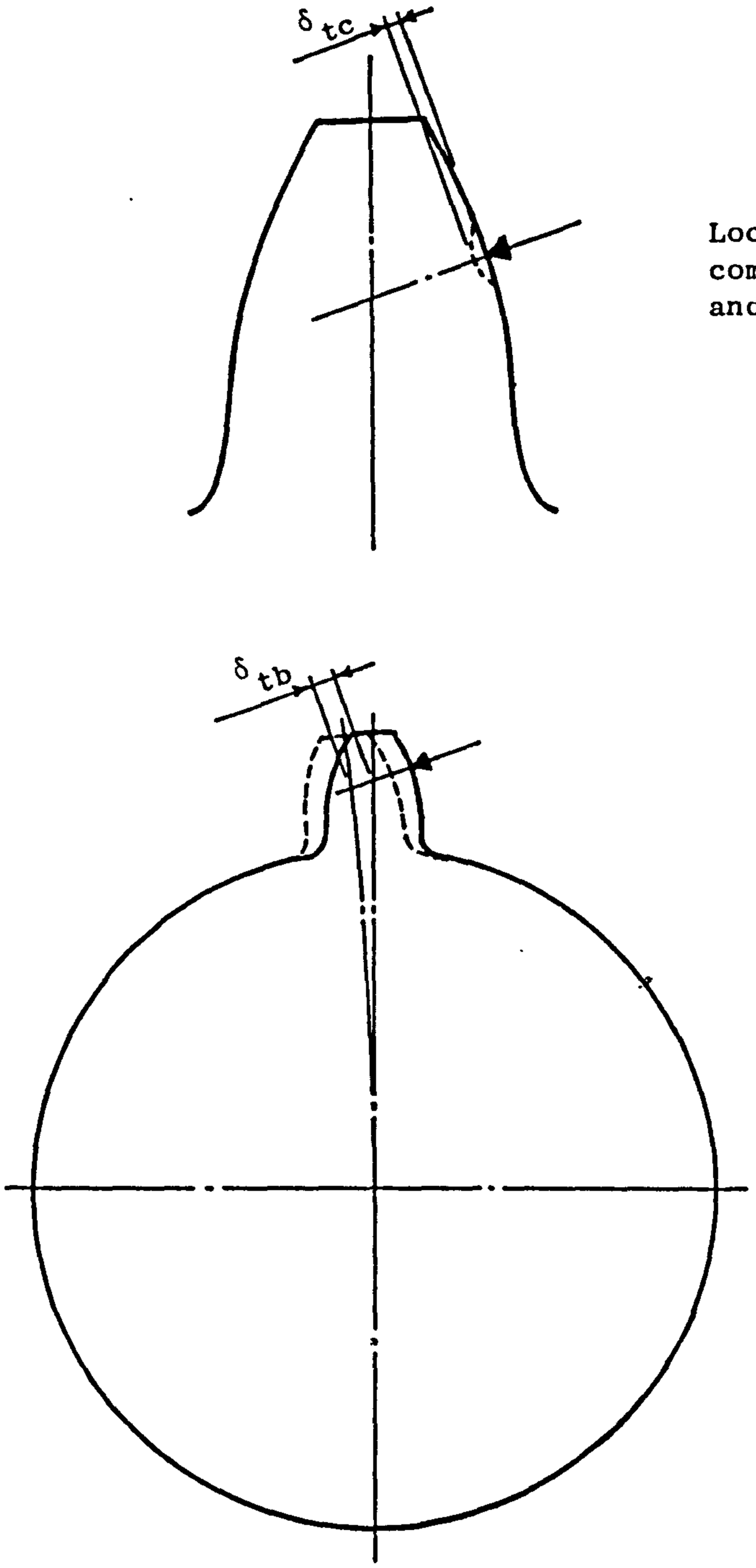

Local tooth contact compression between surface and tooth centre-line

Deflection of tooth centre-line relative to the shaft

Fig. 2.2 Components of Tooth Contact Line Deflection

Compatibility of tooth contact leads to:

$$ft = \delta_{tb} + \delta_{tc} + \delta_s - \delta_e - ct \qquad (2.4)$$

where ft is the transmission error along the base tangent between pinion and wheel. Note that ft is independent of z.

The tooth contact deflection is very localised and so is assumed to be only a function of the specific load at the point of interest. The tooth deflection $\delta(z)$ at z does depend on the load distribution and consequently does include cross terms. Combining equations 2.1 and 2.4 we have:

$$ft = \int_0^b K_{tb}(z.zF)\omega(zF) + K_{tc}\omega(zF) + \delta_s - \delta_e - ct \qquad (2.5)$$

No exact analytical expression exists at present for the tooth bending influence function ktb. Equations 2.3 and 2.5 can be solved by numerical integration to give equations:

$$ft = A[i]\frac{b}{2}\sum_{i=1}^{n} K_{tb}[i,j]\,\omega[j] + K_{tc}[j]\omega[j] + \delta_s - \delta_e - ct \qquad (2.6)$$

$$F_n = A[i]\frac{b}{2}\sum_{i=1}^{n}\omega[i] \qquad (2.7)$$

where A[i] are the weighting factors for the numerical integration. Repeated two point Gauss integration was chosen to minimise integration errors and prevent the unstable modelling which often results from the use of high order polynomial approximations.

Equations 2.6 and 2.7 can be regarded as a set of linear equations for the unknowns w(zF) which can be solved by normal methods (eg Gauss elimination) if the compliance coefficients are constant (linear elastic behaviour). Unfortunately, the contact deflection δ_{tc} is a non-

linear function of the load intensity w(zF) so that the contact compliance is not a constant but decreases with w(zF). For a "negative" w(zF) (ie no tooth contact at zF the "compliance" is evidently infinite.

Equations 2.6 and 2.7 are thus non-linear, appreciably so if the loading is such that no contact occurs over part of the facewidth. This necessitates an iterative solution. An initial estimate of w(zF) is made to allow calculation of the contact compliance. Equations 2.6 and 2.7 are then solved to give an improved estimate of w(zF). This is then used to re-calculate the contact compliances. The process is repeated until convergance is reached. Loss of contact at any point z is indicated by a negative value of w(zF). For these points, the contact compliance is progressively increased so that the convergence process is smooth.

Contact is assumed to occur on up to three pairs of teeth. This takes account of all practical spur gears including the so-called high contact ratio (HCR) spur gears (most spur gears contact on a maximum of two pairs at any one instant). Note that tooth deflection due to loads applied to an adjacent tooth (especially significant in gear wheels) must be included.

2.1.2 Load Intensity Solution at any Arbitrary Position

Section 2.1.1showed how the load distribution at specific points of integration along the contact line(s) could be obtained. Of special interest are the loads at each end of the gear teeth. One method of obtaining the load intensity at any point would be to use a large number of Gauss points in the initial solution and then interpolate but this would be very inefficient.

Hayashi [H1] suggests using the relationship from eqn (2.6)

Rearranging, we obtain the following:

$$w[j] = \frac{ft - A[i]\, b/2 \sum_{i=1}^{n} K_{tb}[i,j]\, w[j] - \delta_s + \delta_e + ct}{K_{tc}[j]} \qquad (2.8)$$

which can be solved for w(zF) by iteration since Ktc is a known function of w(zF). This method has proved to be unsatisfactory and gives unreasonable variations forloading between Gauss points.

A better method is to proceed as follows:

$$W[i] \simeq \frac{ft - \delta_e - ct + \delta_s - \delta_{tb}[i]}{K_{tc}[i]} \qquad (2.9)$$

The tooth contact compliance, Ktc, at any point z is only a function of the load at z. Equation 2.9 can be solved by iterating for the load **w[i]** An initial estimate of the load must be made.

The tooth bending deflection function , Ktb, is known for loads applied at the Gauss points but nevertheless describes the mid-tooth deflection at any point across the facewidth. Tooth bending compliance increases rapidly near the ends of the teeth and at the end of the tooth are extrapolated values so are prone to greater error. This is why Hayashi's method gives spurious results. The method proposed is based on the physical argument that even for severe mal-distribution of load the tooth bending deflection will be "smooth". The bending deflection at the point of interest is accordingly calculated by spline fitting the (already known) Gauss-point values, NOT by calculating new values for Ktb in eqn 2.8. This interpolated deflection is then inserted into equation 2.9 instead of that given by the integral.

2.1.3 Engagement Outside the Kinematically Defined Phase of Mesh

For perfect, infinitely stiff, gears the limit of phase of engagement is easily determined from geometric considerations. For real elastic gears, however, contact occurs outside the theoretical limits of phase of mesh. An example of the effect of this new limit of phase of mesh is in load sharing between adjacent contacting teeth. The loads may or may not be shared between two teeth depending on the difference between adjacent pitches. Consequently, peak contact stresses may at the inner point of single tooth contact due to the low relative radius of curvature (KD), see Fig. 2.3

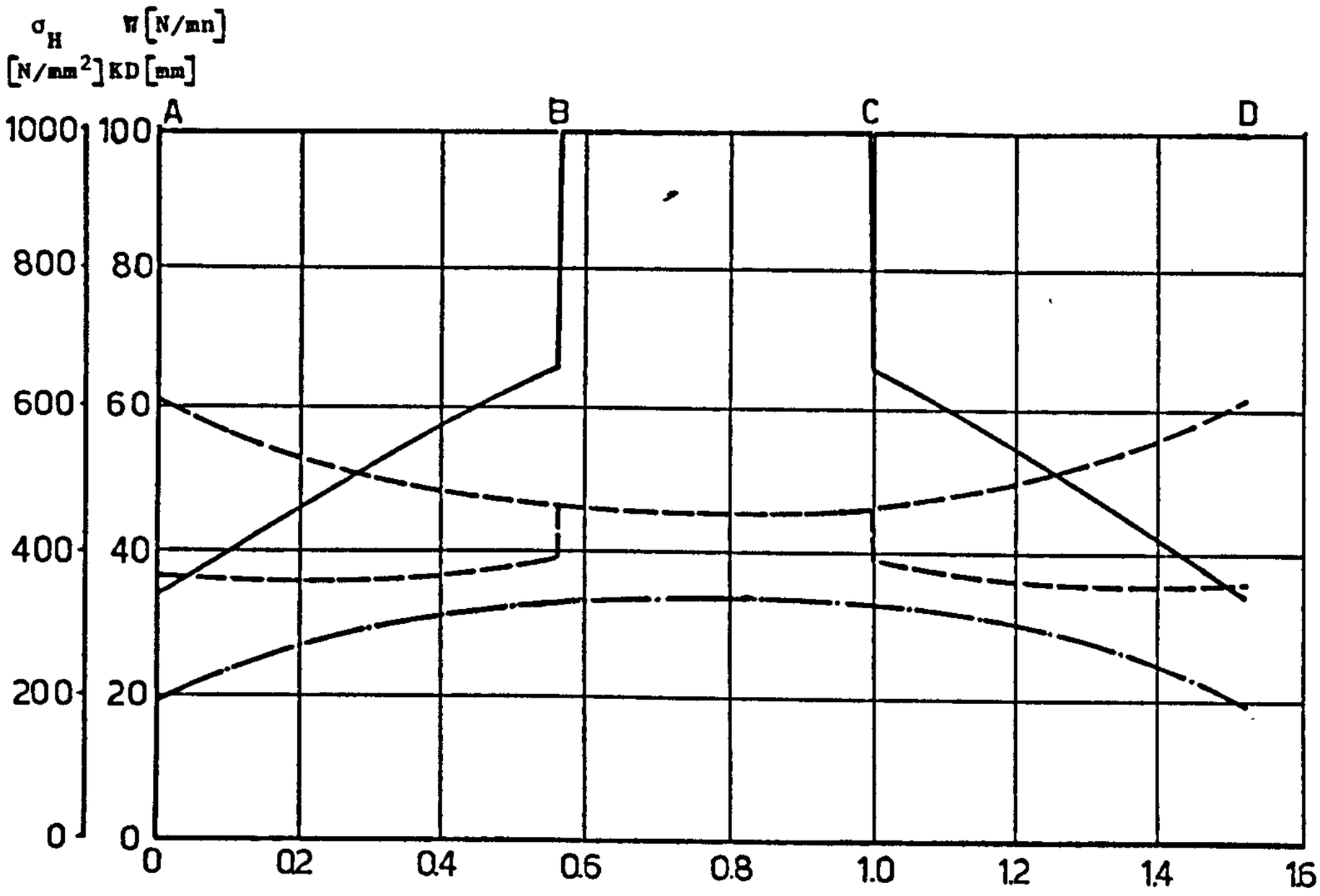

Fig. 2.3 Effect of Pitch Error on Peak Contact Stress

The equation of compatibility for tooth contact (equation 2.4) contains a term, ct, for the initial separation of the two perfect, unloaded teeth. Within the kinematically defined phase of contact ct is zero (ie there is no gap). Where such a tooth pair are just engaging or disengaging contact between the teeth (outside the normal phase angles) can only be between the involute flanks of one gear and the tip (corner) of the mating "flank". Fig. 2.4 shows two gear teeth coming into mesh.

Contact will be on the pinion flank along a line tangential to the pinion base diameter, dbl, and passing through the wheel flank corner, A. The loading diameter, dyl, used to calculate the pinion bending and contact compliances is that intersection between this base tangent line and involute profile. Appendix 2.13 gives the equation for calculating ct and dyl. The wheel compliances are assumed to be those corresponding to normal tip contact, although the actual contact compliance will thus be under-estimated due to the "non-Hertzian" nature of corner contacts (see 2.2.7 below).

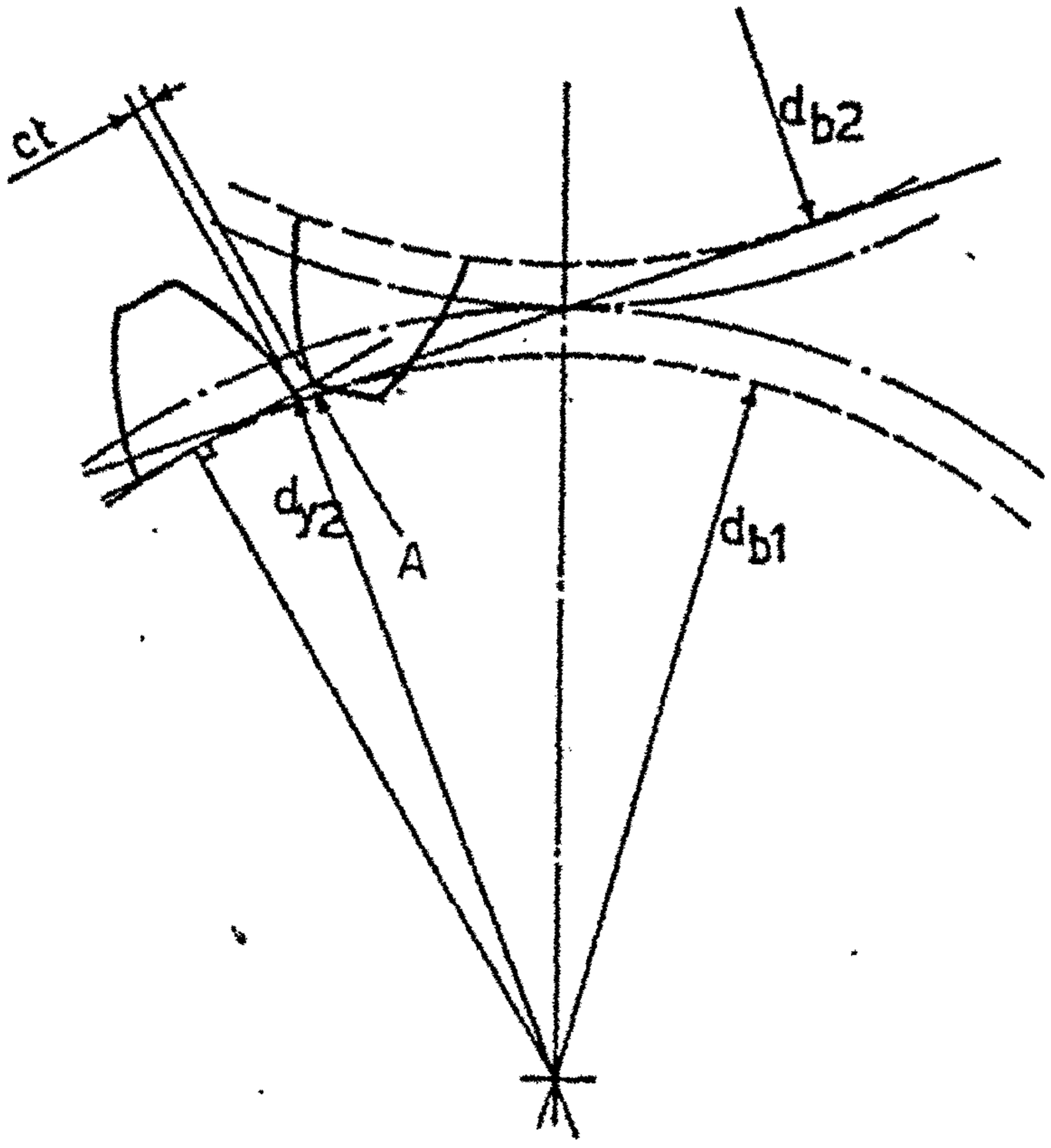

Fig. 2.4 Initial Clearance, ct, and Loading Diameter, dy1 Outside Theoretical Phase of Engagement

2.2 Modelling of Tooth Contact Compliance and Stresses

2.2.1 Introduction

Section 2.1 set out the theoretical equations for modelling spur gear load distribution. Preliminary analysis showed that the tooth contact compliance, Ktc, can contribute up to 30% towards the total contact line compliance. For a non-uniform load distribution and near the tip/root/ends of the tooth flank there is a complicated 3D contact stress field that can not be readily modelled. For "reasonable" load distributions, however, Vedmar [V3] has shown that the contact compliance can be approximated by applying the 2D "Hertzian" pressure applied to an equivalent elastic half space.

In this work, an analytical 2D contact compliance formula has been used to predict the contact deflection. A semi-empirical multiplying factor has been derived to take account of the increase in contact compliance near the tooth tips.

2.2.2 2D Contact Compliance of an Elastic Half Space

The stresses beneath the centre of loading of an elastic half space with an elliptical pressure distribution are (ref. Huber and Fuchs [H11]):

$$\sigma_x / p_o = -2\nu\left[(1+h')^2 - h'\right] \qquad (2.10)$$

$$\sigma_y / p_o = -(1+h'^2)^{\frac{1}{2}}\left[2 - (1+h'^2)^{-1}\right] + 2h' \qquad (2.11)$$

$$\sigma_z / p_o = -(1+h'^2)^{-1/2} \qquad (2.12)$$

Where contact depth h' = h/b and peak pressure $p_o = \frac{4}{\pi}\frac{w}{2b}$ (Dubbel [D5])

* Footnote: There is no Figure 2.5

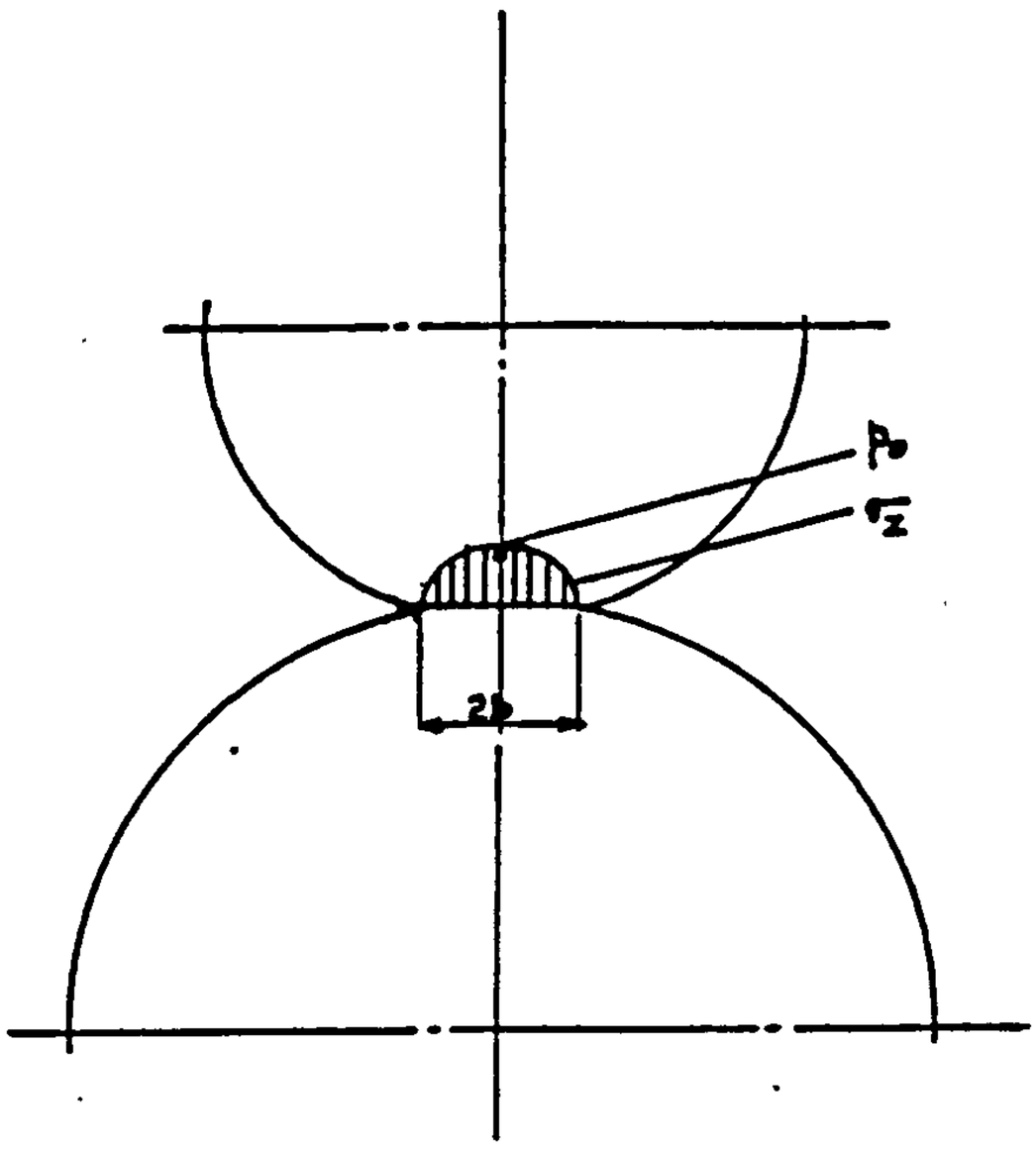

Fig. 2.6 Surface Pressure Distribution with Hertzian Contact Conditions

On the surface of the elastic half space, $z = 0$, we obtain:

$$\sigma_x / p_o = -2\nu \qquad \sigma_y / p_o = -1 \qquad \sigma_z / p_o = -1 \tag{2.13}$$

$$\sigma_x = +2\nu\sigma_z \tag{2.14}$$

The strains are given by:

$$e_z = 1/E[\sigma_z - \nu(\sigma_x + \sigma_y)] \qquad e_x = 1/E[\sigma_x - \nu(\sigma_z + \sigma_y)] = 0$$
$$\Rightarrow \sigma_x = \nu(\sigma_z + \sigma_y) \tag{2.15}$$

$$\therefore e_z = 1/E[\sigma_z(1-\nu^2) - \nu(1+\nu)\sigma_y] \tag{2.16}$$

Whence, inserting equations (2.10) to (2.12) into (2.16) gives:

$$e_z = -\frac{p_o(1-\nu^2)}{E}\left[(1+\frac{\nu}{1-\nu})(1+h'^2)^{-1/2} - \frac{2\nu}{1-\nu}(1+h'^2)^{1/2} - h'\right] \quad (2.17)$$

The contact deflection is obtained by integration, giving:

$$\delta_z = \int_b e_z\, dh' = -\frac{p_o b(1-\nu^2)}{E}\left[\ln(h'+\sqrt{1+h'^2}) - \frac{\nu h'}{1-\nu}(\sqrt{1+h'^2}-h')\right] \quad (2.18)$$

Substituting for p_o from (2.12) and assuming $h' \gg 1$ (typically h' is of order 30 at the tooth centre-line) gives:

$$\delta = -2\frac{(1-\nu^2)}{\pi}\frac{w}{E}\left[\ln(2h') - 3/14\right] \quad (2.19)$$

This expression will be valid for reasonably uniform load distribution away from tooth tip/root/end effects (for which the Hertzian solution is not valid).

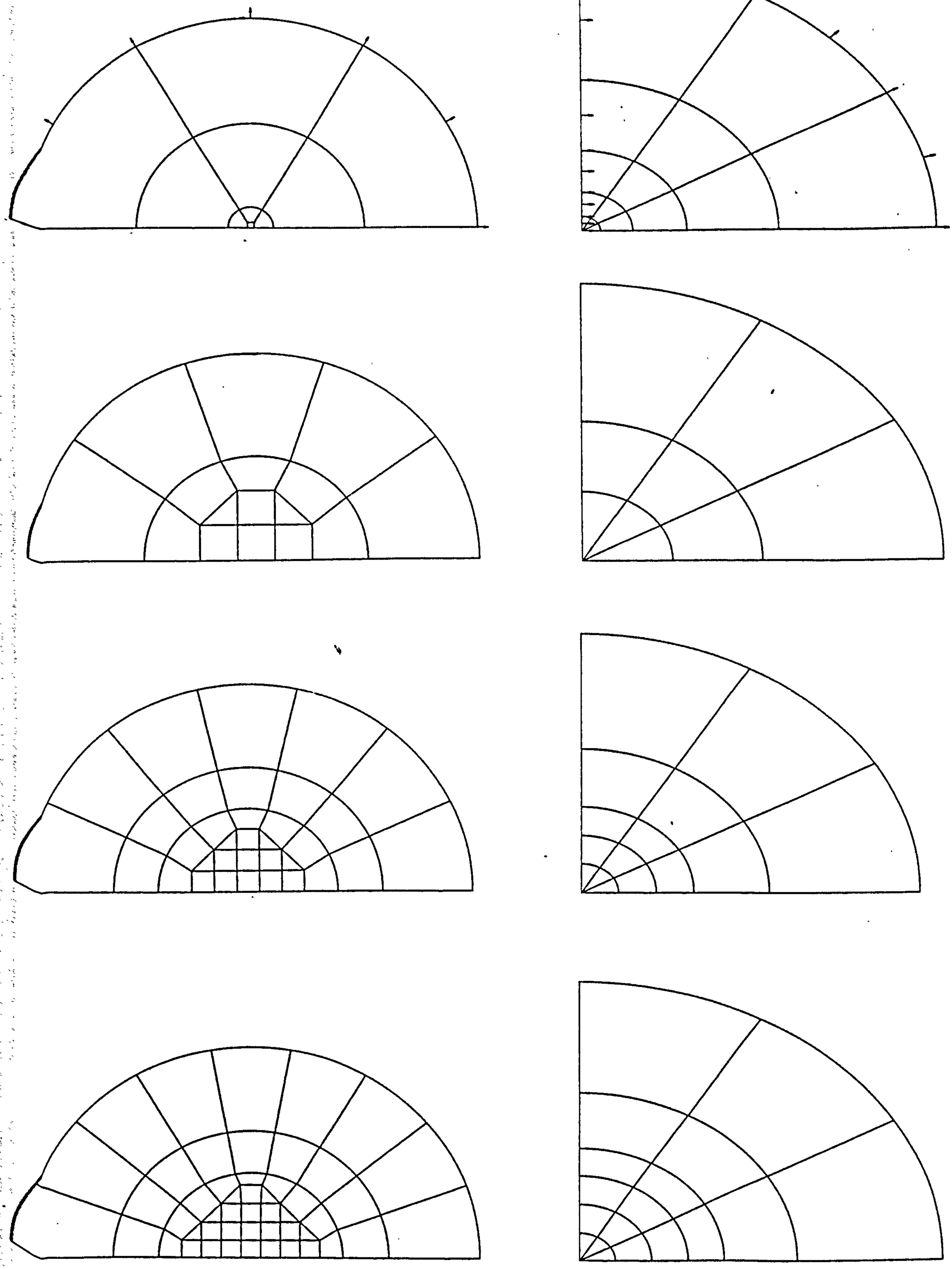

Fig. 2.7 F.E. Modelling of Hertzian Contact Deflections and Stresses

2.2.3 Finite Element Modelling of Contact Compliance and Stresses

In order to verify that seperate modelling of contact compliance was a valid procedure, complete 2D Finite Element modelling of gear tooth stresses including the contact stresses was undertaken (see 2.3.2). This required reliable modelling of the contact region itself, and a seperate study as accordingly made of how this might be achieved with sufficient accuracy.

A second order polynomial approximation (restriction of PAFEC surface loading facility) to the elliptical pressure distribution was applied to several F.E. meshes of an elastic half space, (Fig. 2.7). A specific load of w = 200 N/mm over a contact width of 2b = 0.3mm was applied to the F.E meshes. Far away from the contact patch classical theory shows that the stress system is radial and so radial restraints were applied to the models over semi-infinite boundaries.

The peak shear stress occurs at h' = 0.8b. To correctly model the peak stress gradients the element density is maximum upto a depth of order b.

The two coarsest meshes were also subjected to a "point" load (to a corner or midside node) to investigate the accuracy of a constant contact compliance F.E. model. The Finite Element analysis used in this work is based on linear elasticity so a "point" load produces an elastic approximation to the the contact compliance.

Fig. 2.8 shows the form of the contact deflection; Fig. 2.9 the error in contact deflection as a function of reference depth; Figs. 2.10 and 2.11 the error in z and y for each of the meshes shown in Fig. 2.7.

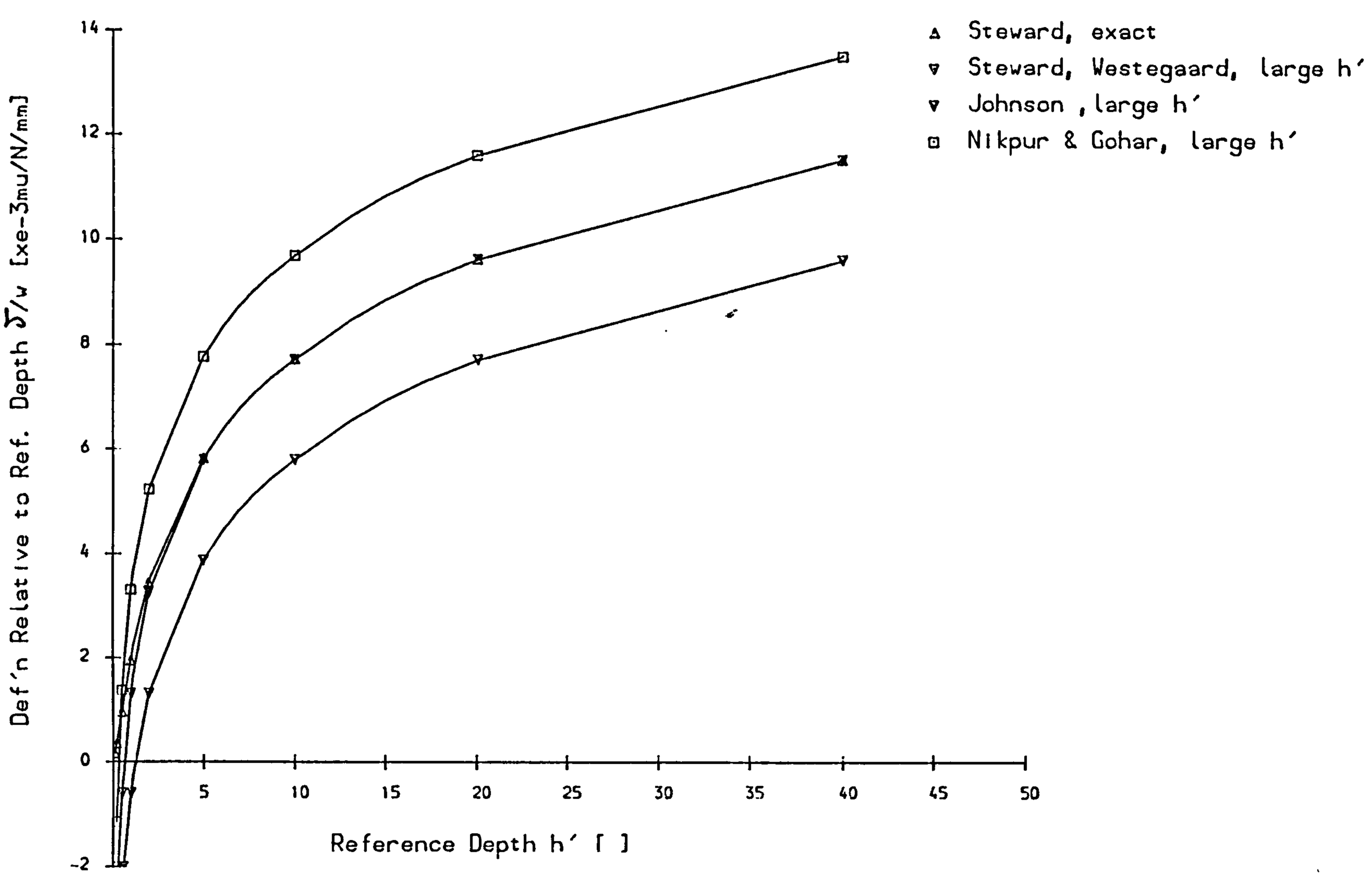

Fig 2.8 Comparison of Formulae for Deflection of an Elastic Half Space

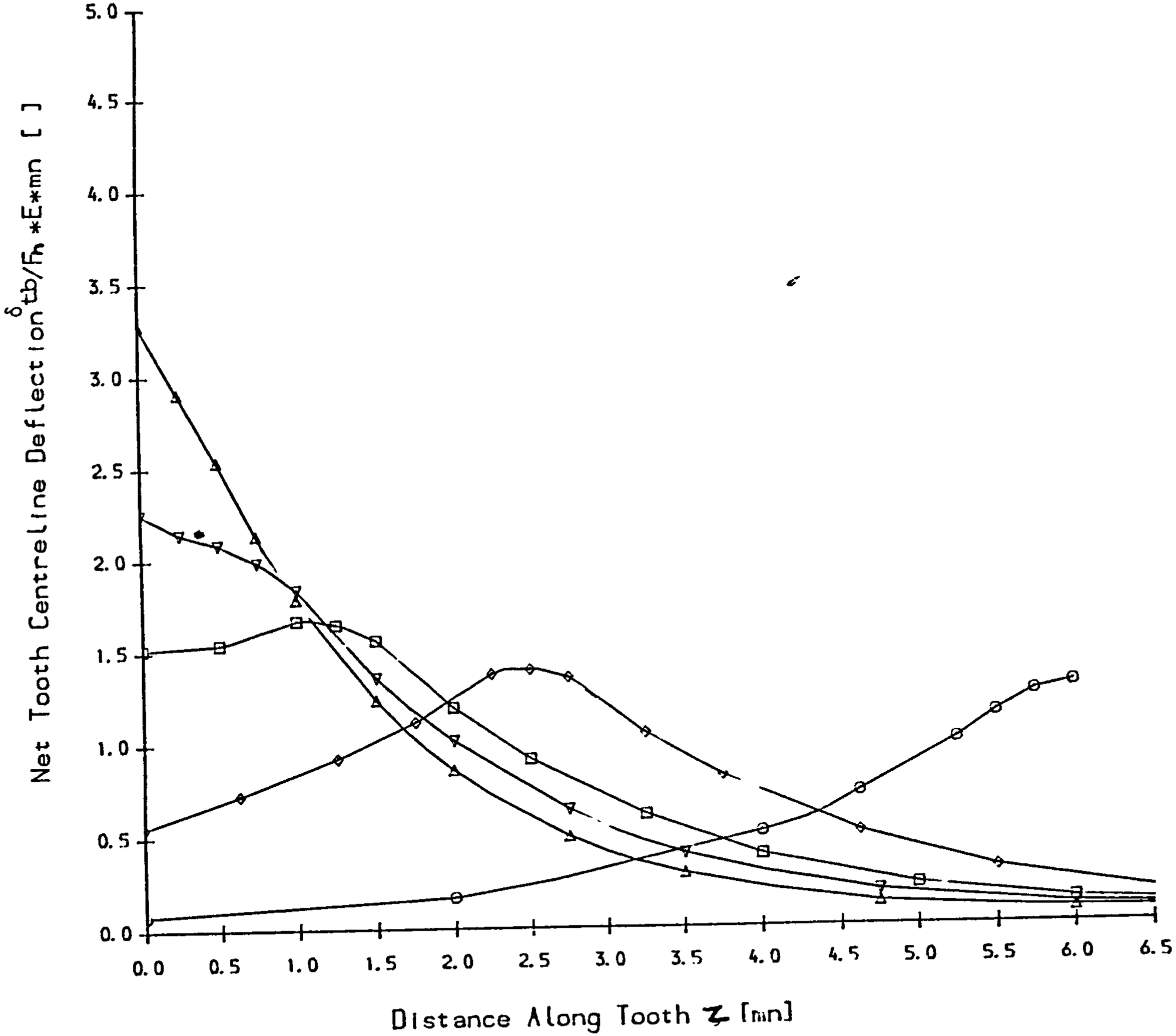

Fig 2.29 FE Results: Reference Dia. Loading; Net Tooth Centreline Deflection; 18 Teeth

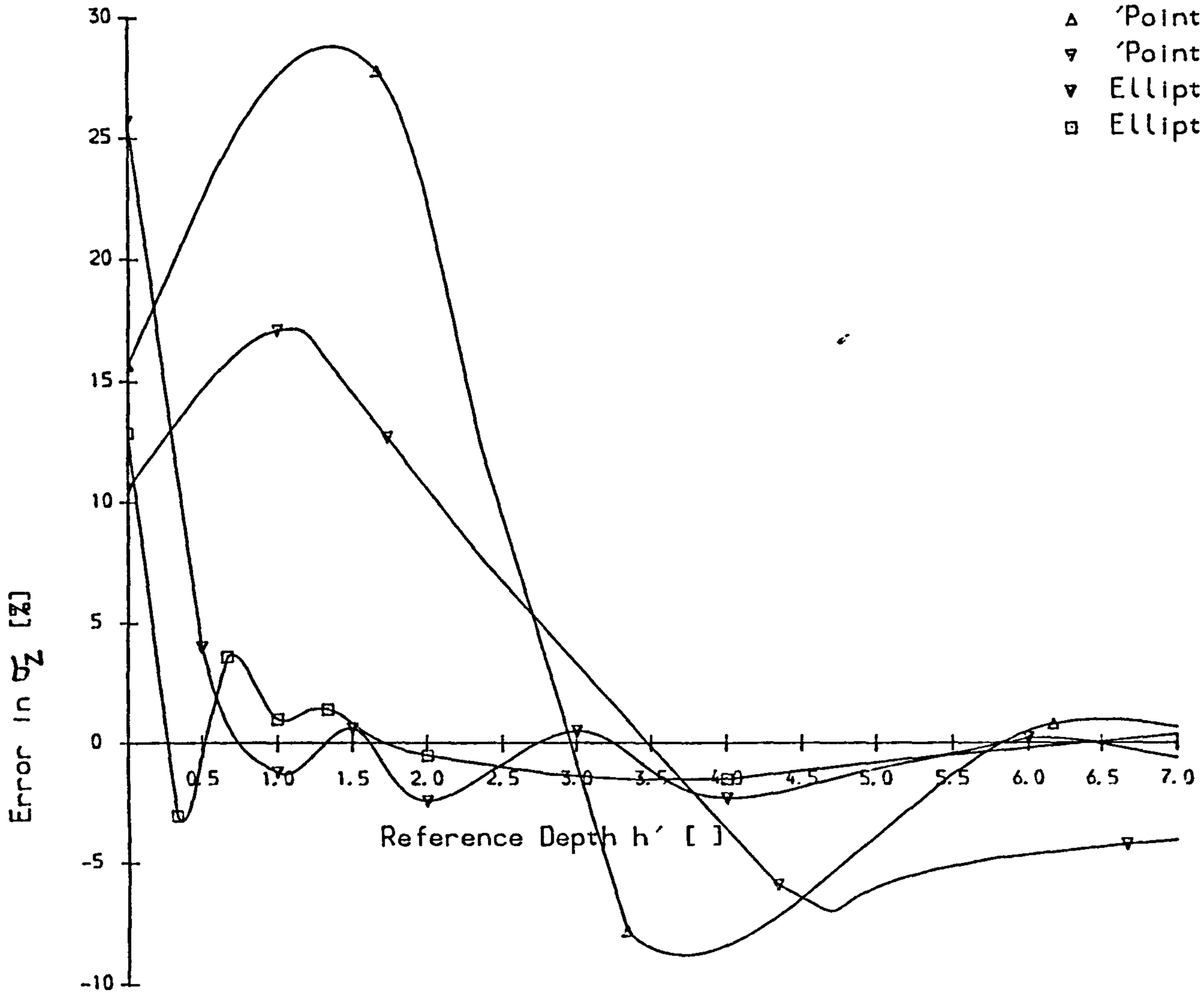

Fig 2.10 Error in FE Modelling of σ_z Below Centre of Pressure

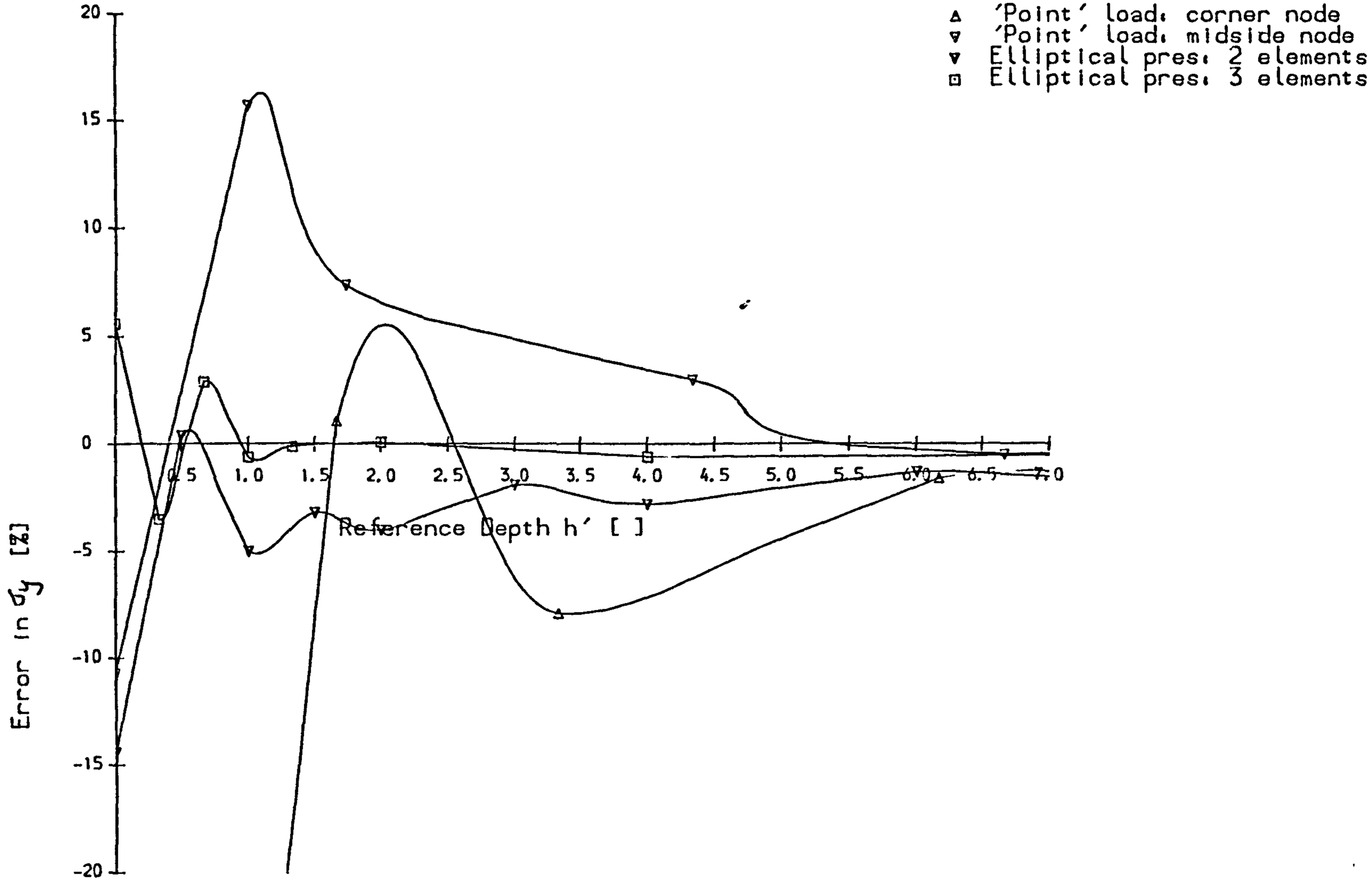

Fig 2.11 Error in FE Modelling of σ_y Below Centre of Pressure

Note:

- The deflections appear to converge to a value approximately 5% greater than the analytical solution. Although the mesh was progressively refined, there is clearly still some region in which the F.E. approximation is inadequate. The edge of the elliptical pressure distribution produces very high stress gradients and seems the most likely source of error. This potential source of error is considered later in this section. The corner-node model is 20% too compliant for h' = 30 (approximate gear tooth reference depth). The midside node model converges to 5% error (acceptable) by the time h' = 30, provided that the loaded element has a width of 2b.

- The stress modelling is less accurate than the deflection modelling near the surface as would be expected. The stresses do not converge to the correct value at the peak stress depth (0.8b) unless three or more 'surface' elements are used to model the applied load.

2.2.4 Comparison of Contact Deflection Results with Published Data

Fig. 2.8 plots a total of four different theoretical contact deflection curves according to various published theories.

Westergaard [H.8] solves for the contact deflection by using stress functions and obtains the same formula as developed here (valid for large h').

Johnson [H.5] quotes Boussinesq's use of potential functions to obtain the deflection of an elastic half space. He again calculates the strains and deflections from the known stress equations but obtains different results. Nikpar and Gohar [H.9] obtain another deflection formula from integrating L'Ure's stress equations, [L.6].

Note:

- The analytical solution developed in this work, eqn (2.19); Westegaard's stress function solution and the F.E. deflection results

all converge to the same value below the surface (h' > 3).

- Johnson's formula and that of Nikpar and Gohar are clearly incorrect.

2.2.5 Investigation of F.E. Surface Loading Discrepancy

If the F.E. model had converged to the correct solution the surface loading output should have exactly correspond to the applied elliptical pressure distribution. In an attempt to compensate for the inaccuracy the surface stresses were subtracted from the required surface loading. The F.E. model was then re-analysed with this error load applied to the surface (by itself) with the total load applied constrained to remain at 200N/mm. Figs. 2.12 and 2.13 show the result of superposing these "corrections" on the original results for the surface load distribution and contact deflection. The modified loading has given a slightly better deflection curve but has not fully explained the 2.5% discrepancy. Very fine mesh modelling of the edge of the loading surface would probably produce better results but is not justified for the increase in accuracy.

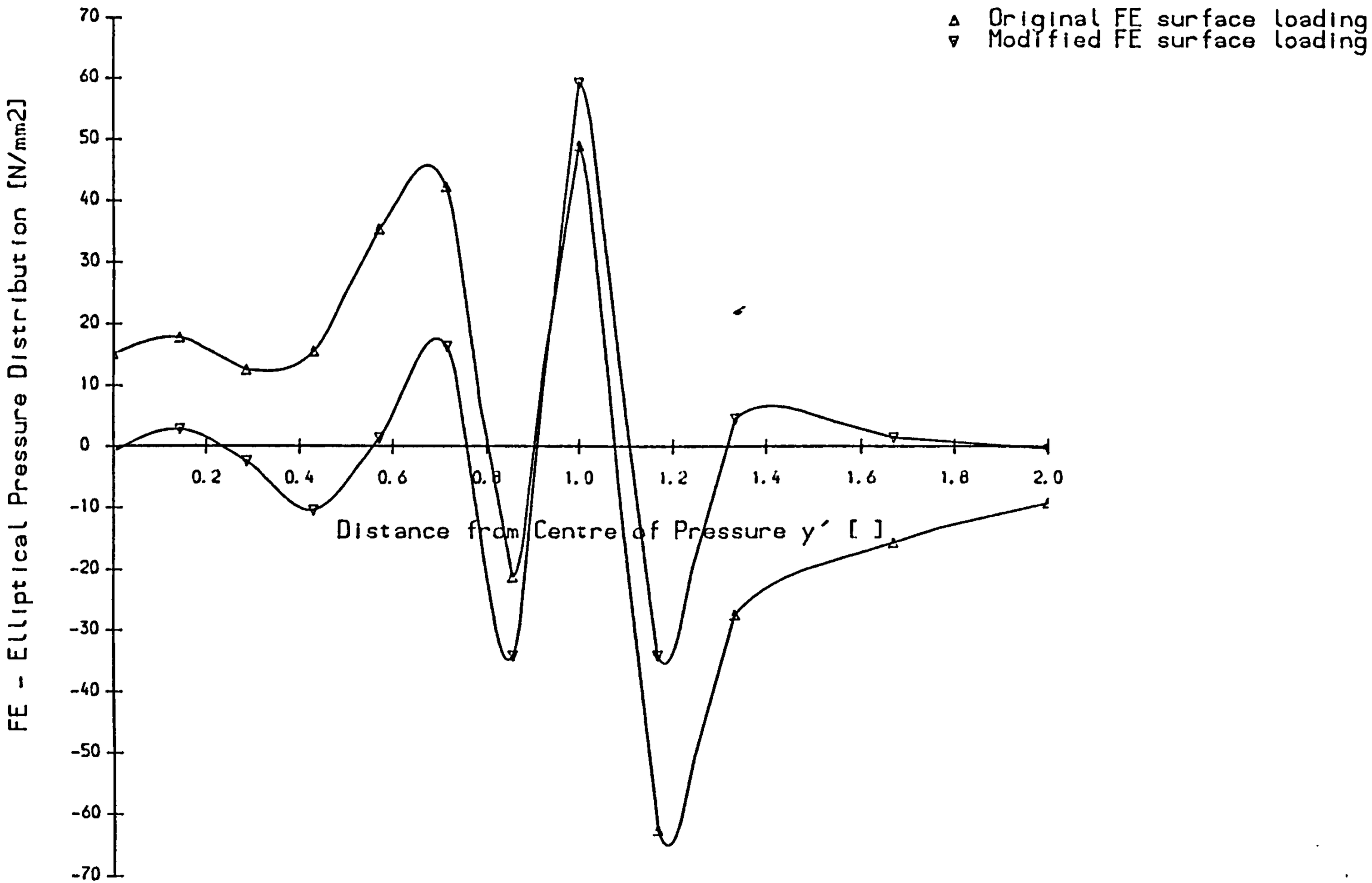

Fig 2.12 Error in FE Modelling of Applied Pressure, 7 Surface Element Model

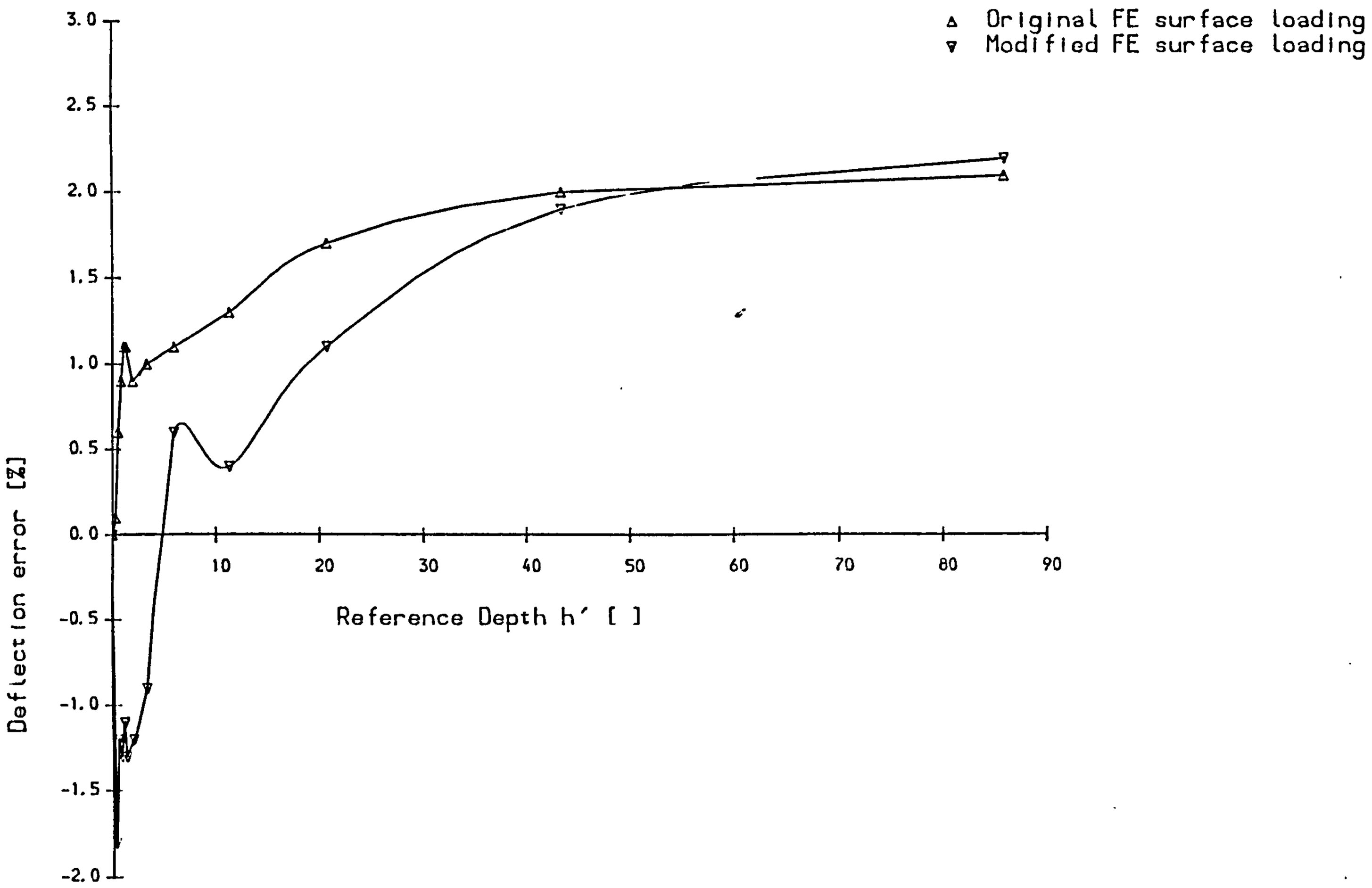

Fig 2.13 Comparison of Deflection Using Modified Nodal Loads

2.2.6 Modelling the Contact Compliance and Stresses of a Gear Tooth

In sections 2.2.2 and 2.2.3, analytical and F.E. solutions for Hertzian contact deflection were developed. Most previous authors assume that these results are valid for a gear tooth flank away from tip/root/end effects. In order to verify this assumption a 2D finite element study of the contact deflections in a typical gear tooth was carried out. The tooth geometry was that used by Winter [W13] for his strain gauge experiments.

Number of teeth	z	:	14
Pressure angle	α	:	20°
Module	mn	:	10.0mm
Addendum modifications	x	:	0.0
Cutter addendum	hao	:	1.2mn
Tool tip radius	rao	:	0.304mn
Tip diameter	da	:	160mm

Three loading diameters were considered corresponding (where possible) to Winter's loading diameters (Fig. 2.14). The root bending stress results could then be compared with Winter's strain gauge data. The three loading diameters (dy = 157.9, 153.6 and 131.94mm) modelled a 'root' loading; a typical OPSTC loading and a 'tip' loading.

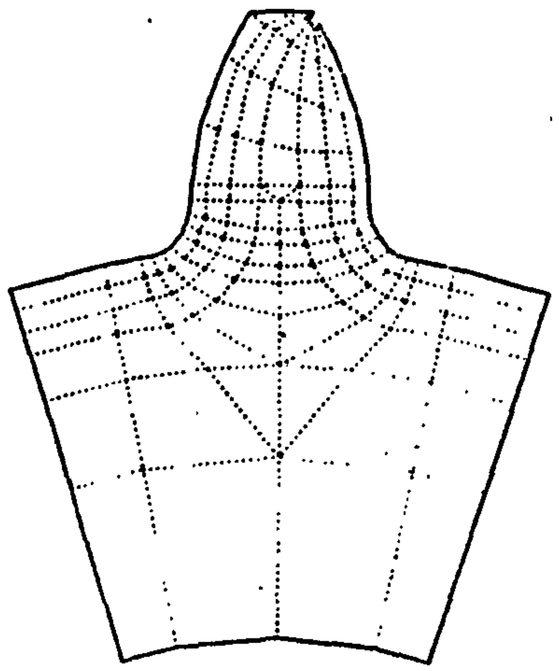

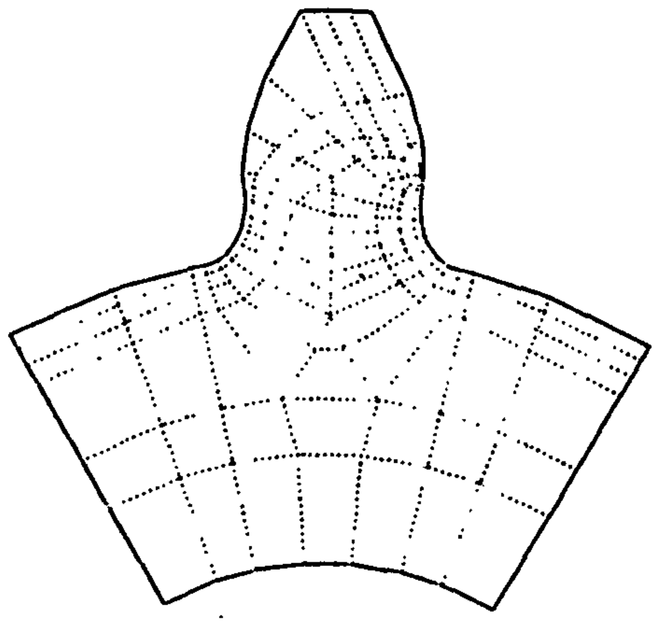

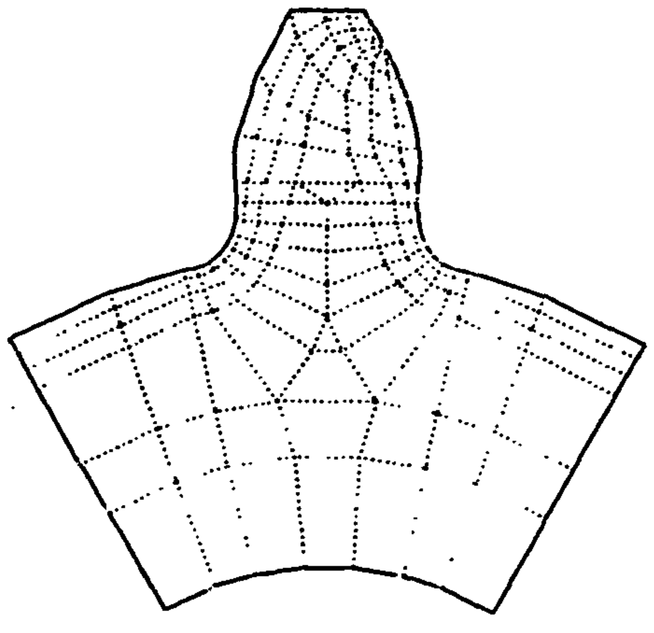

Fig 2.14 Finite Element Study of Gear Tooth Contact Compliance

From 2.2.5, to model adequately the contact region, the mesh of Fig. 2.7 was used. The parabolic approximation to the elliptical loading was applied to two surface elements with the calculated contact width for w = 1300 N/mm. Contact deflections were defined as the deflection of the contact point relative to point A along the LOA.

Loading Diameter dy (mm)	Datum Depth h (mm)	Tooth Flank Deflection (mu)		Error (2-1)/2 x 100% (%)
		F.E. Total Flank Deflection (mu) 1.	F.E. Tooth Bending Analytical Contact Deflection (mu) 2.	
157.90	5.057	80.121	78.051	-2.6
153.60	6.038	69.888	68.562	-1.9
131.94	17.538	35.026	34.349	-1.9

Fig. 2.15 Comparison of F.E. and F.E./Analytical Tooth Surface Deflections

Progressive refinement of the remainder of the mesh in the gear tooth and body (which was insufficiently modelled to give the overall compliance values) showed that modelling of the gear tooth itself was more than adequate.

The results of table 2.15 show that the errors introduced by superposing an analytical contact compliance on the mid-tooth deflections are minimal, except near the tip, so that modelling of the contact region by F.E. is not essential. This had an important bearing on the extension of the work into 3D, since the 3D equivalent of the mesh shown in Fig. 2.14 would have exceed the capacity of the existing computing facilities available to the author.

2.2.7 Contact Compliance Near the Tip/Root of the Tooth

The analytical contact deflection formula (equation 2.19) has been proved valid for a spur gear tooth except near the tip/root. No suitable analytical solution exists for the deflection of the tip of a spur gear loaded with a Hertzian pressure near the tip, as shown in Fig. 2.16. A 2D Finite Element Study has accordingly been carried out on a 20° rack profile to which a Hertzian" pressure distribution was applied at different points along the flank. This approximation represents the contact conditions at the tooth tip, although it does not, of course, ensure, the compatibility of deflections of the two contacting surfaces. The actual pressure distribution will (like the deflections) differ from that given by eqn 2.12.

The resultant contact deflections are plotted as a function of distance from the end of the rack (expressed in contact widths), (Fig. 2.17). The contact deflection is increased by up to 1.6 compared with that for the elastic half space. A second order polynomial was fitted to the curve for h' = 9.816 (corresponding to the centre-line depth of a rack with tip loading). This polynomial provides a semi-empirical multiplier for the half space solution given by eqn 2.16. *

* Footnote

Since this work was completed, an approximate analytical solution to the problem of "Hertzian" contacts near a 90° corner has become available compared to 110° assumed here. This shows that for loading at the corner, the compliance is increased by a factor of 2.3. On the basis that the compliance might be thought to be inversely proportional to the corner angle (cf analytical wedge solutions), a factor of 2 for a 90° and 1.6 for 110° would be expected . This is in good agreement with the work presented here.

This approximation does not account for differences between the rack and spur gear tooth profile, differences in the contact datum depth h' between a rack and a spur gear, changes in tooth profile due to manufacturing errors, running-in etc.

The root loading is applied to a near flat tooth flank so the half space deflection formula has been assumed satisfactory.

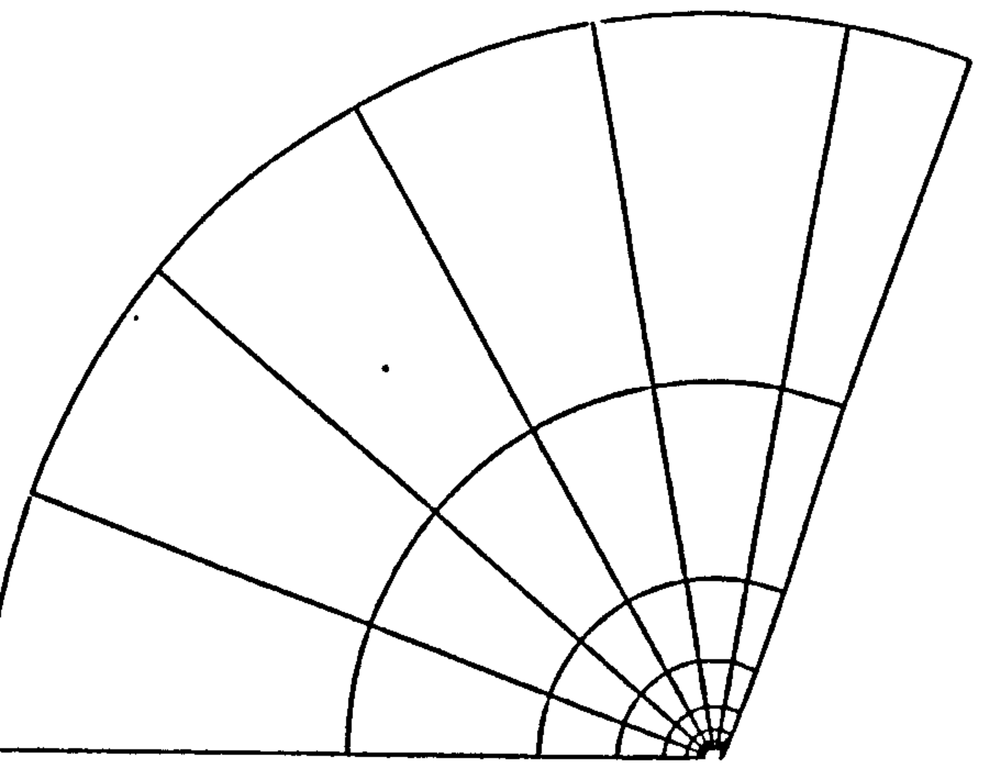

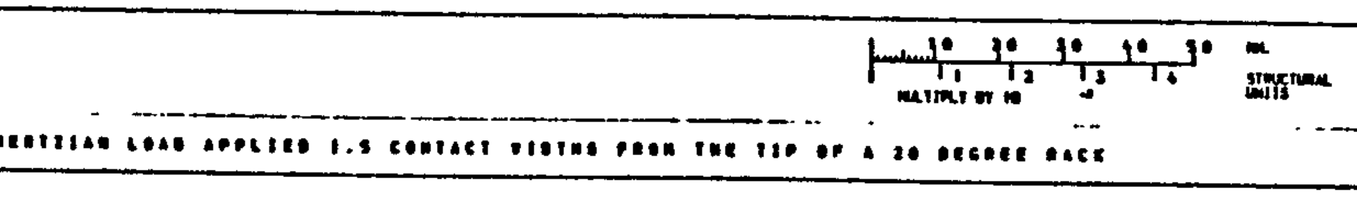

HERTZIAN LOAD APPLIED 1.5 CONTACT WIDTHS FROM THE TIP OF A 20 DEGREE RACK

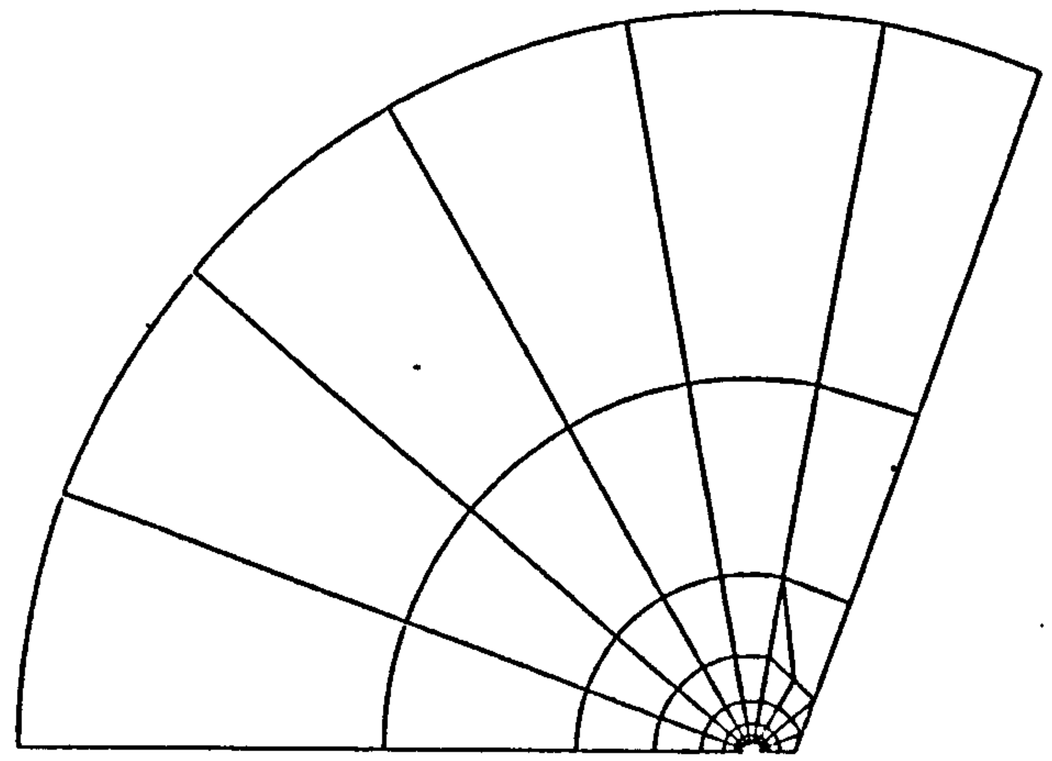

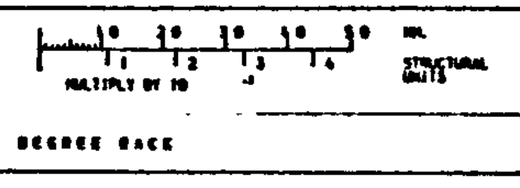

TITLE HERTZIAN LOAD APPLIED 10 CONTACT WIDTHS FROM THE TIP OF A 20 DEGREE RACK

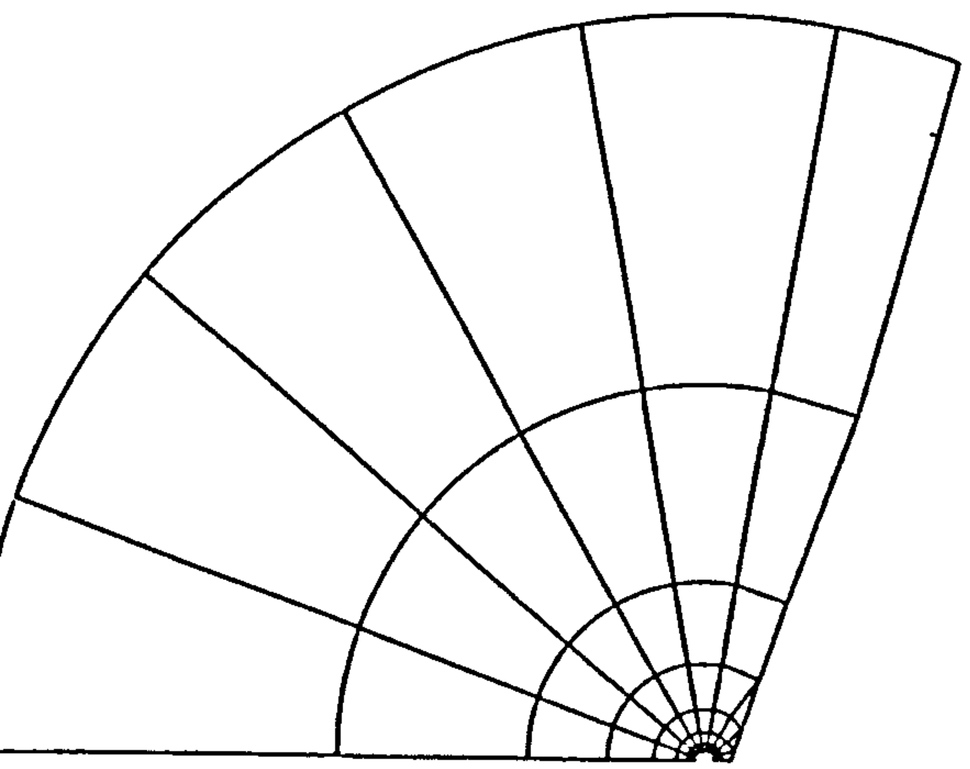

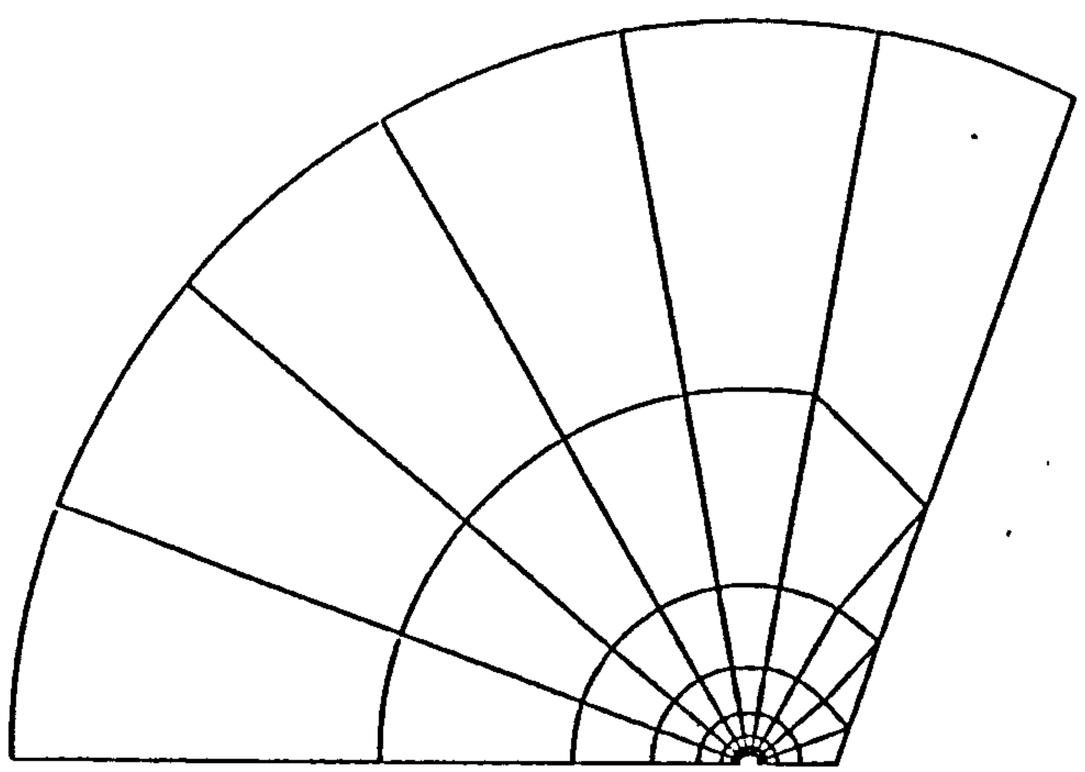

Fig 2.17a F.E. Analysis of Contact Deflections Near the Tip of a 20° Rack Tooth

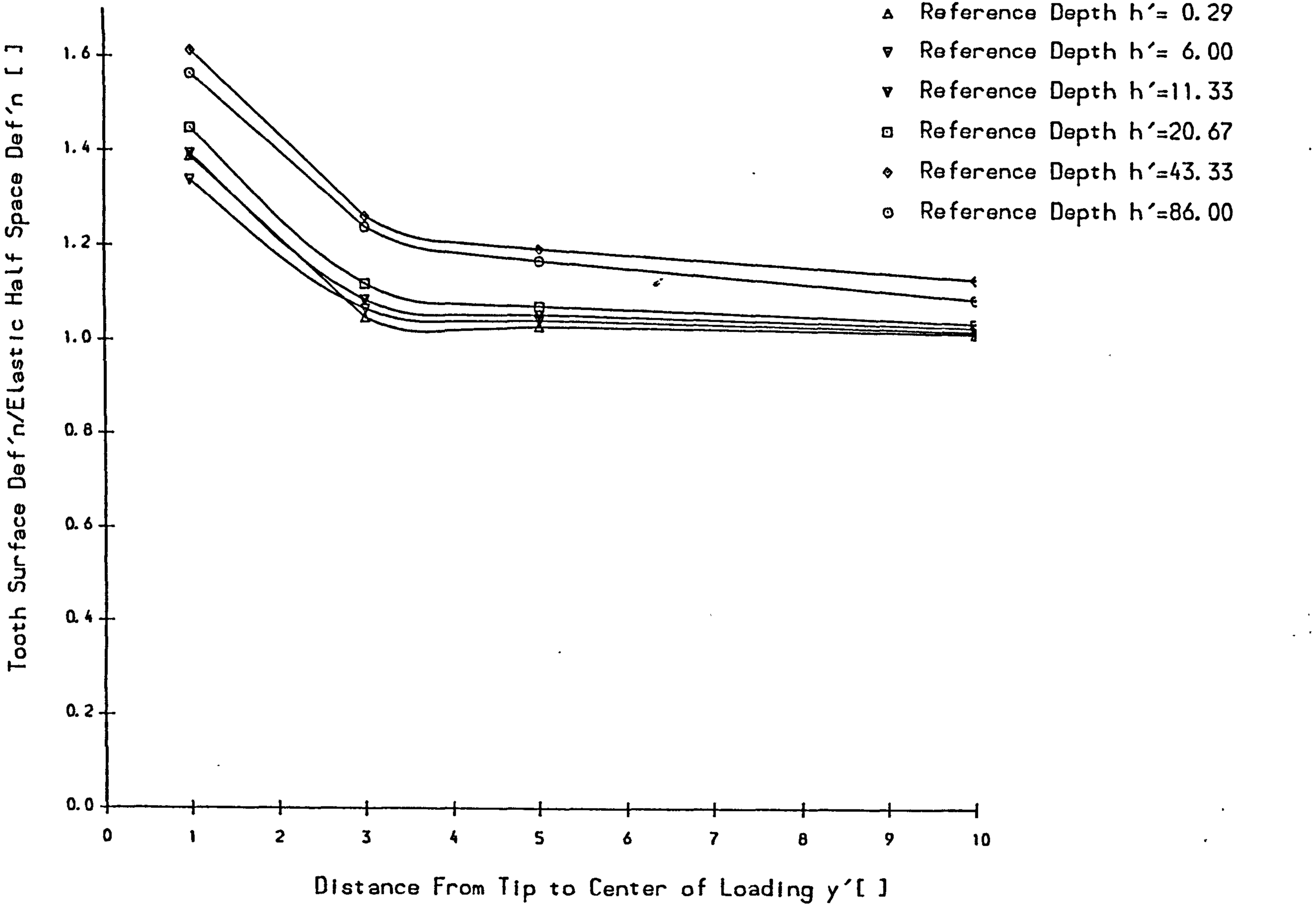

Fig 2.17b Contact Deflection Near the Tip of a 20° Degree Rack Tooth

2.3 Modelling of Tooth Centre-line and Gear Body Compliance

2.3.1 Introduction

Section 2.1 described the theory for modelling spur gear load distribution. The kernel of the tooth deflection integral equation is the tooth centre-line compliance under the action of a point load. This section deals with the modelling of this centre-line deflection using PAFEC Finite Element software.

Firstly, an adequate two dimensional finite element mesh was developed to model with sufficient accuracy the tooth centre-line deflection and also the root stresses. A study of gear body deflections was then carried out by comparing tooth deflections for finite element meshes with various 'depths' of tooth root modelled, to determine how far below the tooth the model needed to extend.

A three dimensional model was then developed based on these results including a length of shaft at each end to ensure that the stress field within the gear blank was correctly represented. The bending deflections of both the loaded tooth and the adjacent teeth were then obtained using the model, with "point" loads applied at various points over the loaded flank.

Finally, the deflection curves for 18, 25, 40 and 100 tooth models were fitted with exponential equations. The coefficients of the fitted equations can be interpolated for intermediate tooth numbers to give tooth stiffness data for any spur gear from 10 to 100 teeth with standard rack form (1.0mn addendum, 1.25mn dedendum, 0.25mn tool tip radius and zero addendum modification).

2.3.2 Two Dimensional Finite Element Modelling of Gear Teeth

To model the deflections and stresses in a gear tooth the finite element model must have a sufficient number of elements to ensure that approximations of the deflection across any element by a second order polynomial is sufficiently accurate. A gear tooth is a cantilever, and the peak stress gradients occur at the tooth root surface. It follows that if a selected mesh is able to model the root stresses correctly it is reasonable to assume it will model the remainder of

the tooth correctly except near the points of load application.

Fig. 2.18 shows two finite element meshes for a 14 tooth spur gear. Equations for calculation of spur gear surface coordinates are contained in Appendix 2.3.2. Coordinates of midside nodes are also calculated to give a smooth root profile with no stress discontinuities. In the tooth root the coordinates of the mesh are selected to satisfy the PAFEC requirement that they bisect the element edge and (like the corner nodes) lie on the calculated trochoid (tooth fillet) curve. The results of section 2.2.3 show that regions of low stress gradient can be modelled adequately by very few elements without degrading the overall result.

Winter [W13] has published experimental results for this tooth profile obtained by strain gauges and quotes 268N/mm2 for the peak tooth root tensile stress. Tooth centre-line deflections (relative to point A) agree within 0.8%.

z = 14
mn = 10.00mm
x = 0.000mm
hao = 1.200mn
rao = 0.304mn

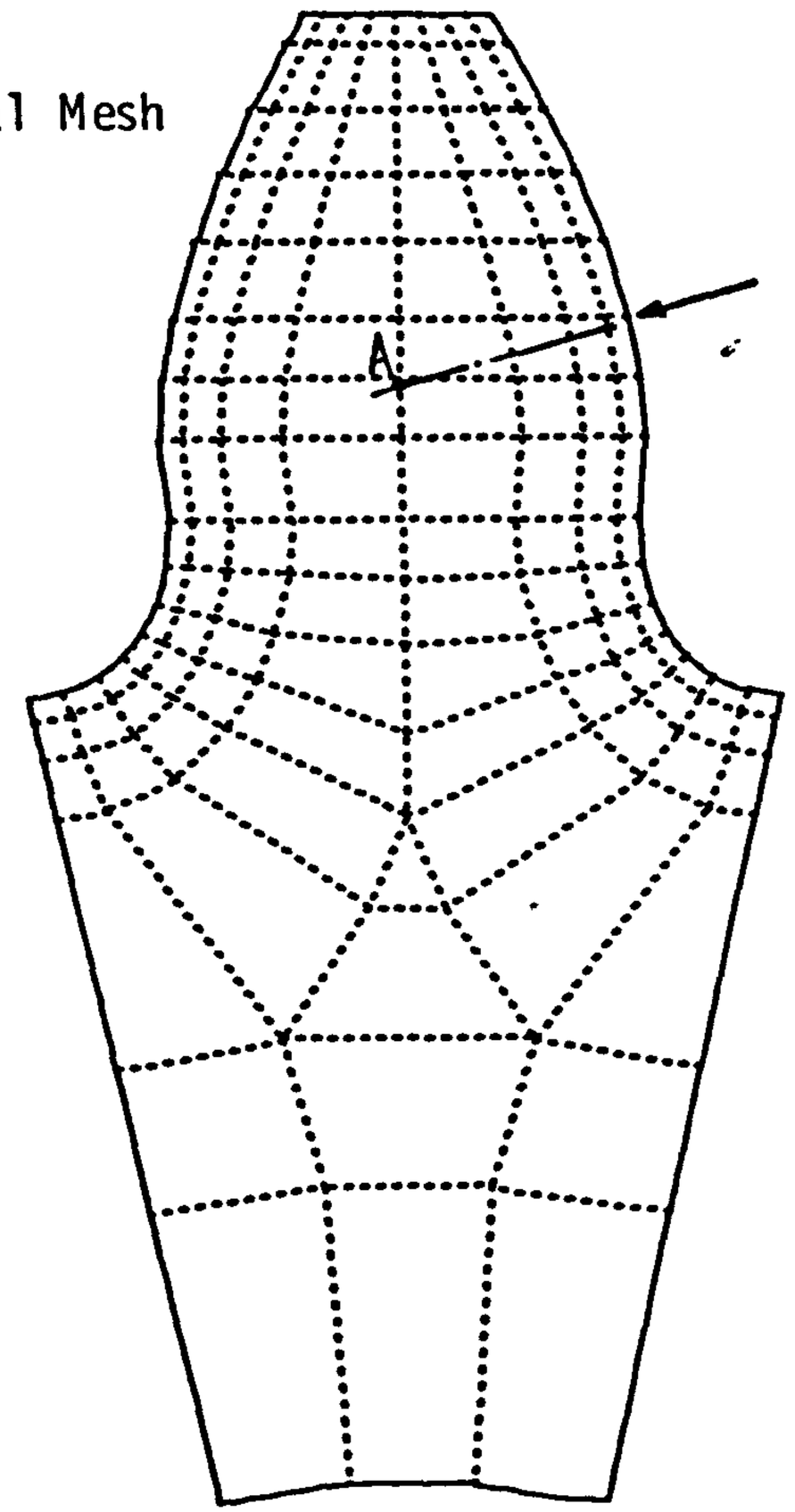

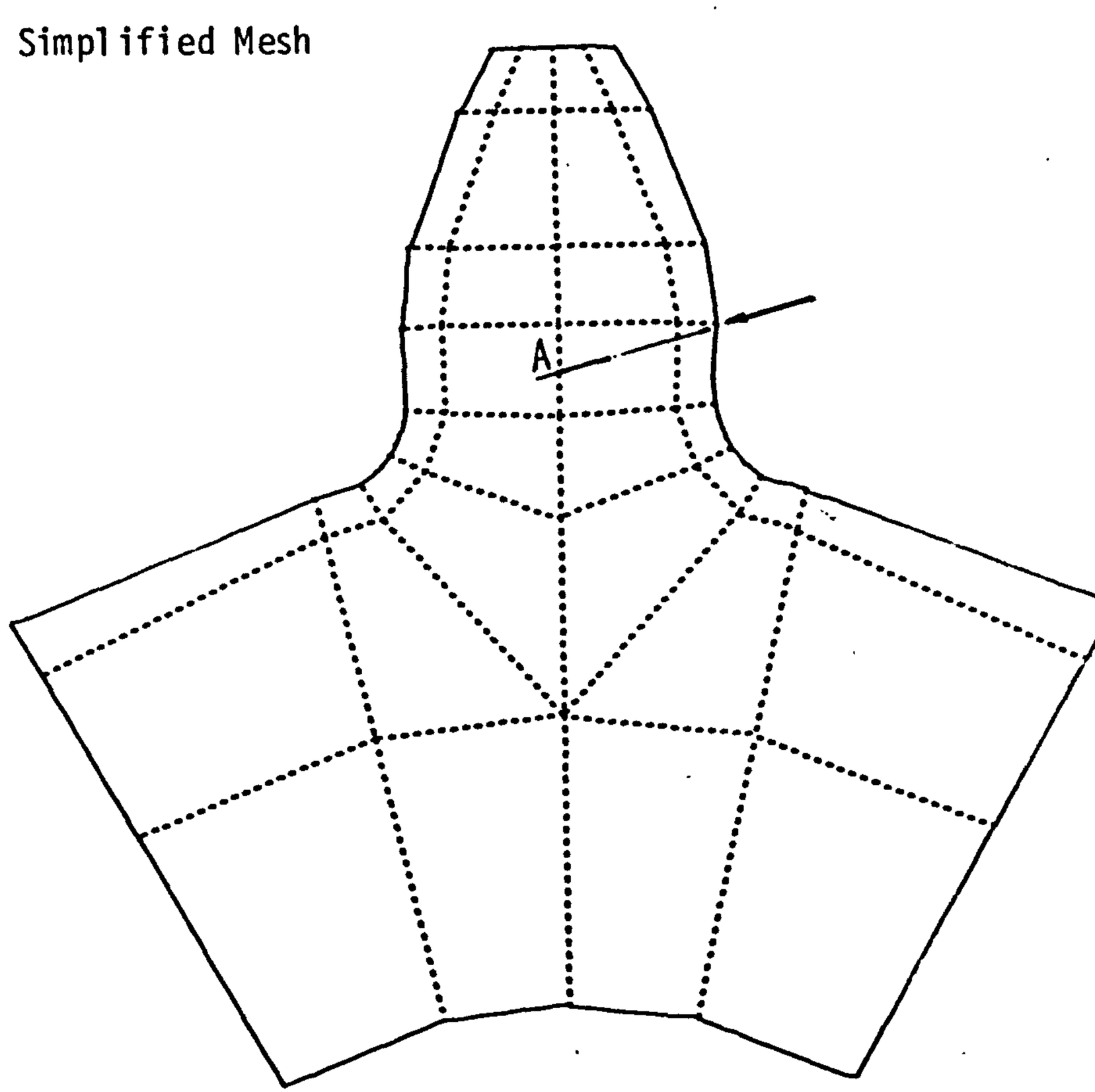

Fig 2.18 Finite Element Modelling of 14 Tooth Gear Used in Winter's Experiments

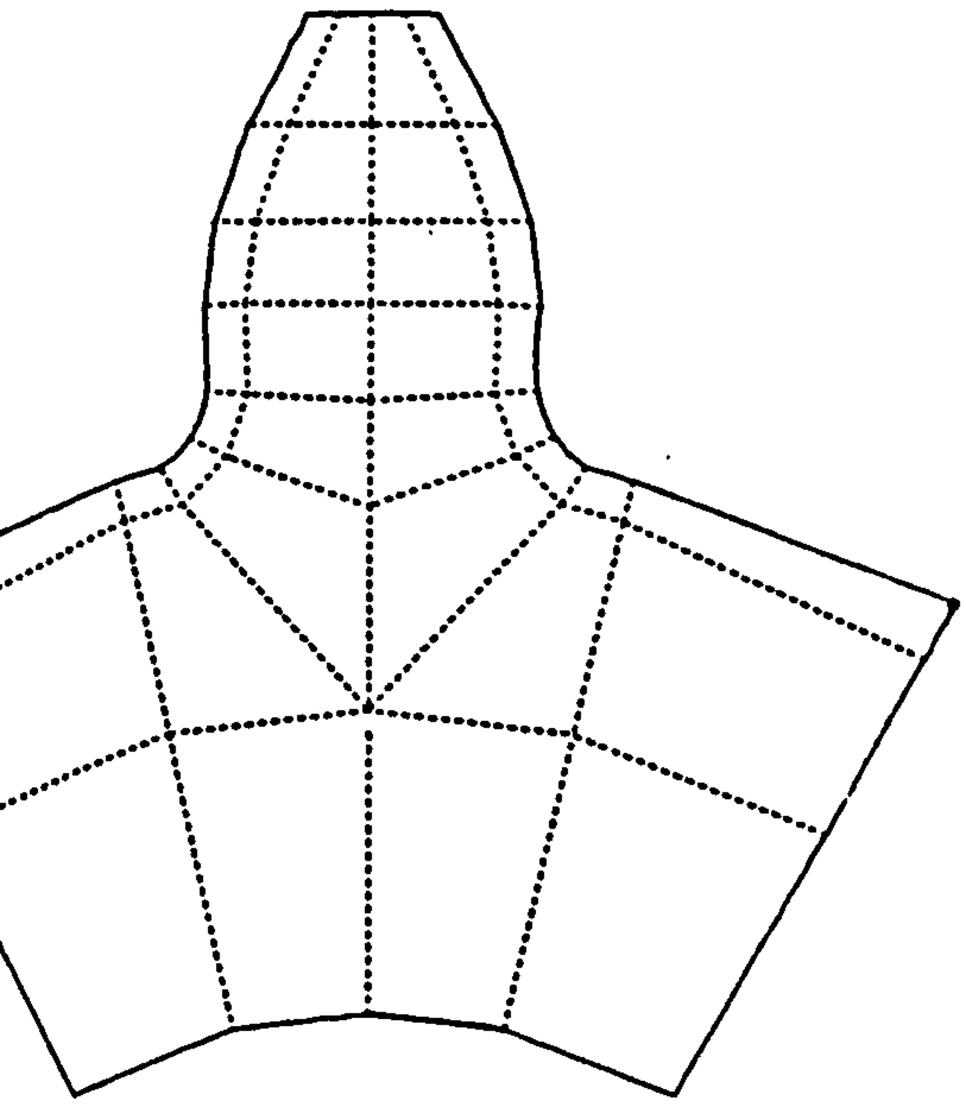

Model 1

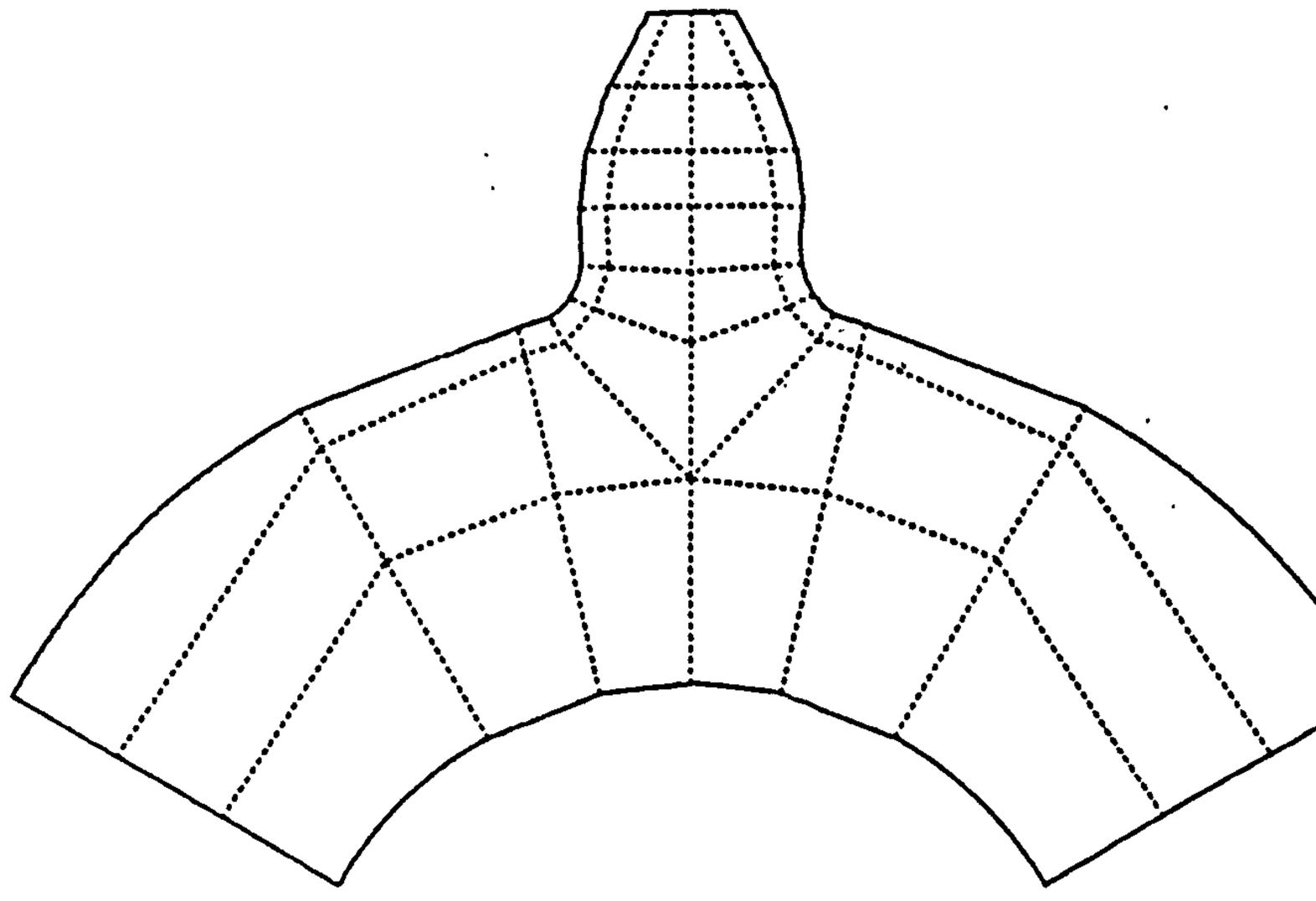

Model 2

z = 14
mn = 10.00mm
x = 0.000mm
hao = 1.200mm
rao = 0.304mn

F.E. Model	$\frac{\delta_{tb}}{w}$ [mu/N/mm]
1	0.0248
2	0.0286
3	0.0313

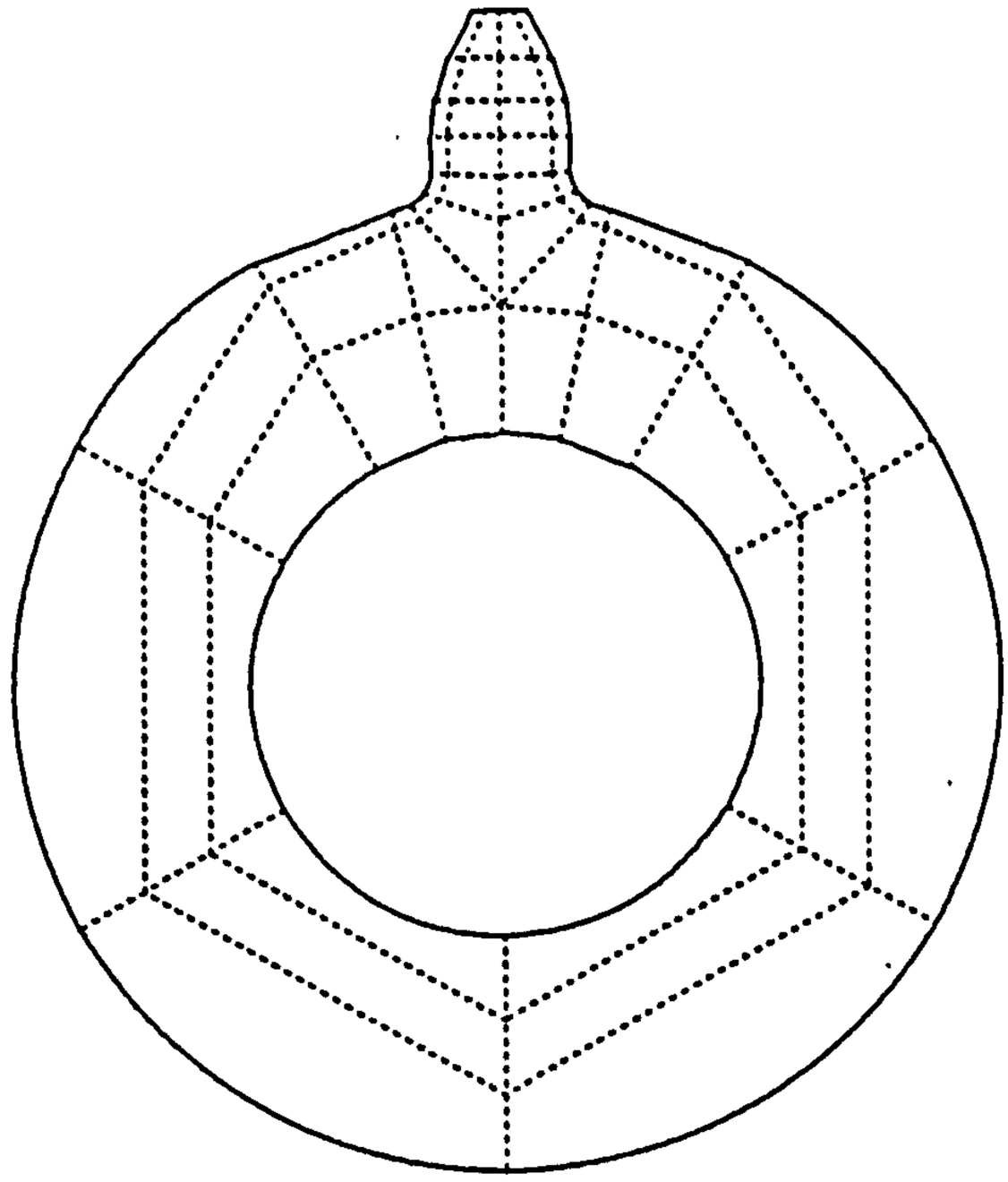

Model 3

Fig 2.19 Two Dimensional Spur Gear F. E. Meshes

2.3.3 A Two Dimensional Study of Gear Body Compliance

The tooth centre-line compliance is made up of two components:- the bending/shear compliance of the tooth acting as a simple cantilever and the compliance of the gear body supporting the tooth. (Note that this is NOT the torsional/shear/bending compliance associated with the shaft). It is not possible to consider individually these two components as the stress fields created by each are not separable.

To demonstrate the significance of the gear body compliance a complete two dimensional slice of a gear was analysed using PAFEC finite element software (see Fig. 2.19). A simple point load was applied at the reference diameter. Finite element models of a sixth, a third and a complete gear body were analysed to investigate the change in the tooth centre-line deflections, resulting from only modelling part of the gear.

The tooth centre-line deflection was found to increase by up to 26% when the whole of the gear body was modelled. Although the exact stress field in the entire gear could not be simulated perfectly, these results are conclusive enough to show that the entire gear must be modelled to give correct values of tooth centre-line compliance.

2.3.4 Three Dimensional Finite Element Modelling of Tooth Centre-line Compliance

The kernel of the integral equation is the tooth centre-line compliance function, Ktb. This has been defined in Section 2.1 as the tooth centre-line deflection at z due to a point load at zF minus the calculated shaft bending, torsion and shear deflections on the gear centre-line.

Fig. 2.20 shows one of the finite element models of an 18 tooth pinion. The gear facewidth is wide enough to ensure that a central point load produces negligible tooth centre-line deflection, except on gears with greater than 40 teeth where there is a significant 'disc' rotation of the gear body. The gear is effectively simply supported by restraining end nodes at one end vertically and horizontally (where the torque is reacted), and radially at the simply

supported end. Approximately half a shaft diameter has been modelled either side of the gear to ensure that local stress concentrations at the support points and the shaft/gear body section change can be adequately modelled by the relatively coarse mesh in these regions.

The tooth centre-line compliance as defined above is assumed not to change appreciably if the shaft mounted configuration is altered (to say, an overhung configuration). The main changes will be those due the different "shaft" deflections, not the local "gear body" deflections associated with transfer of the tooth load to the shaft. A representative shaft diameter, ds must however be used in the F.E. model. Fig. 2.21 shows how the chosen shaft diameter, ds, and gear reference diameter, d, varied with the number of teeth, z. For a 4:1 reduction and a pinion with 20 teeth, the shaft diameter would typically be 16 modules. Torsional strength is proportional to diameter cubed, requiring a wheel shaft diameter of about 25 modules. The shaft diameters shown in Fig. 2.21 are thus close to those that would be used in practice for each tooth number.

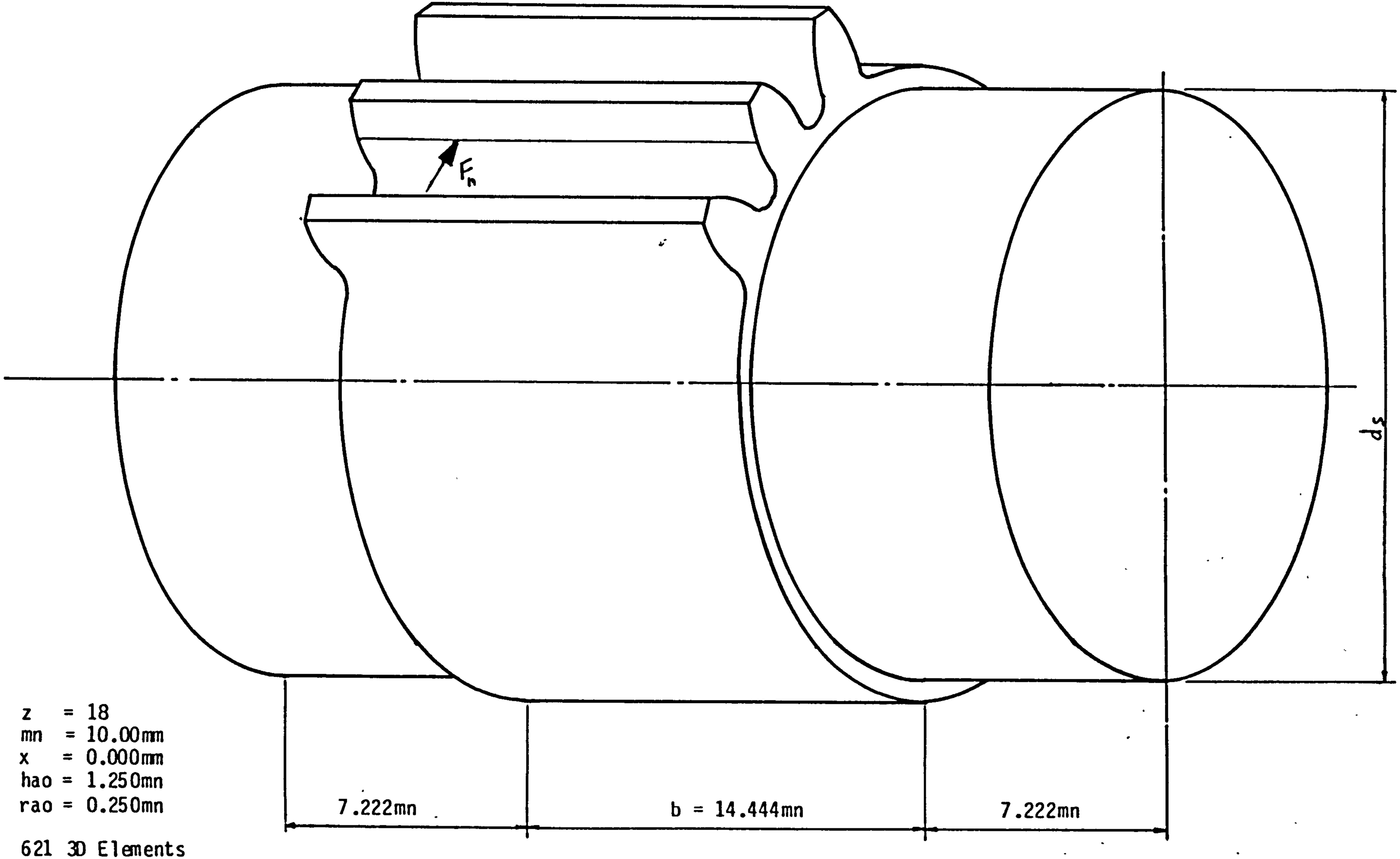

Fig 2.20 Finite Element Modelling of Tooth Centre-line Deflections and Stresses

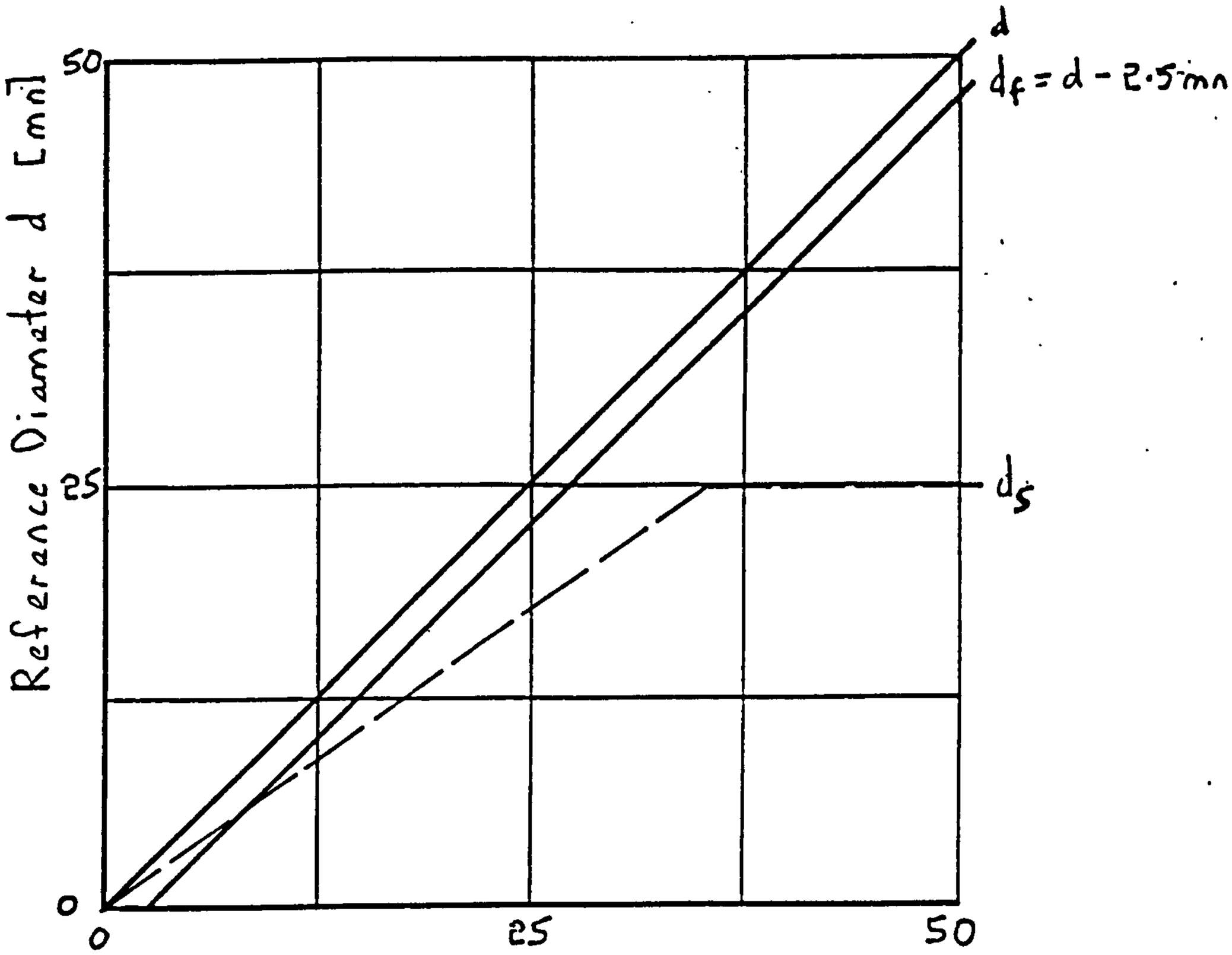

Fig. 2.21 Shaft Diameter for Finite Element Gear Models

Calculation of the shaft bending, torsion and shear deflections is usually based on elementary engineering beam theory using the root diameter, df, as the effective diameter of the gear section. Changes in section diameter are assumed to take immediate effect, which overestimates the shaft stiffness. These same assumptions have accordingly been made when analysing the F.E. results, so that no error is introduced when the same calculated shaft deflections are "added" back in the elastic model deflection vector.

Although the numerical integration is based on the tooth bending compliance due to a point load, the final load distribution is not a series of point loads applied along the contact line(s). It is not possible to apply an "exact" point load to a practical finite element mesh. Depending on whether the load is applied to a corner or midside node the effective applied load distribution is different, (see Fig. 2.22). To approximate a smooth load distribution when the 'point' loads are summed across the flank point loads have been applied to midside nodes in the transverse plane.

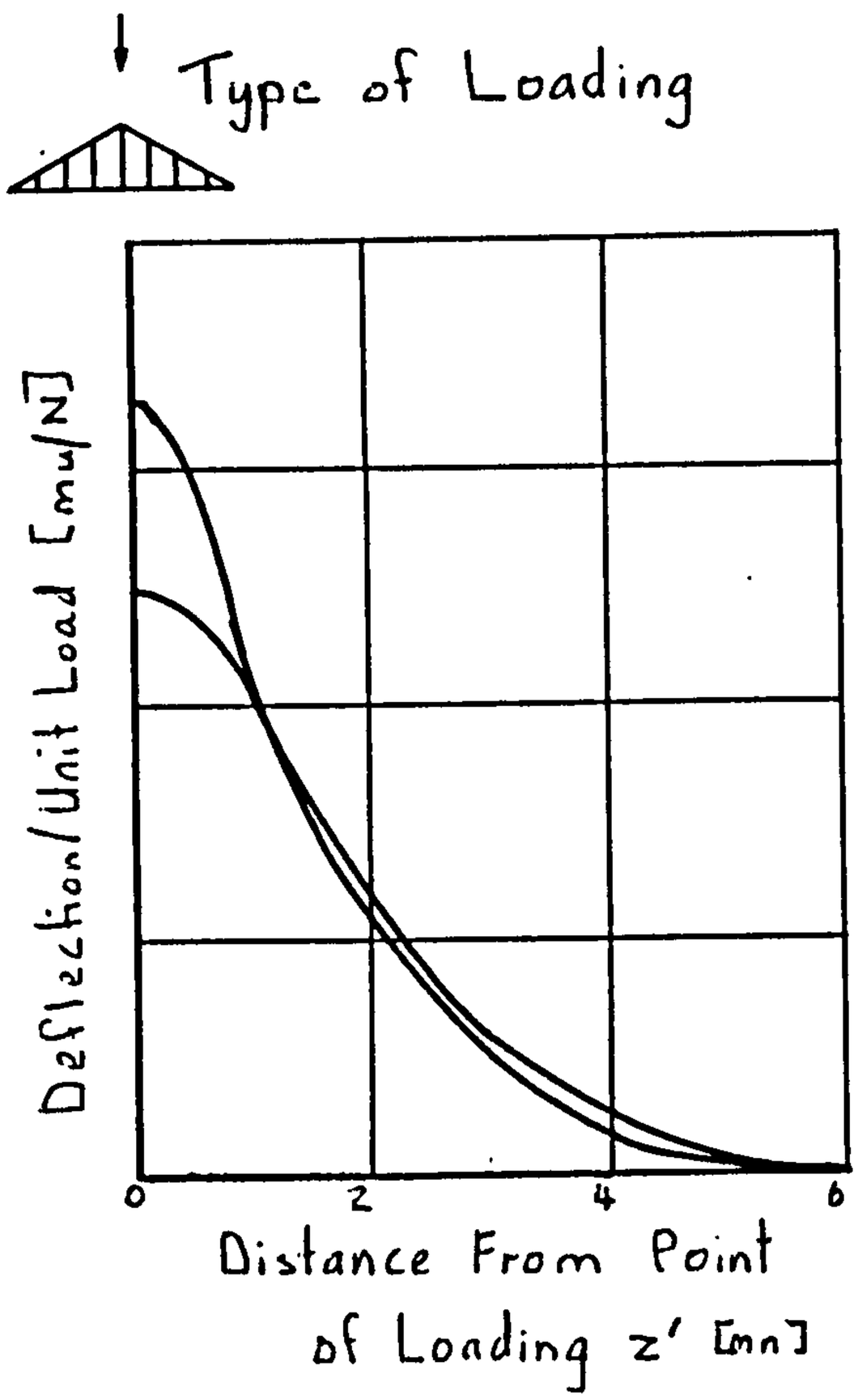

Fig. 2.22 Effect of applying a 'point' load to a midside and corner node of an F.E. mesh

Finite element data has been generated for 18, 25, 40 and 100 teeth for gearswithout addendum modification, generated by cutters of standard geometry (hao = 1.25mm, rao = 0.25mn). These were loaded at 0.25, 0.75, 1.25, 2.5 and 6.0mn from the end of the gear. In each case loads were applied between the tip and root diameter (where still involute) at 1.0mn intervals. Appendix 2.3.4 gives the net tooth bending deflection data generated by these F.E. models, for each load case.

Fig. 2.23 shows the non-dimensionalised tooth bending deflection under the point of load application, $K_{tb}[i,i]$, for the central (mid-face) loading case, together with the equivalent values given by Vedmar[V3].

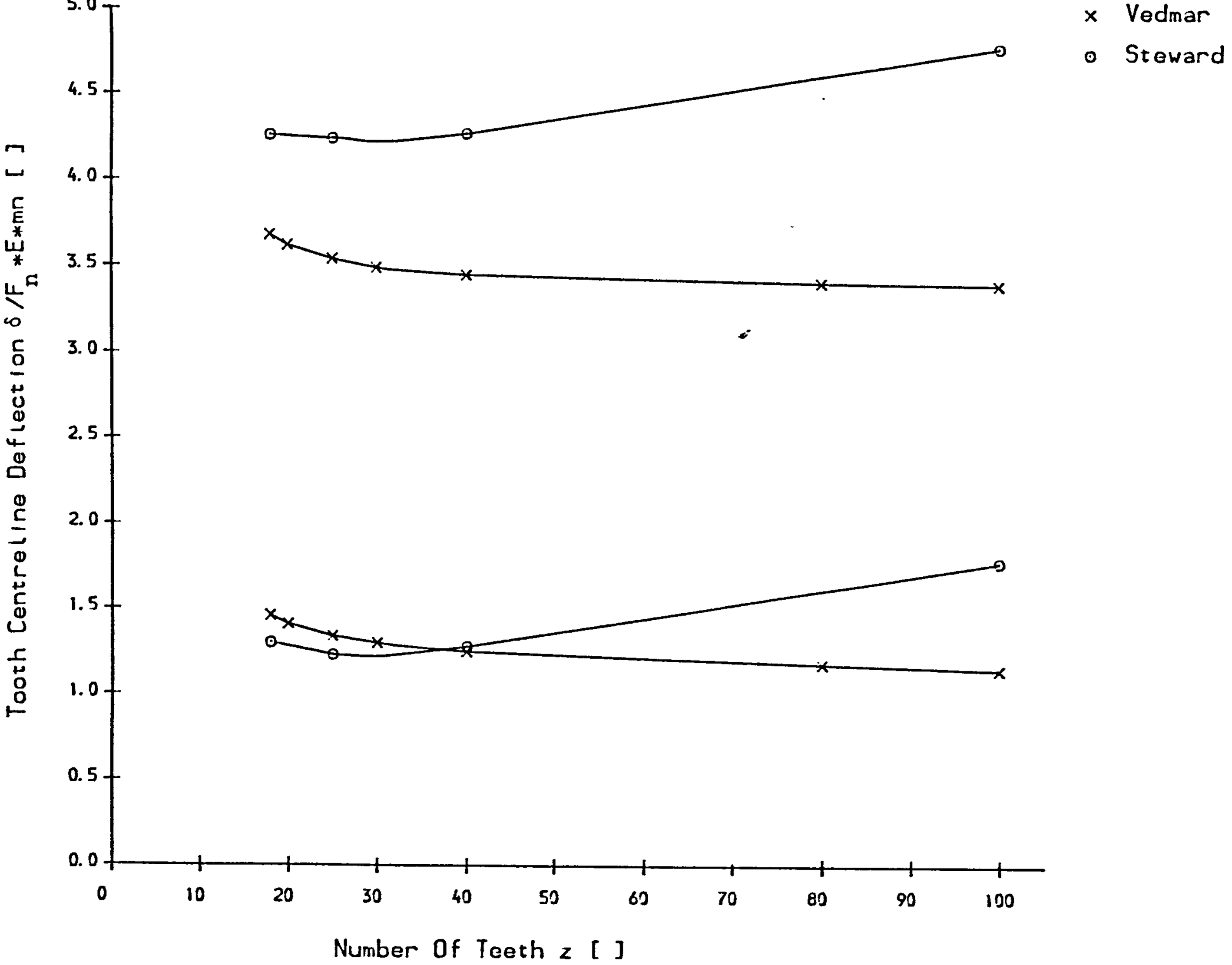

Fig. 2.23 Tooth Centreline Deflection Under Load, Central Loading At Tip & Ref. Diameter

As predicted by the two dimensional F.E. analyses reported in Section 2.3.3, the gear body contributes significantly to the tooth centre-line compliance for large tooth numbers. Vedmar's results are too stiff for large tooth numbers. For smaller tooth numbers the 'disc' rotation effect is reduced, bringing his results closer to those obtained by the author. However, the tooth root region of the gear is still more compliant when the whole gear body is modelled, implying that even for small tooth numbers the tooth compliance should still be greater than that given by Vedmar. This is clearly not true for reference diameter loading.

Vedmar's bending deflection datum is only 0.5mn below the tooth surface, not at the tooth centre-line as in the author's analysis (about 0.84mn deep for reference diameter loading). Timoshenko [T7] gives the surface deflection due to a point load as:

$$\delta = (1 - \nu - 2\nu^2) \frac{F}{2\pi E h} \qquad (2.20)$$

This gives a non-dimensional relative compression between the two deflection datums of 0.40, which should be subtracted from Vedmar's results to give corresponding centre-line values. This explains why Vedmar's reference diameter bending deflections appear to be greater at small tooth numbers.

2.3.5 Modelling of Adjacent Tooth Compliance

Because of the 'disc' rotation of the gear periphery, especially on large gear wheels, the deflection of the two adjacent teeth has been investigated. Fig. 2.24 gives the net deflection of the following adjacent tooth for the 18 tooth gear at various loading diameters.

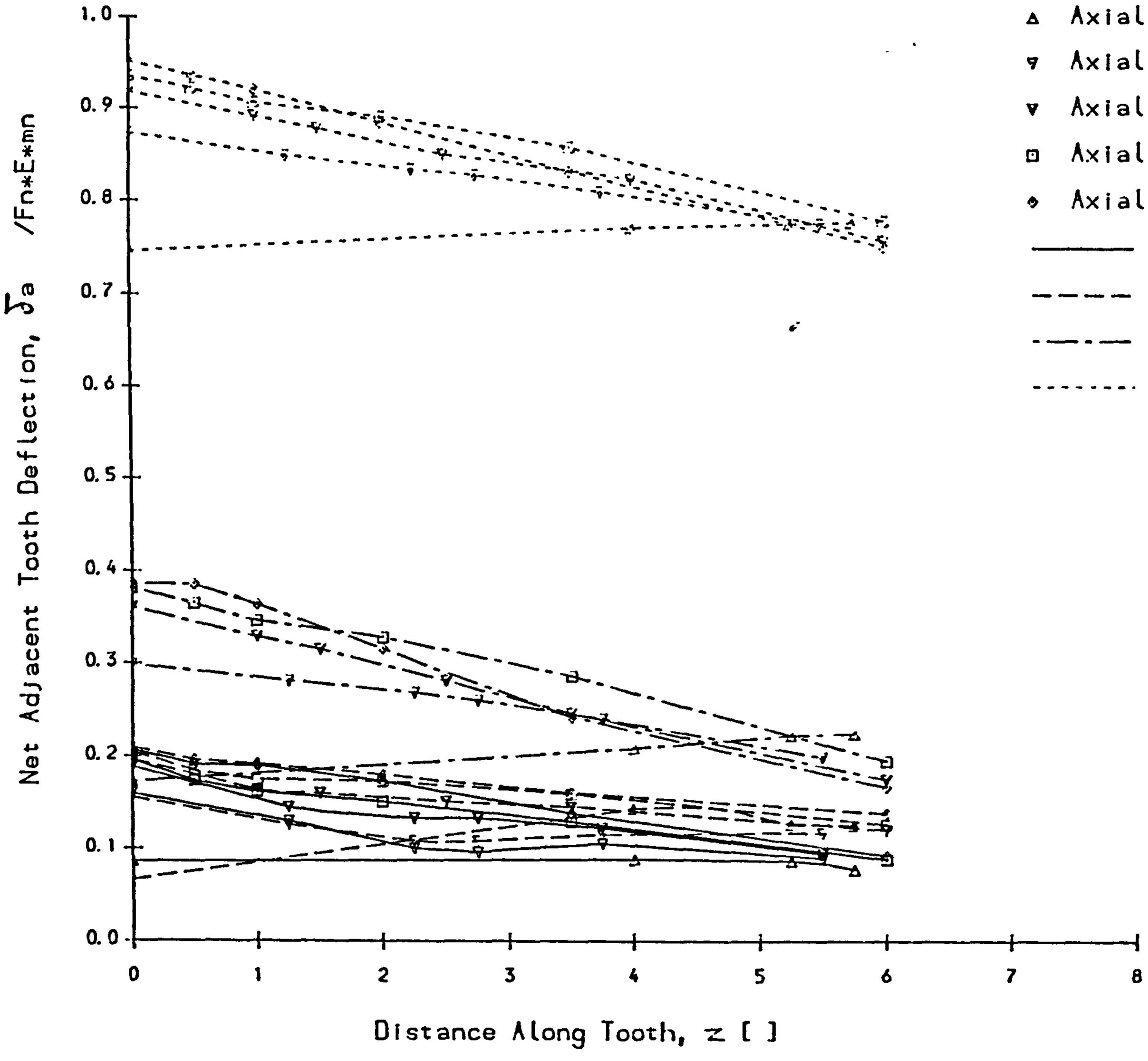

Fig 2.24 Net Adjacent Tooth Surface Deflections, dy=d

As shown the adjacent tooth deflections are found to be largely independent of the loading diameter, dy. By Maxwell's reciprocal theorem, the deflection at point 2 due to a load applied at point 1 equals the deflection at point 1 due to the same load applied at point 2, viz.

$$\delta_{21} = \delta_{12} \tag{2.21}$$

If the adjacent tooth deflection is independent of loading diameter it follows that the deflection on both adjacent (ie preceeding and succeeding) teeth must be equal. Fig. 2.24 shows variation of the non-dimensional adjacent tooth deflection across the facewidth for various tooth numbers. Because these deflections are largely due to rotation of the tooth root they do not vary much with change in axial load position, zF. Gear wheels show the most pronounced deflection.

For a 100 tooth wheel the deflection of the adjacent teeth is 43% of the peak deflection of the loaded tooth. Because the curves are much flatter, (more convective,) the total adjacent tooth deflection due to a complete distributed load is a far greater proportion of the loaded tooth deflection.

2.4 Curve Fitting of Tooth Centre-line/Gear Body Compliance Data

2.4.1 Introduction

The displacements due to tooth bending/gear body deformation have been calculated by F.E. analysis. Since these numerical values of the displacements are evaluated at a finite number of pairs of (z,zF), we must devise a means of interpolating the displacements. An approximate analytical equation for the deflection must be built up for arbitrary values of (z,zF). This is because it impractical to solve for the deflections at arbitrary points using a mico-computer using the 3D finite element analyses reported in previous chapters. It is desirable to have the final load distribution program on a micro for portability and ease of use.

2.4.2 Curve Fitting of Loaded Tooth Deflections

For spur gears of standard rack form without addendum modification the tooth deflection, δ_{tb}, is a function of the following:

- number of teeth, z
- distance of meshing point from reference diameter, ψy
- distance along tooth of load, zF
- distance along tooth of desired deflection, z

The empirical compliance function must satisfy the reciprocal theorem and with this in mind is developed as a symmetric function of z and zF.

$$\delta_{tb}(\psi Z, zF) = \sqrt{G(z) \cdot G(zF)} \cdot F(z') + c \qquad (2.22)$$

where $z' = |z - zF|$

The "master" function F(z') gives the deflection of an infinitely wide gear loaded in the centre of the facewidth, (see Fig. 2.25). The function G(z) accounts for the increase in deflection as the load and/or deflection point near the ends of the tooth, (see Fig. 2.26). The constant, c, takes account of the "disc" rotation in large gear wheels, it is sensibly zero for tooth numbers less than 40.

To obtain the best possible fit for the tooth deflection, several forms of equation were first considered for the 'master' curve F(z') for the reference diameter loading of the 18 tooth Finite Element model. The coefficients to the equations considered were optimised by minimising the rms error relative to the F.E. results. The method of steepest descent (Appendix 2.4.2) was used to minimise the errors together with a simple grid searching procedure to identify the search region and avoid convergence to local minima.

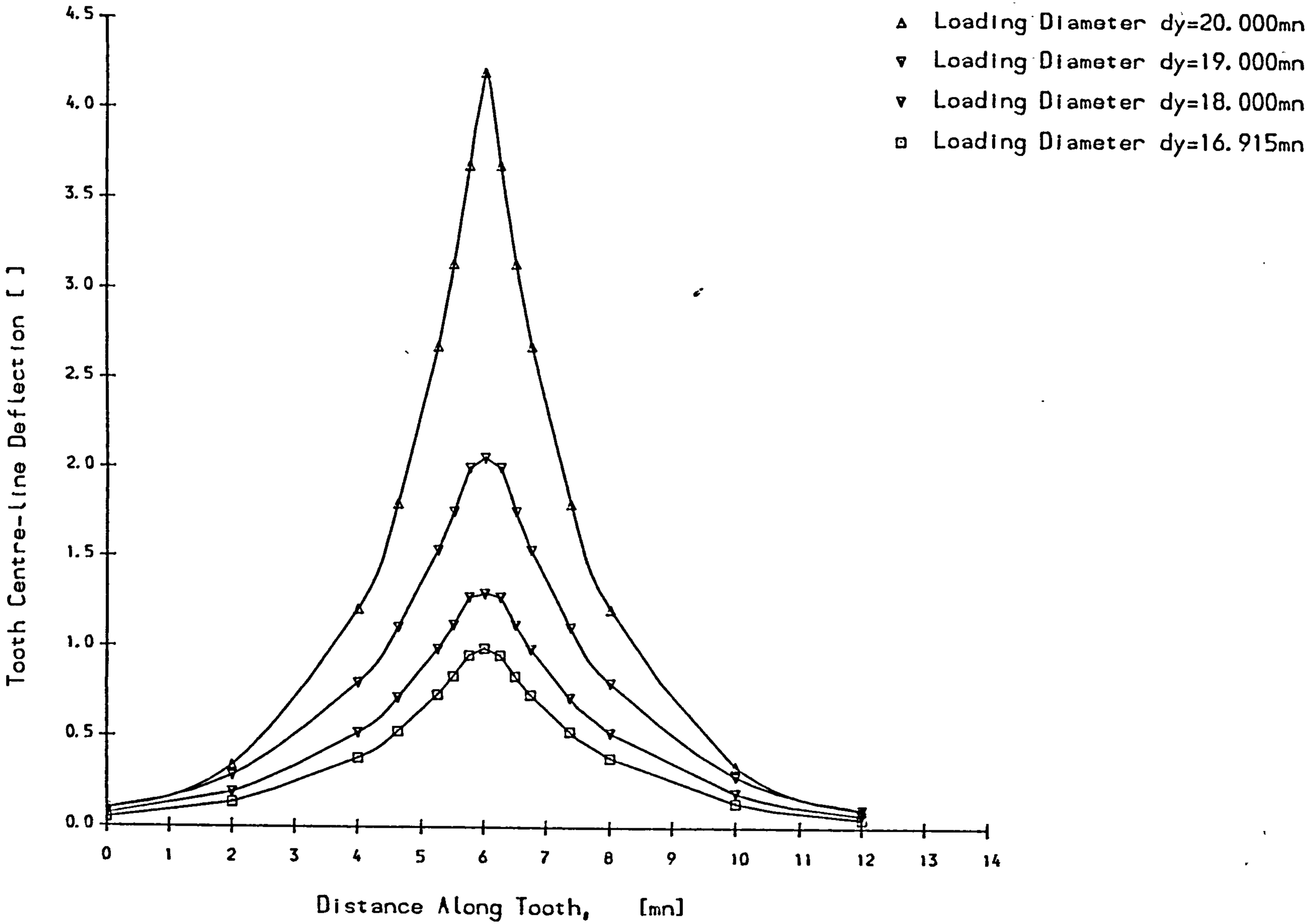

Fig 2.25 Function F(z') Master Tooth Deflection Curves

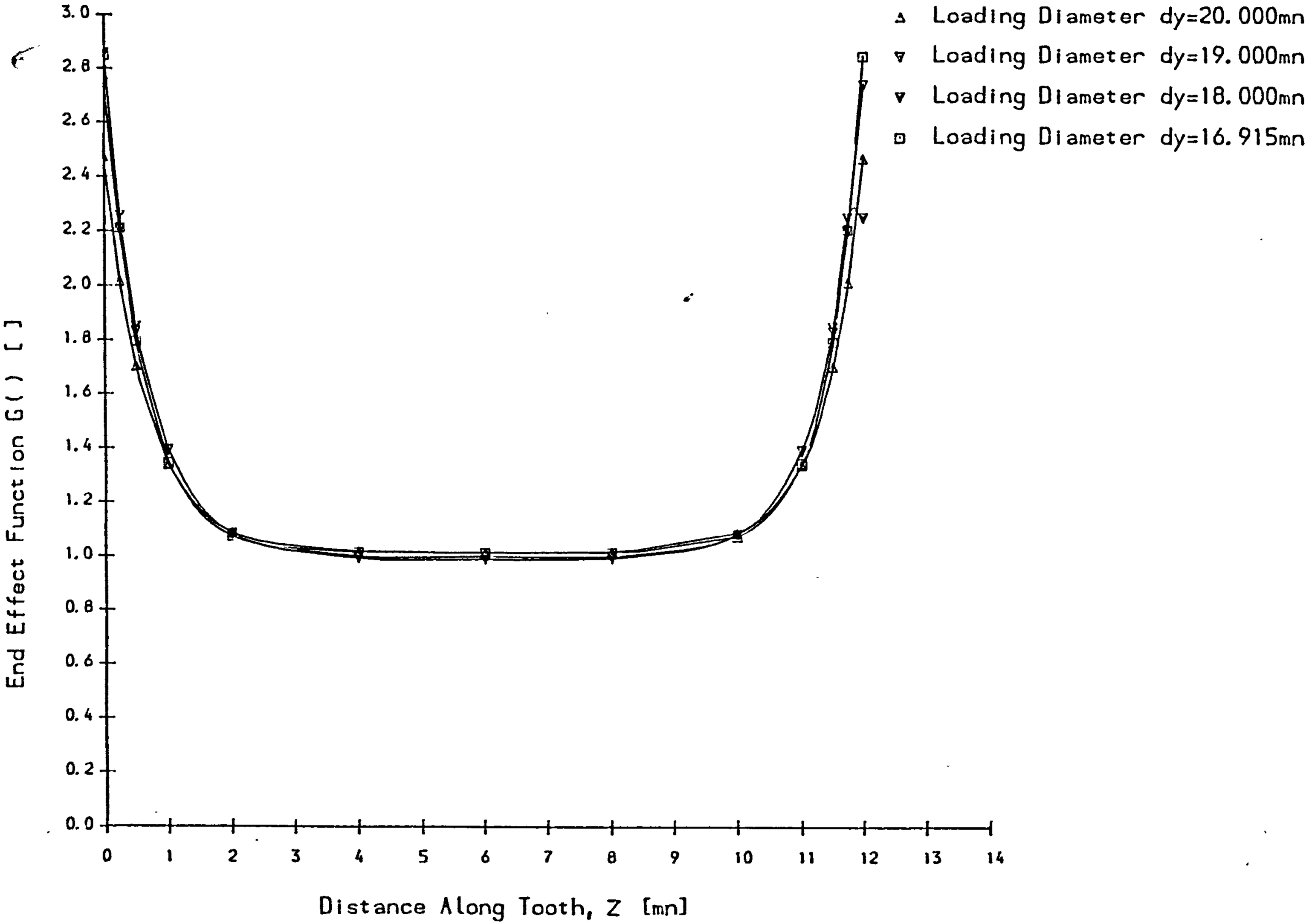
Loading Diameter dy=20.000mn
Loading Diameter dy=19.000mn
Loading Diameter dy=18.000mn
Loading Diameter dy=16.915mn
End Effect Function G( ) [ ]
3.0
2.8
2.6
2.4
2.2
2.0
1.8
1.6
1.4
1.2
1.0
0.8
0.6
0.4
0.2
0.0
0
1
2
3
4
5
6
7
8
9
10
11
12
13
14
Distance Along Tooth, Z [mn]

Fig. 2.26

Note: master curve deflections have been non-dimensionalised by multiplying by E*mn. The following forms for F(z') were considered:

$$F(z') = \frac{C[1]}{\cosh C[2] z'} = \frac{2\,C[1]}{e^{C[2]z'} + e^{-C[2]z'}} \qquad \text{type 1} \quad (2.23)$$

$$F(z') = C[1]\, e^{-C[2](z')^{C[3]}} \qquad \text{type. 2} \quad (2.24)$$

$$F(z') = C[1]\left\{ e^{C[2]z'} + \frac{C[2]}{C[3]} e^{-C[3]z'} \right\} \qquad \text{type 3} \quad (2.25)$$

Note: this is constrained to have zero slope at the line of symmetry, i.e. $z' = 0$.

$$F(z') = C[1]\left\{ e^{-C[2]z'} - C[3]\, e^{-25 z'} \right\} \qquad \text{type 4} \quad (2.26)$$

Equation (2.23) was adopted by Seager [S3]; this effectively only has one coefficient and a scaling factor, C1. Vedmar [V3] used eqns of inverse exponenial form, viz. equation (2.25). Half the symmetric curves are plotted in Fig. 2.27. The last equation was chosen for its closeness of modelling. Note: the second exponential term in eqn. 2.26 only affects the deflections very near the load application point. It was desirable to have very close modelling in this region as it contributes most to the tooth contact line compliance.

Having achieved a satisfactory function for the case of mid-face loading (away from the ends of the tooth), it was necessary to obtain the best fit for the function G(Z) to take account of the increased compliance at the tooth ends. For spur gears G(Z) must clearly be a symmetric function of (z,zF).

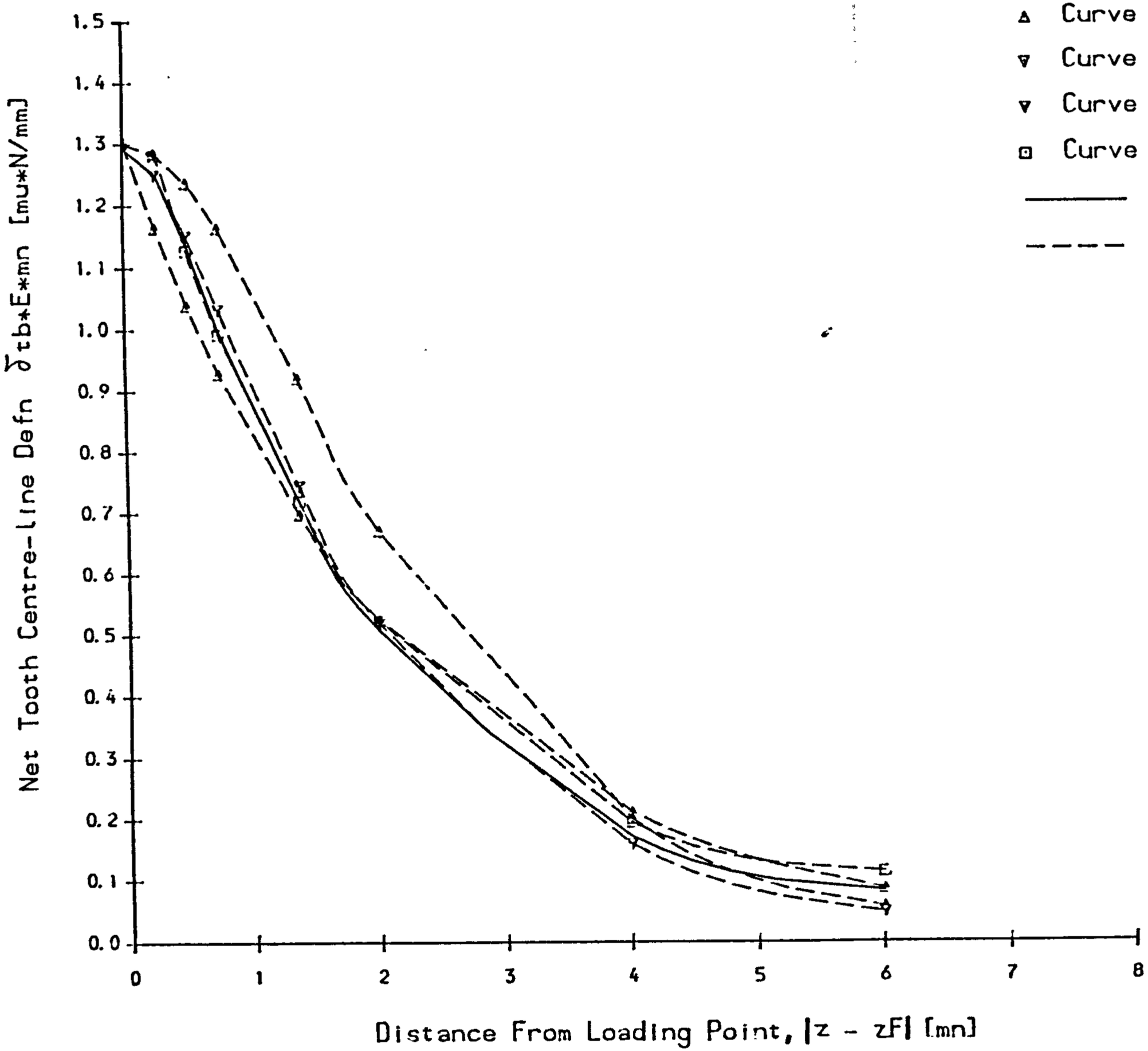

Fig 2.2.7 Curve Fitting of Tooth Centre-line Master Curve

Jaramillo [J1] developed the so-called "moment image" method to deal with this problem. This involved reflecting back the master deflection curve on itself at the ends of the teeth as shown in Fig. 2.28.

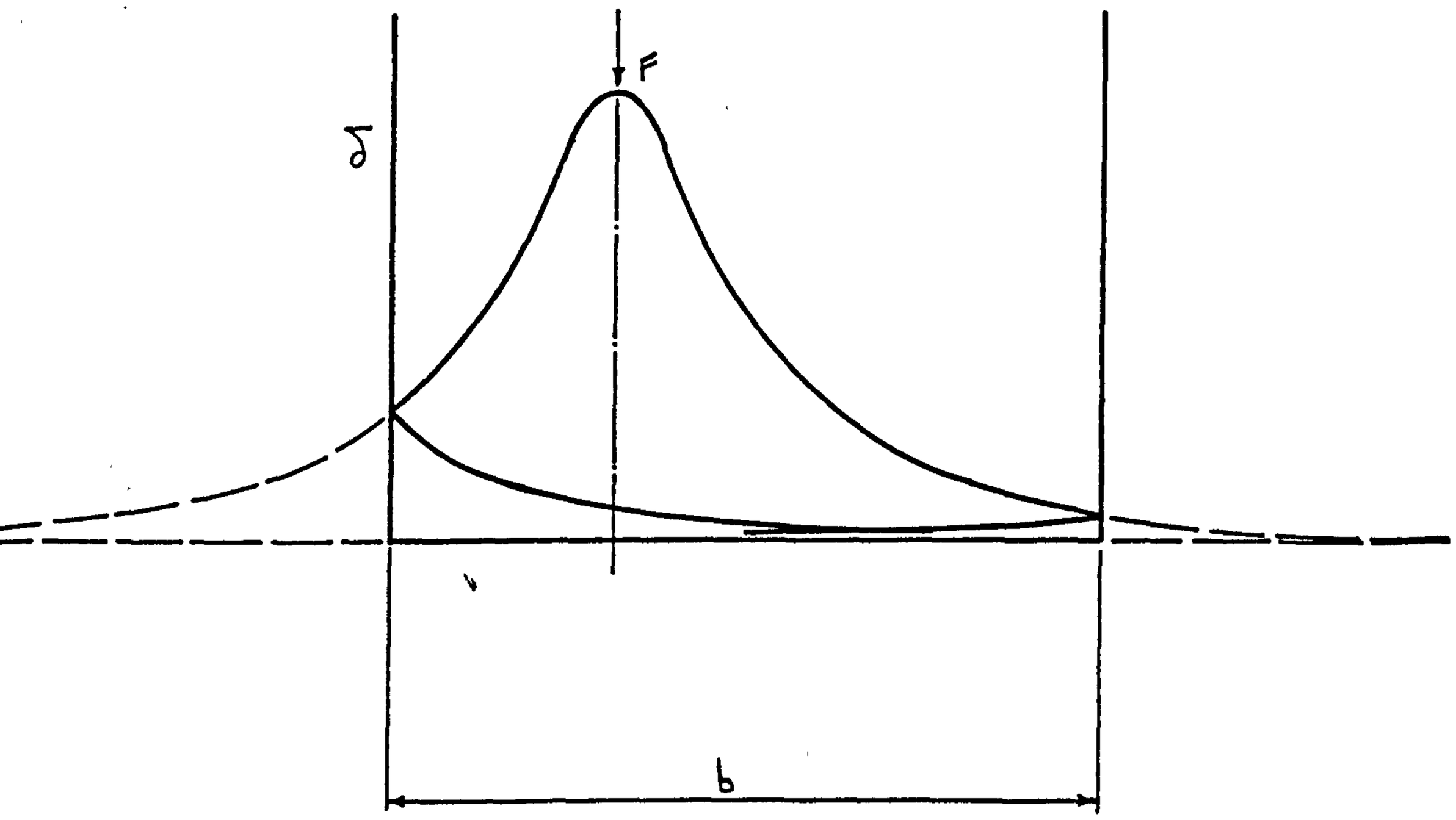

Fig. 2.28 Moment Image Method

Using this method, the tooth deflections at 0 and 1.5 modules from the end of the tooth were found to be 0.76 and 1.13 times the deflections obtained by finite element analysis, indicating that the moment image method does not accurately represent tooth end effects. It can be shown that it models the tooth as though it was continuous, with mirror image load distributions on successive sections of width "b".

For this reason an empirical equation for the end effect function G(z,zF) given in equation (2.26) has been developed such that:

$$G(Z \text{ or } ZF) = C[4] + C[5]\left\{e^{-C[6]Z} + e^{-C[6](b-Z)}\right\} \quad (2.27)$$

For each tooth number analysed by F.E. (18, 25, 40, 100) and each loading height, (-1.0, -0.5, 0, 0.5, 1.0mn), the optimum coefficients were determined for CF[1]..CF[4] and CG[1]..CG[3] using the previously developed minimising routine.

Fig. 2.29 shows results from the optimising program. Note that only the coefficients CG[1] to CG[3] are optimised, the master curve coefficients, CF[i] having previously been fitted. The deflections are given in non-dimensional form by multiplying by E*mn

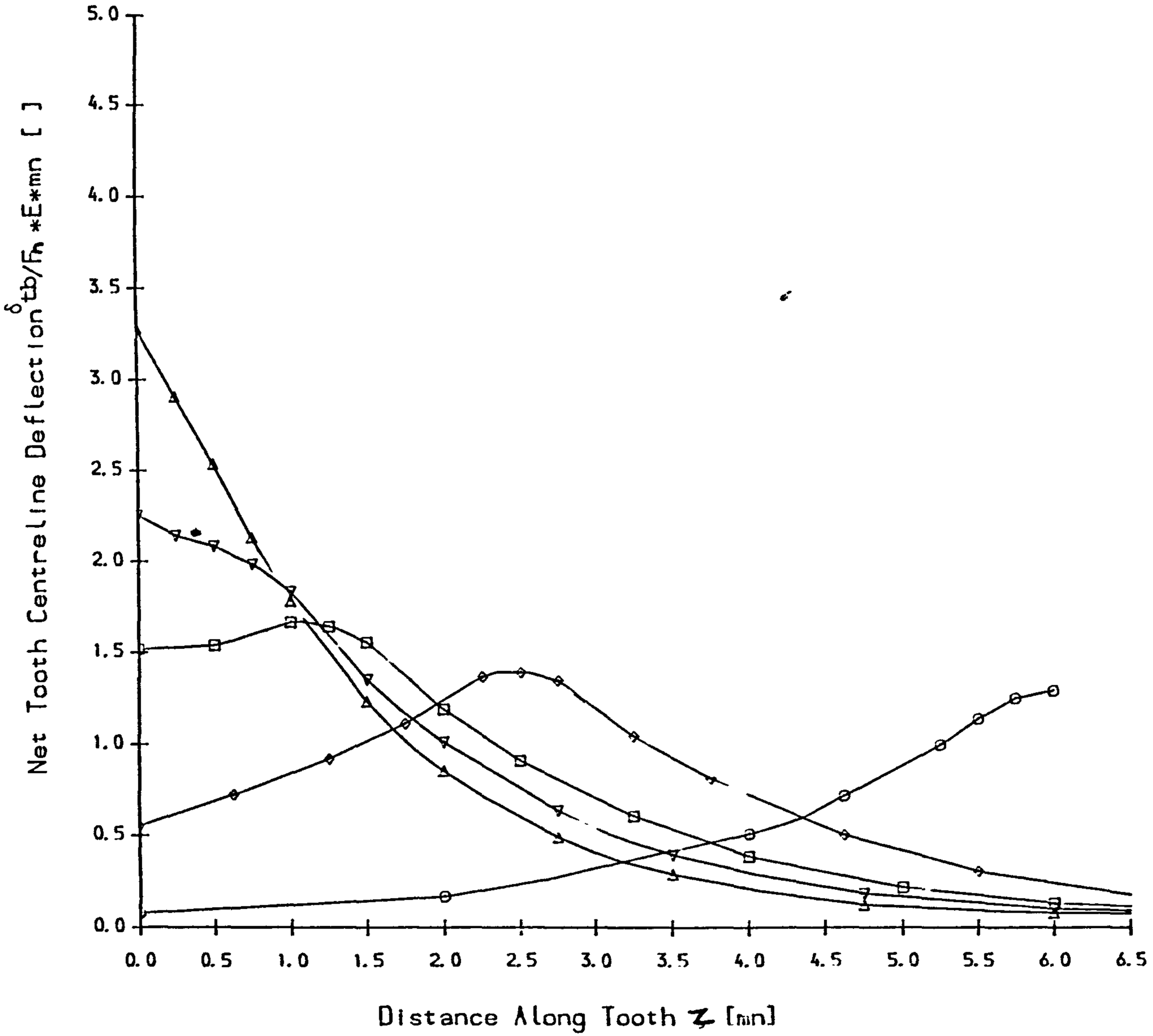

Fig 2.29 FE Results: Reference Dia. Loading; Net Tooth Centreline Deflection; 18 Teeth

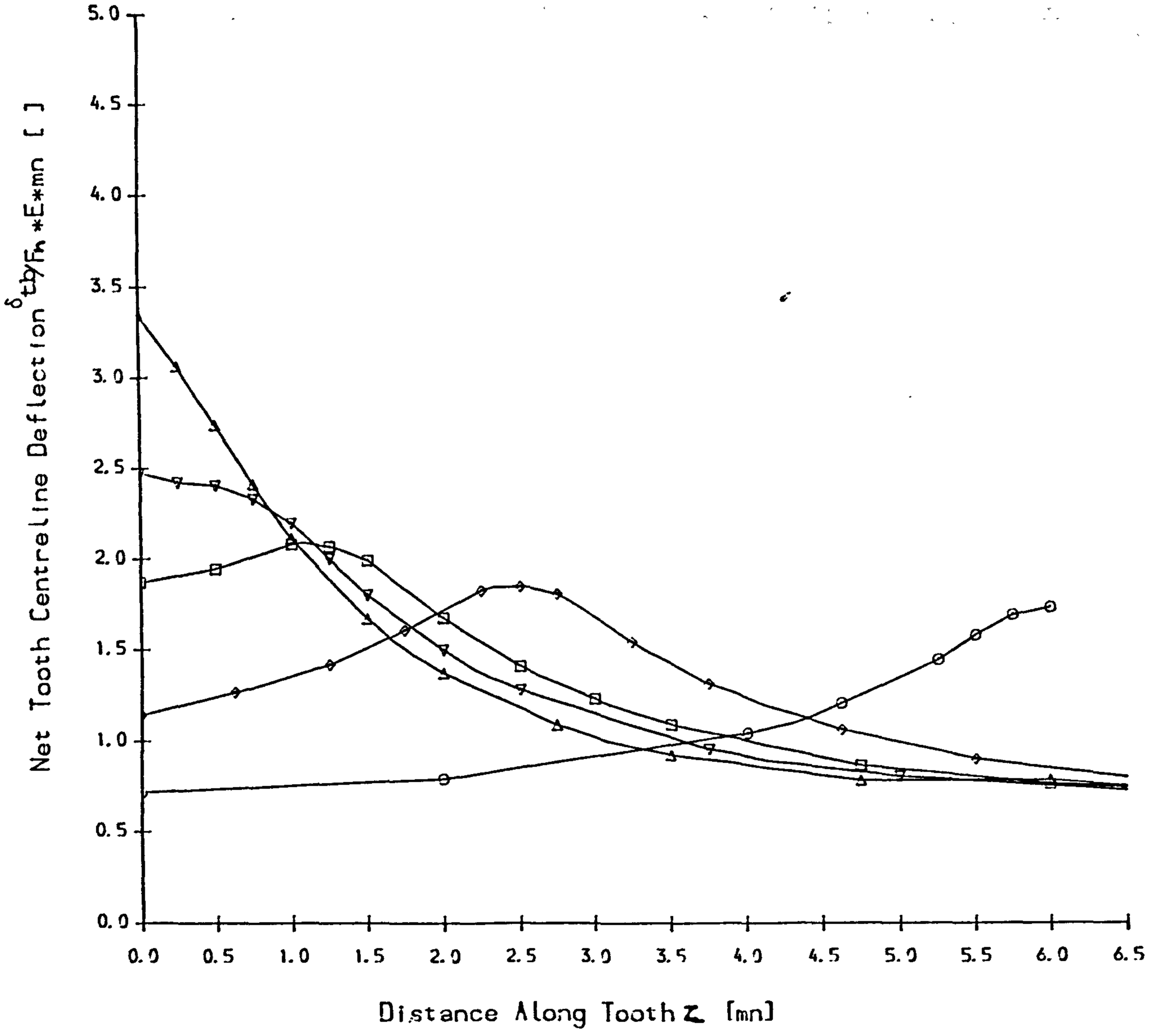

Fig 2.30 FE Results: Reference Dia. Loading; Net Tooth Centreline Deflection; 100 Teeth

2.4.3 Curve Fitting of Adjacent Tooth Deflections

The adjacent tooth bending deflections were fitted using the same optimising routine as for the loaded tooth bending deflections. The deflections are plotted in Fig. 2.24. Because the adjacent tooth deflections are mainly due to disc rotation of the whole tooth, the curves are much flatter so a different form of deflection equation was $\lambda^{\mu sed}$ (with symmetry about z = b/z) viz:

$$\delta_A = C[1] + C[2]\left\{ e^{-C[3](z+zF)} + e^{-C[3](2b-(z+zF))} \right\} \quad (2.28)$$

*****

CHAPTER 3

EXPERIMENTAL INVESTIGATION OF SPUR GEAR COMPLIANCE

3.1 Objectives of the Experiment

In Chapter 2 a theory was proposed for determining the load distribution in spur gears. The tooth contact line compliances were calculated using Finite Element analysis and these results were fitted by suitable approximations. Contrary to most of the previous published work, the gear body deflection was found to be significant and it proved necessary to include in the model the effect of tooth loads on the deflection of adjacent teeth.

In view of this disagreement an experimental investigation of the contact line compliance was carried out on an 18mm module wide face spur pinion.

The primary objectives of this investigation were as follows:

1) To measure the bending deflection of the loaded tooth at various points along each contact line for comparison with the Finite Element results used in the proposed theoetical model.

2) To investigate the shaft deflection component of the tooth deflection and to check that simple engineering theory is sufficiently accurate for practical design analysis (using the appropriate effective diameters).

3) To measure the deflection of the point of loading and verify the tooth contact compliance.

4) To measure the tensile tooth root strains to obtain a stress map from which the position and magnitude of the peak bending stress can be determined.

3.2 Design of Test Rig

A general arrangement drawing of the test rig is included at the end of this thesis. Fig. 3.1 shows a photograph of the rig. The rig applies a 'point' load along the base tangent at any radial or axial position on the loaded tooth. The test gear was chosen to be as large as practicable to give the biggest possible deflection, (typical peak deflection of loaded tooth of order 30mu), and is kinematically mounted to ensure that all the loads applied to it are well defined. All deflections are measured from an unloaded, non-deforming measuring table kinematically supported on the test gear. The measured deflections are relative to this in a rigid frame of reference whose position relative to the gear axis can be precisely defined.

The test gear data was as follows:

Number of teeth	:	$z = 18$	
Pressure angle	:	$\alpha = 20$	
Module	:	$mn = 18.0mm$	
Addendum modification	:	$x = 0.0$	
Cutter addendum	:	$hao = 1.400mn$	} final dimensions
Tool tip radius	:	$rao = 0.400mn$	
Tip diameter	:	$da = 360mm$	
Facewidth	:	$b = 260mm$	
Material	:	708M40 (EN 19A 'T' condition)	
Surface hardness	:	550 HV (flame hardened)	

* Footnote: The friction between the loading anvil and tooth surface will apply a moment to the tooth. However, the high bending compliance of the (aluminium) anvil support column will ensure that the magnitude of the friction force will be small.

Fig. 3.1 Tooth Stiffness Test Rig

The test gear was mounted on two 'thin' plates with negligible bending stiffness. One end of the shaft was torsionally restrained in the desired position by a Ringfeder keyless coupling. The other end was supported radially by a deep groove ball bearing. This ensures that the torque and shear are transmitted to the gear in exactly the same way as in a normal pinion giving the correct distribution of stress in both the gear and adjacent shaft.

3.3 Method of Loading the Test Gear

The gear tooth could be loaded to 24 KN by a hydraulic cylinder in parallel with a load cell and a loading anvil. During a test the deflection gauges were zeroed and then the load s reduced to zero, recording the reverse of the deflection. This procedure was found to produce the most consistent results.

The deflection gauge assembly was mounted on a carriage that could be traversed along the test rig frame such that the loading axis was always vertical and along the base tangent. The axial position of loading, zF, was measured relative to the end of the gear tooth. The adjacent tooth was truncated to allow the anvil to load up the gear tooth. Separate Finite Element investigations showed that this had a negligible on the tooth deflections and stresses.

The loading applied to the teeth had to satisfy two criteria if agreement with the F.E. model was to be obtained; firstly it had to approximate a "point" load with respect to gear tooth centre-line deflection and gear body deflections; secondly, very locally, it had to represent the "Hertzian" contact of two meshing gear teeth. For these reasons a radiused anvil was selected to apply the load, (see Fig. 3.2).

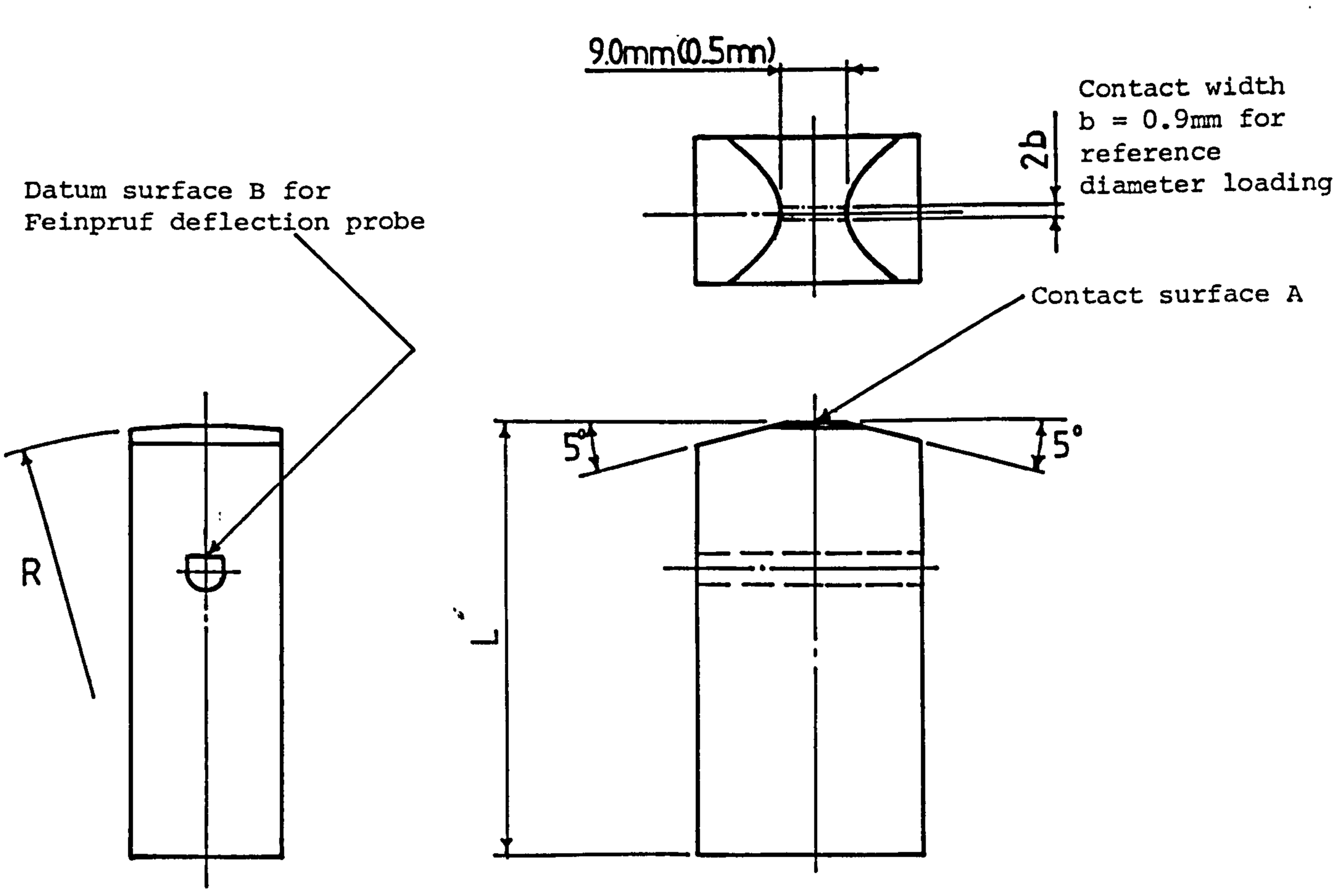

Fig. 3.2 Anvil for Applying 'Correct' Surface Loading to Test Gear

For each of the three loading diameters (324, 342, 357mm), two identical anvils were made. Each anvil had a radius of curvature equal to that of the gear tooth at the corresponding loading diameter and was relieved at each side to give a nominally rectangular contact area 9.0mm wide. Each anvil was provided with a D-shaped hole as shown in Fig. 3.2, through which its axial deflections (at a distance h from the contact surface) could be measured under load with a suitable (LVDT) probe. By loading the two identical anvils together (in a separate calibration rig), at the test load (24 KN), a contact stress system was thus set up identical to that existing when the gear tooth was loaded. The relative deflection of the probes in the D-shaped holes in the calibration rig was thus exactly twice the deflection of the contact surface relative to one of the probes. When loaded against the test gear with the same 24KN load the deflection of the contact surface could then be inferred from measurements taken in the D-shaped hole.

In this way, objective 3 could be met even though direct access to the point of contact with a probe was not possible. To facilitate fine adjustments of the very sensitive probes (claimed measurement resolution of 0.01mu) a fine adjustment lever on the shaft was provided for rotating the gear to the correct angular position. The three anvil pairs had different lengths, l, in order to make contact with the test gear tooth at the correct radius. They were made of 665M17 (EN 34) hardened to 550 HV.

3.4 Measurement of the Static Deflections

As previously explained, all the deflection measurements were made relative to a measuring frame kinematically mounted on the test gear, (see Fig. 3.3). The two shaft sections, A, B, on which the measuring frame are supported define the effective test shaft. They are located away from any local stress concentration (e.g. shaft support points, shaft section changes), so that the stresses at the ends of the effective test shaft would be those given by simple beam theory. The three support points, M1, M2, M3, are all on the neutral axis of the test gear in the direction of loading to minimize 'distortion' of the support point positions under loading. Measuring frame rotation about the gear axis is constrained at the torque-restrained end to minimize absolute rotation of the test gear relative to the frame.

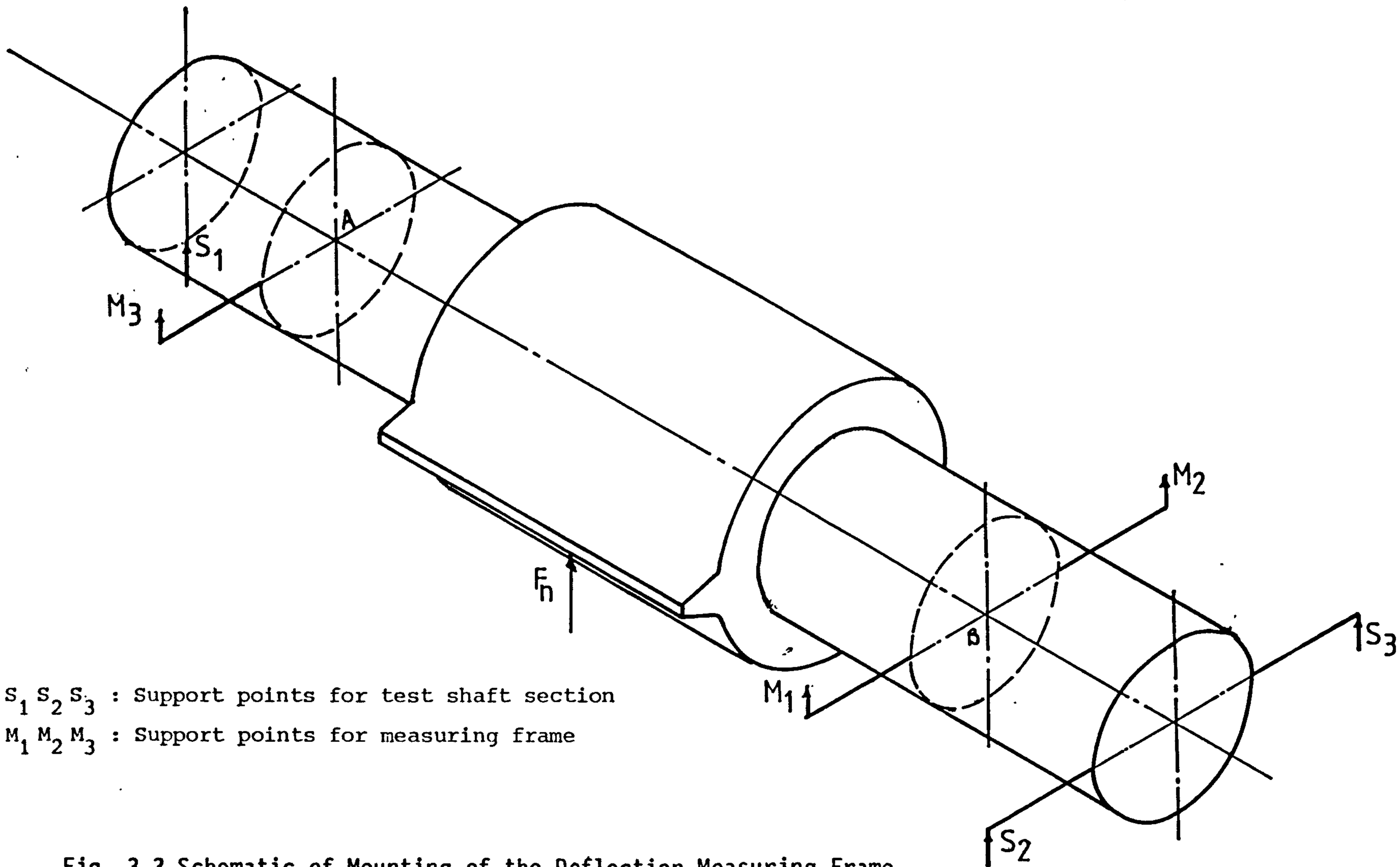

$S_1\ S_2\ S_3$: Support points for test shaft section

$M_1\ M_2\ M_3$: Support points for measuring frame

Fig. 3.3 Schematic of Mounting of the Deflection Measuring Frame

A carriage on the measuring frame carries one or two cantilever LVDT probes (Feinpruf 1320/1 gauge heads, resolution 0.01mu). They were set up to measure the deflection of either flank of the loaded tooth along the base tangent. The unloaded flank is not normal to the base tangent so is fitted with small metal pads providing a perpendicular surface from which to measure off.

The deflection of the shaft relative to the measuring frame is determined using axial LVDT probes (Feinpruf 1301 gauge heads, resolution 0.02mu). The deflection of the tooth flank diametrically opposite to the loaded tooth was also measured as well as those of various other points on the gear at positions along the test shaft.

The axial position (z) of each deflection probe was measured relative to the end of the gear tooth.

3.5 Measurement of Tooth Root Strains

In order to verify the accuracy of the Finite Element modelling and also obtain valuable experimental data on tooth root stressing, the tensile tooth root has been extensively strain gauged, (see Fig. 3.4).

Because of the symmetry of the gear, tooth root stresses are very nearly a symmetric function of the distance of the load/measuring point from the centre of the face (only the torque-restraint at one end disturbs the symmetry slightly). In view of this the tooth root stresses were assumed symmetric for a load applied at the same distance from the end of the tooth. Transverse strain gauge chains (HBM 1/120KY11, 1.0mm pitch, 0.6mm active length), were fitted at selected axial positions across the 30^{o} tangent line to pick up the peak transverse strain and stacked rosettes (WSM WA 06-120R-120) are fitted at equivalent positions from the other end of the fillet to obtain the complete surface strain field.

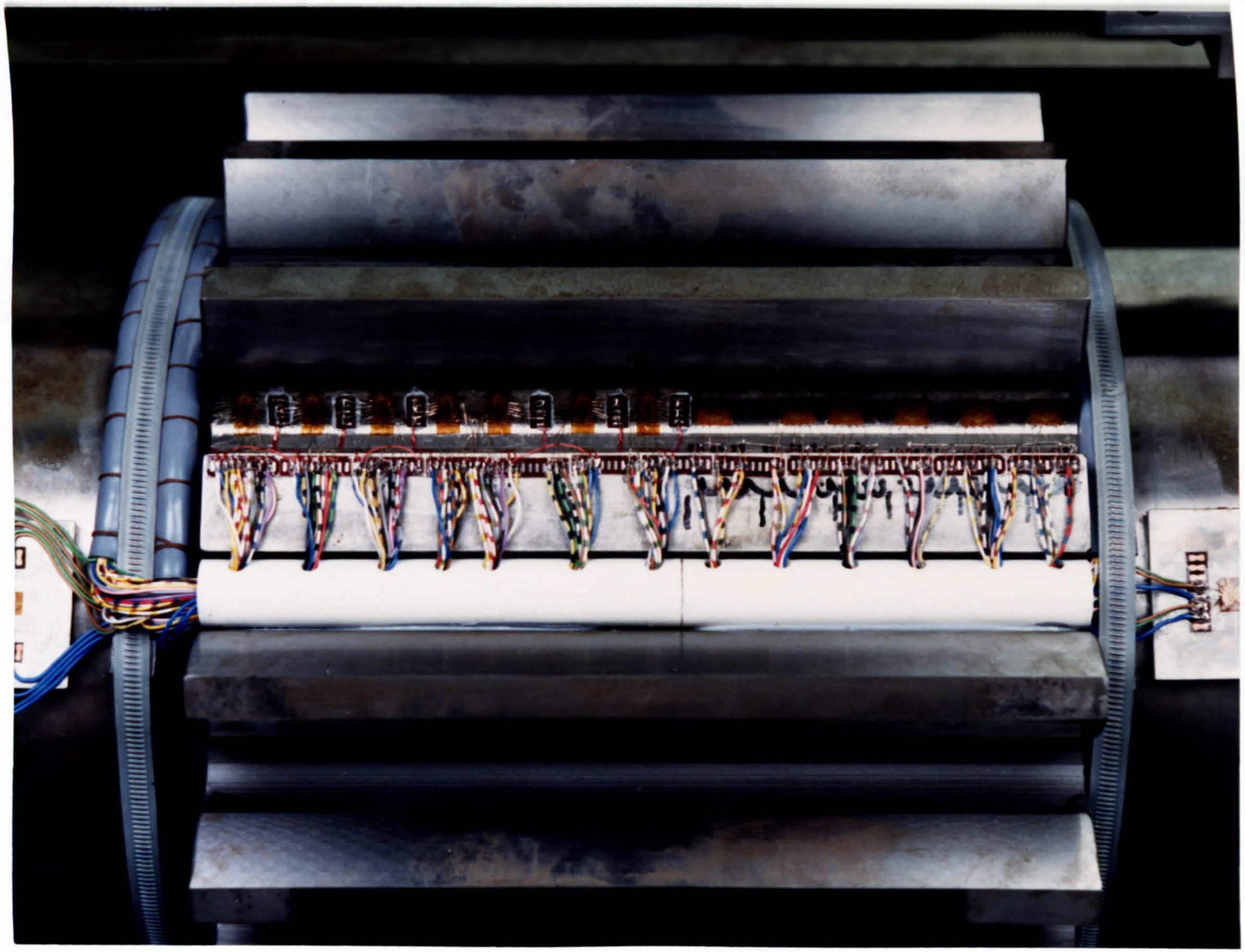

Fig. 3.4 Strain Gauging of Tensile Tooth Root

The strain gauge data (and load cell output) was processed by an HBM UPM60 multipoint measuring unit and stored on a floppy disk using a Data Track Technology Tracker 1400.

3.6 Calculation of Tooth Root Stresses from Surface Strains

On the surface of the tooth root is a state of plane stress. The strain gauge rosettes and chains are positioned to give strains ε_a, ε_b & ε_c in Fig. 3.5. The peak strain value from the chain is used for ε_b.

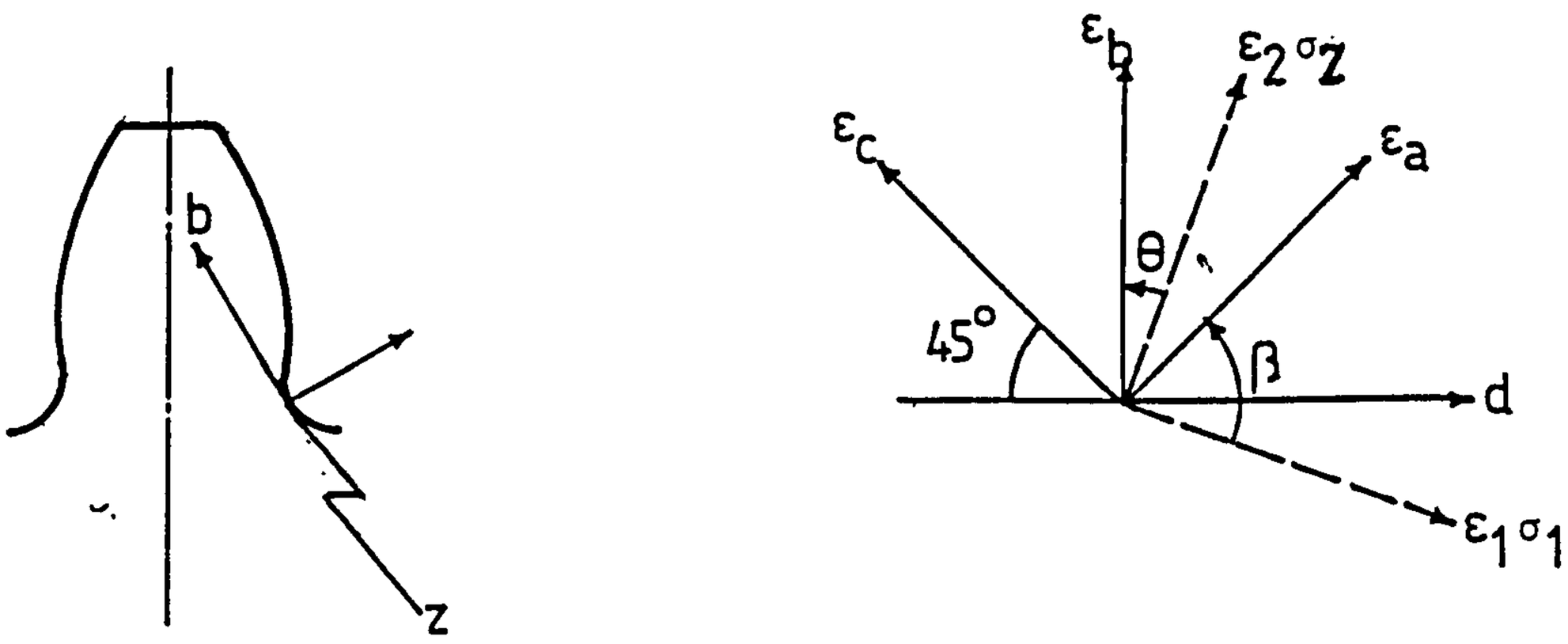

Fig. 3.5 State of Strain in Tooth Root

For plane stress we have the following equations relating the measured and principal strains:

$$\varepsilon^2 - (\varepsilon_a + \varepsilon_c)\varepsilon + [\varepsilon_a\varepsilon_c - \tfrac{1}{4}(2\varepsilon_b - \varepsilon_a - \varepsilon_c)^2] \quad (3.1)$$

and $$\beta = \frac{2\varepsilon_b - \varepsilon_a - \varepsilon_c}{\varepsilon_c - \varepsilon_a} \quad (3.2)$$

Equations 3.1 & 3.2 can be solved to give principal strains ε_1 & ε_2 and the principal stresses σ_1 & σ_2.

$$\sigma_1 = \frac{E}{1-\nu^2}(\varepsilon_1 + \nu\varepsilon_2) \qquad \sigma_2 = \frac{E}{1-\nu^2}(\varepsilon_2 + \nu\varepsilon_1) \quad (3.3)$$

The transverse and longitudinal stresses σ_b & σ_z are then calculated:

$$\sigma_b = \sigma_2 \cos^2\theta + \sigma_1 \sin^2\theta \qquad \sigma_z = \sigma_2 \sin^2\theta + \sigma_1 \cos^2\theta \quad (3.4)$$

A small post processing program has been written to analyse the strains based on these equations.

3.7 Finite Element Model of the Test Gear

The test results were to be compared with Finite Element model of the actual test gear. Only the effective test section of the test gear was modelled by F.E. to simplify analysis of the deflection data. Fig. 3.6 shows the test gear with the F.E. model shaded.

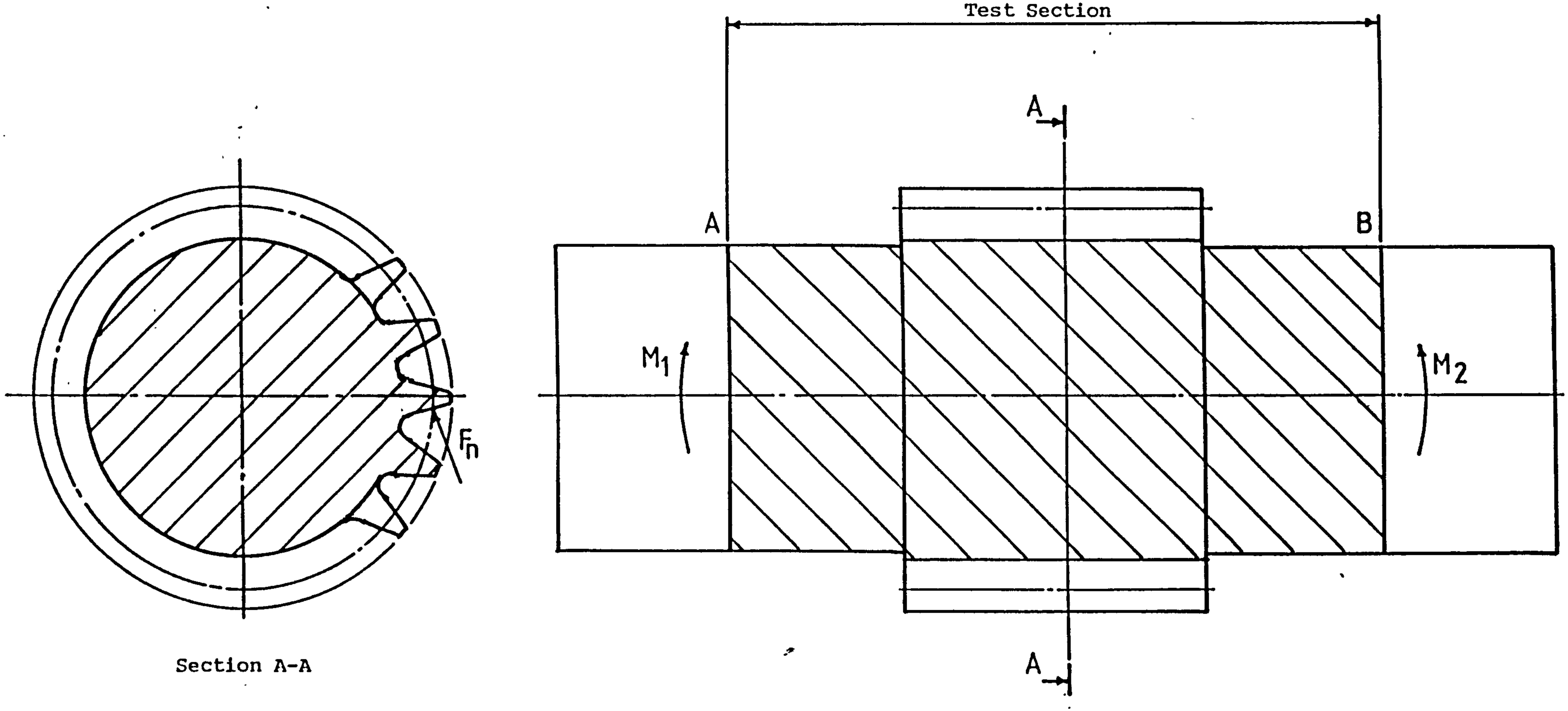

Section A-A

Fig. 3.6 Differences Between the Test Gear & F.E. Model

The Finite Element model is simply supported at sections A & B and torsionally restrained at section B. The extra shaft deflection in the test gear due to M1, M2 has been taken into account when comparing the two sets of deflection results.

3.8 Comparison of Calculated and Experimental Results

3.8.1 Shaft Deflection Results

As a preamble to the measurement of tooth deflection, the shaft /gear body deflections were examined. This also served to verify that simple engineering calculations of the shaft deflections were sufficiently accurate. All the tests were carried out for a reference diameter loading (dy = 324mm), but four separate load cases were considered with the distance from the torque restrained end, zF = 130, 50, 30 and 10mm.

The quantities of interest in this investigation were the vertical deflections of the gear shaft/gear center-line (ie in the direction of loading) and the shaft rotation (twist) again at the shaft centre-line. Simple beam theory predicts no horizontal deflection. Three sources of information of these quantities are available viz:

- simple engineering beam theory
- the results of the F.E. analysis
- measurements taken on the surface of the test gear

Examination of the F.E. results showed that although there was distortion of each shaft and gear cross-section, the vertical deflections at the ends of vertical diameters were very close to that of the centre-line. Rotation and horizontal deflections of the shaft centre could, likewise, be estimated with sufficient accuracy by taking horizontal measurements at the ends of vertical diameters.

Note : 1. The shaft rotated relative to the measuring frame under loading, (lifting up support M3 in Fig. 3.3) so that the shaft centre-line moved vertically at this end relative to the frame. This required a correction to be applied

to any measured deflections. The measured value for the shaft twist between sections A and B, has been used to correct the readings. Calculated values of this twist based on the root diameter for the gear section agree to within 5%.

2. In the plane of loading, tooth 10 rotated by approximately 10% less than tooth 15, demonstrating significant distortion of the gear body. This was confirmed by the F.E. analysis

3. Distortion of the shaft diameter at the measuring frame supports was of the order 0.1mu.

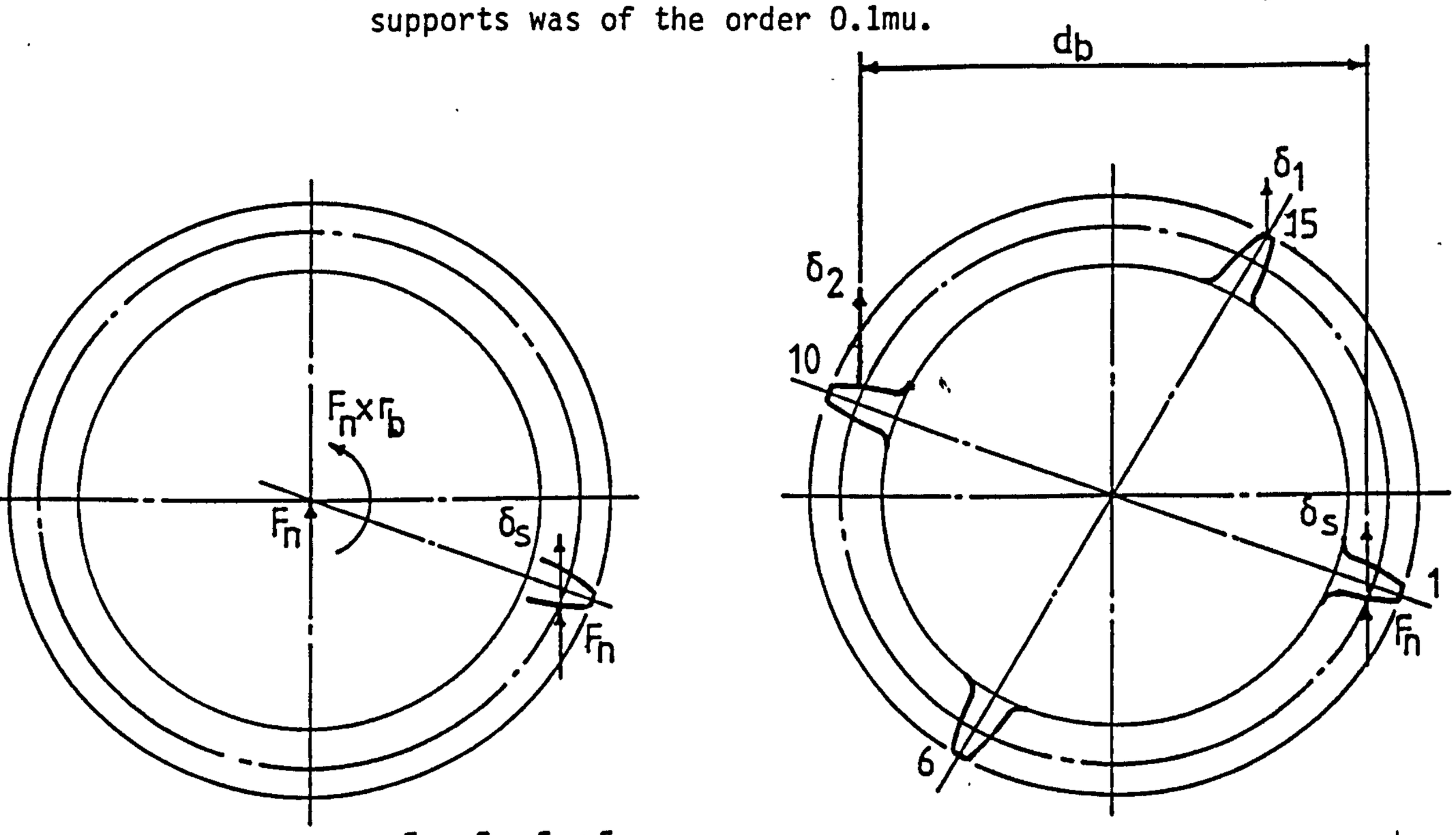

Fig. 3.7 Determination of Shaft Deflection, δ_s at any Section, z

The calculation of shaft deflection by simple engineering theory is made up of 3 components: torsion, bending and shear deflection, (δst, δsb, δss). The following assumptions have been made:

1) Any change in section diameter (e.g. from the shaft to the gear), has been assumed to be fully effective at the step (not a 'cone' of effective diameter). This is perfectly acceptable for a pinion in which the step is small as here.

2) The root diameter, df, has been assumed to be the effective diameter for calculating the torsional deflection.

3) The reference diameter has been assumed effective for calculating the shear and bending deflections.

The results for the four load cases are plotted in Fig. 3.8. The experimental results are generally higher at the ends of the teeth due to the assumed 'step' change in diameter. The repeatability of the deflection measurements was of order $\pm$0.1mu, and thus equal to the discrepancy between measured and calculated values.

There is thus no evidence of any systematic error, and the simple engineering theory can be assumed to predict shaft centre-line deflections within $\pm$5% or $\pm$0.1mu, whichever is greatest.

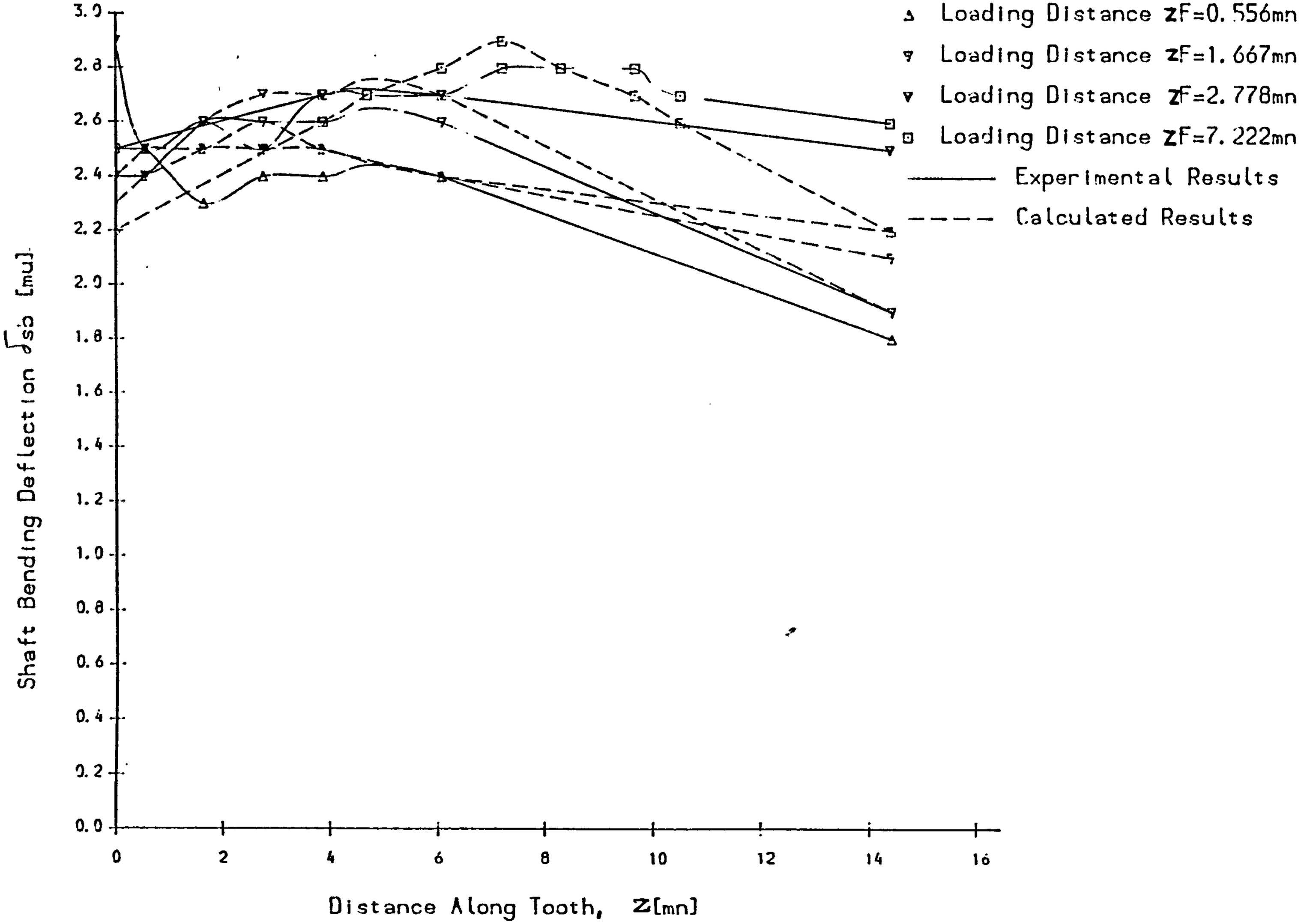

Fig 3.8 Test Gear Shaft Bending Deflection Results, d_y =324mm

3.8.2 Tooth Bending Deflection Results

In this section the results of the loaded tooth deflection, ($\overline{\delta s}$ + $\overline{\delta tb}$), measured on either flank are compared to the tooth centre-line deflections from Finite Element analysis. The total tooth centre-line deflection has been compared because it is near raw data extracted from each model. If the calculated/measured shaft deflections were subtracted from each model an extra error could possibly be introduced. The F.E. deflections have been slightly modified to account for the applied end moments to the shaft ends. Measurements were taken for three loading diameters, (dy = 324, 342 and 357mm) at four axial positions, (zF = 130, 50, 30, 10mm). All measurements were repeated a total of three times with a repeatability of ±0.1mu).

The results of the tooth bending deflections are plotted in Figs. 3.9, 3.10 and 3.11. Where access permitted, both the loaded and unloaded flank deflections were measured and the results averaged to estimate the tooth centre-line deflection. The difference between the two readings was never greater that 5%. In the plane of loading, (z = zF), F.E. deflections are plotted for both the tooth centre-line and the unloaded tooth flank. The in-plane tooth centre-line deflection is greater than that of the unloaded tooth flank showing deformation of the tooth shape. Tip loading shows the largest deformation as expected but this could be partly due to some of the contact deflection still being present at the tooth centre-line. The F.E. results agree very well with the experiments, being on average 6.2% lower. The only plausible reason for this discrepancy (apart from experimental error) is that the F.E. model may not contain enough elements so has not quite converged to the exact solution. Too fewer elements will over-constrain the model and reduce the computed deflection.

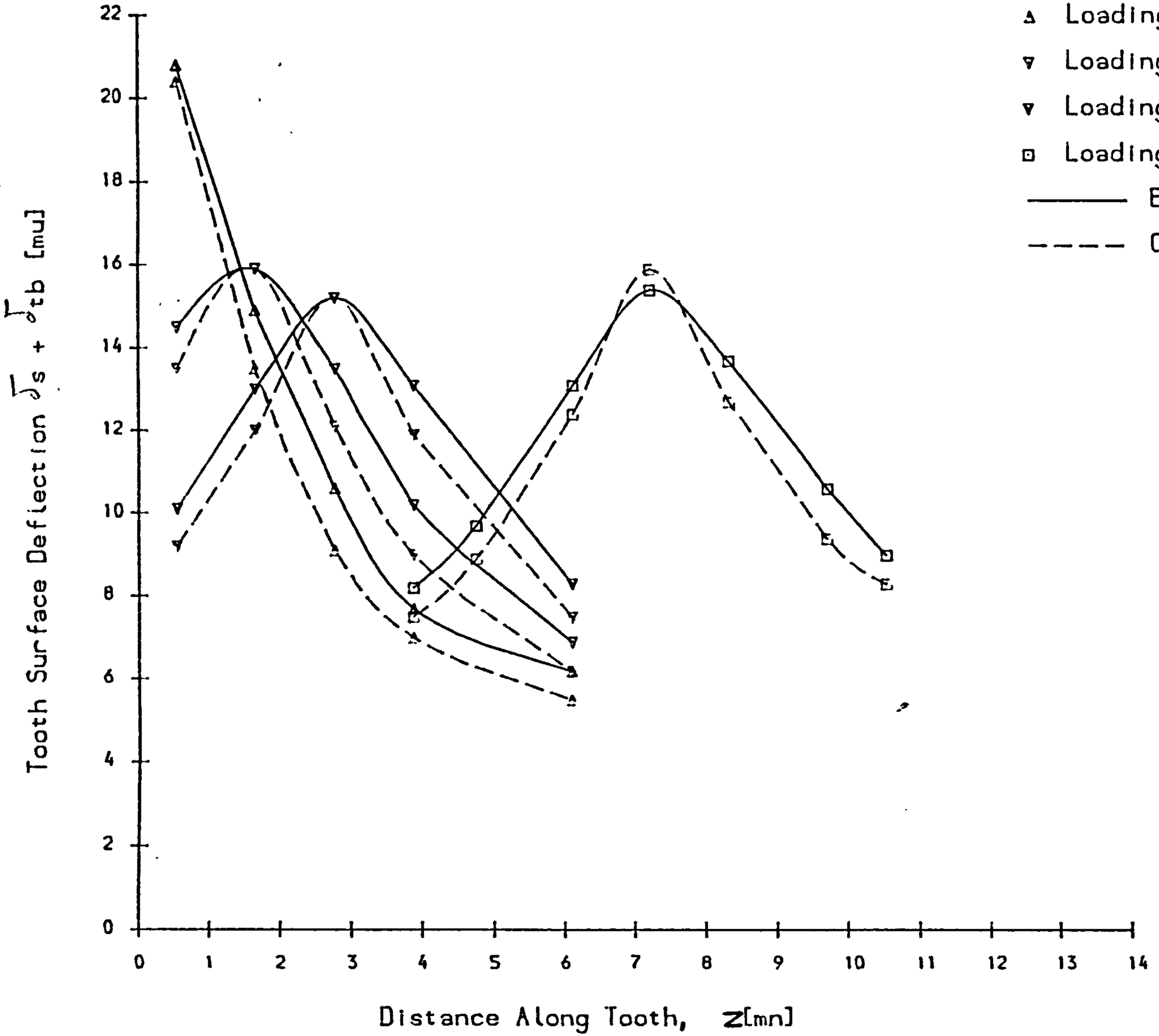

Fig 3.9 Test Gear Tooth Surface Deflection Results, d_y =324mm

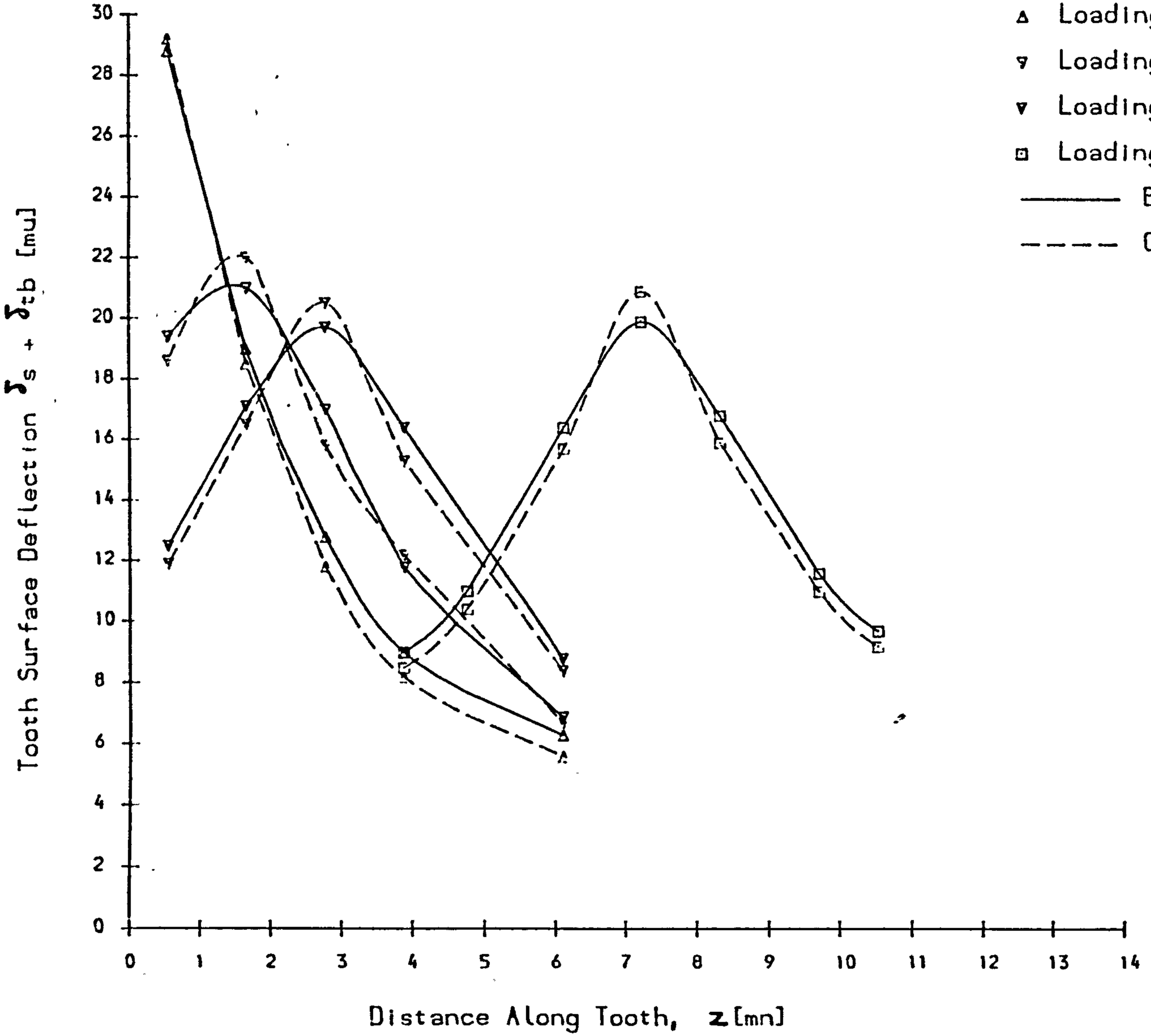

Fig 3.10 Test Gear Tooth Surface Deflection Results, d_y =342mm

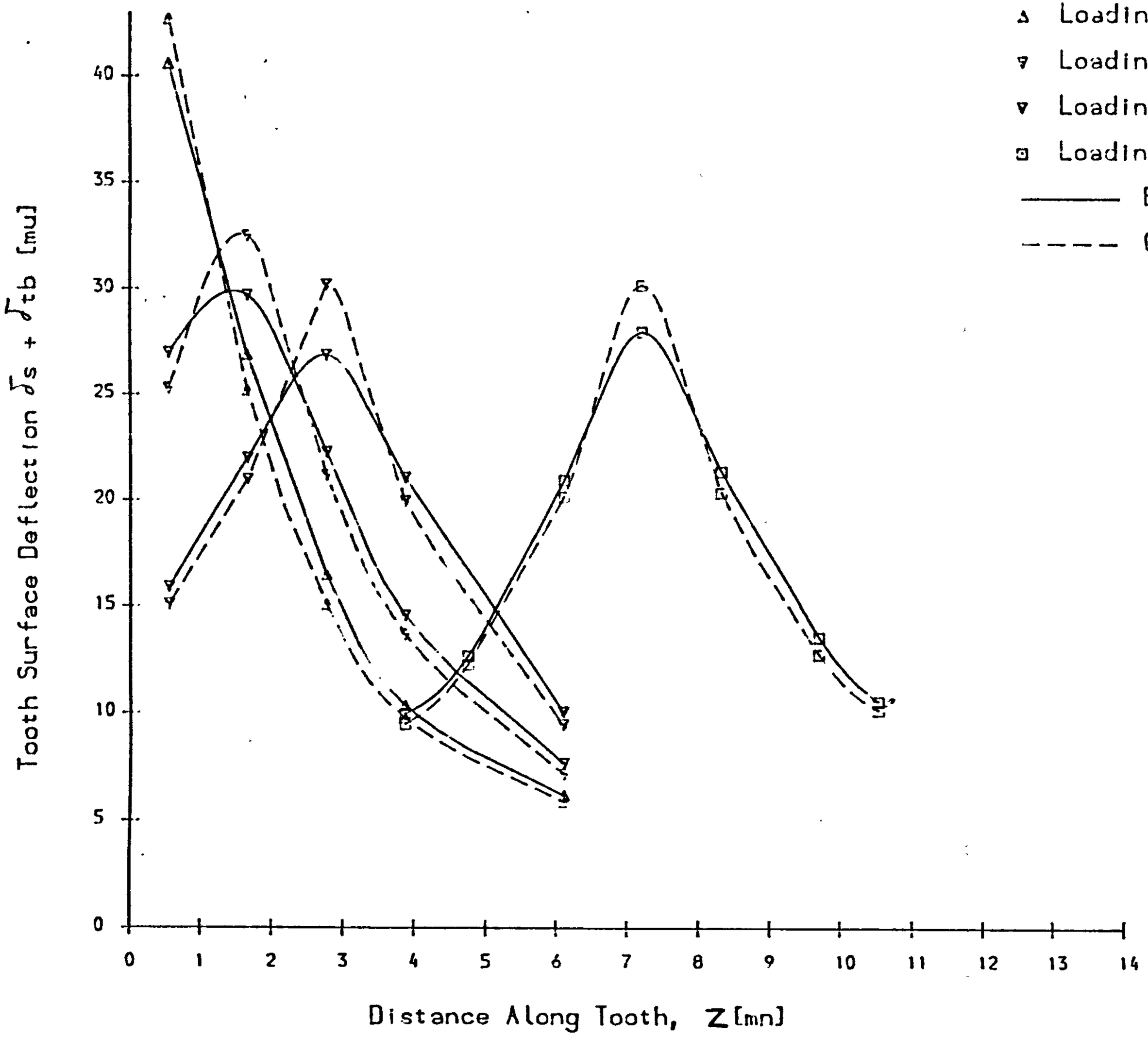

Fig 3.11 Test Gear Tooth Surface Deflection Results, d_y =3.57mm

3.8.3 Tooth Contact Deflection Results

The loading anvil was designed to try and obtain results for the 2D contact deflections occurring between gear teeth. Only the reference diameter contact deflections were investigated. The calculated 2D contact deflections were approximately 21% less than the experimental results.

The experimental contact deflections were obtained as follows. Firstly the loading anvil was calibrated by loading the two identical anvils together. The anvil compression, δ_{AB}, was measured. The test gear was loaded at the reference diameter, (dy = 324mm), following the same procedure as for the tooth bending deflection experiments.

Axial Loading Pos'n of Def'n zF [mu]	Measured Anvil Deflection δ_B [mu]	Derived Tooth Surface Def'n δ_A [mu]	Measured Tooth Bending Def'n δ_{tb} [mu]	Derived Tooth Surface Def'n δ_{tc} [mu]	Error in Contact Def'n [%]
130	59.5	53.2	15.4	37.8	-21.7
50	59.0	52.7	15.2	37.5	-21.1
30	59.2	52.9	15.9	37.0	-20.1
10	65.0	58.7	20.8	37.9	-22.0

δ_{tb} = Deflection measured on unloaded flank

Theoretical 2D contact deflection = 29.6mu

Fig. 3.12 Contact Deflection Results for Test Gear Reference Diameter Loading

The anvil calibration yielded a compression of δ_{AB} = 6.3mu. Equation (2.19) predicts a 2D contact compression of 24.5mu. The length of the line load (2b in Fig. 3.2) is only 0.3 of the total anvil length so a 3D stress field was present in the anvil. If the two mating surfaces of the anvils were flat and the stress assumed to

spread downwards along a double tapered rectangle (see Fig. 3.13) the deflection can be calculated from equation 3.5. This approximation gives an anvil compression of 14.8mu.

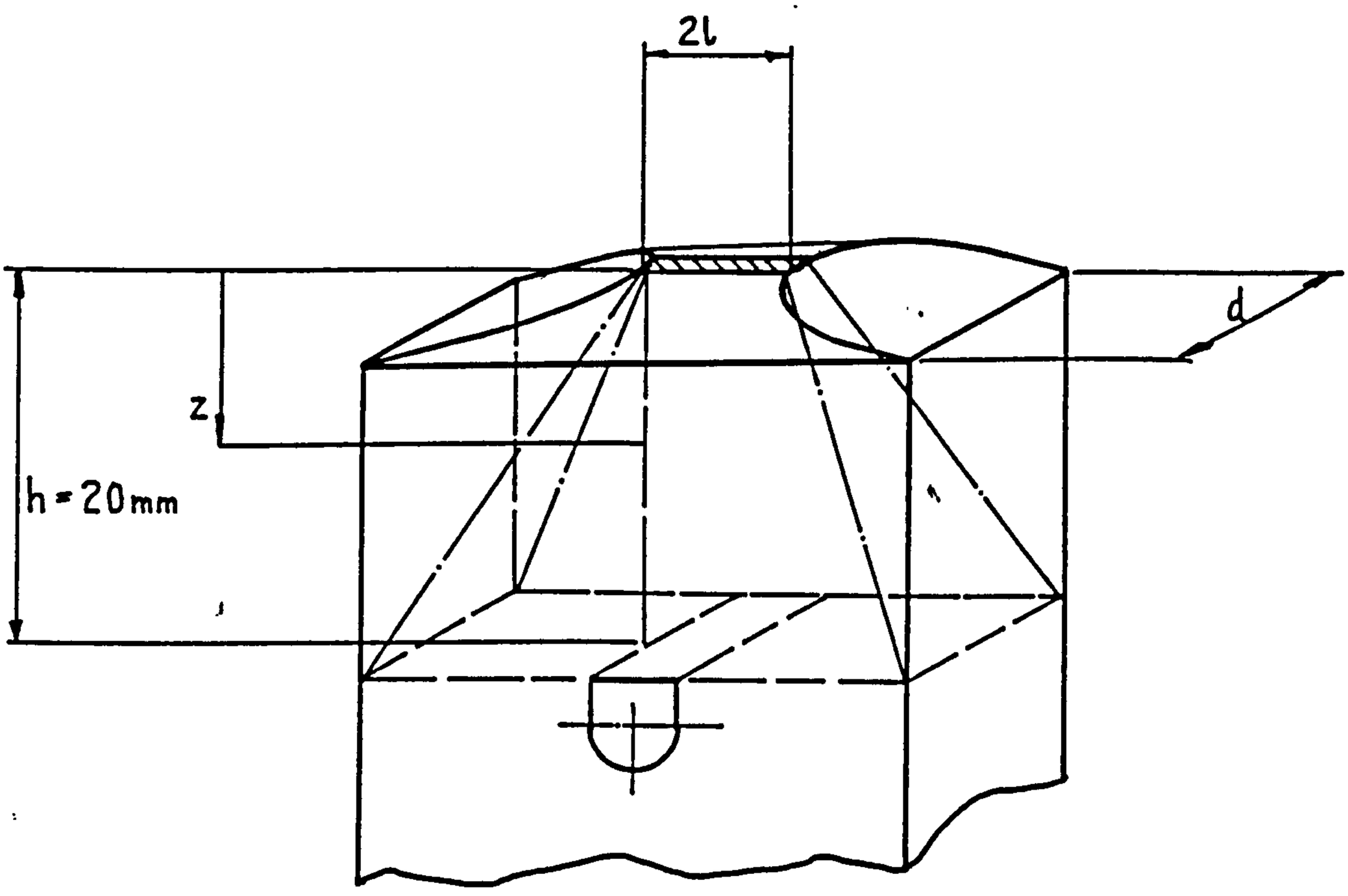

Fig. 3.13 Approximation to the Stress Field in the Loading Anvil

$$\delta_{tc} = \frac{F}{E}\int_{o}^{h}\frac{dz}{A} \qquad (3.5)$$

The deflection should actually be greater than that given by this approximation due to the effect of the surface curvature. No satisfactory explanation can be put forward as to the very low value of anvil calibration deflection (6.3mu) and as such the tooth contact compression results derived from this calibration (given in Fig 3.12) are to be viewed with caution. Note that if the calculated approximation to the anvil compression of 14.8mu is used to derive the loaded tooth surface deflection the derived tooth contact compression is 29.1mu. This gives a +2% 'error'with the calculated 2D contact deflection. This suggests that the contact stress system in the test gear tooth is in fact 2D under the loading anvil throughout the tooth depth which does not seem plausable. It seems more likely that the assumed loading system and corresponding stress system is being distorted, for example by curvature of the tooth in the axial plane due to the 'point' load.

In order to obtain more reliable verification of the contact deflection it would appear necessary to design a new test rig with the following specification:

1) Load up a large module gear to obtain the largest possible deflections, (not a rack because the loading anvil should have the identical contact surface radius).

2) Only the gear tooth plus a suitable depth of gear body, (say 4.0 modules), need be modelled as contact deflections are very localised.

3) Gear facewidth should be wide enough to ensure the central contact deflections are independent of end effect, (5 modules or 100 contact widths).

4) Load must be applied across the entire facewidth to ensure a plane strain stress field in the centre of the gear tooth.

5) The load distribution across the contact line must be uniform, either by accurate control of tolerances or by introducing rotational flexibility into the loading anvil.

3.8.4 Tensile Root Bending Stress Results

The same loading sequence used for the deflection measurements was also used for the root bending stress measurements. Typical peak transverse strain gauged readings were of order 230 micro-strain with a repeatability of better than ±4 micro-strain.

Because only tranverse strains were measured at z = 130mm (b/2) the stress could not be calculated here. At other points, the gauge readings were converted into stress values using the equations given in Appendix 3.8.4. This proceedure was carried out using a computer program that directly read the data files created by the data logger.

The processed strain gauge results are plotted in Figs. 3.14 to 3.16. The corresponing tabulated results of strain and calculated stress are given in Appendix 3.8.4. For the master curve loading, (central loading, zF = b/2), the peak transverse strain was compared with those predicted by F.E. analysis. For the other loading points, the measured strains/stresses were found to agree with those predicted by F.E. analysis to within ± 3% at each loading diameter.

The F.E. mesh used is clearly adequate for practical calculation of the root bending stress, even though analysis of the F.E. results showed typical stress discontinuities over adjacent elements of upto 25%

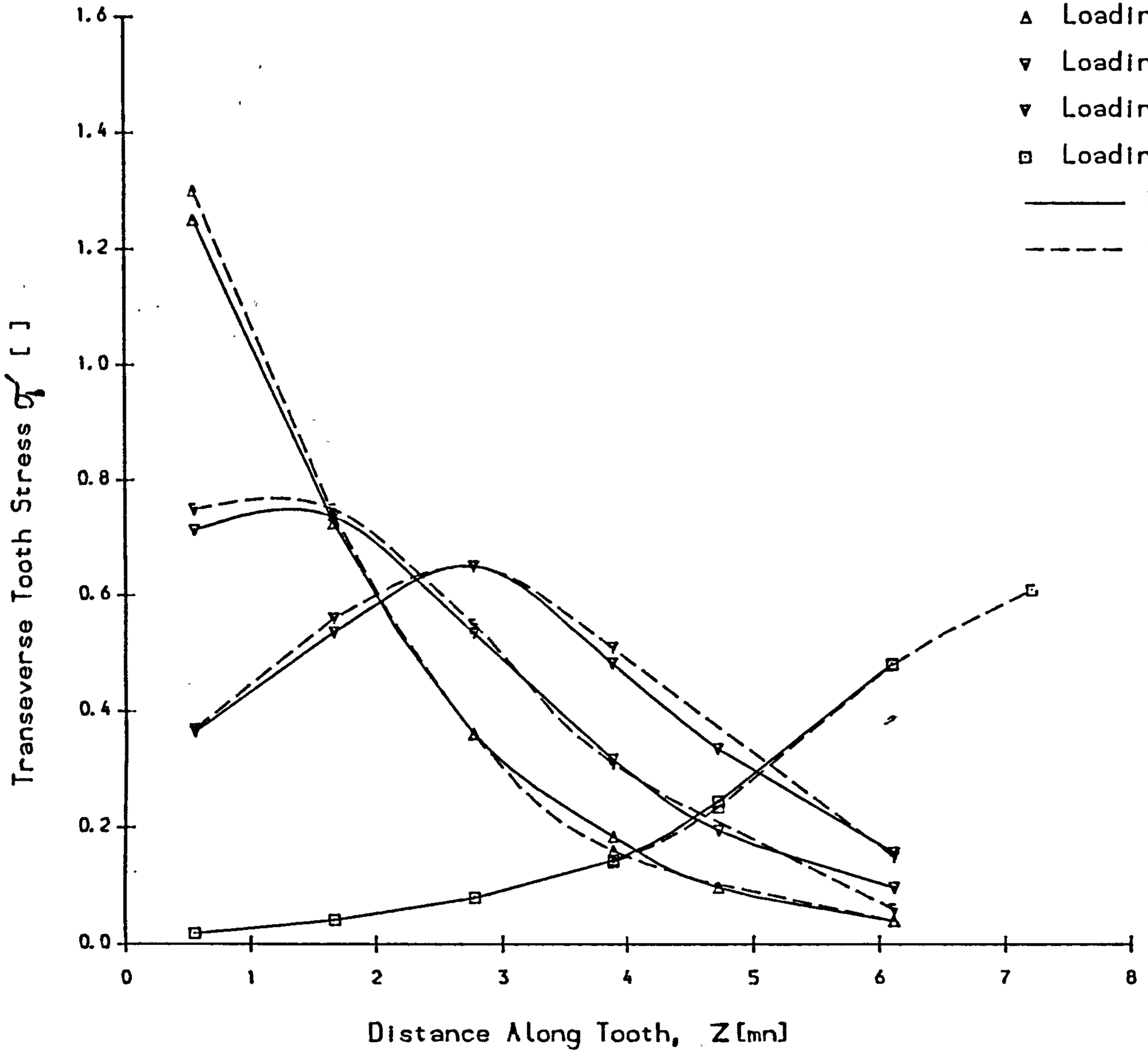

Fig 3.14 Test Gear Transverse Tooth Stresses dy=324mm

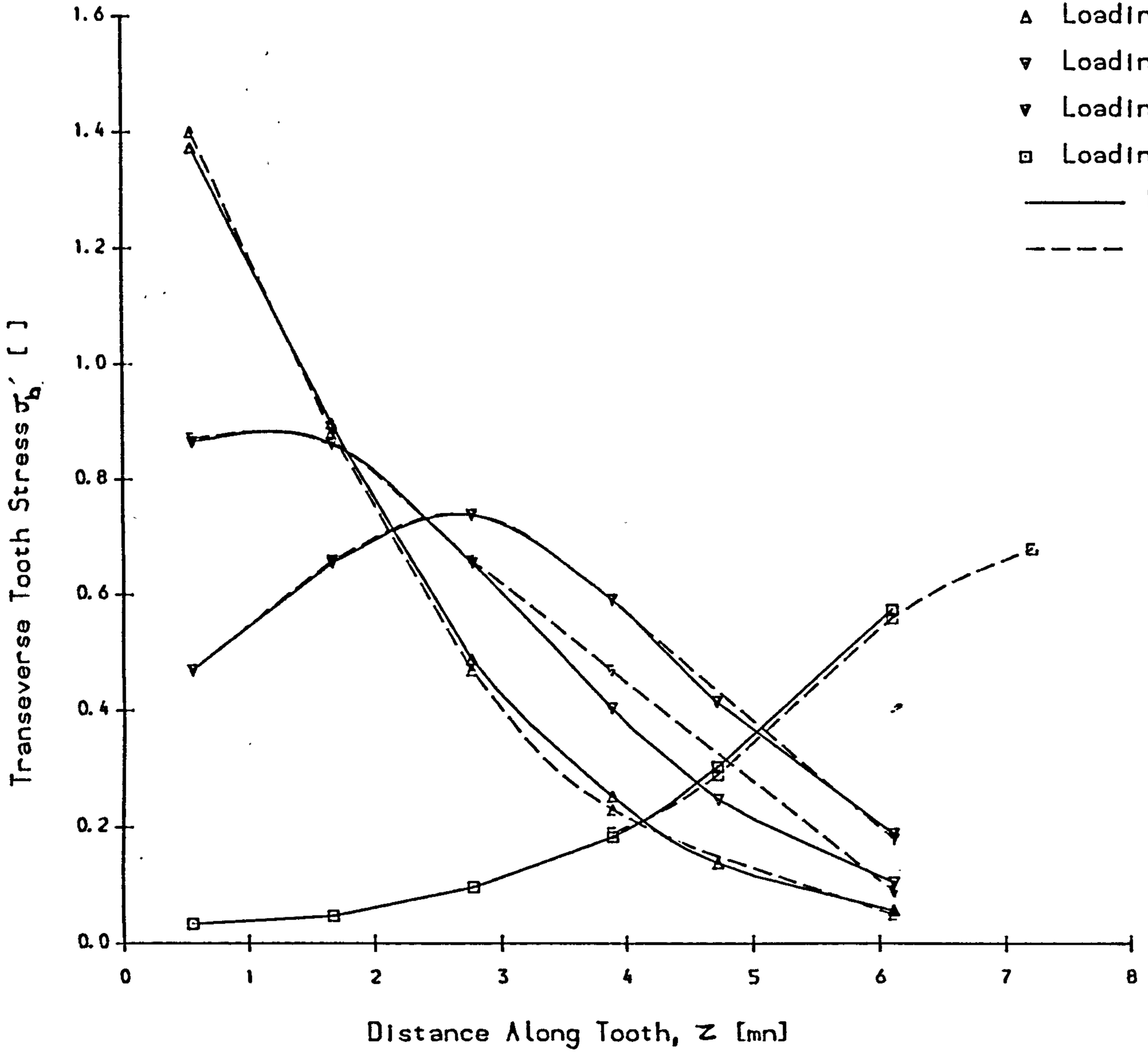

Fig 3.15 Test Gear Transverse Tooth Stresses dy=342mm

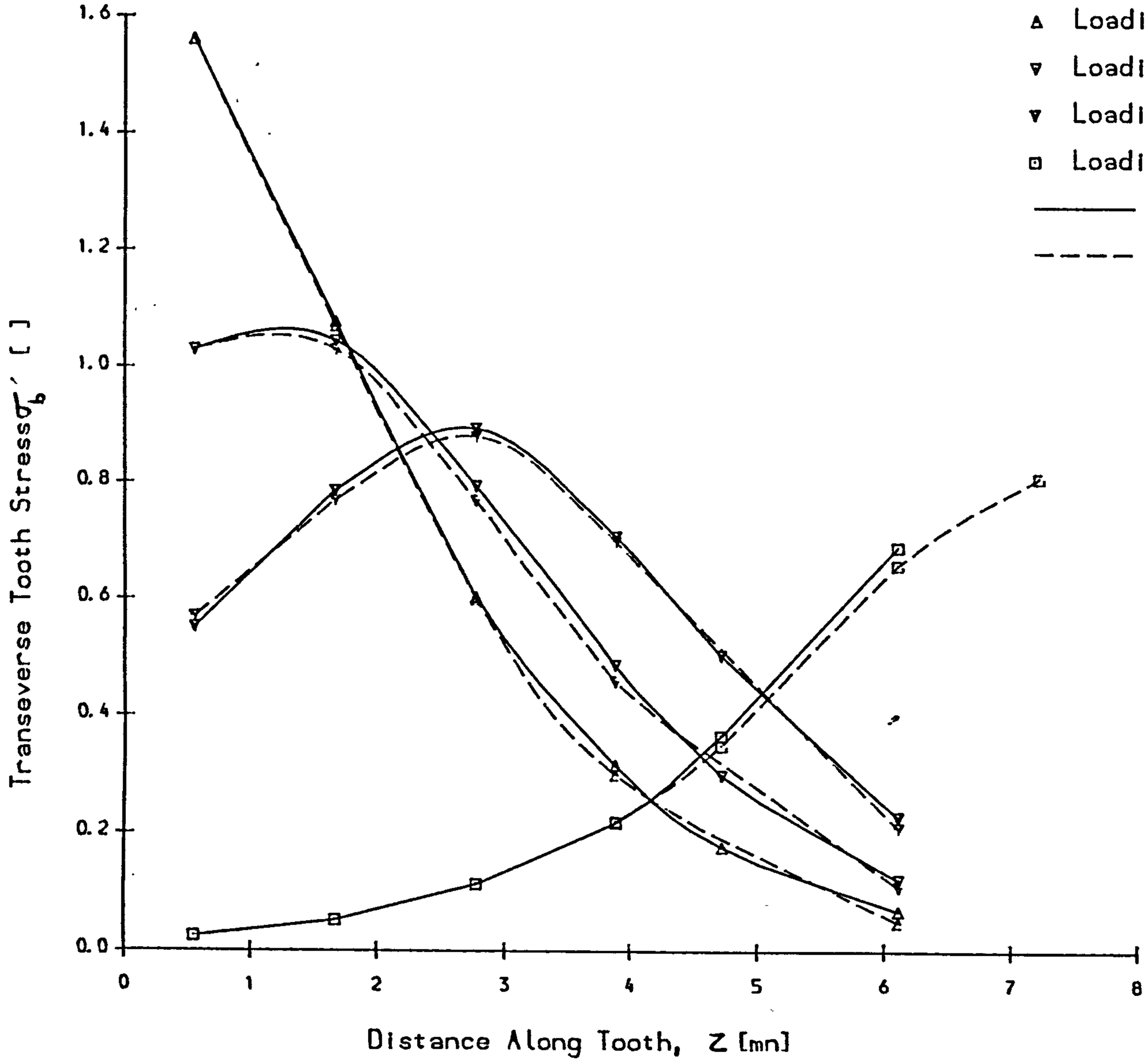

Fig 3.16 Test Gear Transverse Tooth Stresses dy=357mm

3.9 Experimental Error

3.9.1 Tooth Bending Deflection Experimental Error

The error in measured tooth bending deflection arises from two main sources, firstly, the measurement of the deflection (and applied load), and secondly, from the positional accuracy of the deflection probe (and applied load). The errors have been calculated for the tip and reference diameter loadings at axial positions of zF = 10 and 130mm based on the following assumptions:

1) Measurement of deflection: The probes have a resolution of 0.01mu but were found to have an experimental repeatability of ±0.15mu.

2) Measurement of load: ±0.3 kN in 24 kN (1.25%)

3) Error in position of loading anvil: Loading diameter is defined by locking the gear at the required angular position based on a vertical distance, h, from the tooth flank to a datum on the test rig frame. The change in the measured deflection due to applying the load at the wrong diameter is calculated from the F.E.data. Radial position error assumed to be ±0.1mm.

4) Error in position of probe up the tooth flank: Assumed equal to the error in loading diameter.

5) Error in axial position of anvil: As in 3) the change in deflection is estimated from the F.E. data based on a positional accuracy of ±0.2mm.

6) Error in axial position of probe: Assumed equal to 5).

The calculated error bands are tabulated in Table 3.17.

Loading Diameter dy [mm]	Axial Load Pos'n zF [mm]	Tooth Bending Def'n δtb + δs [mu]	Error Band [%]
357	10	42.7	±3.9
357	130	30.2	±4.1
324	10	20.4	±6.0
324	130	15.9	±5.5

Table 3.17 Experimental Error Bands: Tooth Bending Deflection

3.9.2 Tensile Root Bending Stress Experimental Error

Sources of error in the transverse stress based on the strain gauge readings are as follows:

1) Strain gauge factor tolerance: ±0.5%

2) Load measurement tolerance (the load cell was calibrated using another calibrated load cell in series): ±1.25%

3) Radial position error in the point of loading on the tooth: Estimated from F.E. data following the same procedure as for the tooth bending deflections, (3.9.1, Section 3).

4) Gauge misalignment: 45° strain fields assumed constant over positional tolerance of rosettes (±0.3mm). Transverse strain gauge chain pitch is 0.6mm therefore the transverse strain may be measured a maximum of 0.3mm from the peak value. Error in transverse stress estimated from F.E. data.

5) Axial misalignment between gauge position and load: Assumed tolerance of ±0.5mm. Error in transverse stress estimated from F.E. data.

The resultant experimental error in the transverse stress is

tabulated in Table 3.18.

Loading Diameter dy [mm]	Axial Load Pos'n zF [mm]	Tooth Bending Def'n δtb [N/mm2]	Error Band [%]
357	10	115.6	±3.3
357	130	59.8	±3.1
324	10	96.3	±5.2
324	130	45.2	±4.6

Table 3.18 Experimental Error Bands: Transverse Root Bending Stress

3.10 Conclusions

The experiments have satisfactorily proved the validity of the spur gear F.E. models used for determining tooth centre-line deflections and root stresses.

When using engineering beam theory to estimate the shaft deflections the effective diameter of the gear should be assumed to be equal to the root diameter for torsion and the reference diameter for bending and shear.

The calculated (F.E.) tooth bending deflections, (δtb + δs), are, on average, 6.2% lower than those measured. The F.E. model may require further refinement to eliminate this error, but the existing computing facilities at Newcastle University do not permit this to be done at present.

The calculated tooth contact deflections were 21% lower than the experimental results. However, the results do suggest that the plane strain deflection formula is correct. A specification for a test rig to verify this is given in Section 3.8.3. The tensile root bending stresses agreed within 3% The F.E. model is perfectly adequate for obtaining stress results.

CHAPTER 4

COMPARISON OF SPUR GEAR COMPLIANCE WITH PUBLISHED DATA

4.1 Introduction

A large amount of both experimental and theoretical work has been published on spur gear compliance. Weber and Banaschek [W4] obtained 2D analytical expressions for the tooth compliance and these have provided the model for much of the subsequent experimental and theoretical research. The existing European gear design standards [B3, D3, I5] use 2D tooth compliance data based on this work and on later research carried out by Winter and Podlesnik [W12]. Other 2D models of gear tooth compliance are either like those of Weber and Banaschek, with some allowance made for shear and "gear body deformation",based on modified engineering beam theory (Walker[W1], Timoshenko[T7]) or on "exact" solutions obtained by conformal mapping (Cardou and Tordion[C1]) or by F.E or B.E. analysis (CETIM[C2]), Hirt[H9]. One disadvantage of all these theoretical models is that the gear body is in all these cases represented either by a semi-infinite body or by a finite encastre block, so that there always arises the question of whereto determine the 'fixed' datum point from which the tooth deflections are to be measured.

Weber and Banaschek (and Walker) suggest a point "a few pitches" below the pitch-line. Walker integrates his solutions to a point in the semi-infinite solid a distance 'r' below the surfaces. Timoshenko ignores gear body deflections altogether. Results obtained by F.E. analysis of encastre blocks effectively assume the gear to be fixed approximately 3 to 5 modules from the point of loading. By only modelling part of the gear (and, by definition, constraining it at the boundary of the model) the stress/strain field produced is not that which a complete gear will see.

Several authors have used cantilever beam theory to model the 3D behaviour of spur and helical gear teeth, ignoring either the actual tapered involute shape[J1, K1], the finite width of the teeth[J1], the shear deflection or the gear body deflection[H1-H6, S3, S4, V3]. Kagawa[K1] has proposed a beam type model, which gives closed form

solutions for the influence coefficients, and Seager[S3] has developed a similar, semi-empirical model for which the coefficients of the relevent differential equations were deduced from tests on a model tooth. Hayashi[H1-H6] and Zablonski[Z1-Z3] have also published empirical expressions for the 3D influence coefficients.

Vedmar[V3] has determined 3D gear tooth influence coefficients using an elastic model similar to that developed in this thesis. His values can thus be compared directly with those obtained in the present work.

4.2 Theoretical Tooth Compliance at Reference Diameter

4.2.1 Equation used to Determine Tooth Compliance

The European gear design standards (BS, ISO, DIN) define the single tooth stiffness c' as: "The maximum tooth stiffness of one tooth pair". This occurs at reference diameter loading. For an uncorrected gear pair with uniform loading,no manufacturing errors and zero shaft compliance, c' is given by:

$$c' = \frac{w_{bm}}{f_t} \text{ [N/mm/mu]} \qquad (4.1)$$

The single tooth stiffness c' can be used as a basis for comparing both 2D and 3D spur gear compliance models. c' has been calculated for the following gear data:

Specific load	wbm	=	100 N/mm
Module	mn	=	10.0 mm
Facewidth	b	=	100 mm
Pinion teeth	z1	=	18, 25, 40, 100
Wheel teeth	z2	=	18, 25, 40, 100

Weber [W6]

Using Weber's notation the single tooth stiffness is given by:

$$c' = \frac{w_{bm}}{\delta_{tb} + \delta_{tc}} = \frac{W_o}{W_o/E\,(q_1 + q_2 + q_{Hertz})} \qquad (4.2)$$

Where the non-dimensional tooth loading compliance, q, is given (using numerical integration) by:

$$q = \cos\alpha' \left[12 \int_0^{Y_p} \frac{(Y_p - Y)}{(2x)^3} dy + 3{\cdot}12 \left(1 + \frac{\tan^2\alpha'}{3{\cdot}12}\right) \int_0^{Y_p} \frac{dy}{2x} \right. \qquad (4.3)$$

$$\left. + 5{\cdot}2 \frac{Y_p^2}{b^3} + \frac{Y_p}{b} + 1{\cdot}4 \left(1 + \frac{\tan^2\alpha'}{3{\cdot}1}\right) \right]$$

Existing Gear Standards [B3, D3, I5]

The BS, ISO, DIN standards all use the 2D stiffness for uncorrected spur gears given by Winter and Podlesnik [W12] as:

$$c' = \frac{1}{q} \qquad q = 0{\cdot}04723 + \frac{0{\cdot}15551}{z_1} + \frac{0{\cdot}25791}{z_2} \qquad (4.4)$$

Vedmar [V3]

Vedmar gives an empirical expression (fitted to his F.E. results) for the 3D tooth bending influence coefficients, Ktb, at a reference depth of h = 0.5mm below the tooth surface, (see Fig. 4.1). The 2D contact compliance, Ktc, is added on to Ktb to obtain the total tooth compliance.

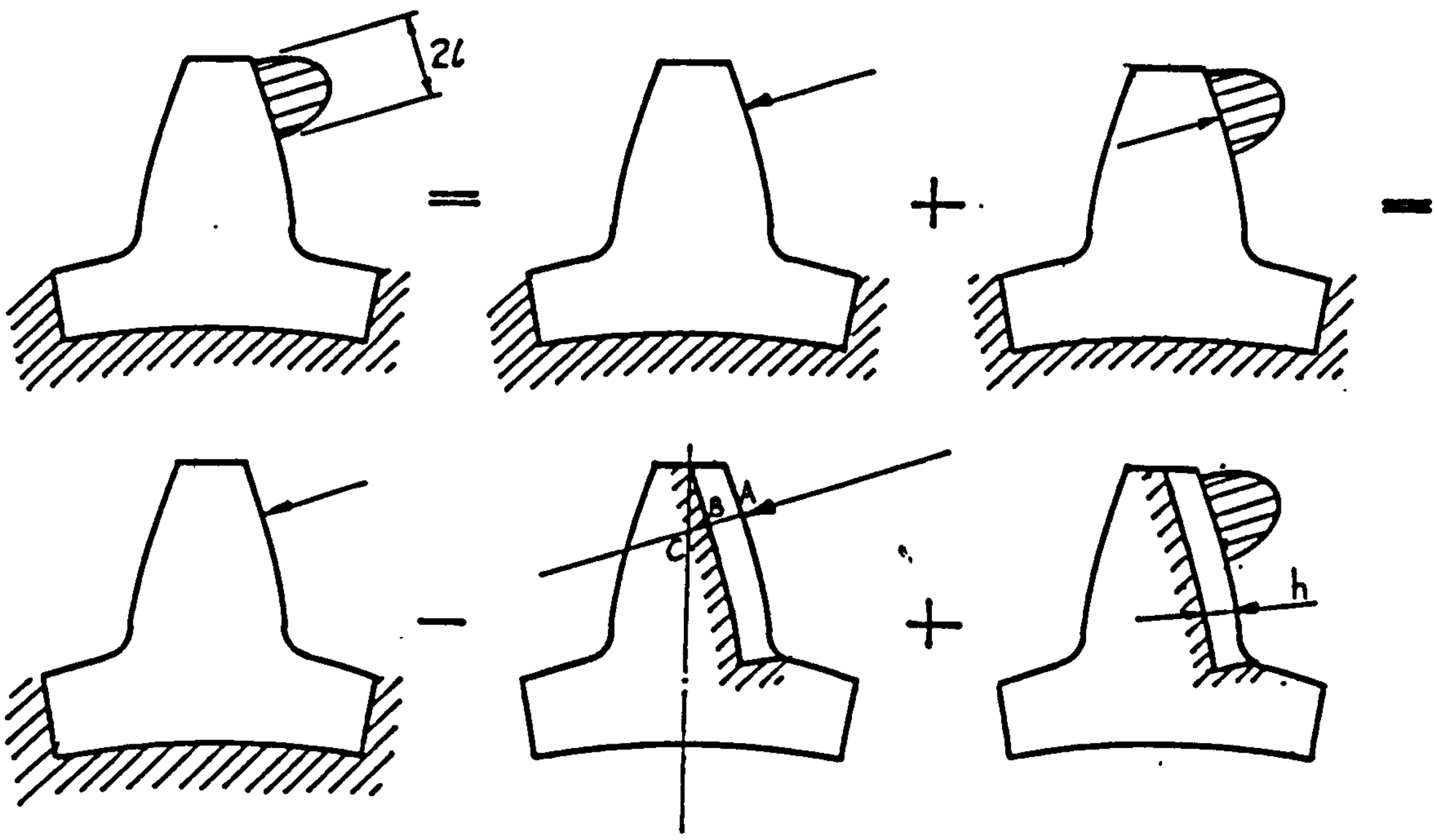

Fig. 4.1 Calculation of Tooth Contact Line Compliance According to Vedmar

The transmission error, ft, used in equation (4.1) is calculated from a simplified form of equation (2.5) for zero errors, and zero shaft compliance giving:

$$ft = \frac{\Delta}{2} \sum_{i=1}^{n} Ktb[i,j]\,w[i] + Kcc[j]\,w[j] \qquad (4.5)$$

Vedmar's bending influence coefficients must be modified if they are to be compared with the tooth centre-line deflection, δtb, determined in this thesis. The smaller reference depth, h, used by Vedmar results in the influence coefficient, Ktb[i,i], containing a larger component of "point load" Hertzian compression. From Timoshenko[T7] the non-dimensional deflections of an elastic half space at a distance h' below the surface due to a point load is given by:

$$\delta_p' = \frac{\delta_p E\, mn}{F} = \left(\frac{1 - \nu - 2\nu^2}{2\pi}\right) \frac{1}{h'} \qquad (4.6)$$

In Vedmar's work, h' = 0.5; in the present work, h' is measured relative to the tooth centre-line (h' = 0.835 for a rack loaded at the reference point). The corresponding non-dimensional contact deflections (0.933 and 0.594 respectively) result in a difference of 0.399 which must be subtracted from Vedmar's tooth deflections to give values at the tooth centre-line. Fig. 4.2 shows the master curve (zF = b/2) derived in this way from Vedmar's results, together with those from the present work.

Let us consider further the consequence of the smaller reference depth h', adopted by Vedmar. Compare the predicted flank surface deflection relative to the tooth centre-line for Vedmar and Steward. Referring to Fig. 4.1 for a reference diameter load of 100 N/mm, we have:

$$\text{Vedmar}: \quad [\delta_p']_{BC} + [\delta_p']_{AB} = 1{\cdot}23 \qquad (4.7)$$

$$\text{Steward}: \quad [\delta_{tc}']_{AC} = 1{\cdot}30 \qquad (4.8)$$

Where $[\delta'_p]_{BC}$ is obtained by numerical integration of the point load equations. (This is a crude approximation as the point load deflection is clearly not a smooth function). There is less than 1% error in the transmission error, ft, between these two methods. As Ktc is nearly linear (Ktb is linear) the load distribution factor kload will be negligibly affected. However, the numerical integration of the contact line deflection does require a smooth function, (taken to the limit of zero reference depth infinite deflection of the contact line will be predicted), and so a tooth bending influence function based on the deeper reference depth will integrate more readily. Vedmar and Steward only model the point load deflection (with relatively crude (too coarse) F.E. meshes). Errors due to F.E. modelling will be greater in Vedmar, since his depth is close to the singularity at h' = 0.

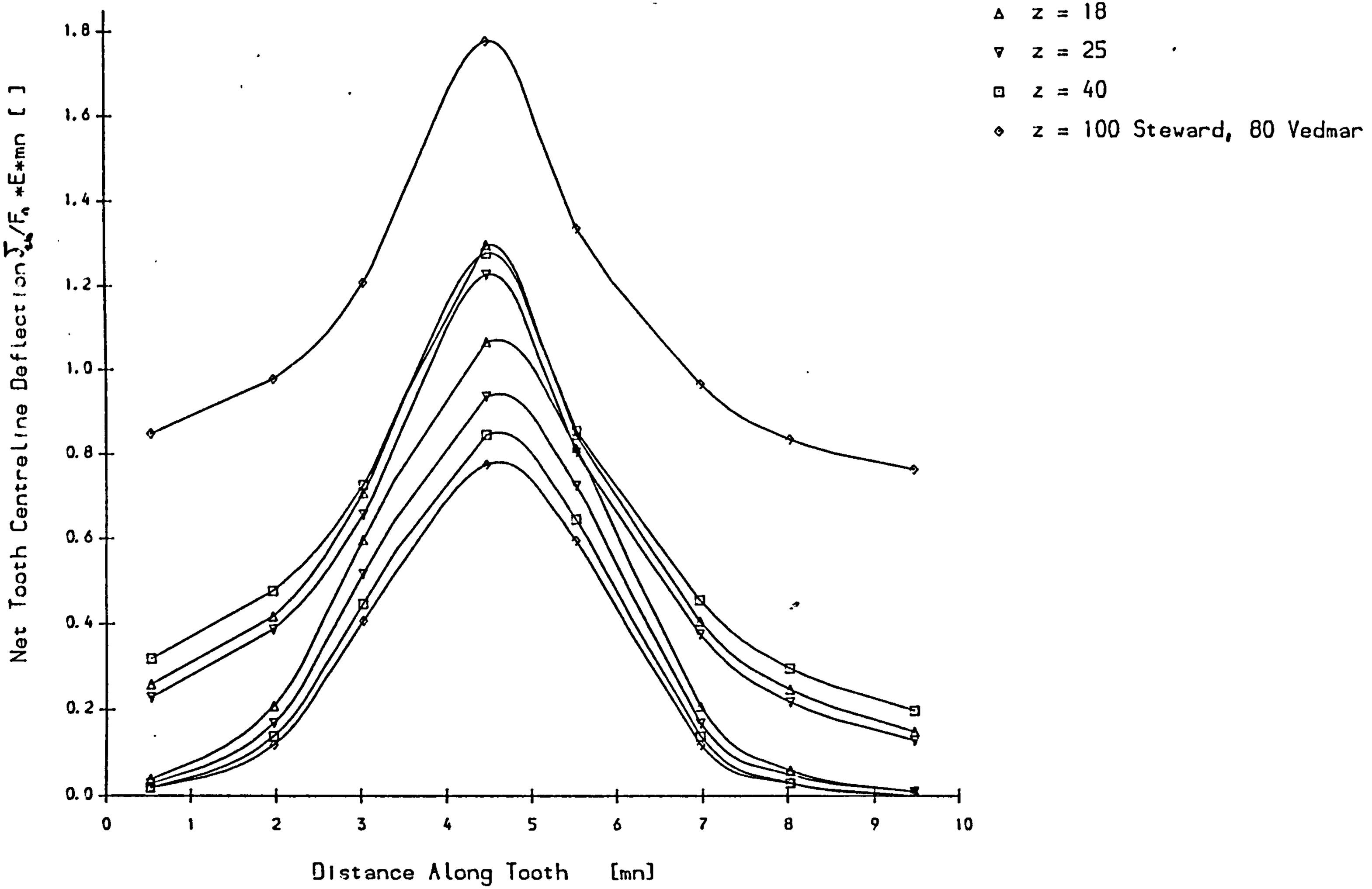

Fig 4.2 Comparison Of Ref. Dia. Master Curves F(z'). Note: Vedmar is lower of each pair of curves.

4.2.2 Comparison of Theoretical Single Tooth Stiffness Results

Figures 4.3 and 4.4 show the calculated stiffness of a single tooth pair according to the various published theories as a function of z and zF. Where the gear body deflections are small (small numbers of teeth) there is good agreement between the values given by all three theories. For larger numbers of teeth, however, Steward gives much lower values of stiffness (higher compliance) due to the inclusion of the substantial 'torsional' compliance of the gear body (ie the rotation of the "rim" relative to the centre of the shaft.

The significance of this additional gear body compliance is shown in Fig. 4.4 in which the tooth stiffness has been calculated from the deflection of the loaded tooth relative to the adjacent loaded tooth. This effectively removes the "rim" rotation component of the gear body compliance, and corresponds roughly to the datum assumed by Weber.

The relative tooth stiffness is given by:

$$c'r = wbm/(\delta_t' - \delta_k') \qquad (4.9)$$

It is generally accepted that compliance of an individual gear tooth decreases as z increases due to a change in shape of the cantilever. This is shown quite clearly when the gear body component of compliance has been removed. All three theories show the same trend in Fig. 4.4 although the agreement between the three theories, as shown in Fig. 4.5, is not good.

The variation of stiffness of one tooth with z is observed in Fig. 4.3 & 4.4 by the fact that each pinion is meshed with several tooth numbers z2. The variation of the stiffness of an individual tooth with z can be investigated by considering only 1:1 ratios, so that the two meshing teeth are identical, with a resultant mesh stiffness c' equal to half that of each tooth.

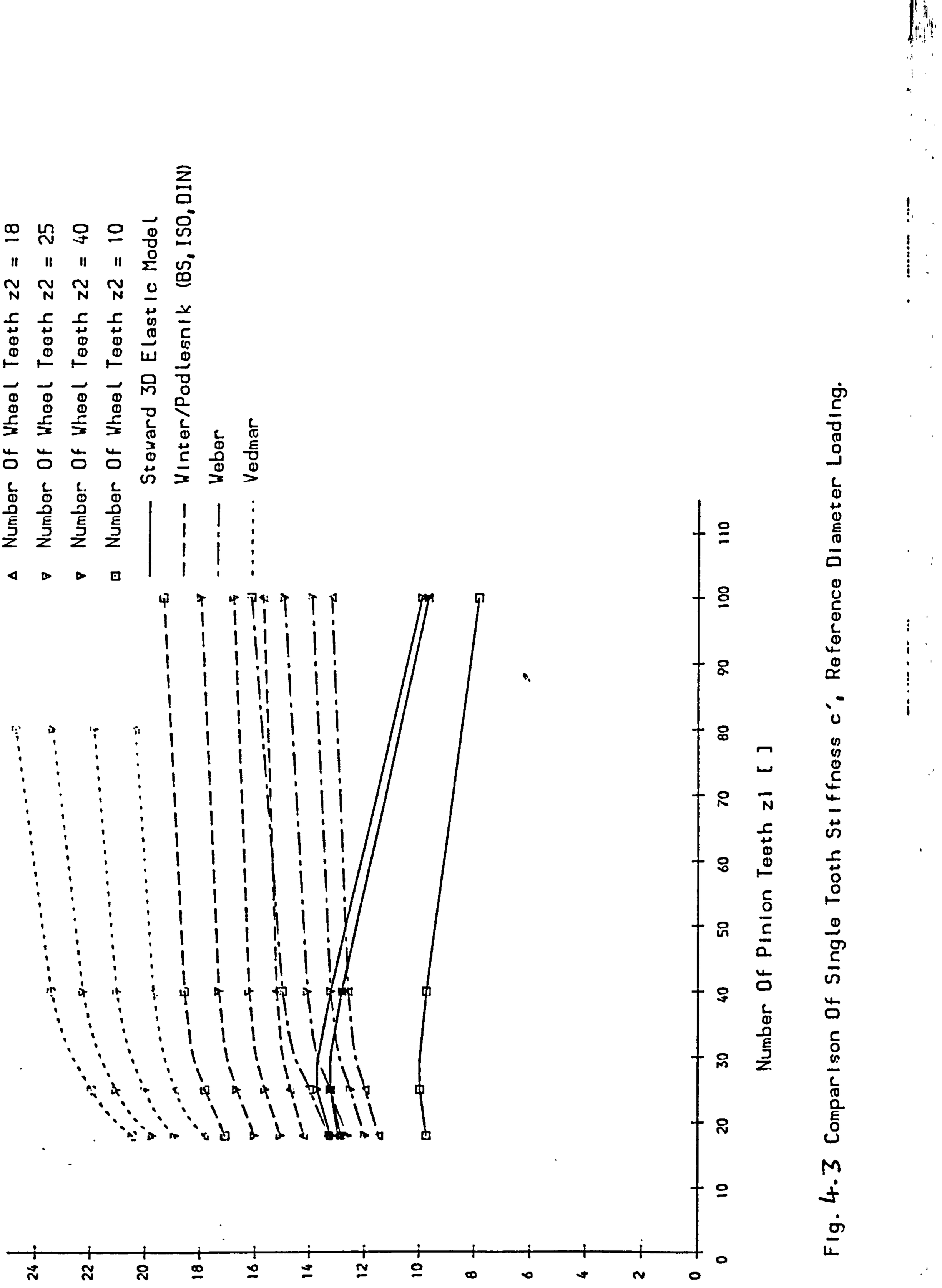

Fig. 4.3 Comparison Of Single Tooth Stiffness c', Reference Diameter Loading.

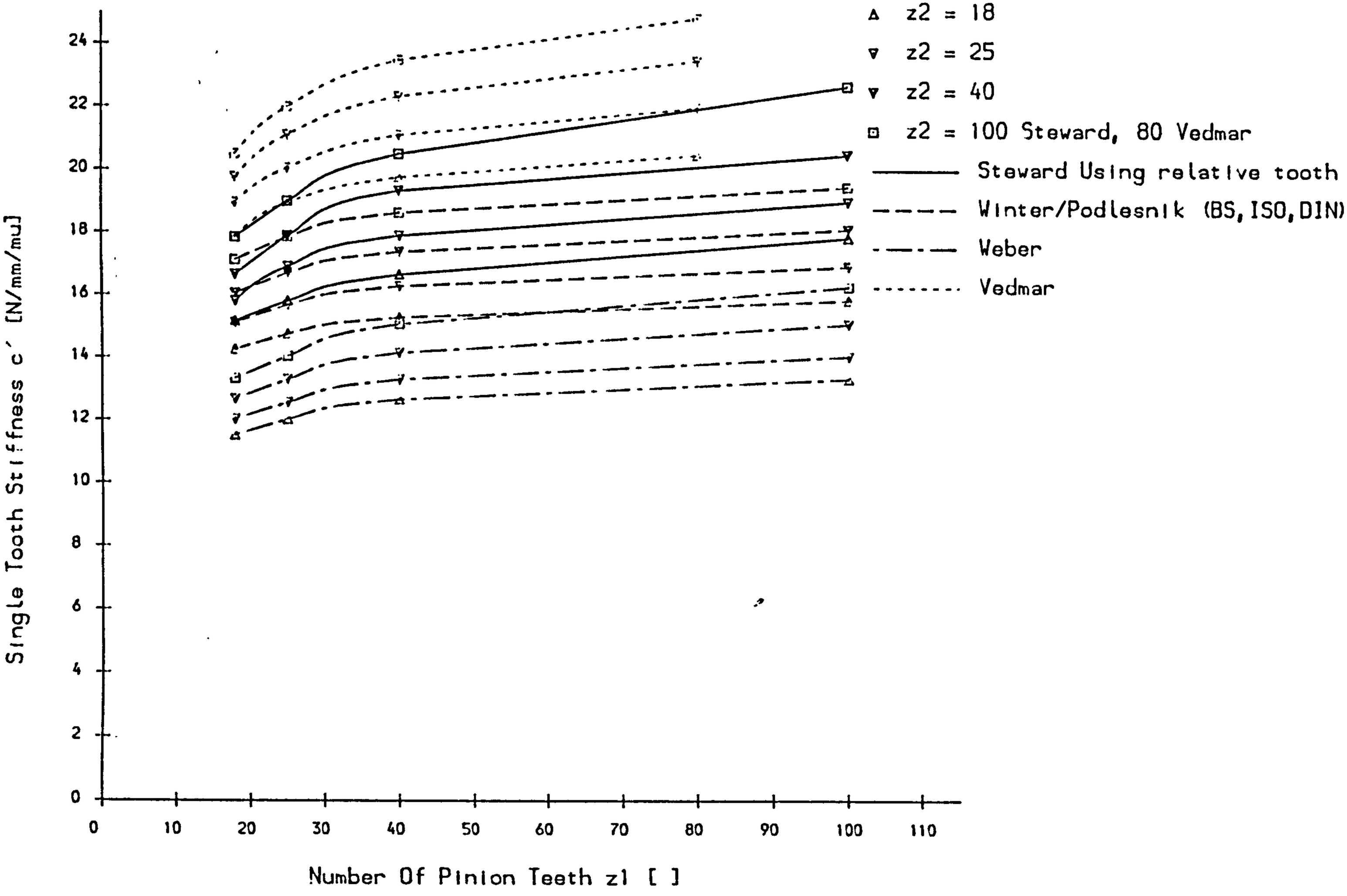

Fig. 4.4 Comparison Of Single Tooth Stiffness c', Reference Diameter Loading.

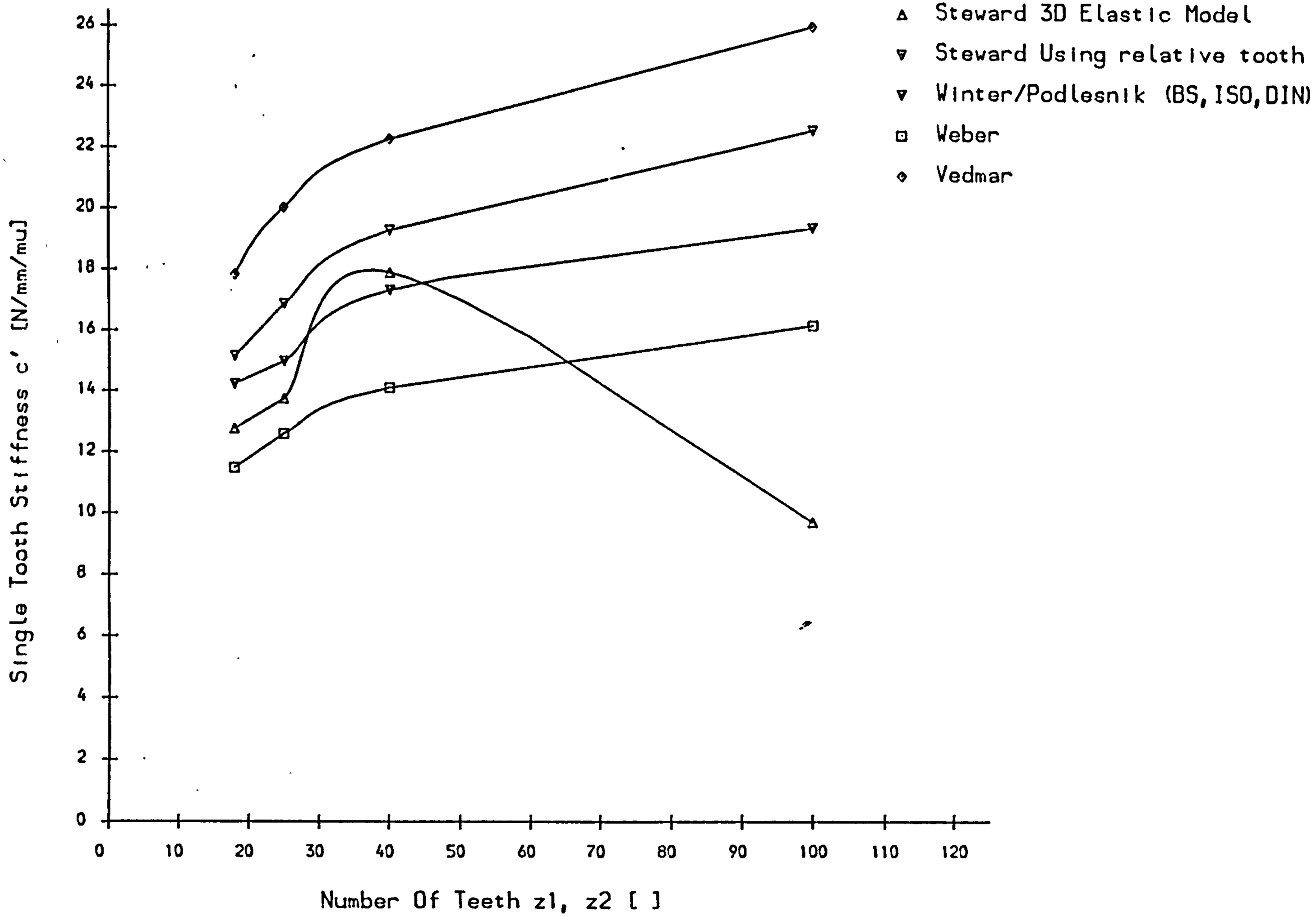

Fig 4.5 Comparison Of Single Tooth Stiffness c', Reference Diameter Loading.

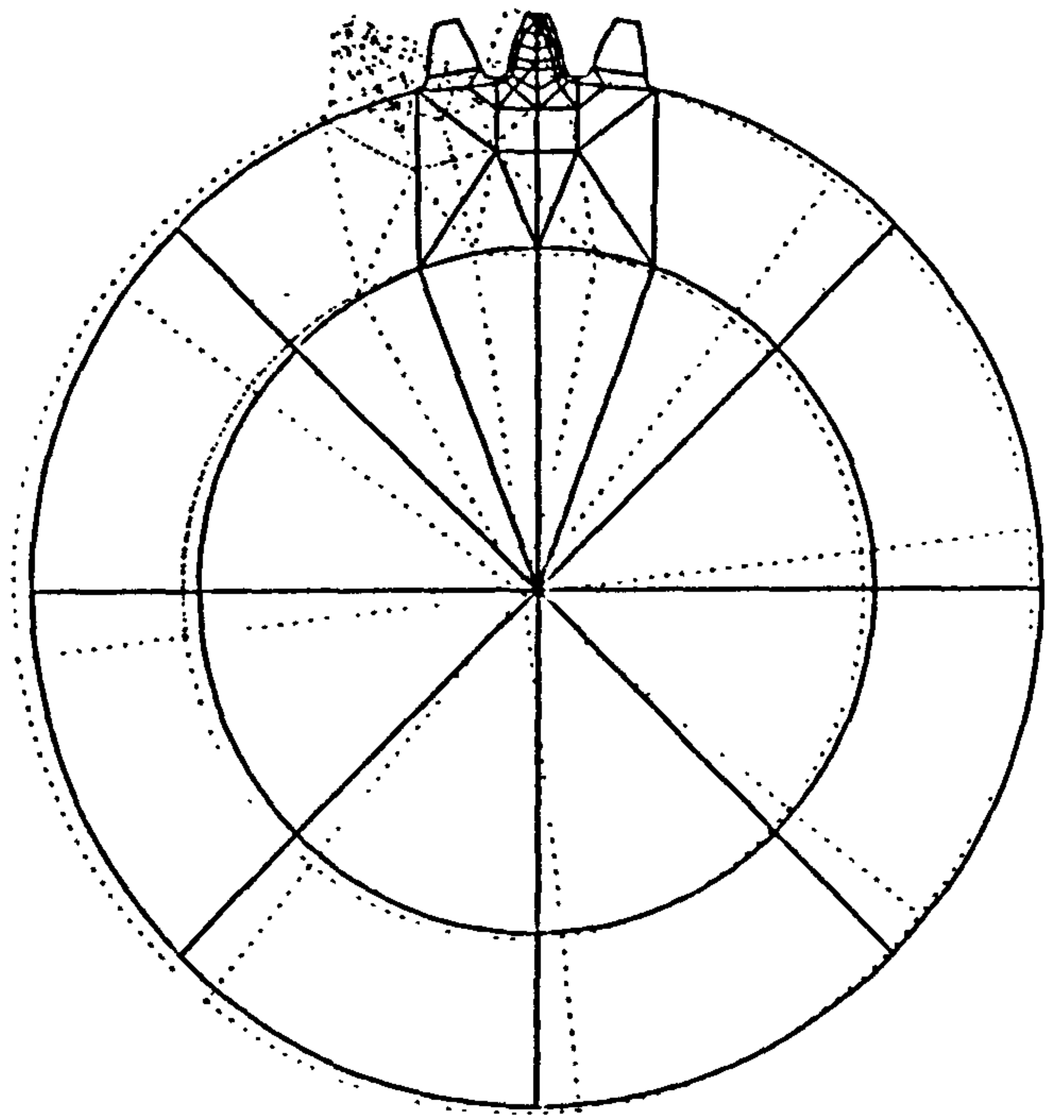

PAFEC

VIEW FROM X = 0.0000
Y = 0.0000
Z = 1.000 0

Z TOWARDS VIEWER

Fig 4.6

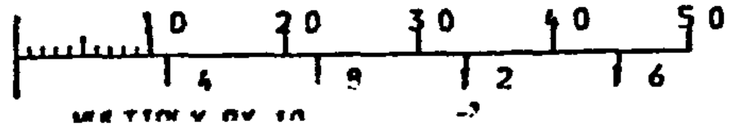

MM.
STRUCTURAL UNITS

LOAD CASE = 1
DISPLACED SHAPE SHOWN DOTTED
SCALE OF DISPLACEMENTS =
0. 3183E - 5 UNITS/CM

ELEMENT GROUPS= 6, 16.

DRAWING NO. 1
SCALE = 0. 2800

4.2.3 Significance of Tooth Stiffness Values

Depending on the type of analysis being carried out, a different tooth stiffness will describe most accurately the behaviour of the gear mesh in a simplified 2D mesh model. A full 3D elastic/plastic model will always describe the behaviour correctly but may be prohibitively expensive in manpower and computing time.

For static stressing of gear teeth during STC contact, (e.g. OPSTC used in BS[B3], ISO method B[I5], DIN[D3]), by definition only one tooth pair is in contact. The single tooth stiffness must be used in this case based on the absolute compliance of the contact line and calculated for the correct phase of mesh.

Note: BS, ISO, DIN use the so called mesh stiffness c_γ for tooth stressing which is typically about 40% greater than c'; AGMA correctly uses c', although the AGMA standard makes only a relatively crude approximation for the stiffness.

For estimating load sharing during double tooth contact it is the relative deflections of the two meshing gear pairs that determines their behaviour. In this case either the relative tooth compliance may be used, or the absolute compliance along with the compliance of the adjacent tooth. If the 2D analysis assumes that each tooth is only deflected by its own tooth loads (as in the BS, ISO, DIN calculation of $K_{H\alpha}$) then the relative tooth compliance c' must be used. The fact that most authors have implicitly calculated the relative compliance (by ignoring the gear body compliance) means that the stiffness values used in the standards for this purpose are reasonably correct. A better approach, however, is to recognise that loads on both meshing tooth pairs influence the deflections of each, and use the correct absolute compliances of the 'loaded' and adjacent tooth to determine how it is shared. Static load distribution of gears in the presence of errors is dealt with in Chapter 5.

For dynamic/vibration analysis of gears it is the inertial forces that are of prime concern. If the gear were to vibrate torsionally as a rigid body, use of the absolute contact line compliance would be appropriate. However, the gear is not rigid so the effective compliance will depend on where the inertial mass of the gear is

deemed to be concentrated. For a thin-rimmed gear, for example, with most of its mass in the rim, the relative (adjacent tooth) compliance c_r' would probably be most appropriate. For solid gears, however, a value somewhere between c_r' and c' is indicated. Fig. 4.6 shows the deflection of a 40 tooth gear from which an estimate of the 2D contact compliance at a given datum diameter could be extracted.

4.3 Two Dimensional Finite Element Model of Seager's Test Gear

Seager's experimental rig [S3] is representative of tests carried out on spur (and helical) gear compliance. A 100 N/mm load has been applied to the tip of a 3/4" rack tooth restrained along the bottom face, (Seager loaded two mirror image blocks together).

Fig. 4.7 shows the F.E. analysis of half of Seager's test gear. The mesh has been extended in the x and/or y direction, (relative to point 0), to investigate the change in deflection and root stress, (Fig. 5.0).

The peak tooth root stresses decrease by 5% if the adjacent tooth is not modelled. Fig. 4.8 shows the tooth tip surface and centre-line deflections.

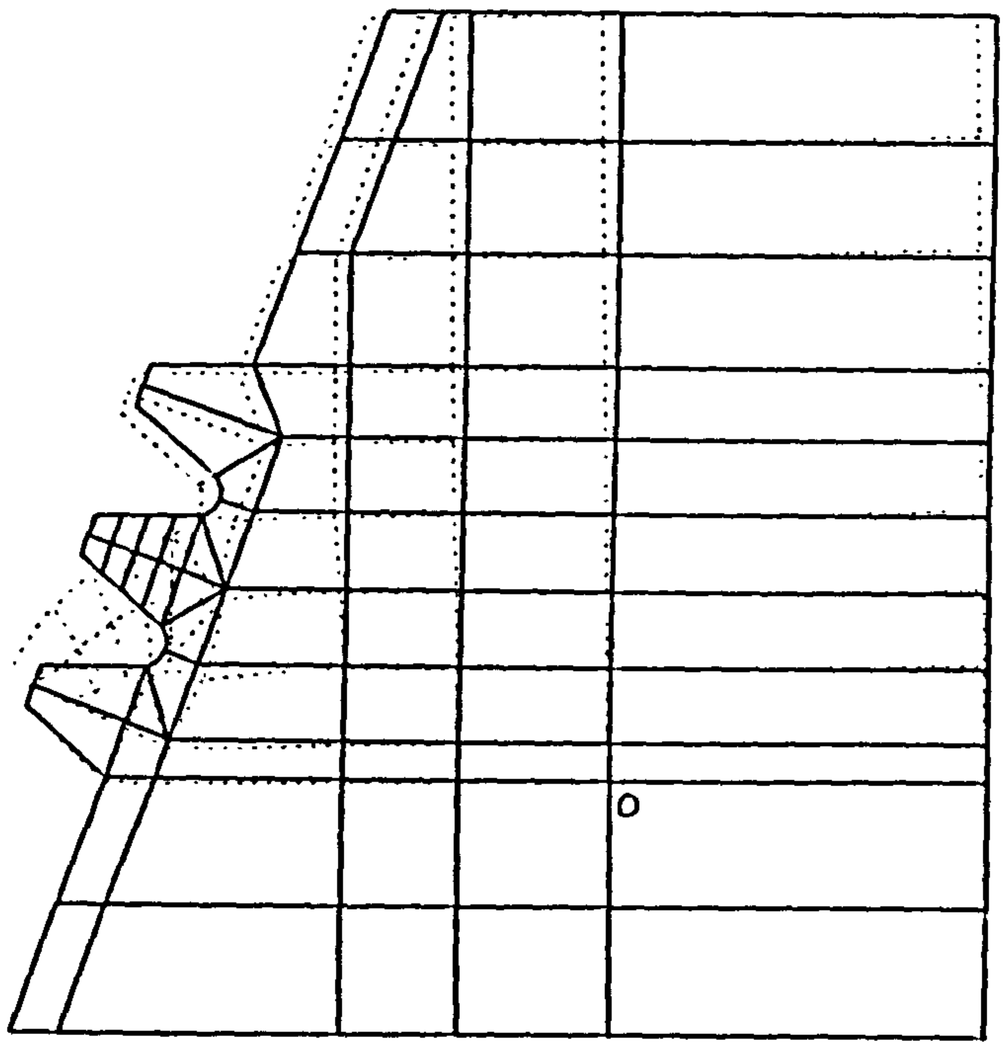

PAFEC

VIEW FROM X = 0.0000
Y = 0.0000
Z = 1.000

Z TOWARDS VIEWER

LOAD CASE = 1
DISPLACED SHAPE SHOWN DOTTED
SCALE OF DISPLACEMENTS =
0. 3527E - 5 UNITS/CM

WHOLE STRUCTURE DRAWN
AS DEFINED IN FRONT. ORDER

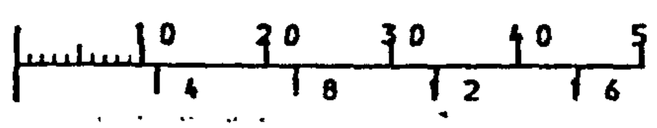

DRAWING NO. 1
SCALE = 0. 2800

Fig 4.7 F.E. Analysis of Seager's Test Gear: The Effect of the Gear Body on the Tooth Contact-Line Compliance

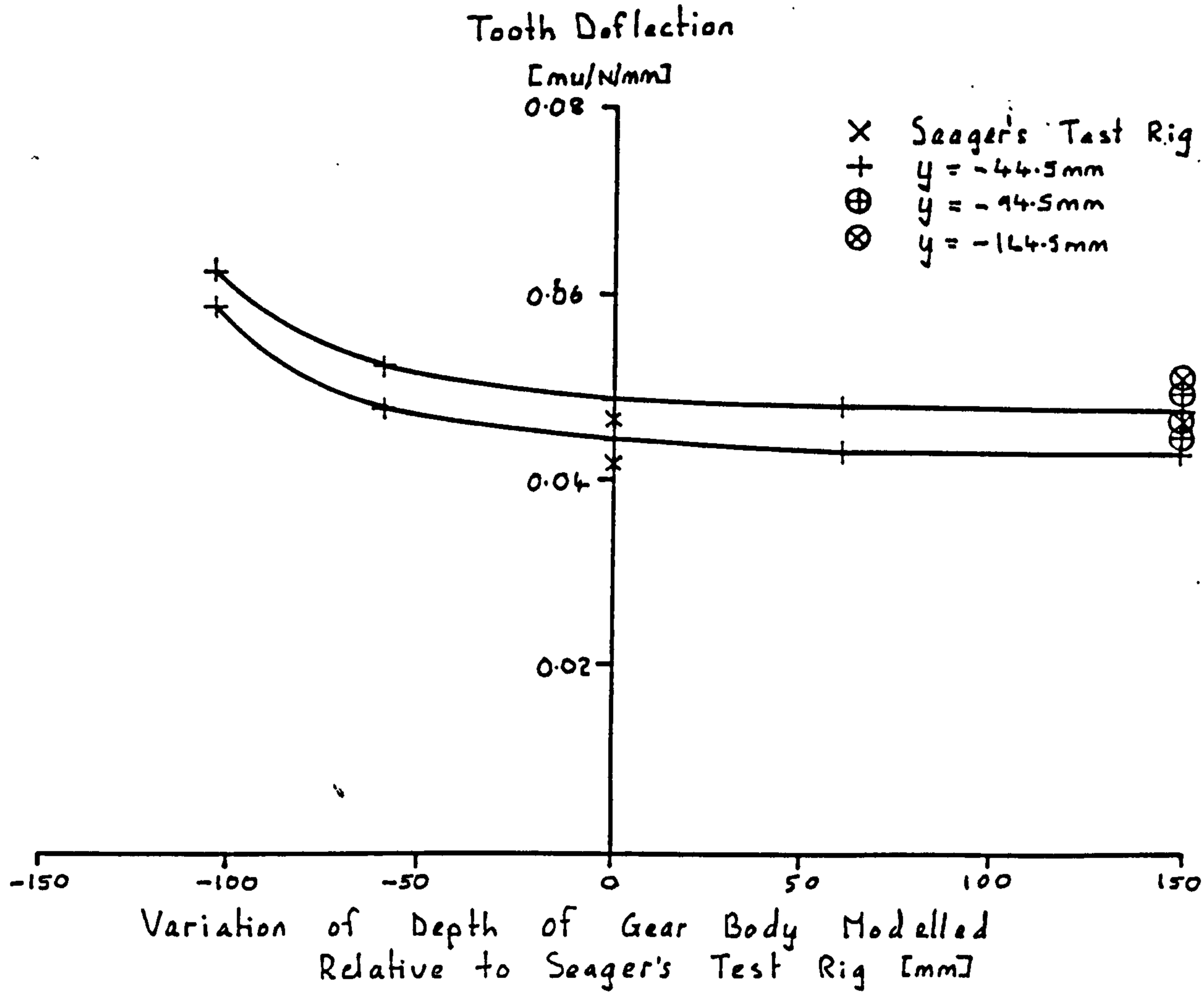

Fig. 4.8 2D F.E. Tooth Contact Line and Centre-line Deflections vs. Gear Body Dimensions

The gear tooth deflection as an encastre cantilever is modelled correctly by Seager (and by all published experimental work). The rotation of the tooth root on the elastic gear body is a localised effect and is modelled correctly by Seager, (x = 0 to -150mm), shown by the slope having nearly reached zero at x = 0. Determination of the correct gear tooth translation requires modelling of the entire gear body. Comparing x = 0 to x = 150mm shows a 7% increase in compliance. The points at x = 150mm include the compression of the extra gear body modelled. This model only serves as a comparison of tooth compliance. As it is based on a rack profile it is difficult to compare with a complete gear model which has an infinite gear body.

*****

CHAPTER 5

EFFECT OF MANUFACTURING ERRORS AND PROFILE MODIFICATIONS ON LOAD DISTRIBUTION

5.1 Introduction

Chapter 2 set out the theory for calculating the contact stresses in real spur gears by generating a 3D elastic model of the meshing gear teeth. Appendix 2.1 explains the program SPURDIST which implements the theory on a micro-computer. In this chapter the program SPURDIST is used to investigate the effect of manufacturing errors and profile modifications on the peak gear tooth stresses (primarily contact stresses).

The BS/ISO/DIN standards have been used to provide comparative values of calculated loads and stresses. SPURDIST only calculates the load distribution and contact stress in the meshing gears. Calculation of tooth root bending stresses σ_F has been based on the BS/ISO/DIN two dimensional formula using peak specific loads output from SPURDIST.

The supporting shafts have been assumed infinitely stiff. Where significant shaft slope or curvature is present, its effects are entirely equivalent to lead errors/corrections of the same form (ie flank misalignment or crowning).

The elemental tooth tolerances examined have been mostly based on those given in BS 436:part 2[B3]. Profile tolerances can be split into profile form tolerances, ff, and profile angle tolerances values based on DIN 3962 [D6].

The stresses are calculated for OPSTC mesh except where pinion root contact conditions give greatly increased contact stresses σ_H due to the smaller effective curvature of the flanks. .

```
**********************************
* DU436. Design Unit Newcastle Univ *
**2000****871216**********************
Disk: BSDATA  File: JHS1     23 Feb 88
```

Pinion:Induct.or Flame Hard. HV550				
Wheel :Induct.or Flame Hard. HV550				
Material quality		B	B	
CL.A Flank	RaH	1.0	1.0	mu
root	RaF	3.0	3.0	"
Case depth	ceff	3.20	3.20	mm
	clim	3.20	3.20	"
Pitting permitted?		NO		
Lube. viscosity nu40/nu50		168/100		

Number of teeth	z	18	54
Normal module	mn	10.000	
Transv. module	mt	10.000	
Gear ratio	u	3.000	
Closed centres	a	360.000	
Ref. centres	a0	360.000	
Facewidth	b	150.000	150.000
Ref. circle dia	d	180.000	540.000
Base circle dia	db	169.145	507.434
Pitch circ. dia	dw	180.000	540.000
Tip diameter	da	200.000	560.000
Root diameter	df	155.000	515.000
Tooth depth	h	22.500	22.500
Ref.pr.ang.Norm	alphan	20.0000	
Ref.pr.ang.Tran	alphat	20.0000	
Wkg.pr.ang.Tran	alphatw	20.0000	
Ref. helix ang.	beta	0.0	
Base helix ang.	betab	0.0	
Addend.mod.coef	x	0.0	0.0
Sum of " coeffs	x12	0.0	

Transv.cont.rat	epsalpha	1.649	
Overlap ratio	epsbeta	0.0	
Total cont.rat.	epsgamma	1.649	
Bsc rack dedend	hfp/mn	1.250	1.250
" " root rad	rofp/mn	0.250	0.250
Protubce u/cut	spr/mn	0.0	0.0
Root chord lgth	sFn/mn	1.883	2.196
Bending mom.arm	hF/mn	1.007	1.105
Root radius	roF/mn	0.504	0.415

Continuous duty			
Application fac	KA	1.000	
Dynamic factor	Kv	1.270	
Required life		10000	Hours
Load cycles		3.00E8	1.00E8
No. of planets	npla	1	
Total power	P	132.84	kW
Torque/npla	T	2537.0	7611.0 Nm
Tang.force	Ft	28188.9	N
R.P.M	n	500.0	166.7
Pitch line vel	v	4.712	m/s
Sliding vel.	vg	1.576	1.822
Singl.stiffness	c'	16.49	N/mm/mu
Mesh stiffness	cgamma	24.51	"
Pin shaft dia.	dsh1	144.0	mm
Lead correction		None	
Accuracy grade		9	
Pitch tolerance	fpe	57.795	mu
Misalgnmt shaft	fsh	3.811	"
" manufac.	fma	54.579	"
Mesh misalgnmt.	Fbetax	59.649	"
Eff mesh misal.	Fbetay	48.500	"
Run-in allowce	yalpha	3.000	"

---TOOTH FLANK---

Face load fac.	KHbeta	3.157	
Transv.load fac	KHalpha	1.276	
Zone factor	ZH	2.495	
Elasticity fac	ZE	189.812	
Cont. ratio fac	Zepsilon	0.885	
Life factor	ZN	1.000	1.000
Lube/Speed fac	ZLZV	0.969	
Roughness fac	ZR	0.920	
Work hardg. fac	ZW	1.000	1.000
Matl. qual. fac	ZM	0.900	0.900
Size factor	ZX	1.000	1.000

---TOOTH ROOT---

Face load.fac.	KFbeta	2.665	
Transv.load fac	KFalpha	1.276	
Form factor	YF	1.731	1.37
Notch parameter	qs	1.870	2.648
Stress corr.fac	YS	1.865	2.19
Helix angle fac	Ybeta	1.000	
Life factor	YN	1.000	1.00
Sensitivity fac	Ydelta	1.028	1.038
Surf. cond. fac	YR	0.907	0.907
Matl. qual. fac	YM	0.900	0.900
Size factor	YX	0.950	0.950

---CONTACT STRESS(N/mm2)---

---BENDING STRESS(N/mm2)---

		U.T.S.		
		sigB	1800.0	1800.0
		sigBcore	800.0	800.0
Yield stress		sigFY	1535.3	1535.3
Resid. stress		sigR	-140.0	-140.0
		sigRcore	450.0	450.0
Endce. limit	sigHlim	1677.9	1747.8	
Permiss. stress	sigHP	1246.0	1402.1	
		sigFO	515.9	515.9
		sigFP	508.1	512.1
		sigFPcore	144.9	144.9
Contact stress	sigH	1118.5	1118.5	
		sigF	262.0	245.5
		sigFcore	50.6	40.0
SAFETY FACTOR	SH	1.20	1.25	
{ SHmin 1.00 }				
SAFETY FACTOR	SF	2.72	2.98	
{ SFmin 1.40 }				

Fig. 5.1

A typical wide faced spur gear mesh with z1:z2 = 18:54 and mn = 10mm and b = 15mn has been chosen as a basis for the comparison. Straddle mounting and a specific load of 200N/mm have been assumed. BS436:part 3[B3] makes provision for estimating the effects of elastic deflection fsh of the pinion shaft aswell as individual gear errors. Both are included in the results shown in Fig. 5.1 which are for BS accuracy grade 9, and which were obtained using the commercially available software DU436[D7] developed at Design Unit, Newcastle University. Where the module is altered the gears are geometrically scaled in all directions.

5.2 Effect of Helix Angle Errors

The main effect of $F_{\beta y}$ is on the face load factor $K_{H\beta}$ describing mal-distribution across the gear flank. The peak bending stress occurs at the OPSTC (defined kinematically in existing design standards), which is actually a function of the transmitted torque and compliance of the two meshing gear teeth and the adjacent tooth compliances. The BS/ISO/DIN standards calculate the face load factor $K_{H\beta}$ from equations 5.2 and 5.3

$$\frac{b_{cal}}{b} = \sqrt{\frac{2\,\omega_{bm}}{F_{\beta y}\cdot c_\gamma}} \qquad K_{H\beta} = \frac{2b}{b_{cal}} \quad \text{for } \frac{b_{cal}}{b} \leq 1.0 \qquad (5.1)$$

$$\frac{b_{cal}}{b} = 0.5 + \frac{\omega_{bm}}{F_{\beta y}\,c_\gamma} \qquad K_{H\beta} = \frac{2\,b_{cal}/b}{(2\,b_{cal}/b - 1)} \quad \text{for } \frac{b_{cal}}{b} \geq 1.0 \qquad (5.2)$$

where $F_{\beta y}$ = equivalent mesh misalignment
c_γ = mean mesh stiffness

To investigate the effect of gear accuracy, the mesh was re-analysed as in Fig. 5.1, with assumed accuracy grade between 4 and 10 (to cover the range of accuracies encountered in typical industrial gearing). For comparison with these results, a pinion helix angle error of ($F_{\beta y}$/b) radians was assumed and the overall load factor KLoad calculated at the OPSTC, using the program SPURDIST.

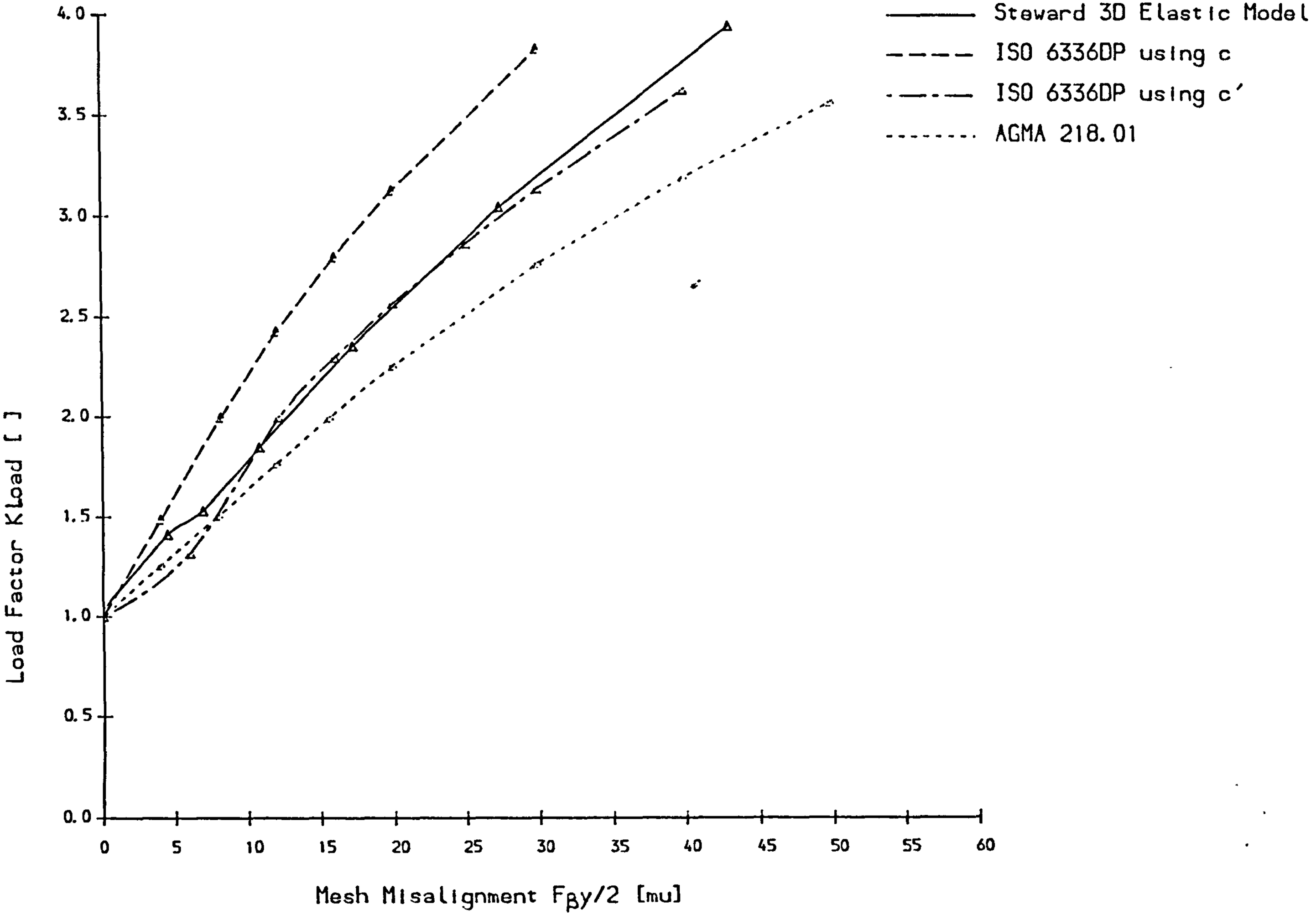

Fig 5.2 Load Factor vs Helix Angle Error, 10.0mm Module Gear

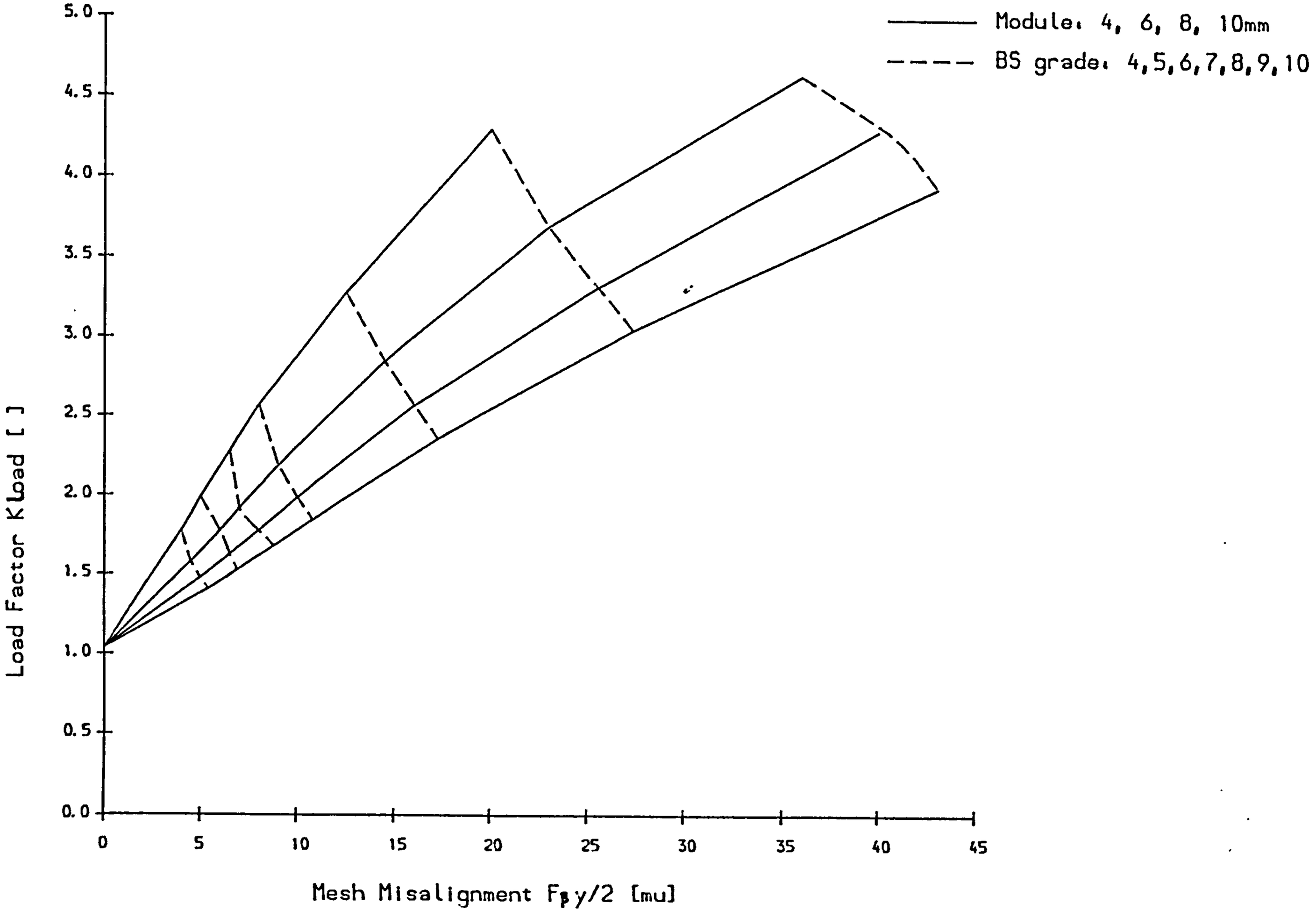

Fig 5.3 Effect of Module & Helix Angle Error on Load Factor Kload

From Fig. 5.2 it is clear that the BS/ISO/DIN standards overestimate KLoad. This is probably because they use the mesh stiffness c_γ rather than the single tooth (pair) stiffness c' in equation 5.1, 5.2. At OPSTC, use of c' is clearly logical (at least for spur gears) and as shown in Fig. 5.2, this gives much better agreement with the results from SPURDIST.

Fig. 5.3 shows the effect of gear accuracy, grade and size (module) on the values of KLoad obtained from SPURDIST. Equations 5.1 and 5.2 show that for geometrically similar gears, the load factor is a function of the ratio given in equation 5.4 (only c' is independent of module).

For gears with a fixed permissible root bending stress, the allowable specific load, and hence the elastic deflection decreases in proportion to the module, whereas for small module gears, the manufacturing tolerances/errors tend towards constant values. The ratio in equation 5.4 is thus always higher for small module gears, which thus have an inherently worse load factor kLoad.

5.3 Effect of Profile Errors

According to BS 436 the profile tolerance limit is defined by two parallel involutes between which the actual tooth profile must lie. In addition, no positive profile deviations may occur outside the central working third of the flank (Fig. 5.4).

DIN 3962 defines two parameters for profile tolerances; a profile form error ff (akin to a base pitch error); and a profile angle error $f_{H\alpha}$ (Fig. 5.4). For the purposes of this investigation only the effect of a profile error is considered, the effect of pitch errors are dealt with in the following section.

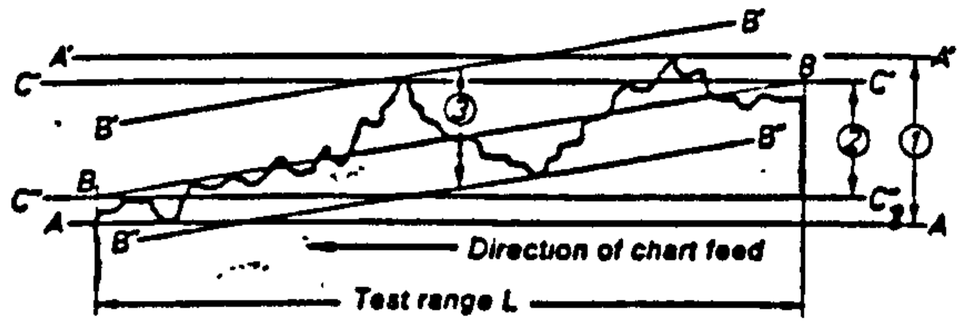

DIN

Figure 40. Flank deviations
Test diagram and survey of deviations

	Profile	Tooth trace	Generator
① ② ③	Total profile error F_f Profile angle error $f_{H\alpha}$ Profile form error f_f	Total alignment error F_β Tooth alignment error $f_{H\beta}$ Longitudinal form error $f_{f\beta}$	Total generant error F_E Generant angle error f_{HE} Generant form error f_{Ef}
Test range	Profile test range L_α	Tooth trace test range L_β	Generator test range L_E
BB	Averaging actual involute	Averaging actual tooth trace	Averaging actual generator
AA, A'A'	Nominal profiles which envelope the actual flank	Nominal tooth traces	Nominal generator
B'B', B"B"	Actual involutes which envelope the actual flank	Actual helices	Actual generator
C'C', C"C"	Nominal profiles	Nominal tooth traces	Nominal generator
	which cut the actual generators or tooth traces at the starting and finishing point, respectively, of the test range		

BS

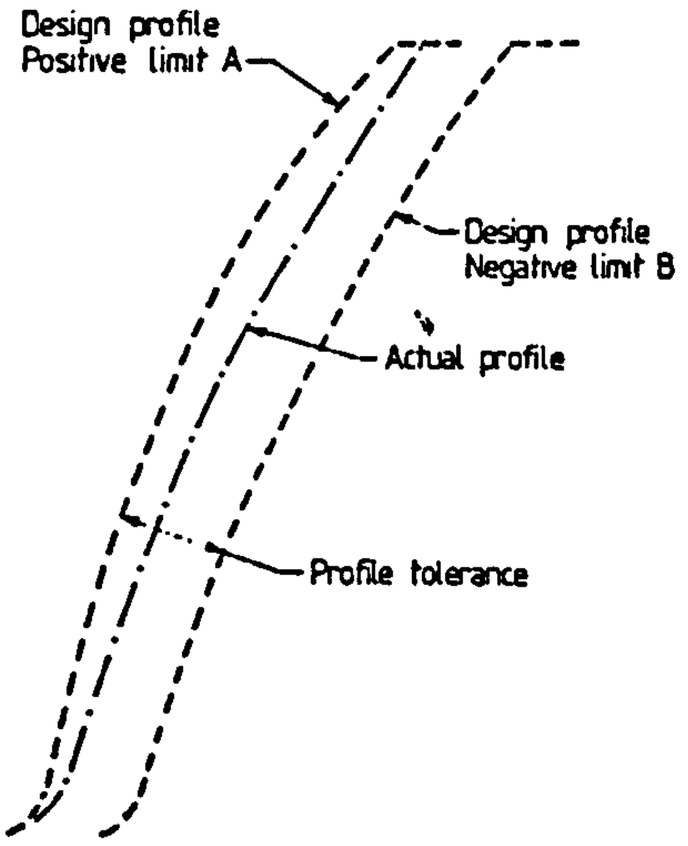

Figure 5a. Tolerance zone of tooth profile error

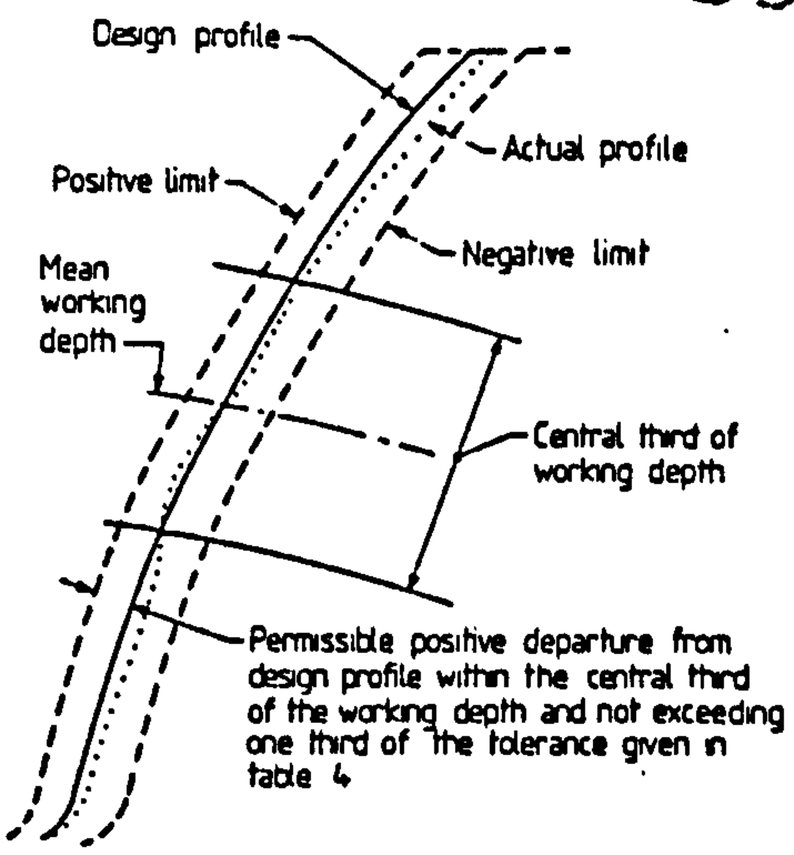

Figure 5b. Control of positive departures from design profile

Fig. 5.4 Definition of Profile Errors According to BS436:Pt.2:1970 and DIN 3962

Positive profile angle errors remove metal at the tooth root increasing the diameter of OPSTC. The bending stress at this point is increased, to a first approximation in proportion to the increase in the moment arm ratio.

The peak bending stress σ_F calculated by SPURDIST at OPSTC can be compared with the geometrically defined peak bending stress σ_{Fa} from the BS/ISO/DIN standards given by:

$$\frac{\sigma_F}{\sigma_{Fa}} = \frac{h_F}{h_{Fa}} = \frac{h_{Fa} + 0.5(d_{y1} - (d_{y1})_a)}{h_{Fa}} \qquad (5.4)$$

The peak contact stress occurs at IPSTC and can be directly compared with that calculated at the geometrically defined IPSTC by the standards. Fig. 5.5 shows the ratio of peak stresses compared with those determined from the BS/ISO/DIN standards as a function of $f_{H\alpha}$. Note: For BS grade 8 there is STC throughout mesh; positive profile errors <u>have</u> been permitted outside the central working third.

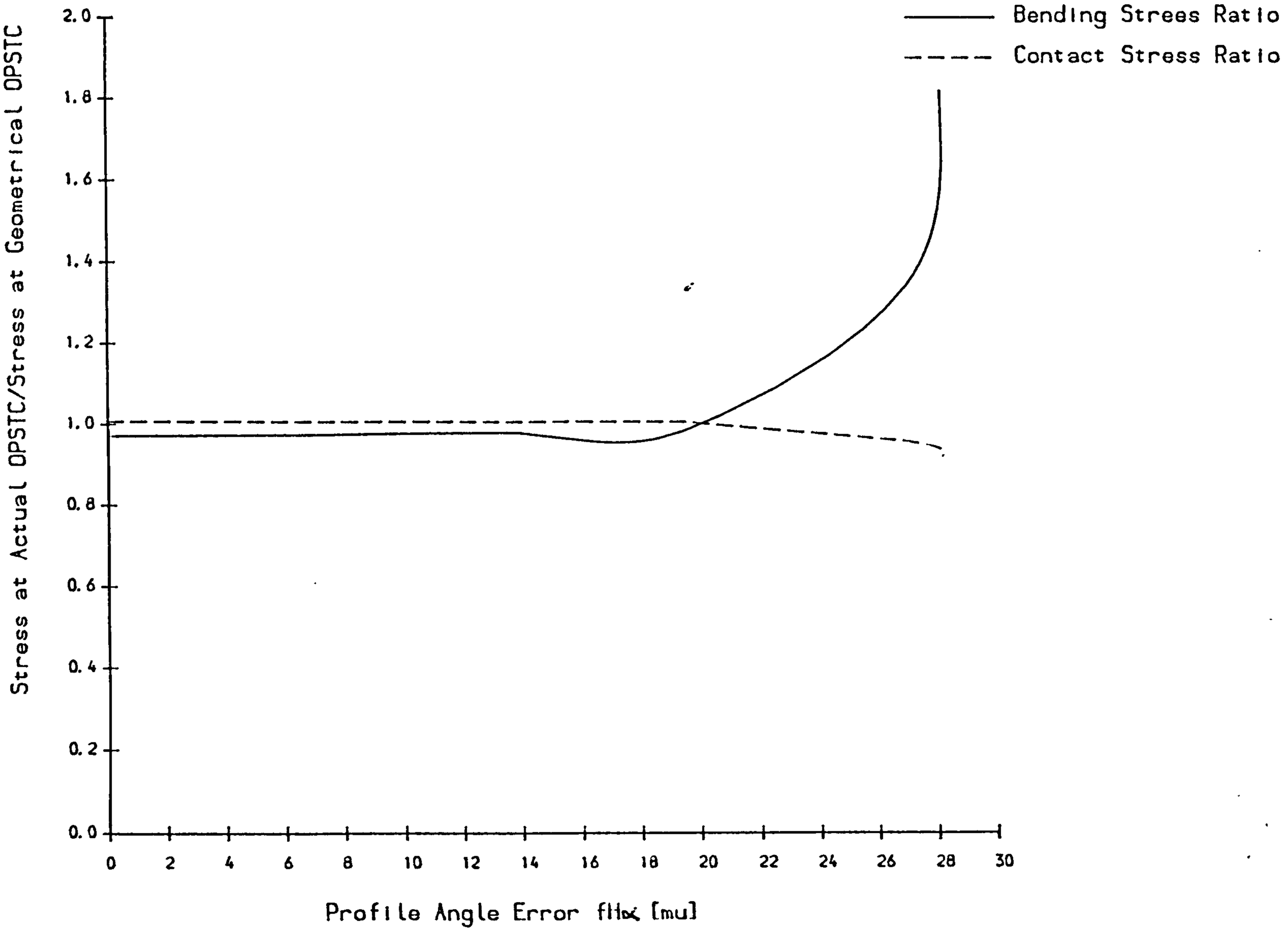

Fig 5.5 Effect of Module & Profile Angle Error on Peak Bending & Contact Stress

Consider in detail the case $f_{H\alpha}$ = 26.9 mn (1.345 mu/mm) (between grade 7 and 8) where there is just DTC during mesh. The adjacent tooth comes into contact when the difference between the elastic deflections exceeds the base pitch error plus any initial tooth clearance:

$$(\delta_{t1} - \delta_{t2}) - [(\delta_{e1} - \delta_{e2}) + c_t] > 0 \qquad (5.5)$$

where '1' = master tooth
'2' = preceeding tooth
$(\delta_{e1} - \delta_{e2}) = f_{p2}$ the base pitch error.

Fig. 5.6 plots the two parameters throughout mesh. For $f_{H\alpha}$ = 26.9mu there will never be DTC except in the presence of other errors.

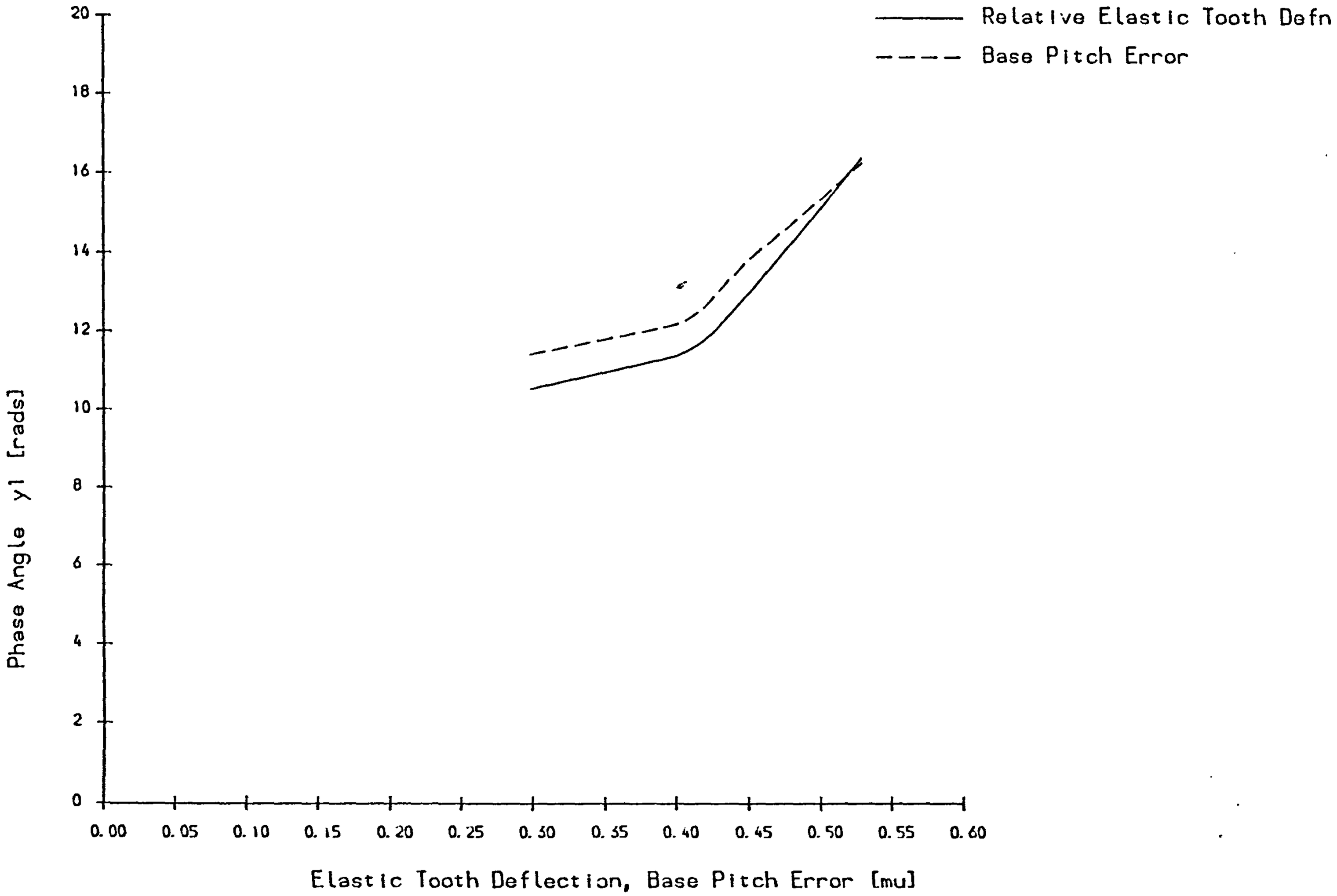

Fig 5.6 Effect of Elastic Tooth Deflection vs Base Pith Error on Region of DTC

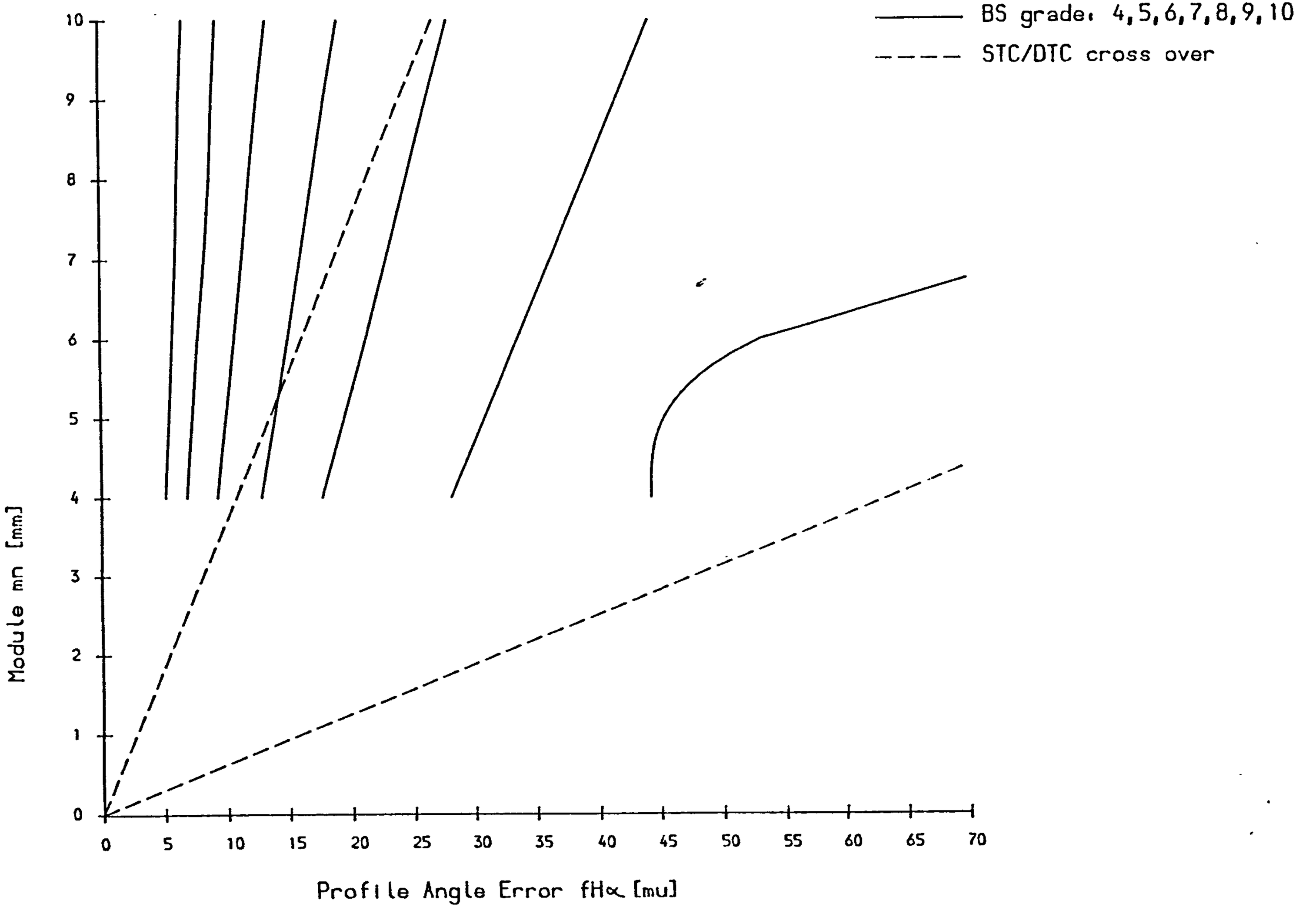

Fig 5.7 Effect of Profile Angle Error on STC Region (Pinion Tip Contact)

For geometrically identical gears of equal nominal σ_F both the base pitch error f_{pe} and the relative elastic deflection ($\delta_{t1} - \delta_{t2}$) are independent of module. For BS profile errors with no positive deviation outside the central working third the gear will behave as if having linear root relief up to the reference diameter. The error will have least effect at tip contact. Fig. 5.7 plots regions of STC and DTC for different BS grades.

Large module gears are less sensitive to profile angle errors due to the tolerance bands being less than proportional to module.

The region of DTC gives approximately reference diameter loading of the preceeding tooth (at dy = d there is no profile angle error), making the effect of positive errors outside the working third very dramatic.

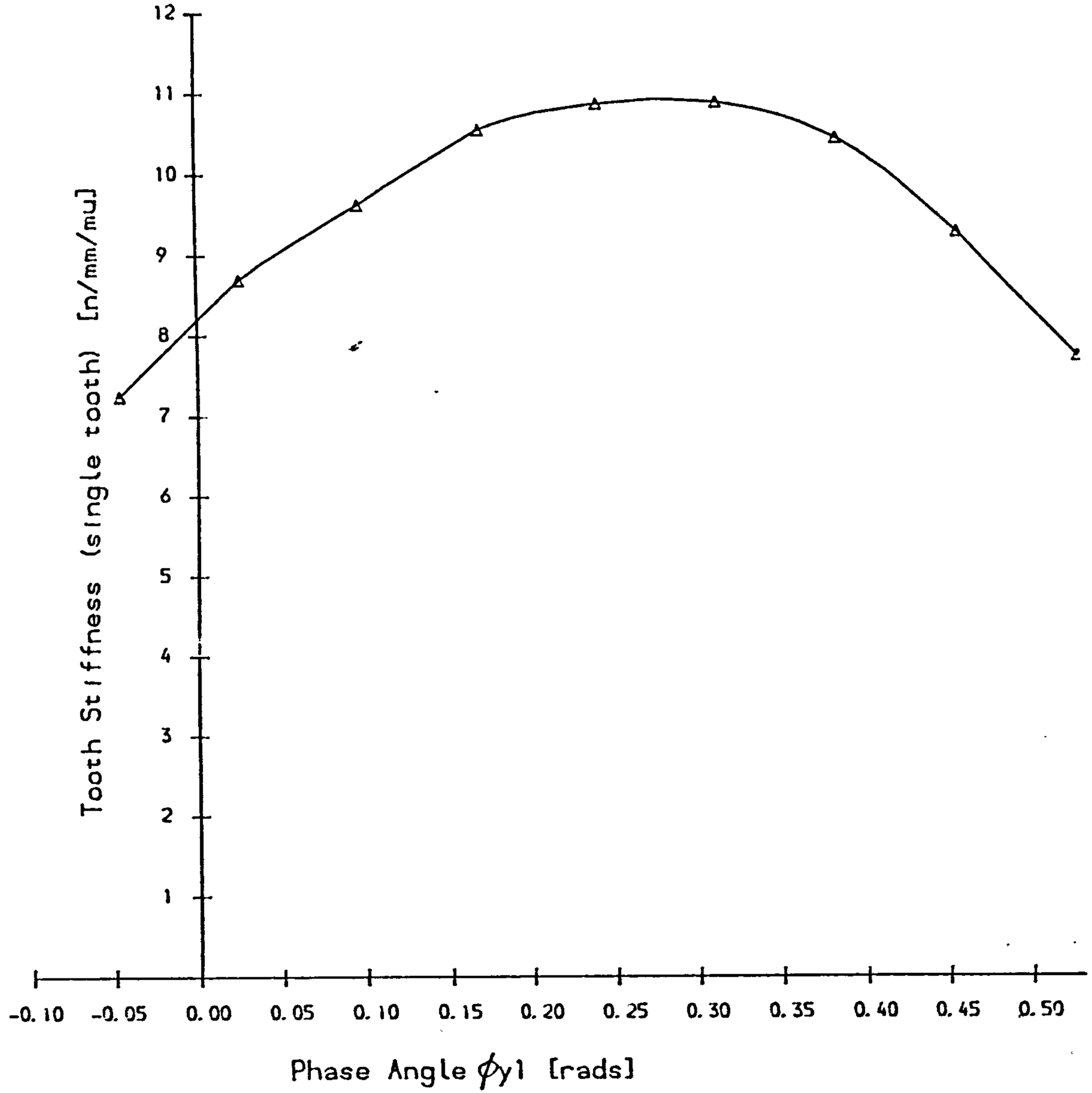

Fig 5.8 Spur Gear Tooth Stiffness Through Mesh

5.4 Effect of Pitch Errors

For a static analysis with, for nearly all cases, only one or two teeth in contact, only adjacent pitch errors need be considered. For wide face gears being investigated here (b/d = 0.8333) the effect of pitch errors can be dealt with two dimensionally provided the correct tooth compliances are used. The adjacent tooth compliance is independent of loading diameter giving a stiffness of c' = 26.67 N/mm/mu for this example.

Fig. 5.8 plots single tooth stiffness for the 18/54 10.0mm module mesh at ω_{bm} = 200 N/mm extracted from the program SPURDIST.

Considering only two potentially meshing tooth pairs in the presence of pitch errors fpe we have, from compatibility of deflection:

$$w_1\left(\frac{1}{c'_{11}} - \frac{1}{c'_{21}}\right) - w_2\left(\frac{1}{c'_{22}} - \frac{1}{c'_{12}}\right) - f_{pe}(ct_1 - ct_2) \qquad (5.6)$$

Assuming DTC sets ct1 = ct2 = 0. Consider only the phase of transition between DTC and STC sets w_2 = 0. Substituting the single tooth stiffness in (5.6) gives:

$$f_{pe} = w_1\left(\frac{1}{c'_{11}} - \frac{1}{c'_{21}}\right) \qquad (5.7)$$

which is the pitch error just producing STC throughout mesh (Fig. 5.9)

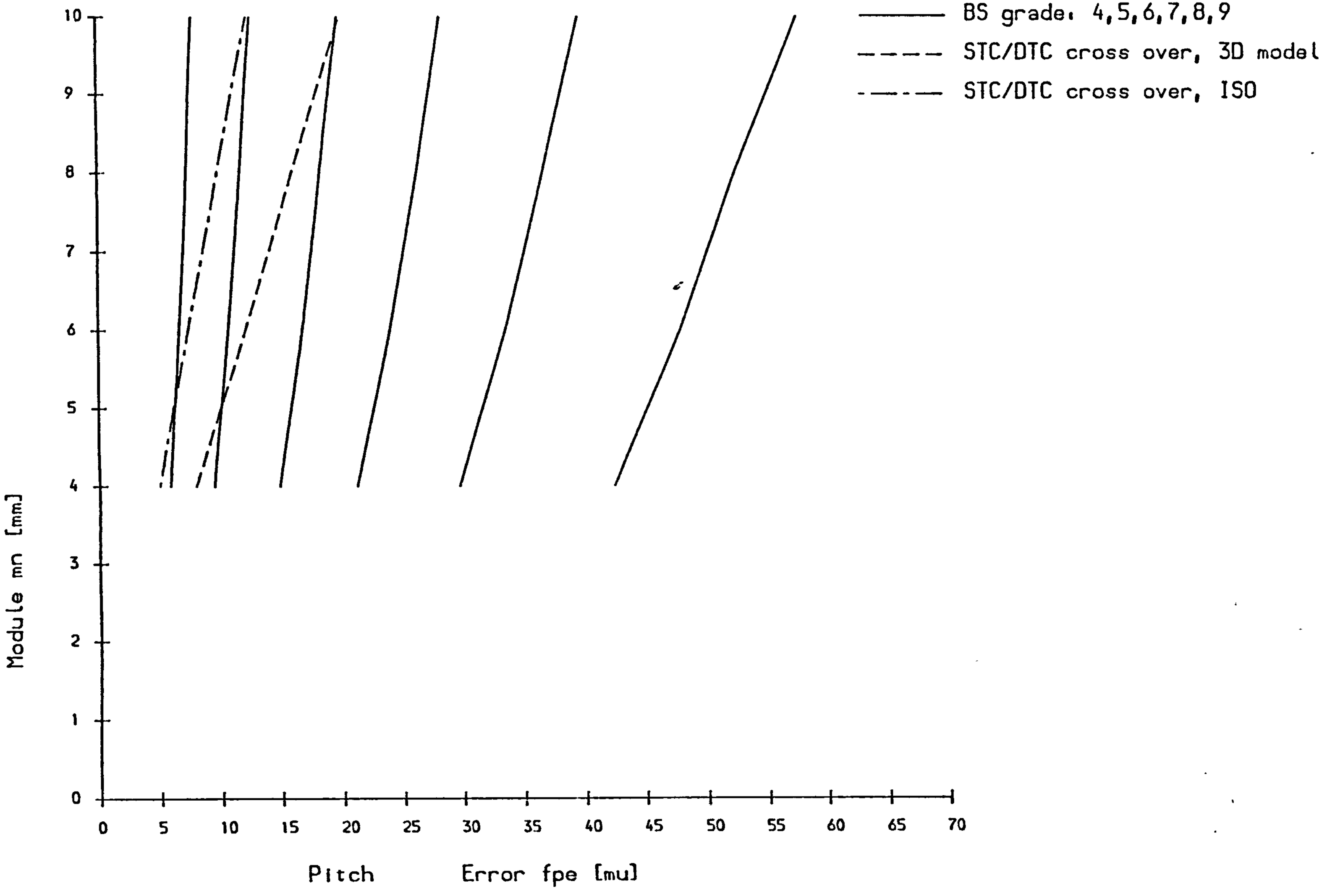

Fig 5.9 Effect of Pitch Error on STC Region (Pinion Tip Contact)

For geometrically similar gears just having STC contact throughout mesh we have

$$f_{p\alpha} = 2.009 m_n \; [\mu] \tag{5.8}$$

Consider the ISO specific load formula for a perfect longitudinal load distribution ($K_{H\beta} = 1.0$) and STC.

$$w_{bn} = Z_\varepsilon^2 K_{H\alpha} \frac{F_t}{b \cos\alpha} = Z_\varepsilon^2 K_{H\alpha} w_{bm} \tag{5.9}$$

substituting for Z_ε^2 and $K_{H\alpha}$ gives

$$1 = \frac{4 - \varepsilon_\alpha}{3} \frac{\varepsilon_\alpha}{2} \left[0.9 + \frac{0.4 c_\gamma (f_{p\alpha} - y_\alpha)}{F_t/b} \right] \tag{5.10}$$

Equation 5.10 reduces to:

$$(f_{p\alpha} - y_\alpha) = 1.24 m_n \; [\mu] \tag{5.11}$$

where y_α = running in allowance

Compared with equation 5.8 the actual pitch errors giving STC are 62% greater than those predicted by ISO. This is mainly due to the use of the mesh stiffness c_γ where STC occurs.

Fig. 5.9 shows the effect of $f_{p\alpha}$ on STC region.

This page is blank

5.5 Calculation of Contact Stress σ_H in the Presence of Pitch Errors According to BS/ISO/DIN

5.5.1 Contact Stress at Pitch Circle

According to BS 436:Pt.3:1986, ISO/DP 6336 and DIN 3990, the contact stress σ_H at the pitch circle for a gear pair with perfect longitudinal load distribution is given by:

$$\sigma_H = \sigma_{H0}\sqrt{K_{H\alpha}} = Z_H Z_E Z_\varepsilon \sqrt{\frac{F_{HE}}{b d_1}\frac{(u+1)}{u}}\sqrt{K_{H\alpha}} \qquad (5.12)$$

Where Z_H accounts for flank curvature and Z_E takes account of material properties. The effect of pitch (and profile) errors is accounted for by $Z_\varepsilon\sqrt{K_{H\alpha}}$.

Effect of $Z_\varepsilon\sqrt{K_{H\alpha}}$

According to ISO/DP 6336 accounts for the influence of transverse contact ratio on specific surface loading.

$$Z_\varepsilon = \sqrt{\frac{4-\varepsilon_\alpha}{3}} \qquad (5.13)$$

$K_{H\alpha}$ accounts for load sharing between adjacent teeth and for spur gears is:

$$K_{H\alpha} = \frac{\varepsilon_\alpha}{2}\left(0.9 + \frac{0.4\, c_\gamma (f_{p\alpha} - \gamma_\alpha)}{F_t/b}\right) \qquad (5.14)$$

where $1/Z_\varepsilon^2 \geq K_{H\alpha} \geq 1.0$

Note: $Z_\varepsilon\sqrt{K_{H\alpha}}$ can NEVER exceed 1.0 and is therefore a stress reducer to account for load sharing between adjacent teeth. For a contact ratio of $\varepsilon_\alpha < 2.0$ (most spur gears) and zero pitch/profile errors $Z_\varepsilon\sqrt{K_{H\alpha}} = 0.82$ underestimating the pitch circle stress

by 22.0% This error is additional to any error due to the incorrect tooth stiffness being used.

5.5.2 Contact Stress away from Pitch Circle

BS and ISO only calculate the contact stress at the pitch circle. DIN includes the pinion single contact factor Z_B to account for the change in equivalent flank curvature KD between the pitch circle and the geometrically defined IPSTC. DIN does not stipulate calculating the contact stress at the start of engagement where the highest stress often occurs on pinions with less than 20 teeth, (see Fig. 5.1D).

The very high slope of the contact stress curve near the start of engagement is due to contact occurring very close to the base diameter where the diameter of curvature D1 is zero. Contact stresses are plotted for perfect gears and also with an adjacent pitch error of greater than 12mu (BS grade 5) which will give STC throughout mesh. Note that this is for $K_{H\beta}$ = 1.0 (uniform face load). In the presence of all gear/shaft/casing errors larger pitch errors will be required to produce STC throughout mesh.

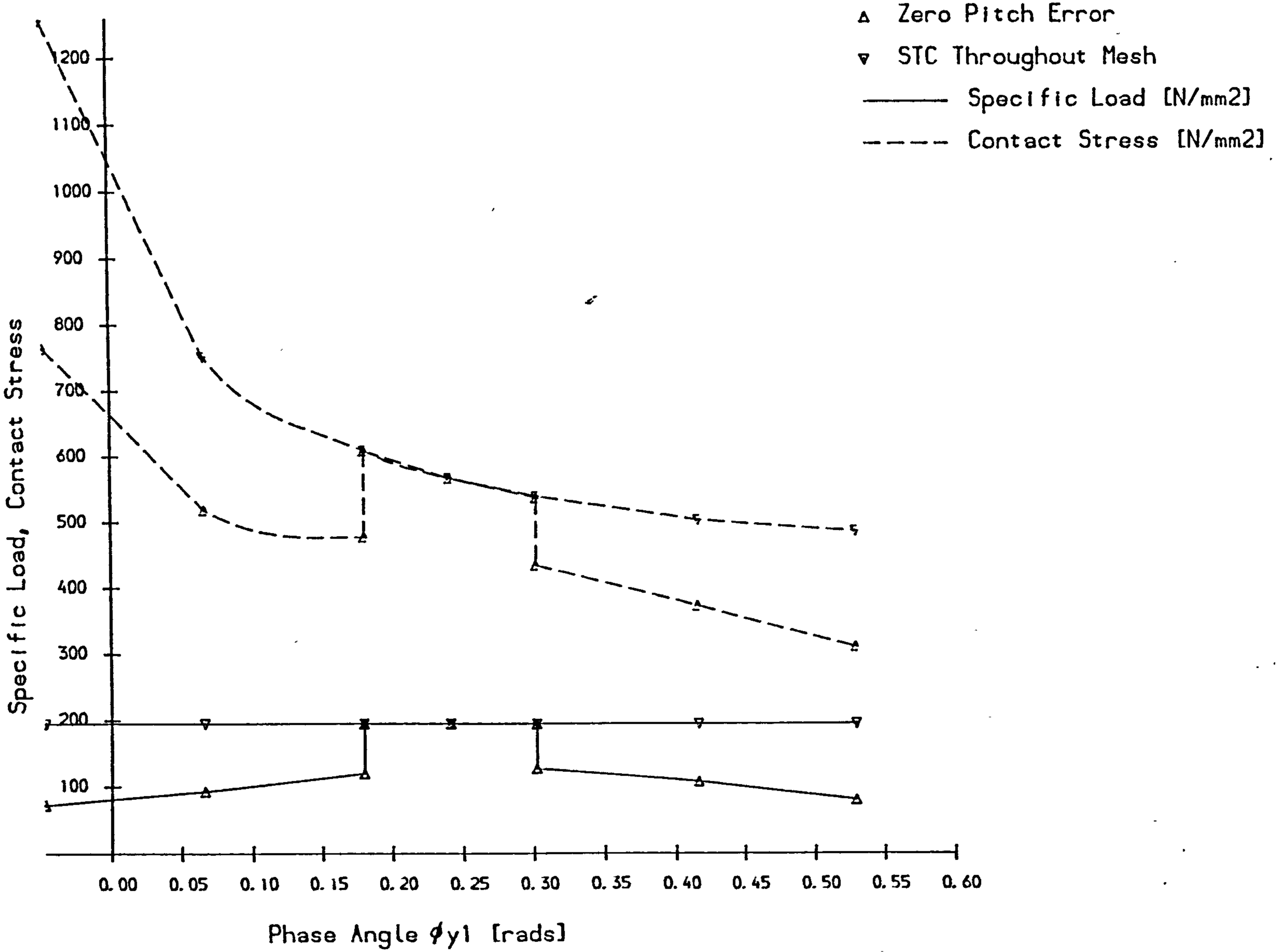

Fig 5.10 Variation of Contact Stress Through Mesh

5.6 Tooth Profile Modifications

5.6.1 Tip/Root Relief

Like pitch and profile errors, tip and root relief are 2D effects governing load sharing between meshing gear pairs. BS 436:Pt.2:1970 specifies upper limits of relief of Ca = 0.2mm applied linearly over no more than 0.6mn of the flank. BS 436:Pt.3:1986 recommends the following:

Height of relief $$C_a = f_p + 0{\cdot}06F_t/b + 5 \rightarrow 25 \ [mu] \quad (5.15)$$

applied in any combination to the pinion and wheel.

The pitch error f_{pe} may be +ve or -ve and with a specific load of $F_t/b \triangleq 20mn \times \cos 20$ the net tooth tip relief is:

$$C_a \geq 0 + 1{\cdot}13mn + 15 \ [mu] \quad (5.16)$$

Equation (5.16) is valid for the 18/54 example of any module.

Tip/root relief is applied to spur gears to reduce noise generated by the difference in mesh stiffness between STC and DTC (c' and c_y). For a small pinion (less than 20 teeth) it is desirable to reduce the specific load near the root diameter loading (small equivalent diameter of curvature). It is strongly recommended that tip/root relief be confined to the wheel tip wherever possible. Fig. 5.11 shows the 10.0mn module 18/54 mesh with wheel tip relief.

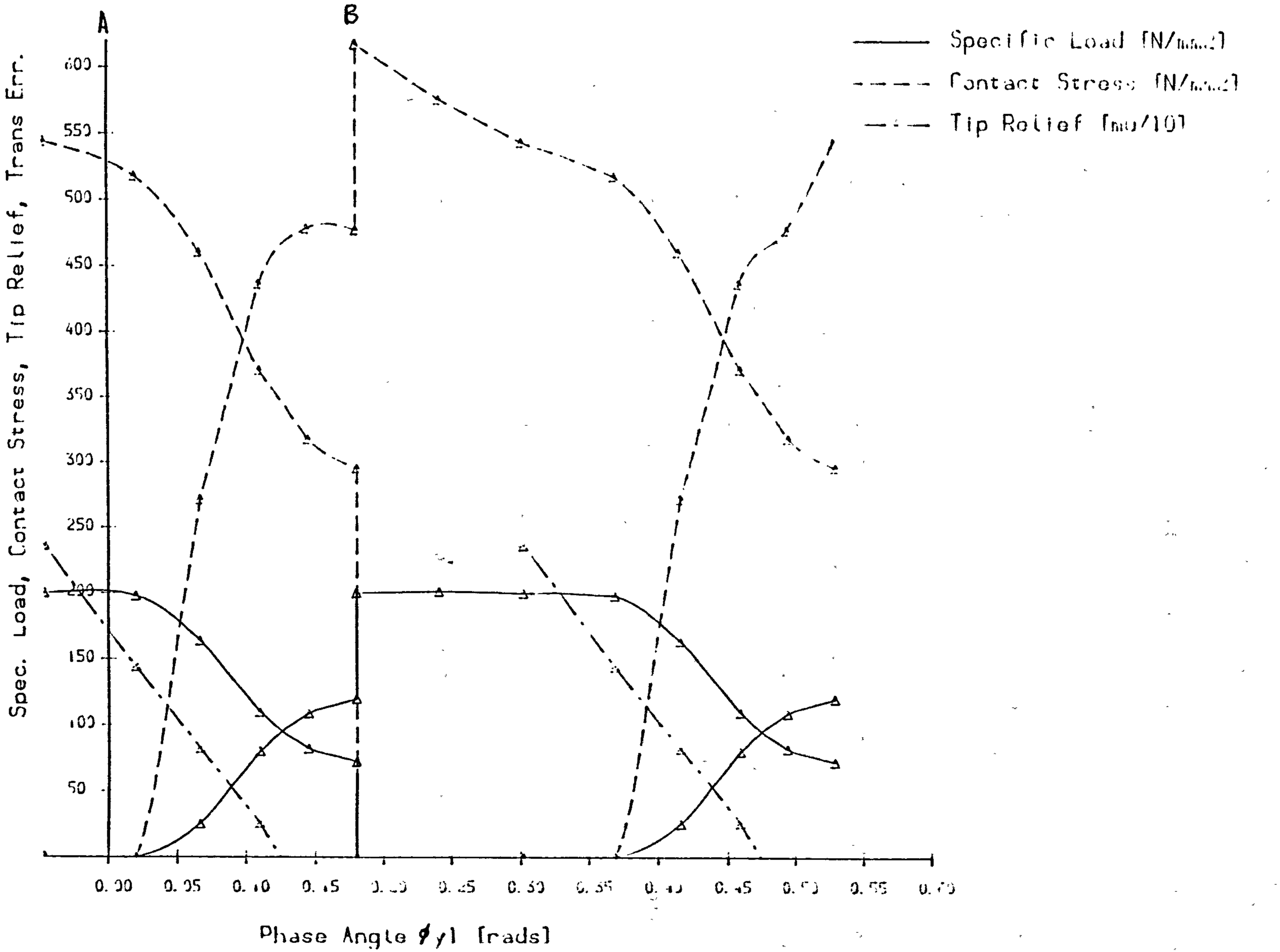

Fig 5.11 Effect of Wheel Tip Relief on Contact Stress

Note:

- Contact stress at point A would be 1274 N/mm2 if no tip relief were applied. Peak contact stress is now at point B (618 N/mm2), a factor of 2.1 smaller.

- Wheel tip relief increases OPSTC for pinion and thus the peak bending stress

- There is still a step change in transmission error ft in the DTC/STC transition (point B).

- To obtain a continuous transmission error curve, sufficient height and depth of tip relief would be needed to reduce the specific load to zero at point B.

5.6.2 Crowning

Crowning is a crude form of helix modification that partly compensates for manufacturing errors and gear deflections under load. Helix modification or lead correction applies the inverse of the contact line deflection to the gear profile at a given design torque especially applicable to drives with a fairly uniform load spectra. Helix modification requires knowledge of the total contact line deflection so has not been dealt with in this section.

BS436:Pt.3:1986 recommends crowning only where the calculated $K_{H\beta}$ is greater that 2.0 for the uncrowned gear pair. Recommended crown height is given by:

$$C_a = F_{\beta y} + 0 \rightarrow 20 \quad [mu] \qquad (5.17)$$

For the 18/54 10.0mm module example the elastic deflection (equal to ft) is 18.5mu. Fig. 5.13 plots the load factor at point C vs. peak error for various degrees of crowning.

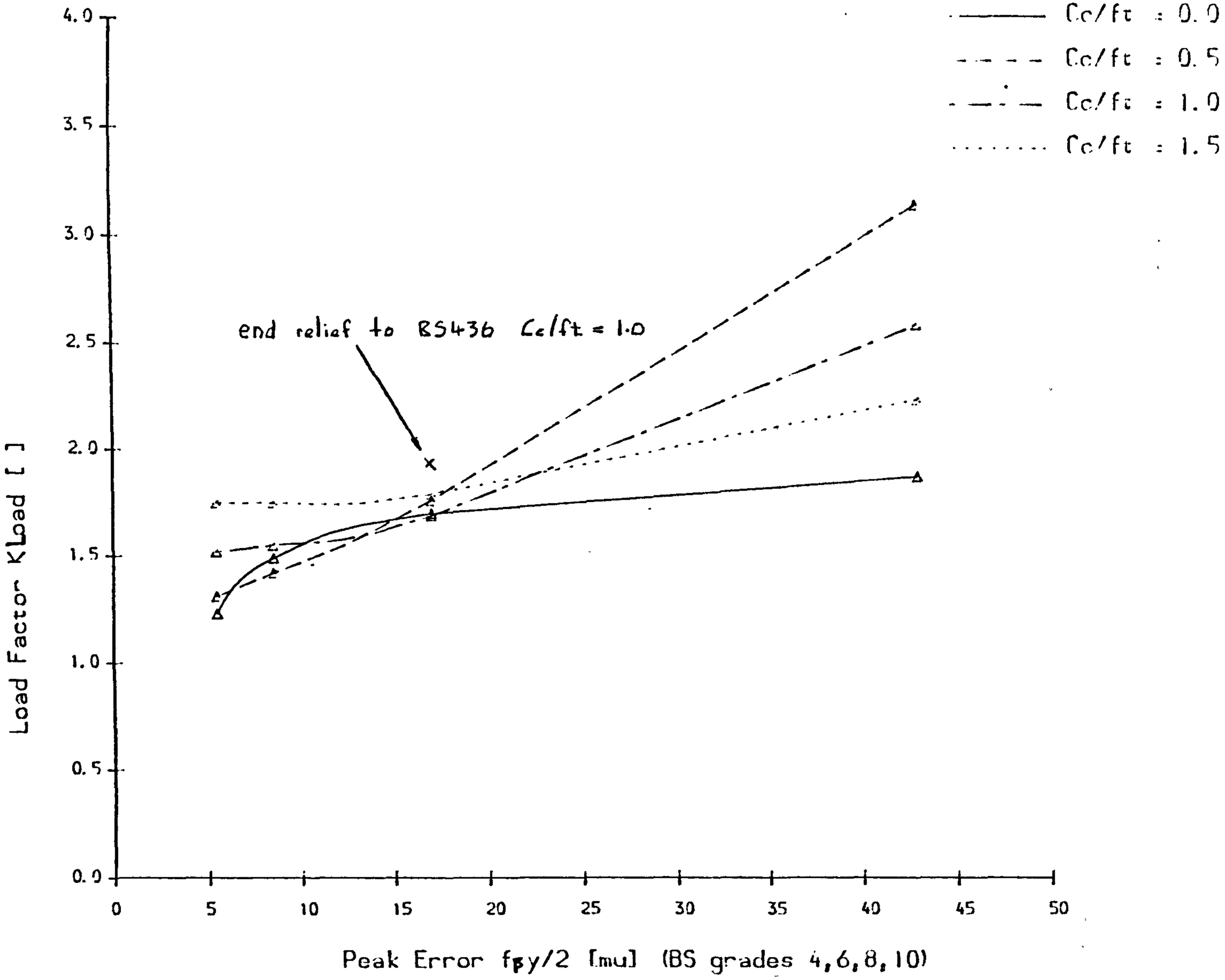

Fig 5.12 Effect of Crowning Height Cc on Load Distribution Factor Kload

Note:

- Crowning of a perfectly aligned gear increases the peak specific load (KLoad > 1.0).

- Less accurate gears require more crowning to reduce the peak specific load. For very inaccurate gears a load factor of KLoad ≈ 1.7 appears to be the lowest attainable.

- Accurate gears require only a small amount of crowning. (Hence the cross-over point on the graphs, approximately BS grade 8-9).

5.6.3 End Relief

End relief is a crude form of crowning and inherently produces a worse load distribution due to the flank discontinuity. As the type of profile modification is a function of the gear cutting machine used and, after running-in, the end relieved and crowned gear will possess near identical fatigue strength, only one analysis has been carried out to BS 436 recommendation. This is for a BS grade 8 gear $f_{\beta y}$ = 34mu; Cb = 18.5mu; $L_c/2$ = 5.625mm. This is shown on Fig. 5.12.

*****

CHAPTER 6

LIMITATIONS OF THE EXISTING SPUR GEAR ANALYSIS AND AREAS FOR FUTURE STUDY

6.1 Limitations of the Existing Spur Gear Analysis

A three dimensional elastic model has been developed for calculating the load distribution, transmission error and contact stresses in wide faced spur gears, and a computer program SPURDIST has been written to implement the model on a micro-computer. Elemental gear errors, tooth profile modifications, and the compliance of the two shafts (a function of the mounting configuration) and the phase of mesh are all input variables.

The contact line compliances of the loaded teeth (including adjacent tooth coupling compliances) are automatically calculated for wide faced solid spur gears 18 <= z <= 100 and standard rack profiles (hao = 1.25 mn, rao = 0.25 mn, b = 12.0 mn) using the results obtained from thirty separate 3D Finite Element analyses of complete spur gears of this type.

The model and the program SPURDIST naturally have limitations. These are compared with those of other published elastic meshing models in Fig. 6.1 The main limitations of the present work are as follows:

1. Thin rimmed gears

No tooth compliance data is available for the thin rimmed spur gears used extensively in the gear industry. Analysis of a thin-rimmed sun gear for an industrial epicyclic gearbox has shown that the tooth compliance can increase by a factor of 2 due to localised rotation, of the rim. The root stresses also increase correspondingly due to the thin rim deformation. Thin rim effects will increase the 'adjacent tooth' compliance terms and completely alter the pattern of load sharing between the contacting teeth.

2. Narrow faced gears

The compliance data generated has been for wide faced spur gears where the effects of increased flexibility of each end of the gear teeth do not overlap. In narrow face gears, (for example, as used in the automotive industry), the tooth compliance will be largely dependent on the overlapping effects of the tooth ends.

A variation of Jaramillo's moment-image method [J1] could be used to model this effect but as it has already been shown to be in error for wide faced gears its validity to narrow face gears must be questioned. The model developed in this thesis will analyse narrow faced gears but its accuracy has not been verified.

Factors taken account of in load distribution models	Thesis (UK)	Existing Gear Design Standards (BS, ISO, DIN)	Vedmar (Sweden) [5]	Seager (UK) [4]	Schmidt Based on Weber & Banaşhek (Germany) [2]	Hayashi (Japan) [1]
3D elastic model	✓	X (2D)	✓	✓	✓	✓
Adjacent tooth compliance	✓	X	X	X	X	X
Compliance of gear body	✓	X	X	X	✓	X
Arbitrary tooth modifications (barrelling, tip relief etc.)	✓	✓	✓	✓	✓	✓
Tooth contact outside geometrically defined phase of mesh	✓	X	X	✓	X	X
Tooth compliance due to thin rim	X	X	X	X	X	X
Narrow face-width gears	✓	✓	✓	✓	✓	✓
Addendum modified gears	X	✓	X	X	✓	✓
Increased contact compliance near tip	✓	X	X	X	X	✓
Increased contact compliance near ends of tooth	X	X	X	X	X	X
Calculation of tooth root bending stress	X	✓	✓	✓	✓	✓
Plastic deformation of gear	X	X	X	X	X	X

Note: Table does not specify whether factors are correctly modelled, only if they have been considered by the author.

Fig. 6.1 Summary of Significant Factors Included in Various Spur Gear Load Distribution Models

3. Addendum modified gears

Especially for small numbers of teeth the tooth compliance will decrease with positive addendum modification. For an 18/54 spur gear mesh the single-tooth stiffness c' according to BS/ISO/DIN is respectively 18.0, 16.15 and 15.15 N/mm/mn for a pinion shift of x1 = 0.5, 0.0 and -0.5mn respectively. No 3D finite element analysis has been carried out for modified gears to allow correct modelling of their compliance.

4. Contact compliance at the tip and ends of the tooth

The increase in contact compliance near the tip of the tooth has been modelled by assuming a Hertzian pressure distribution applied to a rack profile tooth. No account has been taken of the change in pressure distribution caused by the adjacent tooth tip or of the effect of different tooth numbers.

The increase in contact compliance near the ends of the tooth flank has not been modelled. However the tooth is very compliant at the ends of the gear so the percentage error is small.

5. Calculation of peak tensile tooth root stress influence coefficients

The peak tooth root stress at any point can be calculated by numerical integration, from the calculated load distribution and the stress influence coefficients.

$$\sigma_F = \int_0^b K_\sigma(z, zF) . \omega(zF)\, dz \qquad (6.1)$$

Work is in hand to extract values of the influence coefficients K(z,zF) from the results of the F.E. analyses reported in chapter 2 and fit them with approximating functions using the same techniques as for the deflection coefficients.

6. Plastic deformation of the gear flank and tooth root

These two effects lead to 'bedding in' of the teeth and improved contact conditions. Existing standards, (and the model developed in this thesis), although allowing for 'normal' running in wear, are otherwise based on elastic theory and are unable to accommodate plastic deformation or work hardening of the gear teeth. A substantial effort would be involved in developing a full elastic/plastic tooth meshing model. All the influence coefficients would become functions of the applied load and load history (unless tooth root plasticity is neglected or approximated by an equivalent 'elastic' compliance). There are areas of study in gear technology that would improve gear rating far more readily than a full elastic/plastic model at present, particularly in view of the move away from the use of soft or through hardened gears towards surface-hardened types in which plastic deformation is unacceptable.

7. Movement of the Line of Contact

Gear teeth that have profile modifications or manufacturing errors are not truely of involute form, and thus do not make contact exactly in the theoretical base tangent plane. The same is true of perfect involute gear teeth under load.

The analyses reported only allow for gross departures from the 'theoretical' plane of contact (eg during tip contact) but does not allow for the small departures caused, away from the tooth tips, by profile errors, modifications or elastic distortions.

A further step would be to redefine the contact points each time the loads and deformations were calculated but it would be necessary to recalculate the stiffness matrix and this would be too time consuming.

6.2 Areas for Further Study

The shortcomings of the spur gear analysis listed in section 6.1 provide the basis for much further research into the understanding of spur gear stress analysis. The existing program SPURDIST could be directly linked to commercially available design standards software,

(DUISO, DU436 [D7]), to give an improved overall gear design package. Such features as an automatic output of the optimum lead or profile corrections are immediate possibilities. The complete synthesis of optimum gear geometry and mounting configurations are further possibilities, but present a formidable task which is possibly insoluble.

The general influence coefficient theory and load distribution/stress analysis approach used in this thesis can be applied to all types of gearing:

a) Helical gears: These have an oblique line of contact and a transverse section that is rotated about the gear axis but are in principal the same as spur gears. The influence coefficients are not symmetric about zF = b/2 due to the different stiffness of the two angled tooth ends. The peak tooth root stress will probably be in the normal NOT transverse plane except near the ends of the tooth (plane stress). The 2D contact deflection formula will be less accurate along an oblique contact line with continuously changing curvature and specific load even for perfectly aligned gears.

The theory is not really applicable to crossed helicals as geometrically they have point contact and are rarely used for torque transmission purposes.

b) Worm gears: These also exhibit line contact and so are well suited to analysis by the influence coefficient method. Worm gears have sliding contact and the frictional forces may have a significantly greater effect on the tooth deflection and contact stress field. Movement of the line of contact under load is well known, and must be clearly be included in any analysis of worm contacts.

c) Bevel gears: Again the line contact present means that the influence coefficient method can be readily applied. The majority of bevel gears have an overhung mounting configuration potentially producing very bad load distributions although this is normally improved by crowning. An accurate study of the bearing and shaft compliances would be a prerequisite of a meaningful 3D elastic model of bevel gears.

d) Spiral Bevel, Hypoid, Spiroid gears: Spiral bevel gears are to bevel gears what helicals are to spurs, with low sliding speeds and quieter operation at higher pitch line velocities due to a more constant length of line of contact. In hypoid and spiroid gears the shaft axes are offset as the pinion starts to resemble a tapered worm gear and sliding contact occurs. The influence coefficient approach is applicable to all three gear types with the potential problem areas analagous to bevels and worms respectively.

--------oOo--------

Bibliography

[A1] Aida T., Teranchi Y., : ~Tooth Stresses~
Trans. JSME (in Jap) (1961-6) 27 (178) p.853

[A2] Aida T., Teranchi Y., : ~Tooth Stresses~
Trans. JSME (in Jap) (1961-6) 27 (178) p.862

[A3] Aida T., Teranchi Y., : ~Tooth Stresses~
Trans. JSME (in Jap) (1961-6) 27 (178) p.863

[A4] Aida T., Fujio H., Murata S., Iwasaki T., : Deflections and Moments of Wide Plate With Varying Thickness in Direction of Height"
Bull. JSME (1973-2) 16 (92) pp.387-394

[A5] Ajapetov E.L. : "Contact Deformation on Gear Teeth"
Russ. Engg. Jnl. 1967 (5) pp.44-47

[A6] Arai N., Harada S., Mori N., Okamoto M., : "Study on Stresses at the Root Fillet of Tooth, Deformation and Accuracy Deterioration of Spur Gear With a Thin Rim When Rate of Load Distribution Under Dynamic Condition is Considered".

[A7] Attia A.Y., : " Deflection of Spur Gear Teeth Cut in Thin Rims"
Ein Shams University, Cairo

[A8] AGMA 218.1 "The Rating of Spur and Helical Gears" Dec. 1982

[A9] Atkinson L.V., "Pascal Programming"
Wiley 1983

[B1] Baethge J., : ~Drehwegfehler, Zahnfederharte und Geransch bei Stirnradern~ Diss. T.U. Munchen 1969

[B2] Baethge J., : VDI-Z (1970-71), 112 (4) p.205

[B3] BS436 Spur and Helical Gears
:Part 2 Basic Rack Form , Modules ans Accuracy (1 to 50 metric module)

:Part 3:1986 Method for Calculation of Contact and Root Bending Stress Limitations for Metallic Involute Gears

[B4] Buckingham E,. : "Analytical Mechanics of Gears" McGraw-Hill 1949

[B5] British Steel Corperation : "Iron and Steel Specifications", 1986

[C1] Cardou A., Tordion G.V., : "Calculation of Spur Gear Tooth FLexibility by the Complex Potential Method" Trans. ASME, Vol.107, Mar. 85

[C2] Chabert G., : " Evaluation of Stresses and Deflection of Spur Gear Teeth Under Strain" C.E.T.I.M. Senlis. Fr. ASME 72-PTG-27 Oct. 1972, p.16

[C3] Conry T.F., Seireg A., : "A Mathematic Programming Method for the Design of Elastic Bodies in Contact" Jnl. App. Mechs., Trans ASME 93E(1), 1971, pp.387-392

[C4] Conry T.F., Seireg A., : "A Mathematical Programming Technique for the Evaluation of Load Distribution and Optimal Modification in Gear Systems" Trans. ASME, Jnl. Engg. for Ind. (Nov.1973)

[C5] Cornell R.W., : "Compliance and Stress Sensitivity of Spur Gear Teeth" ASME, Jnl. Mech. Des., Vol. 103, April 1981

[C6] Case J., Chilver A.H., : "Strength of Materials and Structures" Edward Arnold 1978

[D1] Davies W.J., : "Some Design Considerations Affecting Performance and Reliability of High-Duty Spur and Helical Gearing for Aircraft" Proc. Int. Conf. Gearing, I.Mech.E. London (1958), pp.82-90

[D2] Davis A.W., : "Marine Reduction Gearing" Proc. Inst. Mech. E. 170 (16) 1956, pp.477-498

[D3] DIN 3990 Calculation of Load Capacity of Spur, Helical and Bevel Gears

[D4] Dolan T.J., Broghammer E.L., : "A Photoelastic Study in Gear Tooth Fillets"
Univ. of Illonois Engrg Expt. Station Bulletin No. 335, 1942

[D5] Dubbel, : "Taschenbuch fur den Maschinenbau"
Springer Verlag, 1974

[D6] DIN 3961 : "Accuracy of Cylindrical Gears: General Bases" 1978

[D7] DU436 Computer program implementing BS436 gear stress analysis standard [B3]. Design Unit, University of Newcastle upon Tyne

[D8] Dobrovolsky V. : "Machine Elements"
Mir Publishers, Moscow 1977

[D9] DIN 3960 : "Concepts and Parameters Associated With Cylindrical Gears and Gear Pairs With Involute Teeth" 1980

[D10] DIN 3962 : "Accuracy of Cylindrical Gears: Tolerances for Individual Errors" 1978

[E1] Elkholy A.H., : "Tooth Load Sharing in High-Contact Ratio Spur Gears"
Pratt & Whitney Canada Inc., Ontario

[F1] Fujio H., Aida T., : "Varying Thickness Plate (Greens and F.E. Analysis)"
Preprint JSME No. 710-6 (1968-4), p.113
Preprint JSME No. 192 (1971-4), p.161, (in Jap.)

[F2] Fujita K., : Trans. JSME (1960-3) 26 (163) p.430, (in Jap)

[F3] Fujita K., Obata F., Miyanishi K., : "Gear Tooth Stress Calculation Method for Heavily Crowned Gears"

Bull. JSME (1974) 17 (104), pp.264-272

[F4] Fujita K., : "Heavily Crowned Gears"
Machinist (In Jap.), (1967-12) 11 (12), p.24

[F5] Furrow R.W., Mabie H.H., : "The Measurement of Static Deformation of Spur Gear Teeth"
Jnl. Mechanisms, 5 1970, pp.147-168

[G1] Gromann M.B., : "Load Distribution in Gear Teeth"
Russ. Engg. Jnl. 1967, 5, pp.44-47

[G2] Geick K., : "Technical Formulae"
Geick-Verlag 1982

[H1] Hayashi K., : "Load Distribution on Contact Line of Helical Gear Teeth", (Part 1 : Fundamental Concept)
1963 Bull. JSME 6 (22), pp.336-343

[H2] Hayashi K., Sayama T., : "Load Distribution on the Contact Line of Helical Gear Teeth", (Part 2 : Gears of Large Facewidth)
1963 Bull. JSME 6 (22), pp.344-353

[H3] Hayashi K., : "Analysis of Loading in Cylindrical Gears"
Proc. JSME Semi Internat. Symp., Tokyo 1967, pp.181-188

[H4] Hayashi K., : Trans. JSME (1962-3) 28 (193), p.1093 (In Jap.)

[H5] Hayashi K., Sayama T., : Trans. JSME (1962-3) 28 (193), p.1102 (In Jap.)

[H6] Hayashi K., Sayama T., : "Load Distribution in Marine Reduction Gears"
Bull. JSME (1962) 5 (18), pp.351-359

[H7] Holl D.L., : "Cantilever Plate with Concentrated Edge Load"
Jnl. Appl. Mechs., Trans. ASME 59 (1937), pp.A8-10

[H8] Hertz H., : "Gessamelte Werke," vol. I, Leipzig, 1895.

[H9] Hirt M.C.O., : "Stresses in Spur Gear Teeth and Their Strength as Influenced by Fillet Radius"
English translation of Phd Thesis by John Maddock, 1976
Published by AGMA

[H10] Heywood R.B., : "Tensile Fillet Stresses in Loaded Projections"
Trans. Inst. Mech. Engrs., 1948

[H11] Huber M. T., Fuchs S., : "Spannungsverteilung ben Beruhrung"
Physik. Zeitschr XV, 1914

[H12] Hofmann D.A., : "The Importance of the New Standards BS 436(1986) and DIN 3990 (1986) for Gear Design in the UK"
TransIMarE(TM), Vol. 99, Paper 14, 1987

[I1] Inoue K., Tobe T., : "Longitudinal Load Distribution of Helical Gears"
Tohoku University, Sendai, Japan

[I2] Ishikawa J., : Trans. JSME (1951) 17 (59) p.103 (In Jap.)

[I3] Ishikawa J., : Bull. T.I.T. (3) 1957 (Tokyo Inst. Technol.)

[I4] Ishikawa J., : On the elastic problem of cantilever subject to combined bending and twisting"
15 (90) 1972

[I5] ISO/DP 6336 Gear Loading PARTS I, II, III AND IV.

[J1] Jaramillo T,J., : "Deflections and Moments due to a Concentrated Load on a Cantilever Plate of Infinite Length"
Jnl. Appl. Mechs. 17, 1950 Trans. ASME 72

[J2] Johnson K.L., : "100 Years of Hertz Contact"
Proc. Inst. Mech. Engrs., Vol 196, 1982

[K1] Kagawa T., : "Deflection and Moment due to a Concentrated Edge Load on a Cantilever Plate of Finite Length"
Proc. 11th Jap. Nat. Congress of Applied Mechanics 1961

[K2] Kasuba R., : "Extended Model for Determining Dynamic Loads in Spur Gearing"
Trans. ASME, J. Mech. Des. 103, 1981 pp.398-409.

[K3] Kubo A., : "Estimation of Gear Performance"
Kyoto University

[K4] Kugimiya H., : Trans. JSME (1965) 31 (231), p.1722

[K5] Kugimiya H., : "Profile Modifications of Helical Gear Teeth"
Bull. JSME (1966) 9 (36), pp.829-841

[L1] Lewis F.M., : "Load Distribution of Reduction Gears"
Jnl. App. Mech. June 1945, pp.A87-A90

[L2] Linke H., : "Untersuchungen Zur Ermittlung der Breiten Lastverkilung und Erhohung der Betastbarkeit Durch Breitenballige Verzahnungen"
Int. Con. 'Infert 1978', Tech. Univ. Dresden, Vol. 1 p.321

[L3] Little R.W., : "Bending of a Cantilever Plate"
MS Thesis (Mechanics), Univ. Wisconsin (1959)

[L4] Loo T.T., : "Effect of Curvature on the Hertz Theory for Two Circular Bodies in Contact"
Jnl. Appl. Mechs., Trans. ASME 80 (1958), pp.122-124

[L5] Lundberg G., Sjovall H., : "Stress and Deformation in Elastic Contacts"
Chalmres Univ. of Tech., Gotenburg, 1958

[L6] Lur'e A. I., : "Three Dimensional Problems of the Theory of Elasticity"
Gostekhizdat Moscow 1955, Translated by Interscience 1964

[L7] Lennox S.C., Chadwick M., : "Mathematics for Engineers and Applied Scientists", Heinemann 1977

[M1] MacGregor C.W., : "Deflection of a Long Helical Gear Tooth"

Mech. Eng. 57 1935 pp.225-227

[M2] Merritt H.E., : "Gears"
Pitman, London 1942

[M3] Monch E., Roy A.K. : "Spannunesoptische Untersuchung einer Schragverzahnden Stirnrads"
1957 Konstruktion 9 (11), pp.429-438

[M4] Monch E., Roy A.K. : "Photoelastic Investigations of a Helical Spur Gear"
Engineers Digest, 19 (1958) pp.53-57

[M5] Munro R.G., Seager D.L. : "Tooth Loading on the IAE Gear Rig"
Proc. Symp. Gear Lub., Inst. Petrolium, I, pp. 73-78 (1958)

[M6] Munro R.G., : "The Dynamic Behaviour of Spur Gears"
PhD. Thesis, Camb. Univ. (1962)

[N1] Niemann G., Schmidt G., : "Untersuchungen uber den Einfluss von Zahnbreite und Schragungswinker auf die Zahrbelastung bei Stirnradern" (1971) VDI-Z 113 (2), pp.165-170

[N2] Niemann G., Baethge J., : VDI-Z (1970-71) 112 (4), p.205

[N3] Niemann G., Richter W., : "Tragfahigste Evolventen - Schragverzahnung"
Essen Conv. on Transmission Techniques (1954), p.16

[N4] Nengebauer G., : "Experimentelle Untersuchung der Lastverteilung uber der Zalmbreite bei Schragverzalmten Stirnradern im Lauf"
Maschinenbautechnik 11 (1962) (2), pp.93-103

[N5] Niemann G., Winter H., : "Maschinenelemente"
Springer-Verlag 1983

[P1] Portitsky H., Sutton A.D., Pernick A., : "Distribution of Tooth Load Along a Pinion"

Jnl. Appl. Mechs. Trans ASME 67 (1945), pp.78-86

[P2] Premilhat A., Tordion G.V., : "An Improved Determination of the Elastic Compliance of a Spur Gear Tooth Acted on by a Concentrated Load"
ASME, Jnl. Eng. Ind. (1974)

[P3] PAFEC : "Data Preparation User Manual"
"Theory and Results"
PAFEC 1982

[R1] Rao A.C., : "On Load Sharing by Pairs of Gear Teeth"
J. Inst. Eng. (India) 58 Pt. ME (1978) pp.265-267

[R2] Rademacher J., : "Ermittlung von Lastverteilungsfaktoren fuer Stirnradgetriebe"
Industrie-Anzeiger 69 (17), (1967) pp.31-34

[R3] Richardson H.H., : "Static and Dynamic Load, Stress and Deflection Cycles in Spur Gear Systems"
ScD. Thesis, MIT (1958)

[R4] Roark R.J., Young W.C., : "Formulas for Stress and Strain"
McGraw-Hill 1975

[S1] Schmidt G., : "Berechnung der Walzpressung Schragverzahnter Stirnrader unter Berucksichtigung der Lastverteilung"
Diss. T.U. Munchen 1973

[S2] Schmidt G.R., : "Optimum Tooth Profile Correction of Helical Gears"
ASME Paper 80-C2/Det-110

[S3] Seager D.L., : "Some Elastic Effects in Helical Gear Teeth"
PhD Thesis Cambridge Univ. (1976)

[S4] Seager D.L., : "Tooth Loading and Static Behaviour of Helical Gears"
Trans. ASLE 13 (1), 1970, pp.66-77

[S5] Sigg H., : "Profile and Longitudinal Corrections on Involute Gears"
AGMA Paper 109.16, Oct. 1965

[S6] Small N.C. : "Bending of a Cantilever Plate Supported From an Elastic Half Space"
(1961) Trans. ASME 83E, pp.387-394

[S7] Shigley J.E., : "Mechanical Engineering Design"
McGraw-Hill 1981

[T1] Terauchi Y., Nagamura K., : "Study on Deflection of Spur Gear Teeth - 1. Calculation of Tooth Deflection by Two-Dimensional Elastic Theory"

[T2] Terauchi Y., Nagamura K., : "Study on Deflection of Spur Gear Teeth - 2. Calculation of Tooth Deflection for Spur Gears With Various Tooth Profiles"
Bull. JSME 24 (188) 1981, pp.447-452

[T3] Terauchi Y., Nagamura K., : "On Tooth Deflection and Profile Modification of Spur Gear Teeth"

[T4] Tobe T., Katsumi I., : " Longitudinal Load Distribution Factor for Straddle and Overhung-Mounted Spur Gears"
ASME pap. (80-C2/DET-45) 1980, p.8

[T5] Trbojevic M.D., : "Load Distribution in Helical Gear Teeth"
The Engineer (1957) 204 (5298) pp.187-190, (5290) pp.222-224

[T6] Trobjevic M.D., : "Load Distribution in Helical Gear Teeth"
The Engineer (1957) 204 pp.483-488

[T7] Timoshenko S.P., Goodier J.N., : "Theory of Elasticity"
McGraw-Hill 1985

[T8] Tuplin W.A. : "Load Capacity of Helical Gears"
The Engineer (1966) Sep., pp.483-488

[U1] Umezawa K., : "Meshing Test on Helical Gears under Load Transmission"
3rd Report, Bull. JSME (1974 Oct.), 17 (112) pp.1348-1355

[U2] Umezawa K., : Bull. JSME (1969-70) 12 (53) p.1204

[U3] Umezawa K., : Bull. JSME (1971-1) 15 (79) p.116

[U4] Umezawa K., : Bull. JSME (1972-12) 15 (90) p.1632

[U5] Umezawa K., : "The meshing test on Helical Gears under Load Transmission" 2nd Report :- "The Approximate Formula for Bending Moment Distribution of Gear Teeth"
(1972-3) Bull. JSME 16 (92) pp.407-413

[U6] Umezawa K., Ishikawa J., : "Deflection due to Contact Between Gear Teeth With Finite Width"
Bull. JSME (1972-73) 16 (97), pp.1085-1093

[U7] Umezawa K., : "Thick Plate Theory, Finite Length"
Trans. JSME (1969-2) 35 (270) p.423 (In Jap.)

[U8] Umezawa K., : "Practical Equation for Deflections and Stresses"
Trans. JSME (1970-71) 36 (288) p.1385, (In Jap.)

[V1] Van Zandt R.P. : "Beam Strength of Spur Gears"
Quart. Trans. SAE (1952), pp.352-357

[V2] Vathayanon B., : Diss. (1965) Univ. Illinois, Urbanar, Ill.

[V3] Vedmar L., : "On the Design of External Involute Helical Gears"
Lund Inst. Tech. (Sweden)

[W1] Walker H., : "Gear Tooth Deflection and Profile Modification"
The Engineer 166 (1938)

[W2] Walker H., : "Helical Gears"
The Engineer 1946 (i) July 12, pp.24-26 182 (ii) July 19, pp.46-48 (iii) July 26, pp.70-71

[W3] Waterworth N., : "Effect of Deflections of Gears and their Supports"
Proc. Int. Conf. Gearing, Inst. Mech. Engrs. Sept. 1958

[W4] Weber C., Banascheck K., : "Formanderung und Profilrucknahme bei gerad und schragverzahnten Radern" Schriftenreihe Antriebstechnik Ht 11 (1955), p.54

[W5] Weber C., Thuss W., : "Belastungsgrenzen bei gerad und schragverzahnen Stirnradern"
Antriebstechnik H5, 1952

[W6] Weber C., : "The Deformation of Loaded Gears and the Effect on their Load Carrying Capacity"
Part 1. DSIR (London)
Sponsored Research (Germany), Report 3 (1949). See also [W7]

[W7] Weber C., Banascheck K., : "The Deformation of Loaded Gears and the Effect on their Load Carrying Capacity"
Part 5. DSIR (London)
Sponsored Research (Germany)m Report No. 6 (1950). See also [W4]

[W8] Wellauer E.I. Seireg A., : "Bending Strength of Gear Teeth by Cantilever Plate Theory"
Trans. ASME 82B (3) Aug. 1960, pp.213-222

[W9] Wellauer E.I., : "Bending Strength of Gear Teeth by Cantilever Plate Theory"
Trans. ASME Paper 58-A-50

[W10] Winter H., Stolzle K., : "Tragfahigkeitsberechnung von Zahnradgetrieben"
Antriebstechnik 10 Jrgg (2) Feb. 1971

[W11] Winter H., : "Experimentelle und Theoretische Ergebnisse zur Last - und Spannungsverteilung bei Schraegverzahnten Raedern"
Int. Conf. (Infert 1978) 1 pp.347-357

[W12] Winter H., Podlesnik., : Research work quoted in BS436 draft spur and helical standard., full reference not given

[W13] Winter H., Hirt M., : " The Measurement of Actual Strains at Gear Teeth, Influence of Fillet Radius on Stresses and Tooth Strength"

[W14] Westegaard H.M., : "Bearing Pressures and Cracks" Journal of Appl. Mechanics, March 1988

[Z1] Zablonskii K.I. : "Load Distribution on Gear Drive Contact Lines" Russ. Engg. Jnl. (1969) (8) pp.26-31

[Z2] Zablonskii K.I., et al, : "Automation of the Calculations of the Load Concentration Factors in Gears" Vestnik Mashniostroeniya 63 (1) 1983, pp.33-37 (Sov. Engg. Res. 3 (1), pp.28-32

[Z3] Zablonskii K.I., : "Gears" Tekhnika, Kiev 1977, p.208

[Z4] Ziegler H., : "Verzahnungssteifigkeit und Lastverteilung Sehragverzahnter Stirnrader" Diss. T.H. Aachen 1971.po 0

-----oOo-----

APPENDIX 2.1

PROGRAM SPURDIST FOR THE ELASTIC ANALYSIS OF SPUR GEARS

Appendix 2.1 explains the computer program SPURDIST for determining the load distribution, contact stress and transmission error in any pair of meshing real spur gears. The elastic equations used are set out in Section 2.1.

Fig. 1 shows the menu hierarchy and Fig. 2 a summary of the main commands. The program defines a master tooth (tooth 3) which is used for specifying the phase of mesh (see Fig. 4 procedure PHASE). Up to two teeth either side of the master tooth may be in mesh at any one time. A tooth is assumed to be potentially in mesh if the tooth tip is within 0.25 base pitches of the 'mating' tooth surface (ie touching when inside the geometrically defined phase of mesh). Elemental gear error datafiles are manipulated using procedure ERROR. Error datafiles are permanently stored on disk.

The solution is obtained and output by calling procedure ANALYSE (Fig. 4) which calls CALCMAT (Fig. 5) and LOADDIST (Fig. 6). CALCMAT generates the tooth compliance matrix (not including the load dependent contact compliance). The tooth centre-line deflection coefficients C[1..7] (for 10 to 100 teeth at = -2, -1, 0, 1, 2 modules) are permanently stored on datafile COEFDATA. The coefficients have been calculated by fitting natural splines to the F.E. result coefficients in two 'directions'

LOADDIST completes the compliance matrix, by adding in the estimated contact deflection (Function CONDEFN) inverting the compliance matrix and solving for the load distribution. Each contact line has 8 gauss points (2 point integration over successive quarters of the facewidth) giving a 25 x 25 augmented compliance matrix for 3 teeth in contact. The solution is iterated until all gauss point loads have converged to values greater than -wbm/1000. When negative loads are predicted (i.e. teeth are separated), the contact compliance is multiplied by 10 at each iteration. This reduces the estimated gauss load in a smooth process until it approximates to zero or

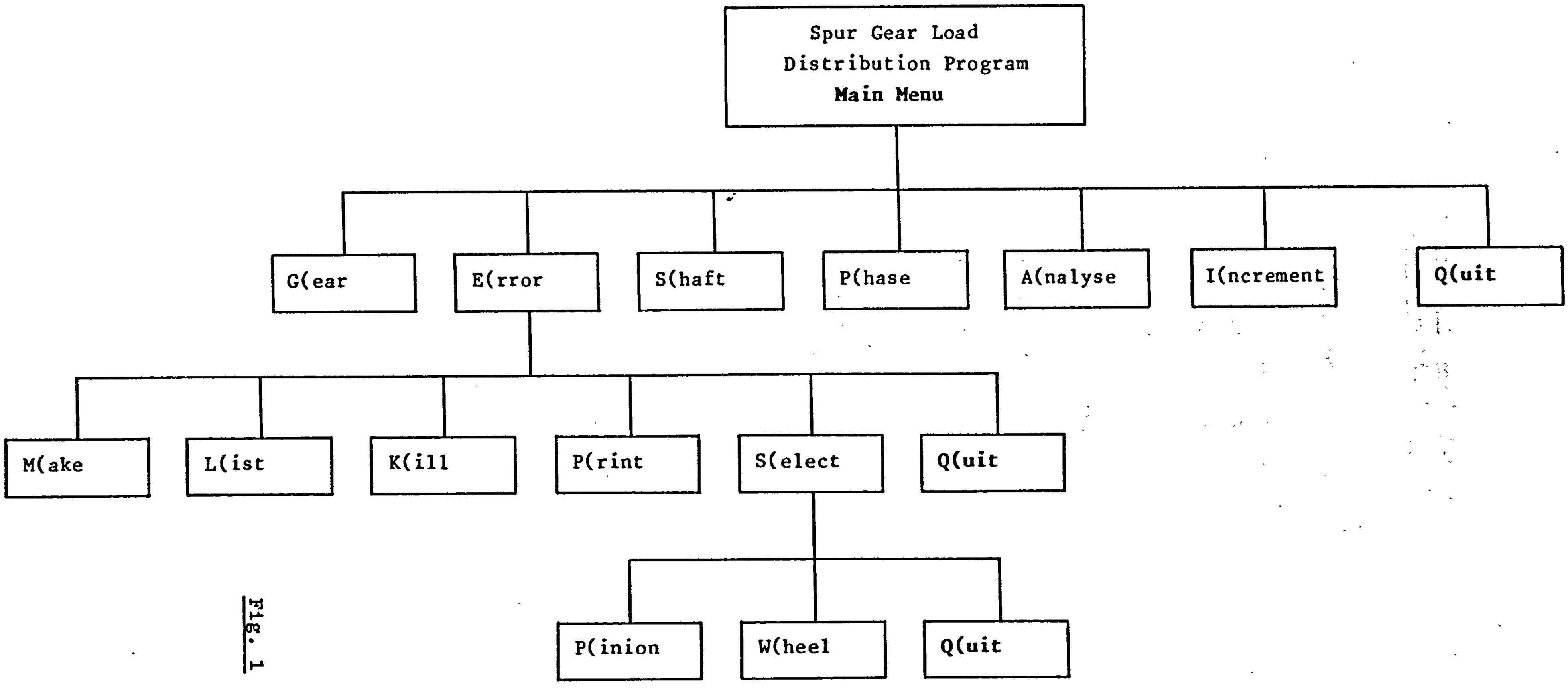

Fig. 1 Menu Heirarchy
Program SPURDIST

Commands for Spur Gear Load Distribution
Program Version 04. 26-10-87

G(ear : Prompts for gear tooth geometry independent of phase of mesh

E(rror : Returns the error file menu for handling the elemental gear tooth errors and profile modificaitons (pitch, profile, barrelling, crowning, tip, root and end relief)

- M(ake : Creates a new error datafile
- L(ist : Lists an existing error datafile on the screen
- K(ill : Destroys an error datafile
- P(rint : Lists an existing error datafile on the printer
- S(elect : Assigns an error datafile to each tooth of the 5 possible engaging tooth meshes (maximum of 3 at any phase of mesh)
  - P(inion : prompts for pinion tooth number 1-5
  - W(heel : prompts for wheel tooth number 1-5
- Q(uit : Returns to main program menu

S(haft : Prompts for shaft deflections at the gauss integration points

P(hase : Prompts for the phase of mesh and displays which tooth pairs are potentially in mesh

A(nalyse : If all mandatory input data is present the mesh is analysed and the results output to the printer

I(ncrement : A(nalyse is performed for seven phases of mesh corresponding to points A, B, C, D and the 3 midpoints on the roll angle graph

Q(uit : Exits the program

Fig. 2

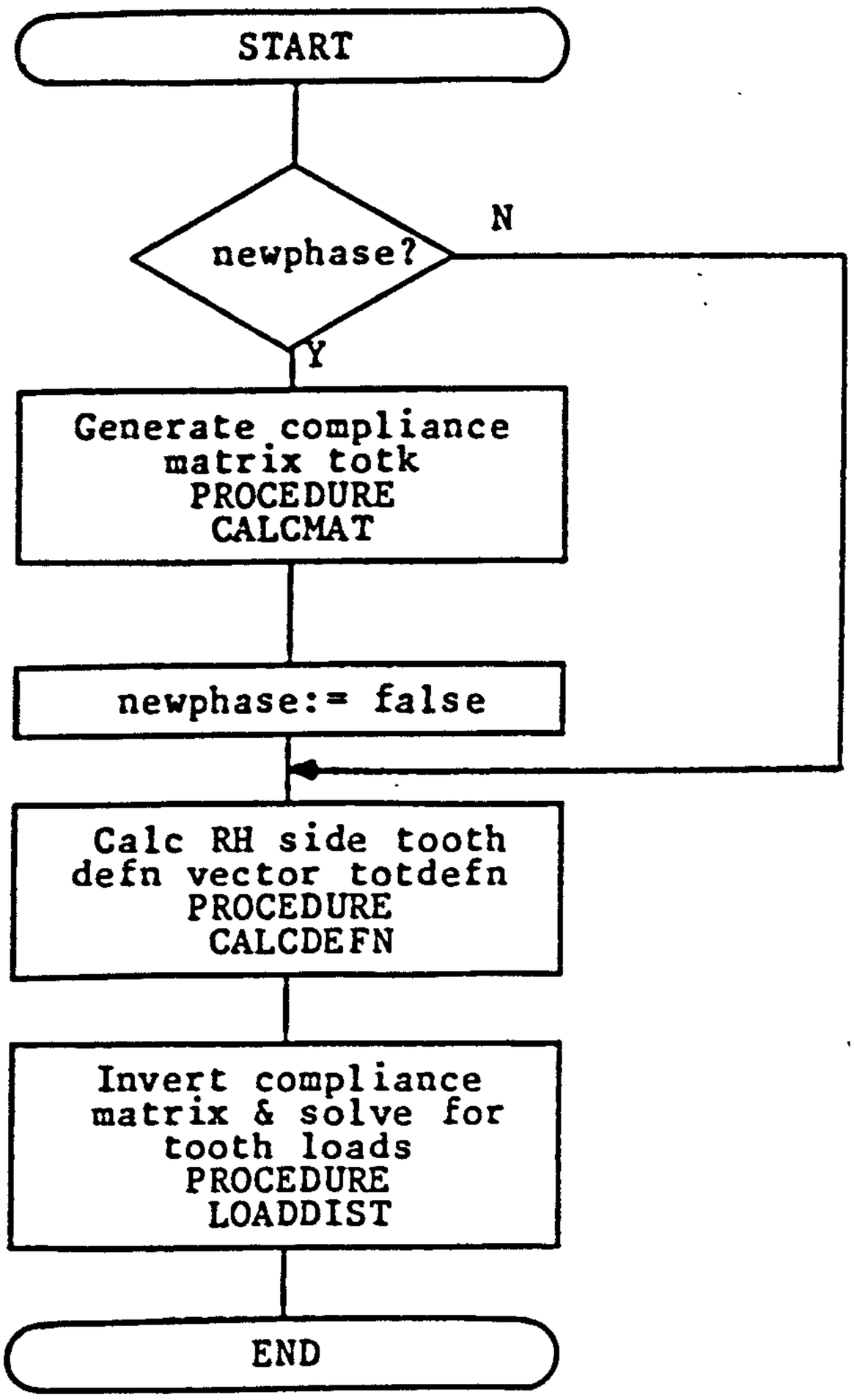

Fig 3. Spur Gear Load Distribution Program Procedure ANALYSE

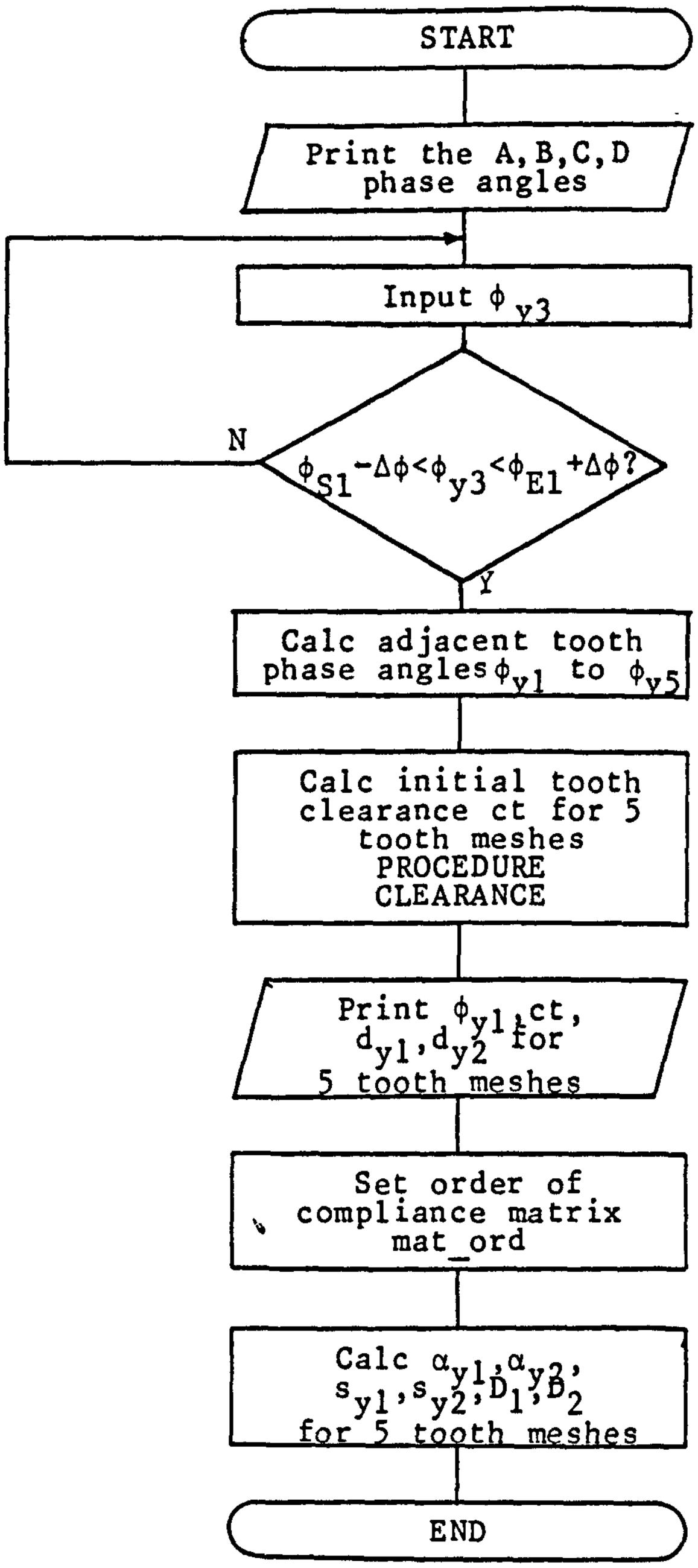

Equations for calculating the tooth clearance ct dealt with in Appendix 2.1.3

Fig 4. Spur Gear Load Distribution Program Procedure PHASE

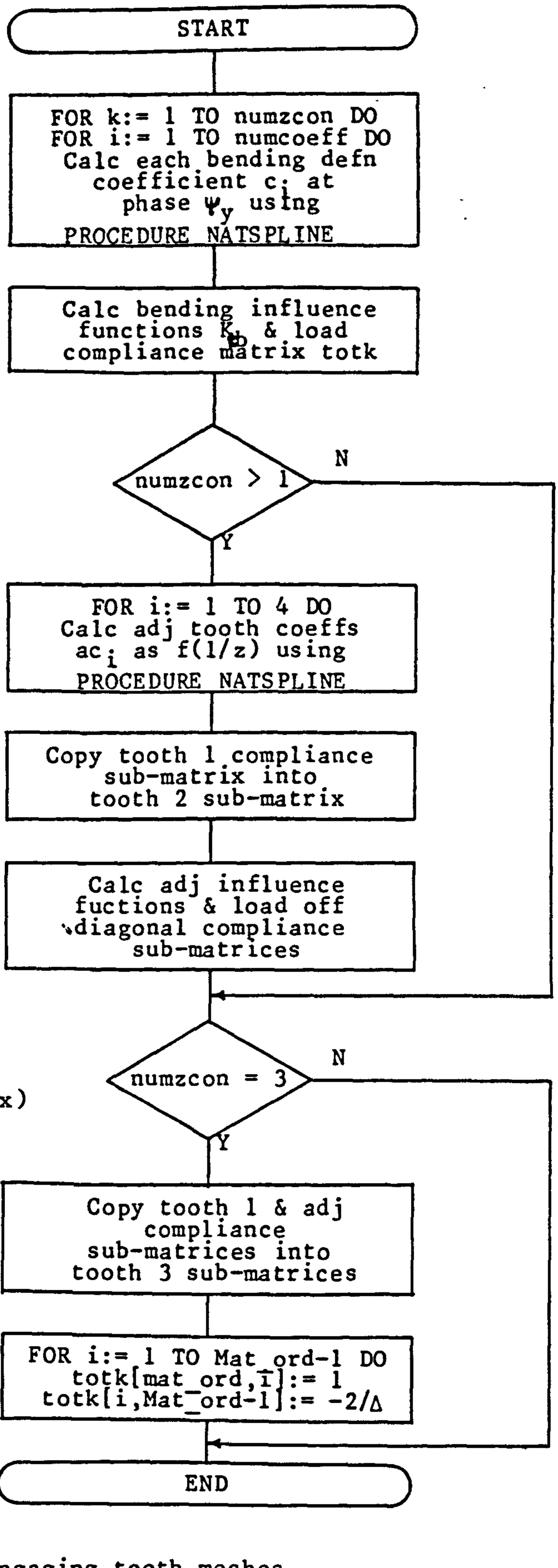

(Fig2.3 shows 3 tooth mesh compliance matrix)

numzcon : number of engaging tooth meshes
numcoeff: number of bending defn curve fit coefficients c_i (7)

Fig 5. Spur Gear Load Distribution Program Procedure CALCMAT

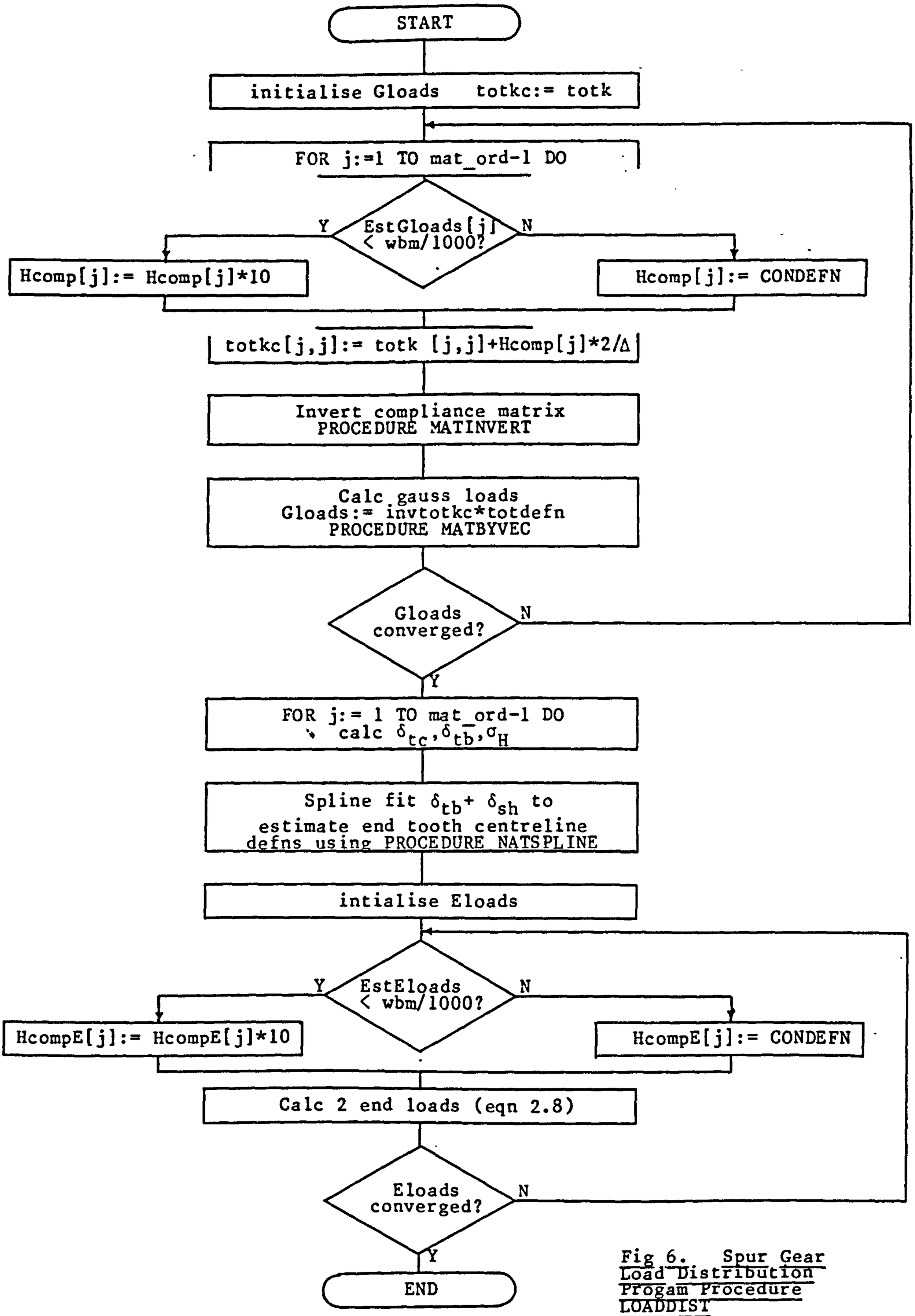

Fig 6. Spur Gear Load Distribution Progam Procedure LOADDIST

converges too a stable positive load. The tooth centre-line deflection is fitted with natural splines to obtain the end tooth centre-line deflections. The specific load is calculated at the end of each meshing tooth from equation 2.8.

★★★★★

APPENDIX 2.1.3

CALCULATION OF LOADING DIAMETER, dy, AND INITIAL TOOTH CLEARANCE, ct, OUTSIDE THEORETICAL RANGE OF MESH

Appendix 2.1.3 covers calculation of dy and ct at the end of pinion engagement. It is valid for spur gears of any pressure angle with profile modification.

The following calculations determine the co-ordinates at the pinion tip at a given phase angle ϕ_i. A tangent is joined between this point and the wheel base circle. The intersection between the tangent and the wheel involute defined as the wheel meshing point, defining the tooth clearance, ct, and the mesh diameter, dy2. This procedure has been repeated for the start of pinion tooth engagement.

Referring to Fig. 1 we have for the pinion:

$$L_1 = \sqrt{\left(\frac{d_{a1}}{2}\right)^2 - \left(\frac{d_{b1}}{2}\right)^2} \qquad \text{(A2.1.3.1)}$$

$$\phi_{s1} = \tan^{-1}\left(\frac{2(i_1 - q)}{d_{b1}}\right) - \lambda_{s1} \qquad \text{(A2.1.3.2)}$$

$$\alpha = \cos^{-1}\left(\frac{d_b}{d_y}\right) \qquad \text{(A2.1.3.3)}$$

$$\lambda = \frac{S}{d} + \text{inv}\,\alpha - \text{inv}\,\alpha_y \qquad \text{(A2.1.3.4)}$$

$$L_{y1} = (\phi_{y1} - \phi_{s1}) \frac{d_{b1}}{2} \qquad \text{(A2.1.3.5)}$$

$$d_{y1} = \sqrt{\left(L_{s1} + L_{y1}\right)^2 + \left(\frac{d_{b1}}{2}\right)^2} \qquad \text{(A2.1.3.6)}$$

$$\omega_{y1} = \phi_{y1} - \alpha_{\omega} \qquad \text{(A2.1.3.7)}$$

$$\theta_{y1} = \omega_{y1} \tau \lambda_{y1} \qquad \text{(A2.1.3.8)}$$

where ϕ = phase angle relative to base normal
ω = angle between tooth centre-line and line joining centres
θ = angle between meshing point and line joining centres

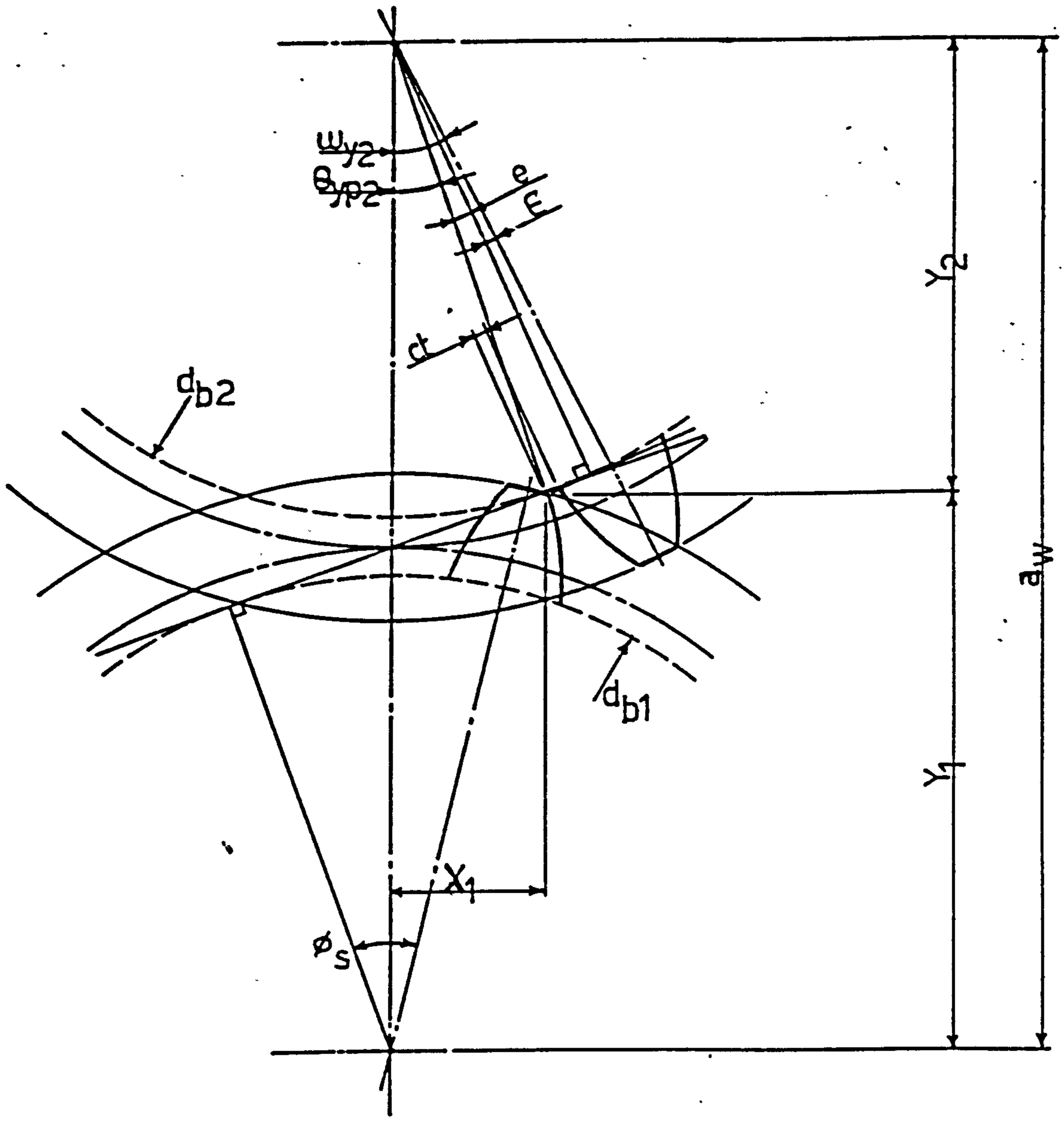

Geometry of Tooth Clearance, ct, outside the Geometrically Defined Phase of Mesh

Now consider the gear pair:

$$X = \frac{d_{a1}}{2} \sin \theta_{y1} \qquad \text{(A2.1.3.9)}$$

$$Y_1 = \frac{d_{a1}}{2} \cos \theta_{y1} \qquad \text{(A2.1.3.10)}$$

$$Y_2 = a_w - Y_1 \qquad \text{(A2.1.3.11)}$$

$$d_{yp2} = \sqrt{X^2 + Y_2^2} \qquad \text{(A2.1.3.12)}$$

$$\theta_{yp2} = \tan^{-1}\left(\frac{X}{Y_2}\right) \qquad \text{(A2.1.3.13)}$$

$$e = \cos^{-1}\left(\frac{d_{b2}}{d_{yp2}}\right) \qquad \text{(A2.1.3.14)}$$

where suffix 'yp2' refers to the tip of pinion relative to the wheel axis.

The equation of the tangent to the wheel base circle can now be calculated.

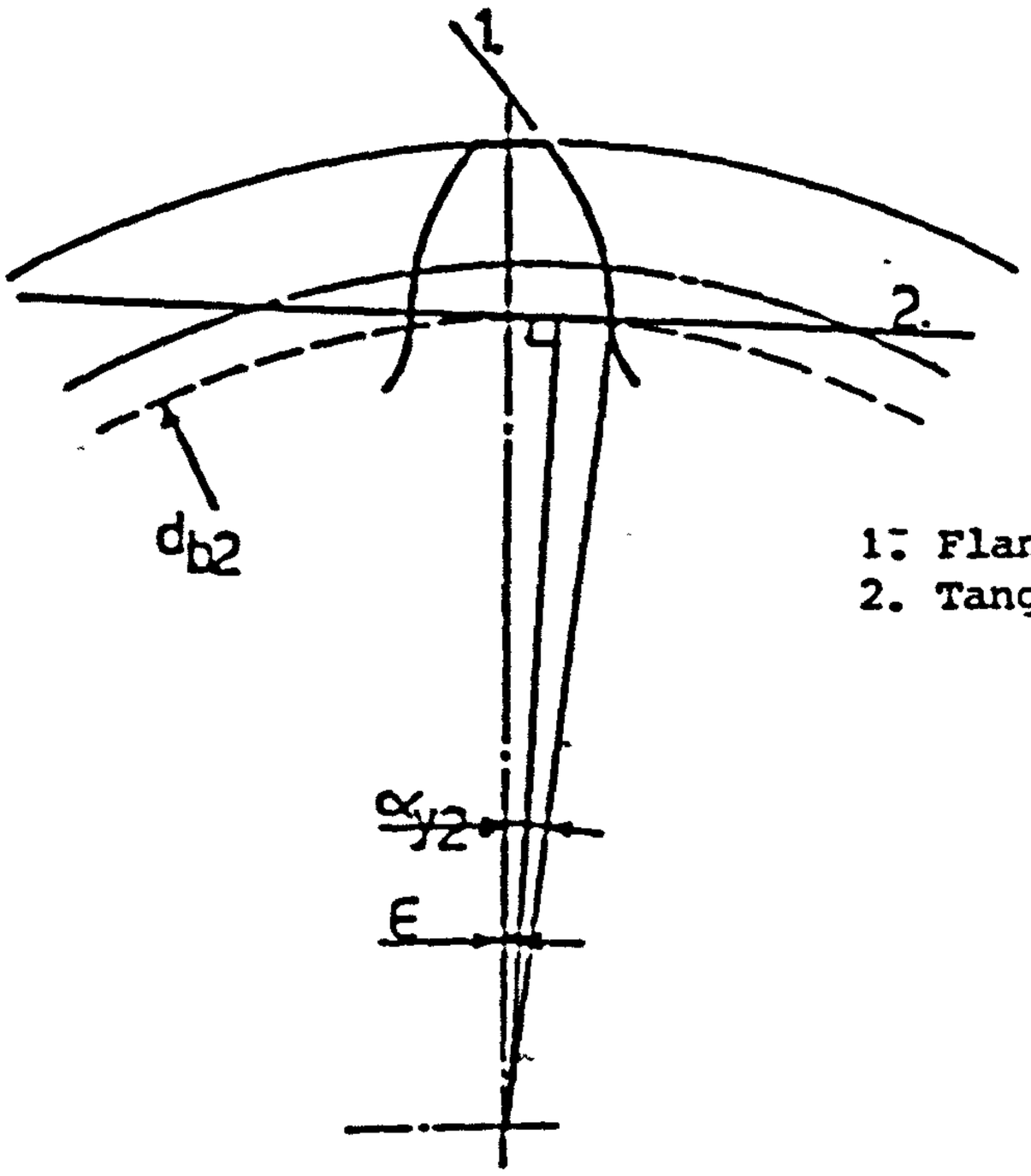

1. Flank involute
2. Tangent to wheel base circle

Fig 2. Wheel Contact Point Outside the Geometrically Defined Phaase of Mesh

Referring to Fig. 2 we have

$$\epsilon = (\omega_{y2} - \theta_{yp2} - e) \qquad \text{(A2.1.3.15)}$$

The equation of tangent line 2 is:

$$y = \tan \epsilon . x + \frac{d_{b2}}{2 \cos \epsilon} \qquad \text{(A2.1.3.16)}$$

Transforming this to polar co-ordinates gives:

$$d_{y2} = \frac{d_{b2}}{\cos \epsilon \left(\cos \lambda_{y2} - \tan \epsilon \sin \lambda_{y2} \right.} \qquad \text{(A2.1.3.17)}$$

For the wheel involute profile, line 1:

$$\alpha_{y2} = \cos^{-1}\left(\frac{db2}{dy2}\right) \qquad \text{(A2.1.3.18)}$$

$$\lambda_{y2} = \frac{S_2}{d_2} + \text{inv}\,\alpha - \text{inv}\,\alpha_{y2} \qquad \text{(A2.1.3.19)}$$

The wheel mesh diameter, dy2, can be solved iteratively. The tooth clearance, ct, is the distance along the assumed base tangent given by:

$$ct = \frac{1}{2}\left[\sqrt{d_{yp2}^2 - db2^2} - \sqrt{d_{y2}^2 - db2^2}\right] \qquad \text{(A2.1.3.20)}$$

*****

APPENDIX 2.3.2

SURFACE CO-ORDINATES OF A SPUR GEAR WITH ADDENDUM MODIFICATION

This appendix sets out the procedure for calculating the rectangular and polar co-ordinates of spur gears with addendum modification. The primary purpose for this was to generate mesh data for Finite Element analyses so a procedure for determining the midpoint of two surface co-ordinates is included.

Required data for profile generation:

number of teeth	:	z
module	:	mn
pressure angle	:	α
addendum modification	:	x
tool addendum	:	hao
tool tip radius	:	rao

For involute generation: input radius ry

reference radius $r = z.mn/2$ (A2.3.2.1)

base radius $r_b = r \cos \alpha$ (A2.3.2.2)

tooth thickness $S = mn(\pi + 2x \tan \alpha)$ (A2.3.2.3)

surface pressure angle $\alpha_y = \cos^{-1}(r_b / r_y)$ (A2.3.2.4)

surface angle co-ordinate $\lambda_y = \frac{S}{d} + inv\,\alpha - inv\,\alpha_y$ (A2.3.2.5)

rectangular co-ordinates $X = r_y \sin \lambda_y \quad Y = r_y \cos \lambda_y$ (A2.3.2.6)

For trochoid generation:

The fillet form of the tooth has been calculated based on work by Buckingham [B4]. Co-ordinates are calculated for a rack cutter with a tool radius.

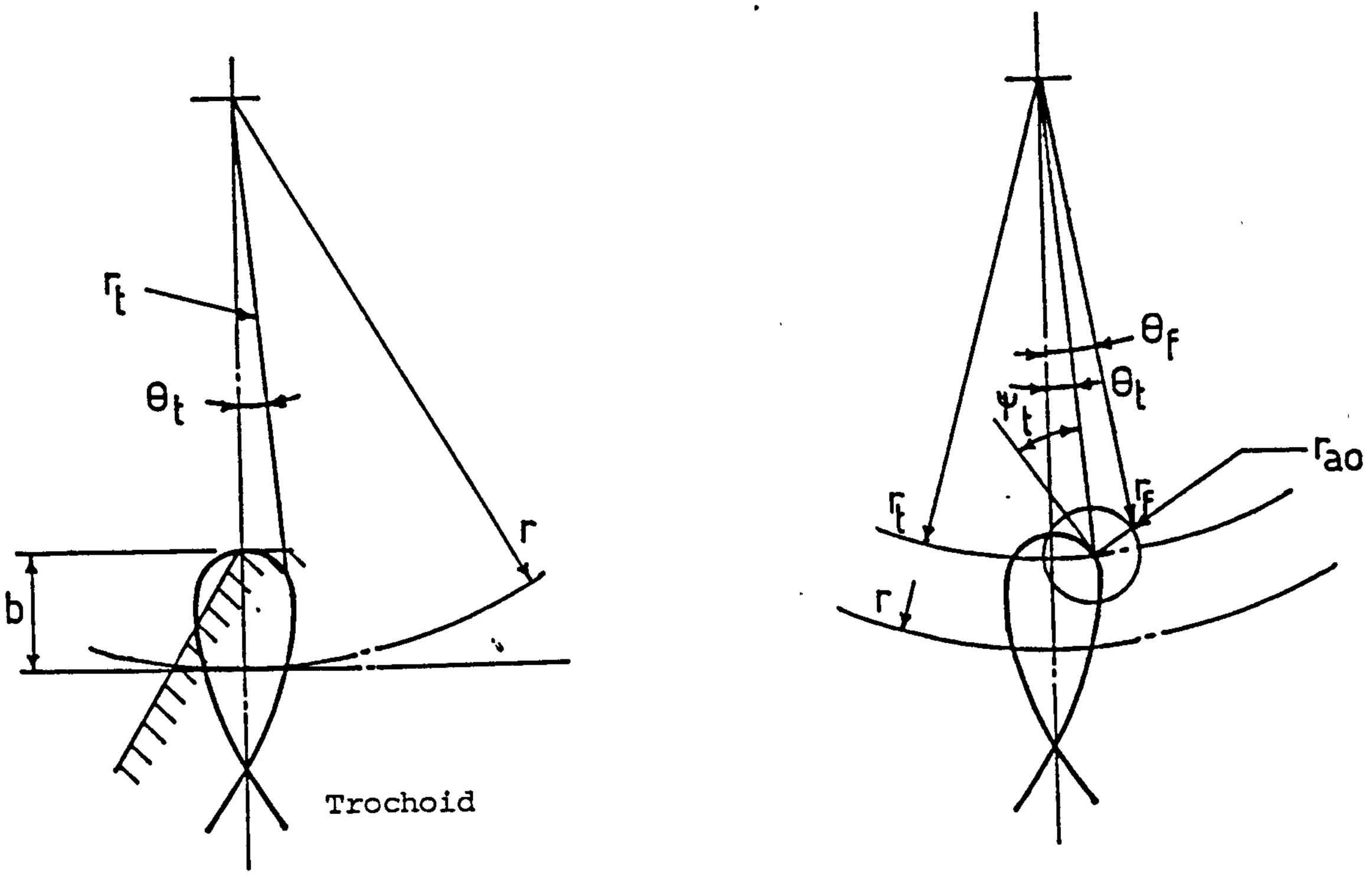

Fig. 1 Geometry of a Spur Gear Root Fillet

For no undercut the trochoid will be tangent to the generated involute profile. From the geometry of Fig. 1 for the corner of a rack tooth we have:

$$\theta_t = \tan^{-1}\left[\frac{\sqrt{r_t^2 - (r-b)^2} - \sqrt{r_t^2 - (r-b)^2}}{r}\right] \qquad \text{(A2.3.2.7)}$$

$$\tan \psi_t = \frac{r_t \, d\theta_t}{dr_t} = \frac{r(r-b) - r_t^2}{r\sqrt{r_t^2 - (r-b)^2}} \qquad \text{(A2.3.2.8)}$$

where rt = any radius of trochoid (input)
b = distance from rack reference line to origin of rack radius
θ_t = vectorial angle of trochoid

For the rounded corner of rack tooth shown in Fig. 1 we have:

$$r_f = \sqrt{r_t^2 - r_{ao}^2 - 2 r_{ao} r_t \sin \psi_t} \qquad \text{(A2.3.2.9)}$$

$$\theta_f = \theta_t + \cos^{-1}\left[(r_t - r_{ao} \sin\psi)/r_f\right] \qquad \text{(A2.3.2.10)}$$

where rf = any radius of fillet form
θ_f = vectorial angle of fillet form

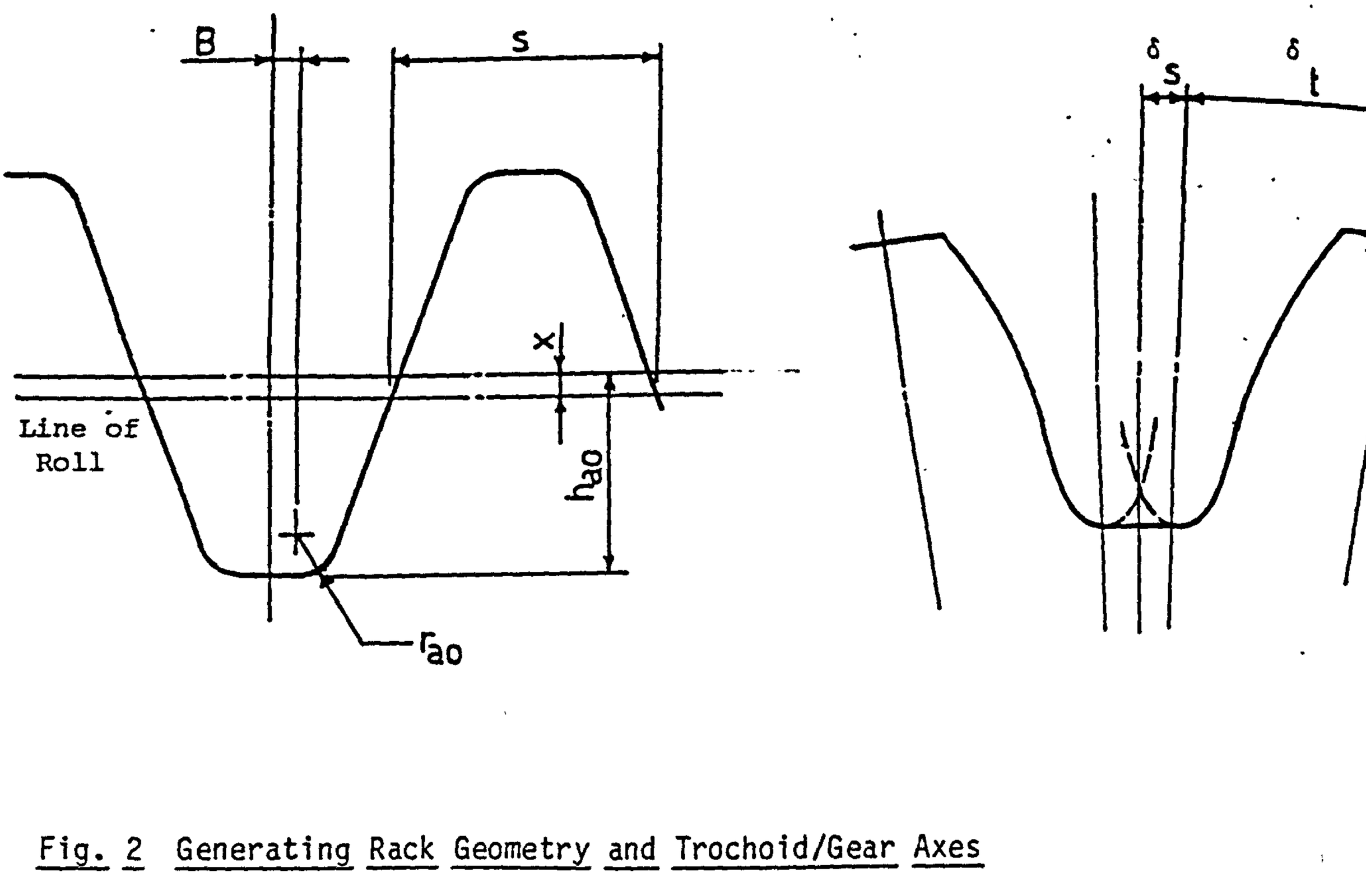

Fig. 2 Generating Rack Geometry and Trochoid/Gear Axes

Now consider the generating rack given in Fig. 2. The origin of the tool tip radius is offset by:

$$B = m_n \left[\pi/4 - (h_{ao} - r_{ao}) \tan \alpha \frac{-r_{ao}}{\cos \alpha} \right] \quad \text{(A2.3.2.10)}$$

The co-ordinates of the trochoid are defined relative to the tooth centre-line which is offset from the trochoid axis by where:

$$\delta_t = \frac{\pi m_n - B}{\Gamma} \quad \text{(A2.3.2.11)}$$

The polar co-ordinates of the trochoid are given by θ and rf (equation A2.3.2.10) where:

$$\theta = \gamma_t - \theta_f \qquad \text{(A2.3.2.12)}$$

Rectangular co-ordinates are obtained using equation A2.3.2.6. Note that the trochoid co-ordinates are not obtained directly from the trochoid radius rf but by inputting rt, the radius of the tool tip origin.

Calculation of Midside Node Co-ordinates

If midside node co-ordinates are omitted from the F.E. input the elements are assumed to have straight sides, (shown dotted). To ensure a correct trochoid profile the midside node co-ordinates must be calculated. The midpoint is defined as a point on the trochoid of equal distance from points 1 and 2.

Equations given for the trochoid are not closed form so the midpoint is determined by iteration between the two calculated corner node co-ordinates.

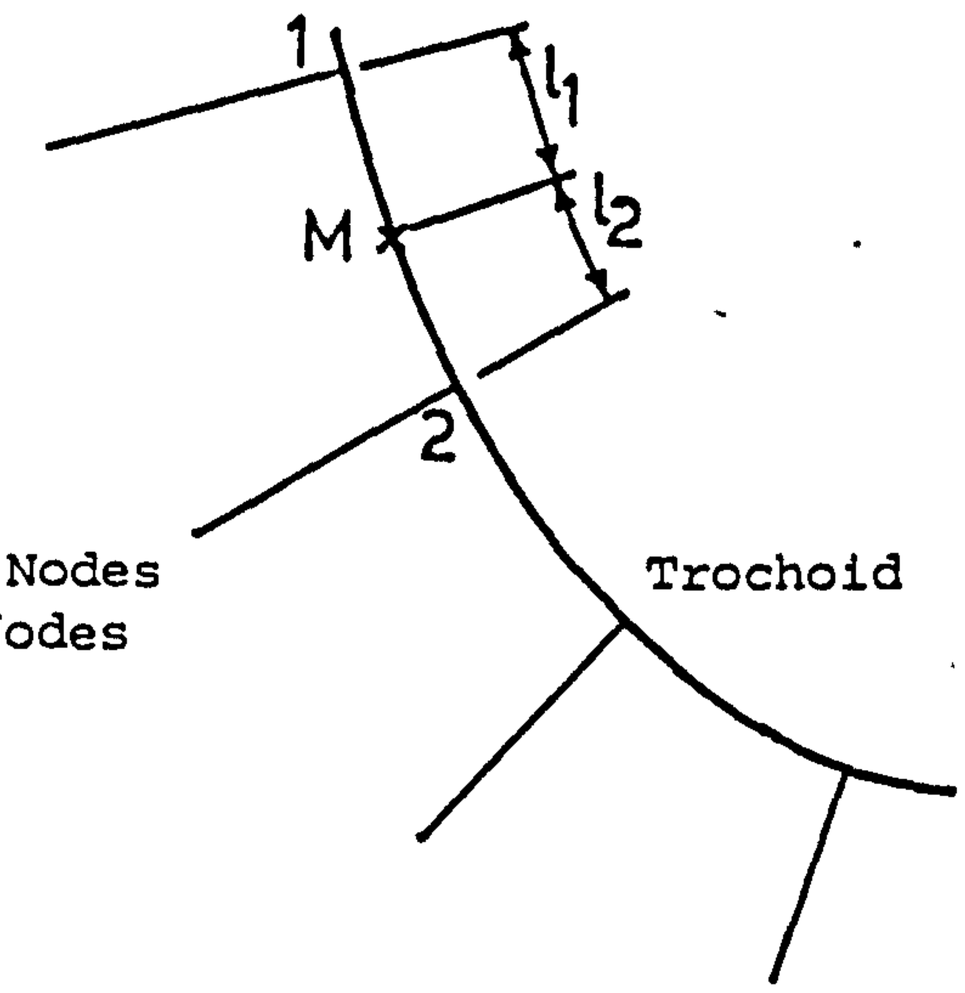

Fig. 3 F.E. Midside Node Calculation

The flow diagram for the iteration is given in Fig. 4. The program successively divides the trochoid in half and detects which section the midpoint must lie until further subdivision produces no improvement in midpoint co-ordinates.

*****

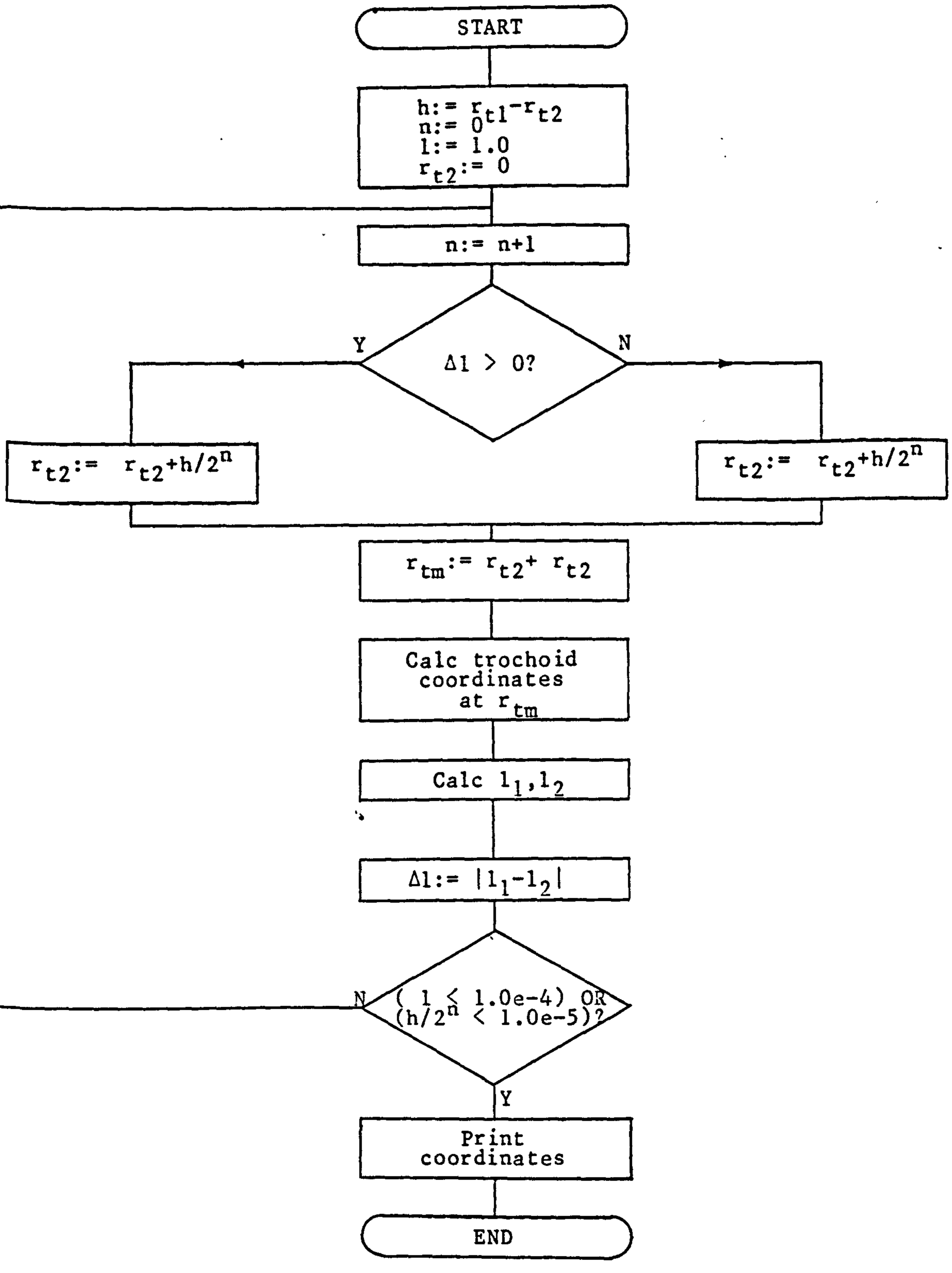

Fig 4. Trochoid Midpoint Coordinate Routine

APPENDIX 2.3.4

PLOTS OF F.E. NETT TOOTH CENTRE-LINE DEFLECTION RESULTS

The following graphs plot the tooth centre-line deflections along the tooth axis. The results are extracted from PAFEC 3D F.E. analyses of 18, 25, 40 and 100 teeth. The calculated shaft deflections of the F.E. model, due to a point load, have been subtracted from the F.E. results.

The plots of adjacent tooth deflection are in Section 2.3.5.

*****

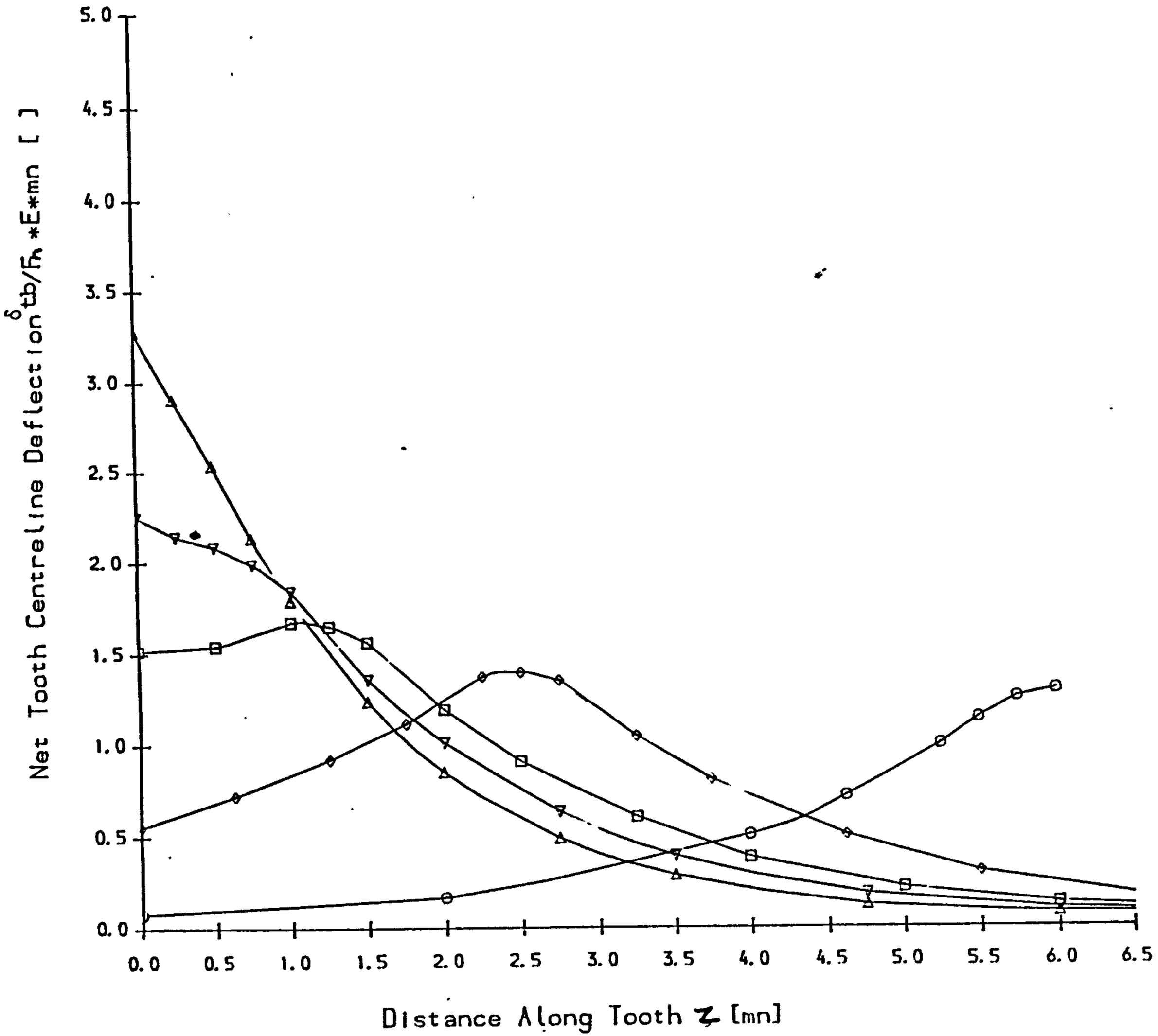

Fig1 FE Results: Reference Dia. Loading; Net Tooth Centreline Deflection; 18 Teeth

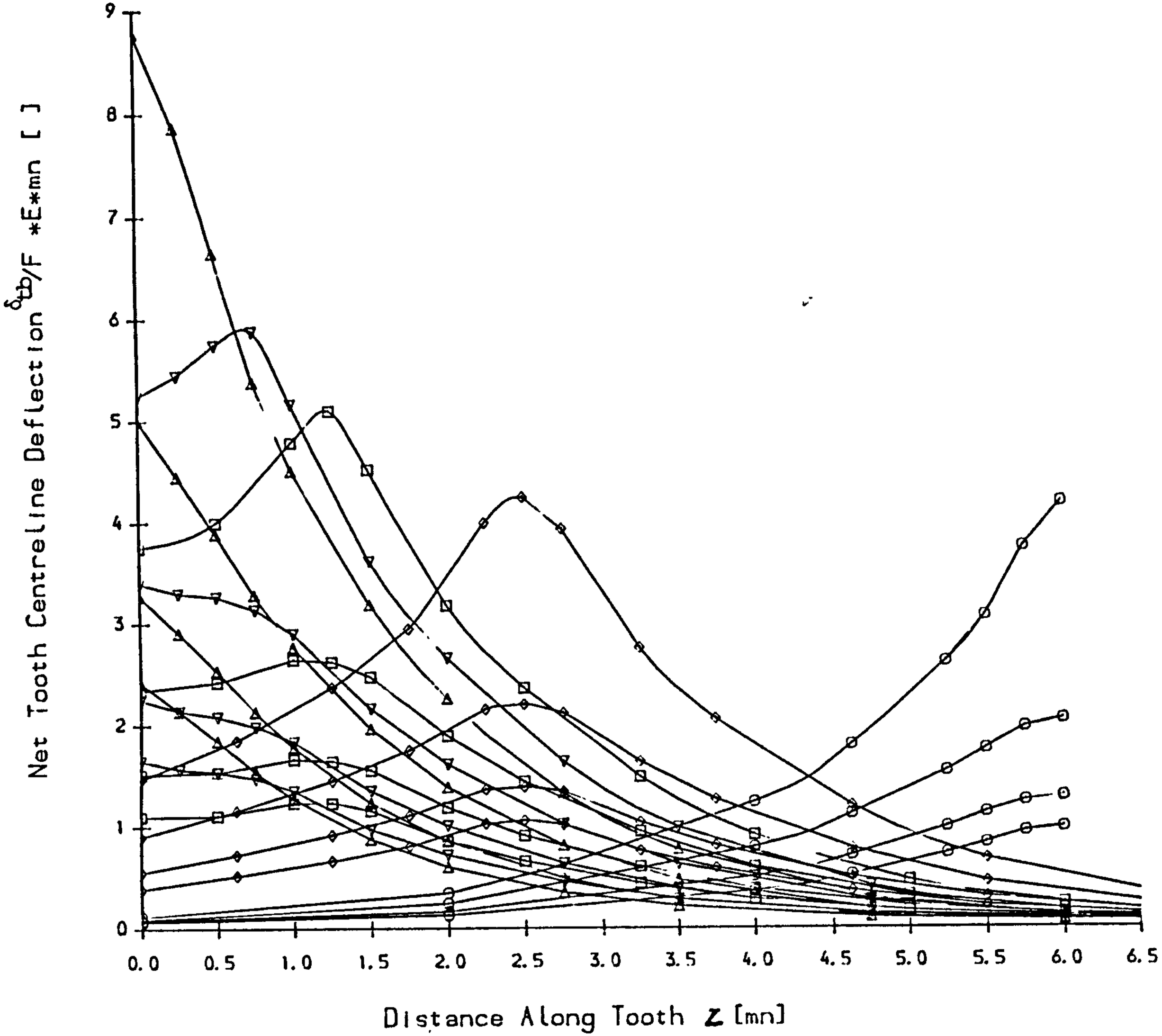

Fig 2 FE Results: Net Tooth Centreline Deflection, 18 Teeth

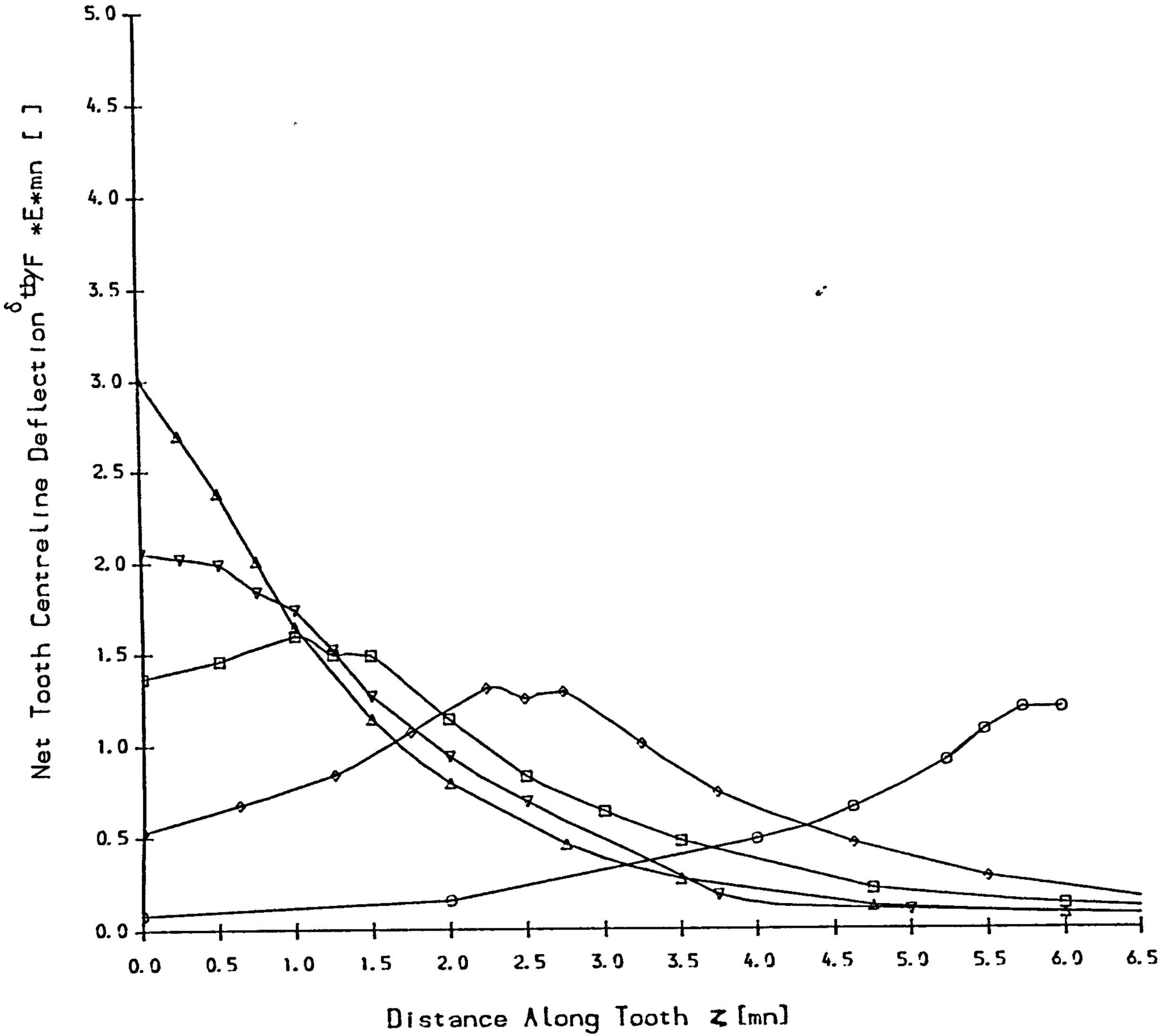

Fig 3 FE Results: Reference Dia. Loading; Net Tooth Centreline Deflection; 25 Teeth

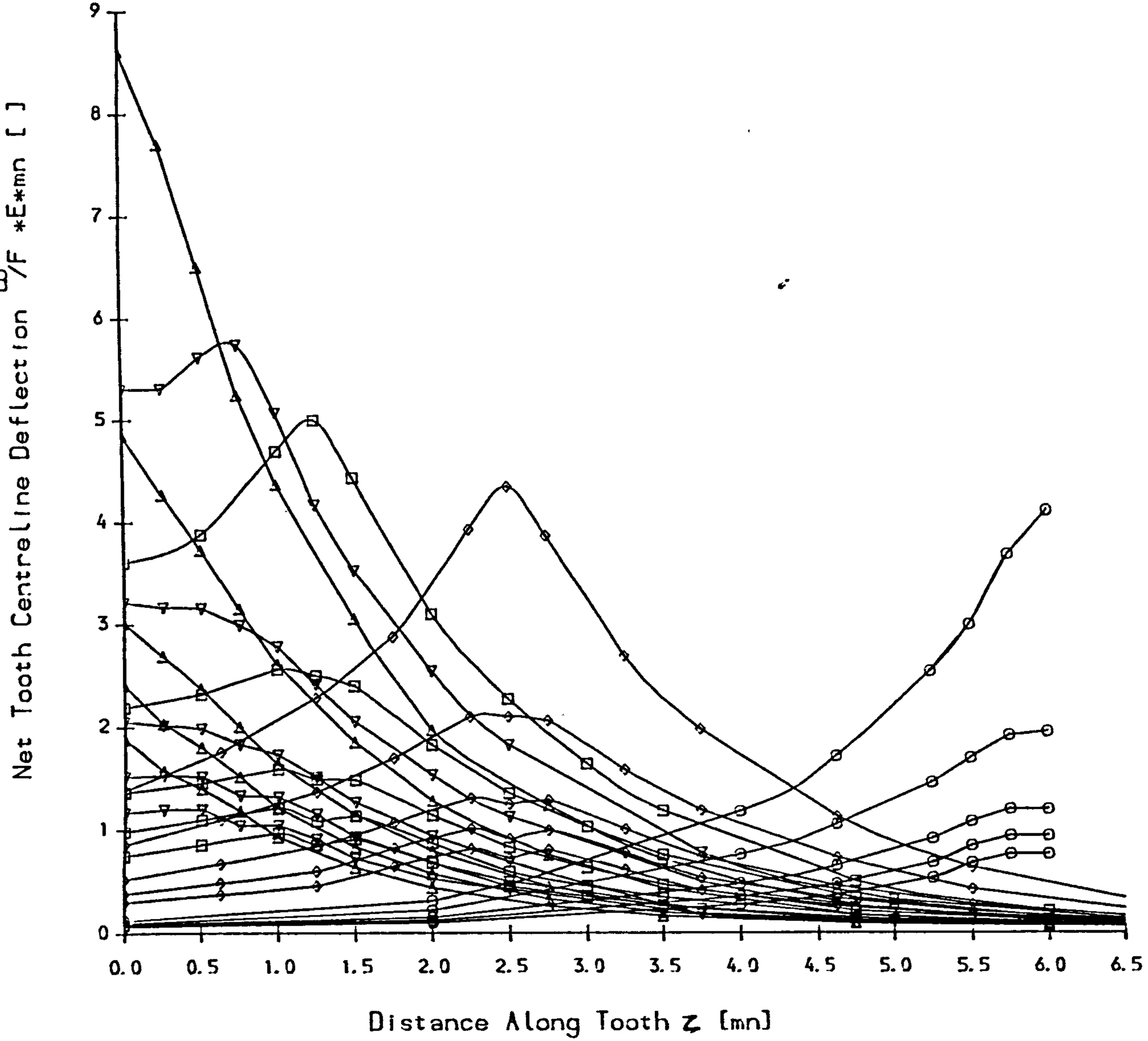

Fig 4 FE Results: Net Tooth Centreline Deflection; 25 Teeth

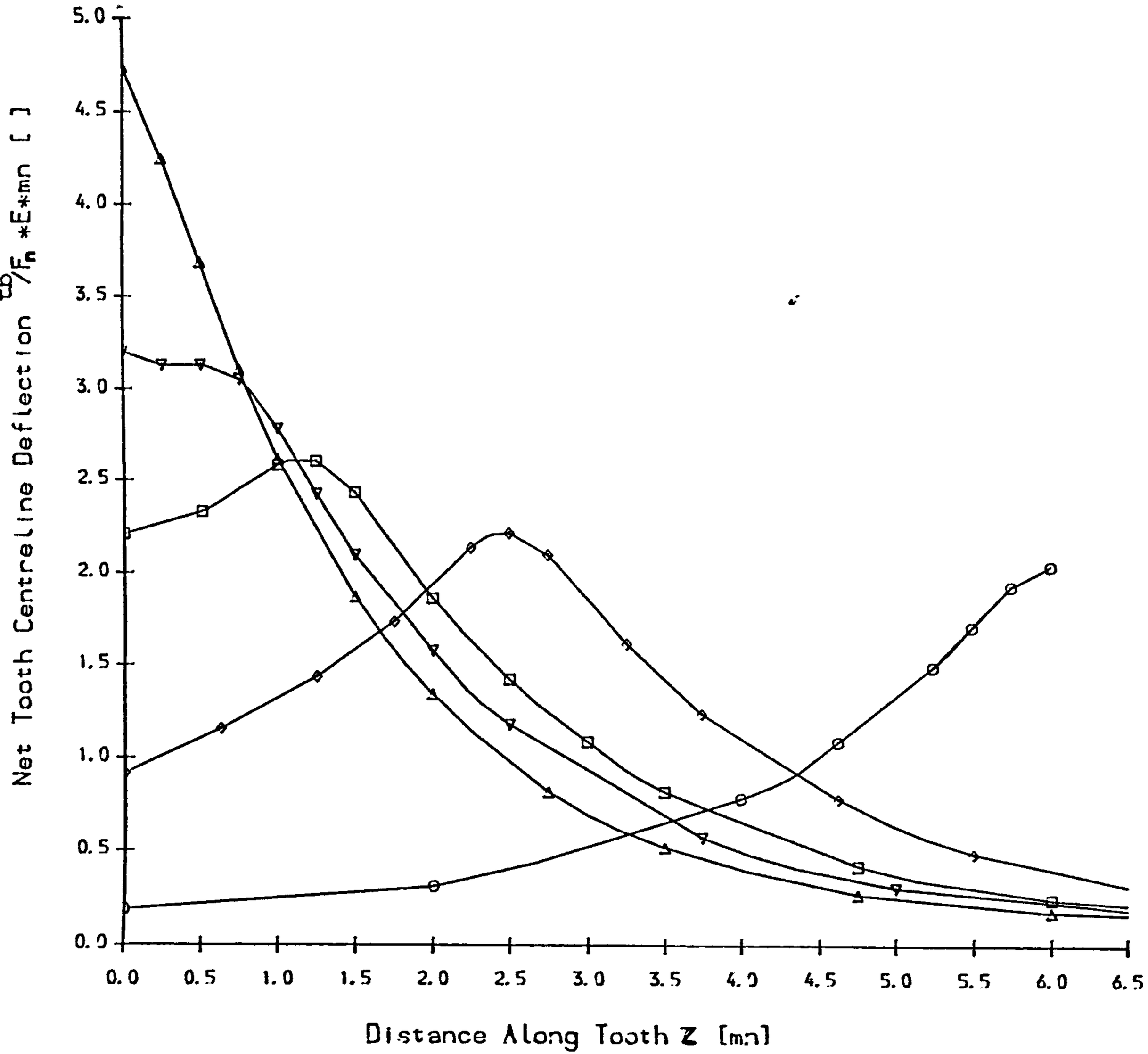

Fig 5 FE Results: Reference Dia. Loading; Net Tooth Centreline Deflection; 40 Teeth

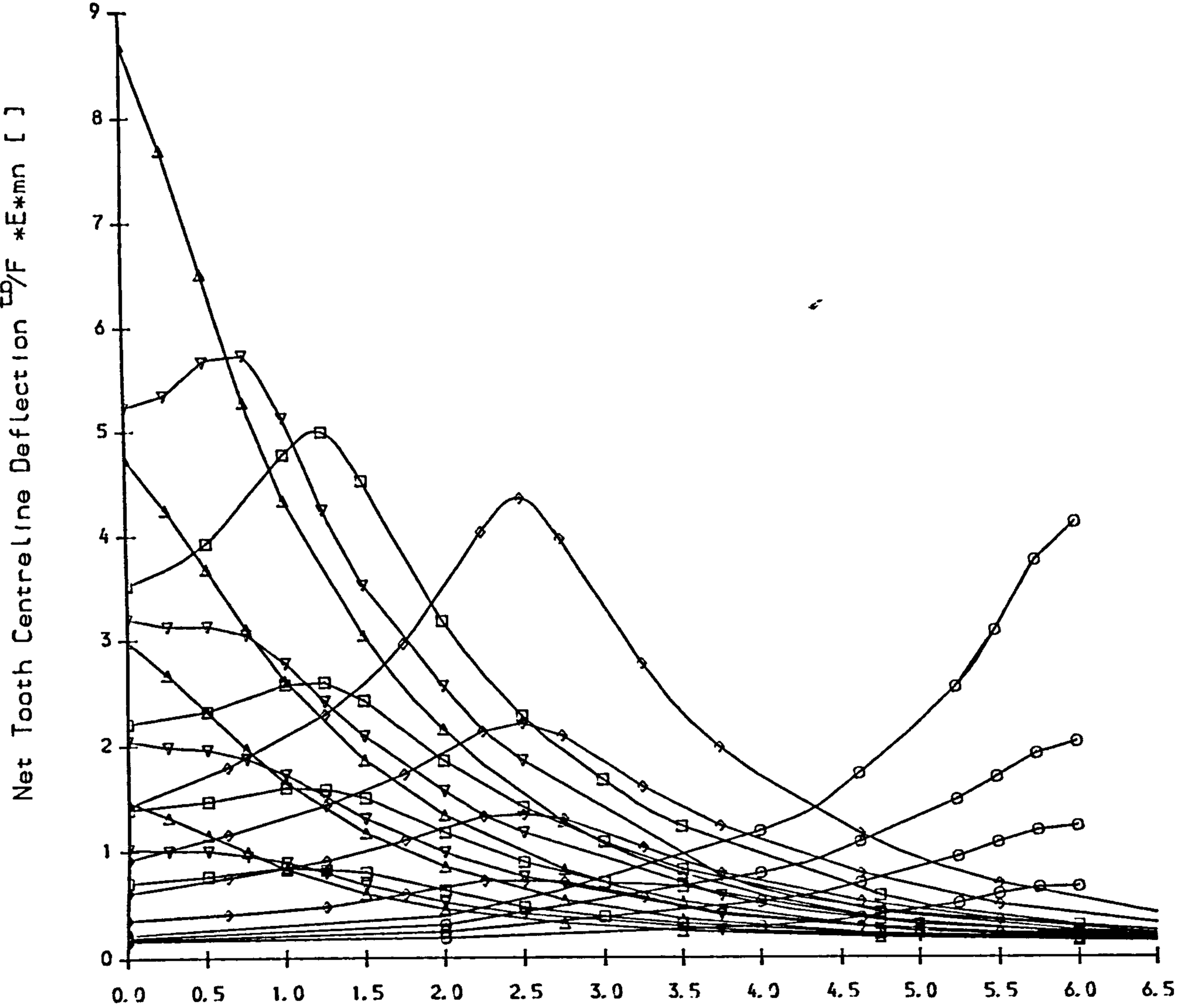

Fig 6 FE Results: Net Tooth Centreline Deflection; 40 Teeth

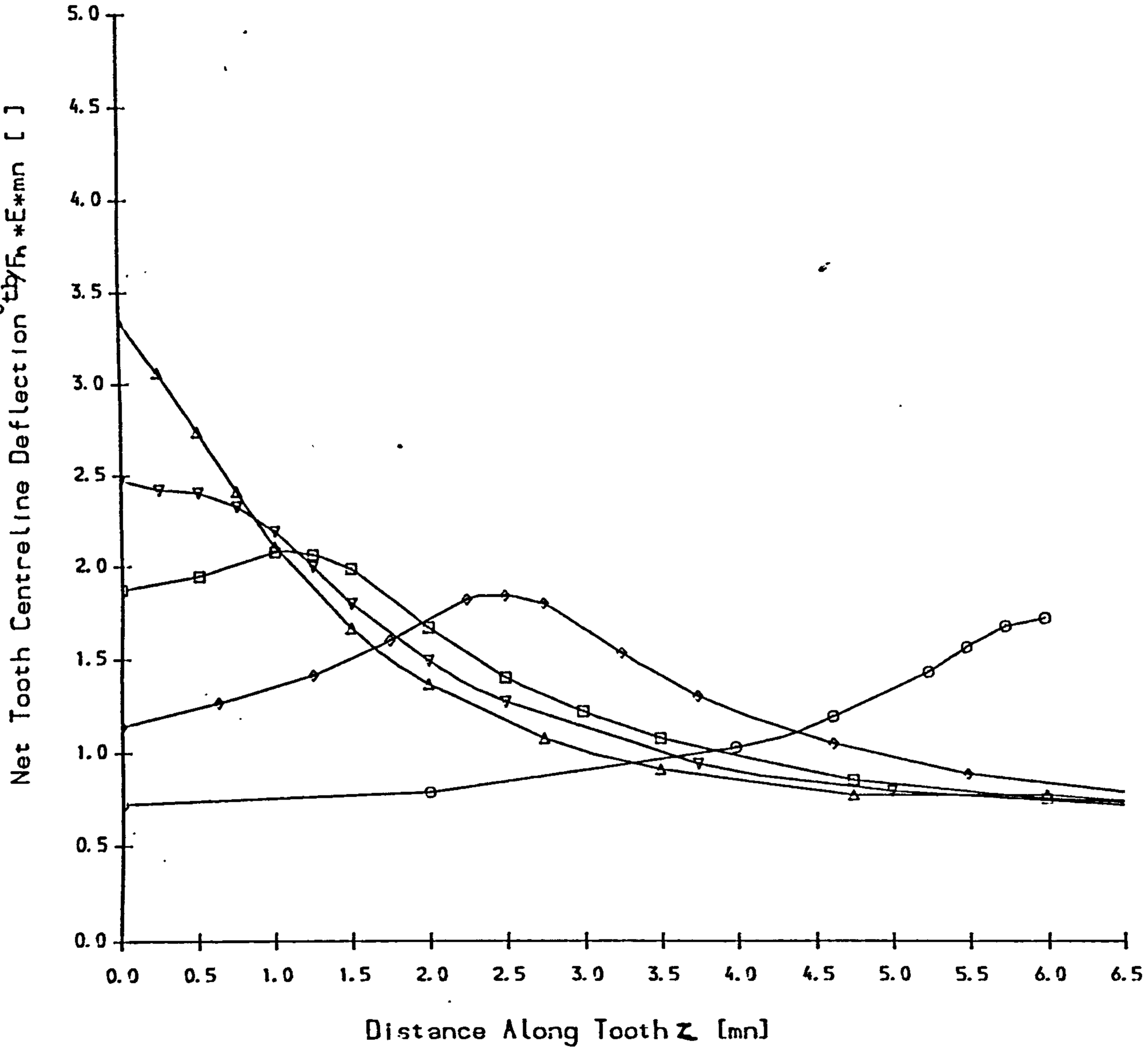

Fig 7 FE Results: Reference Dia. Loading; Net Tooth Centreline Deflection; 100 Teeth

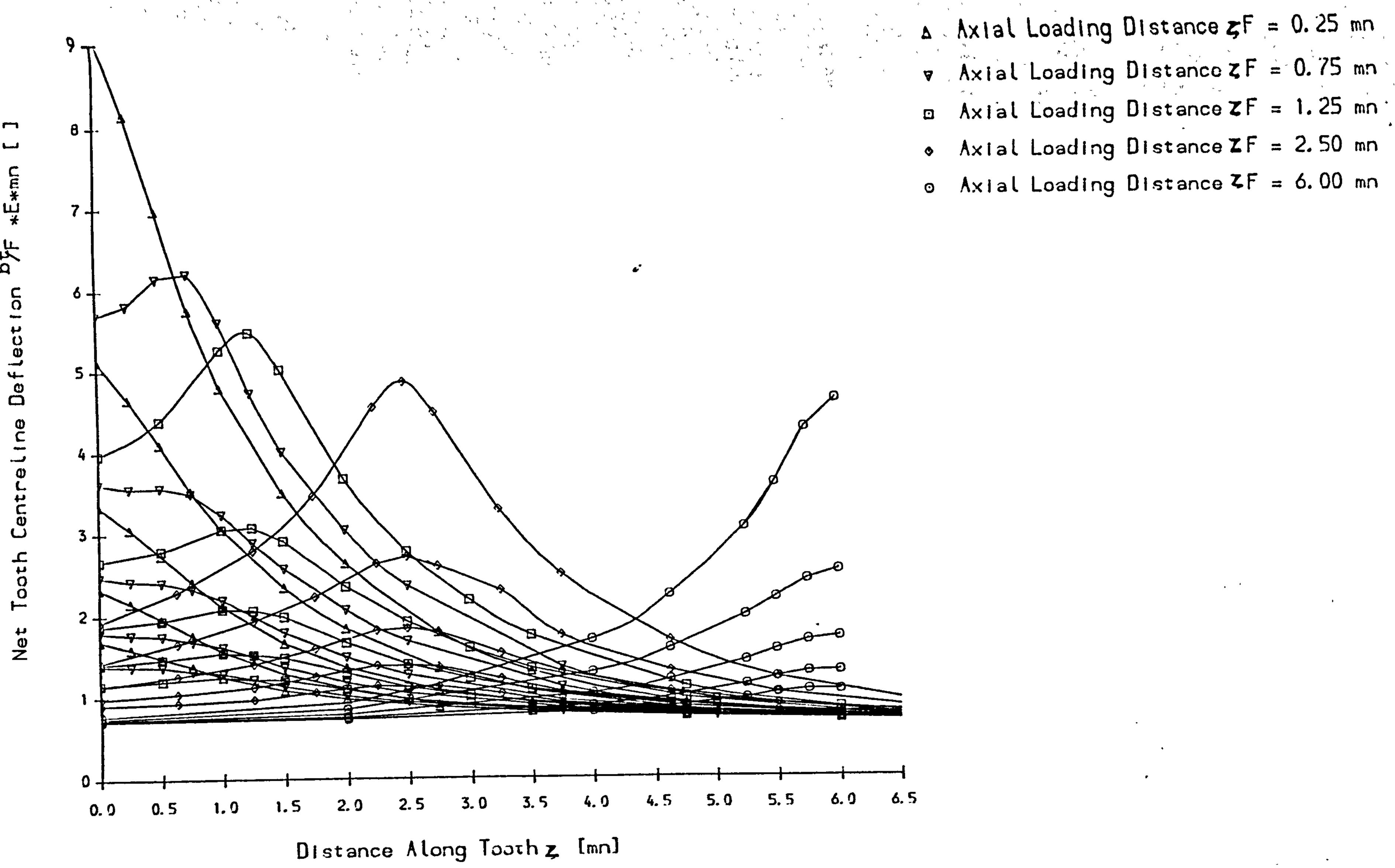

Fig 8 FE Results: Net Tooth Centreline Deflection; 100 Teeth

APPENDIX 2.4.2

OPTIMISATION ROUTINE FOR CURVE FITTING OF FINITE ELEMENT TOOTH DEFLECTION DATA

To minimise the error between the F.E. tooth deflection results and the mathematical fitting function the coefficients of F( ) and G( ) were optimised by computer. The method used was a modified gradient method. The procedure is set out below.

For a given function, F, with n variables the gradient in any direction is approximately given by:

$$\nabla F_i = \frac{F(x_i + \delta x) - F(x_i)}{\delta x} \qquad \text{(A2.4.2.1)}$$

where x is a small distance.

The vector $-\nabla F$ represents the direction of steepest descent for the function. For each of the n variables the gradient in the direction of steepest descent is given by:

$$\nabla' F_i = \frac{\nabla F_i}{|\nabla|} \qquad \text{(A2.4.2.2)}$$

where $$|\nabla| = \sqrt{\sum_{i=1}^{n} (\nabla F_i)^2} \qquad \text{(A2.4.2.3)}$$

For the n-dimensional space an initial guess for each of the n coefficients is made; the gradient is found from equations A2.4.2.1 and 3. Now proceed in this direction until a miminum is found. This method has been adopted so that the gradient is not recalculated for every new set of coefficients.

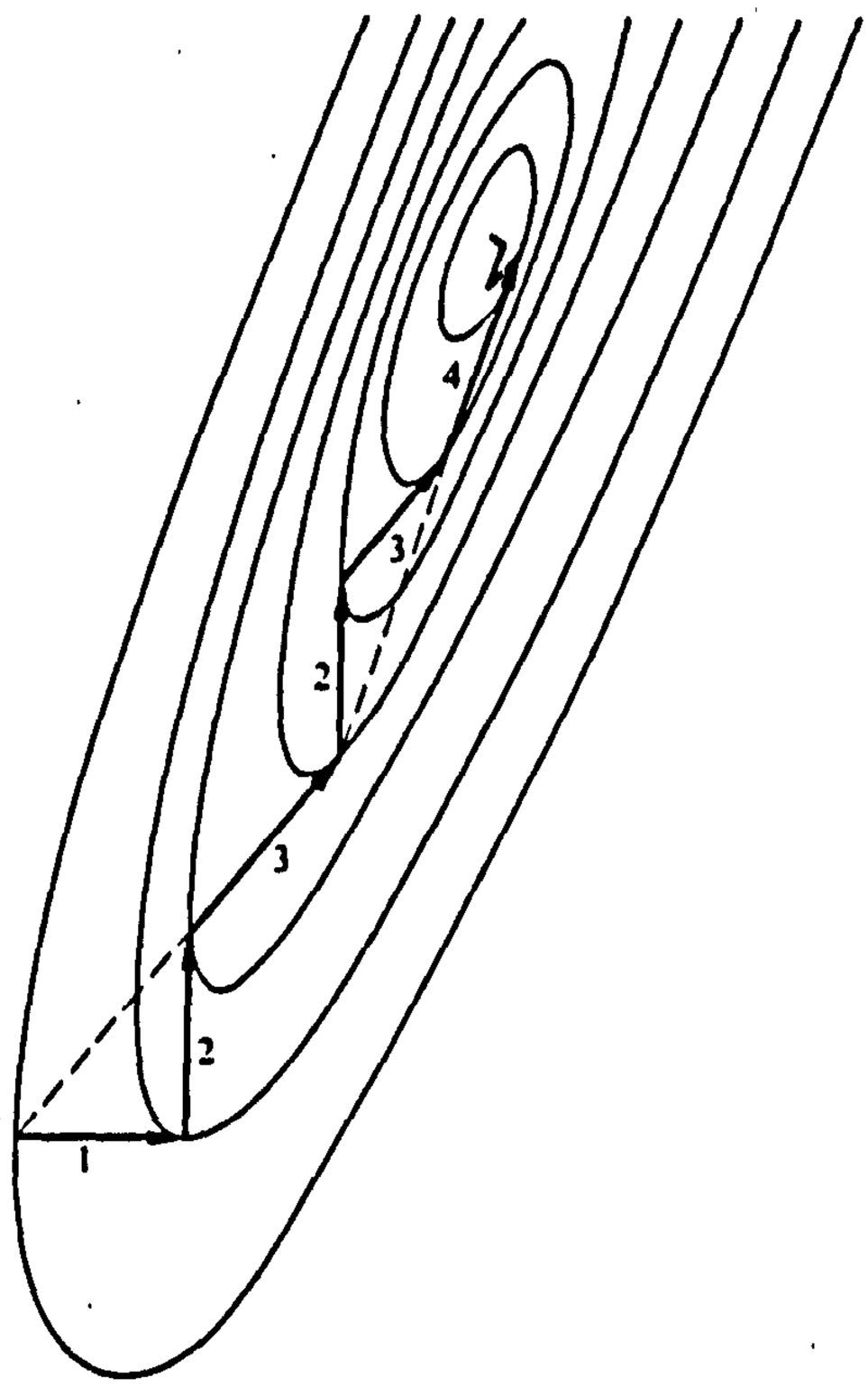

Fig. 1 Modified Gradient Minimisation (Powell's Method)

To minimise the function F in a particular direction quadratic interpolation was adopted. The steplength for the calculated gradient position is increased until the 1 dimensional minimum is passed, see Fig. 2. The last three points evaluated are approximated to a parabola of form:

$$F = a + bx + cx^2 \qquad \text{(A2.4.2.4)}$$

The minimum of this curve is at:

$$x_4 = \frac{-b}{2c} \qquad \text{(A2.4.2.5)}$$

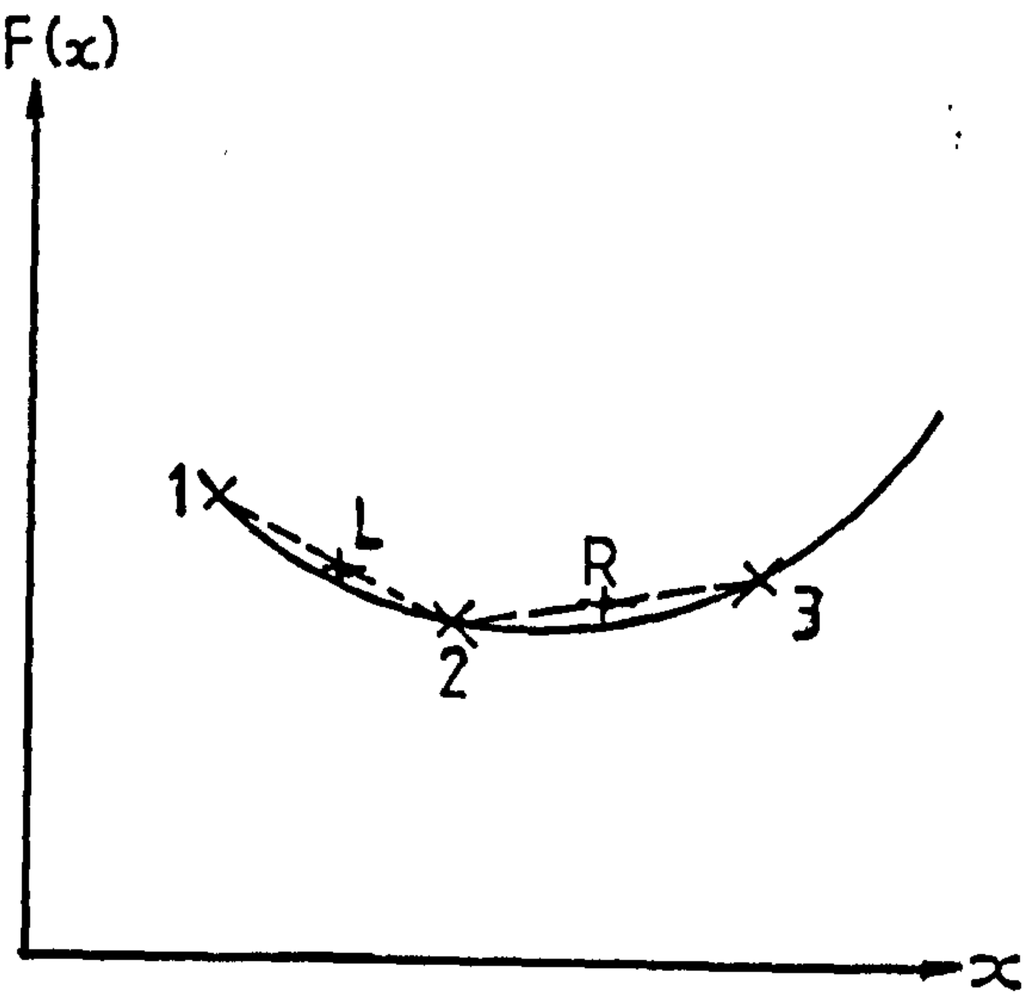

Fig. 2 Quadratic One Dimensional Minimisation

The slopes at the two midpoints L, R can be linearly approximated. Inserting this into equation A2.4.2.5 gives a good estimate of the ordinate of the minimum x4.

$$x = \tfrac{1}{2}\left[x_1 + x_2 + (x_3 - x_1)\frac{S_L}{S_L - S_R} \right] \qquad \text{(A2.4.2.6)}$$

This method quickly converges to the one dimensional minimum.

*****

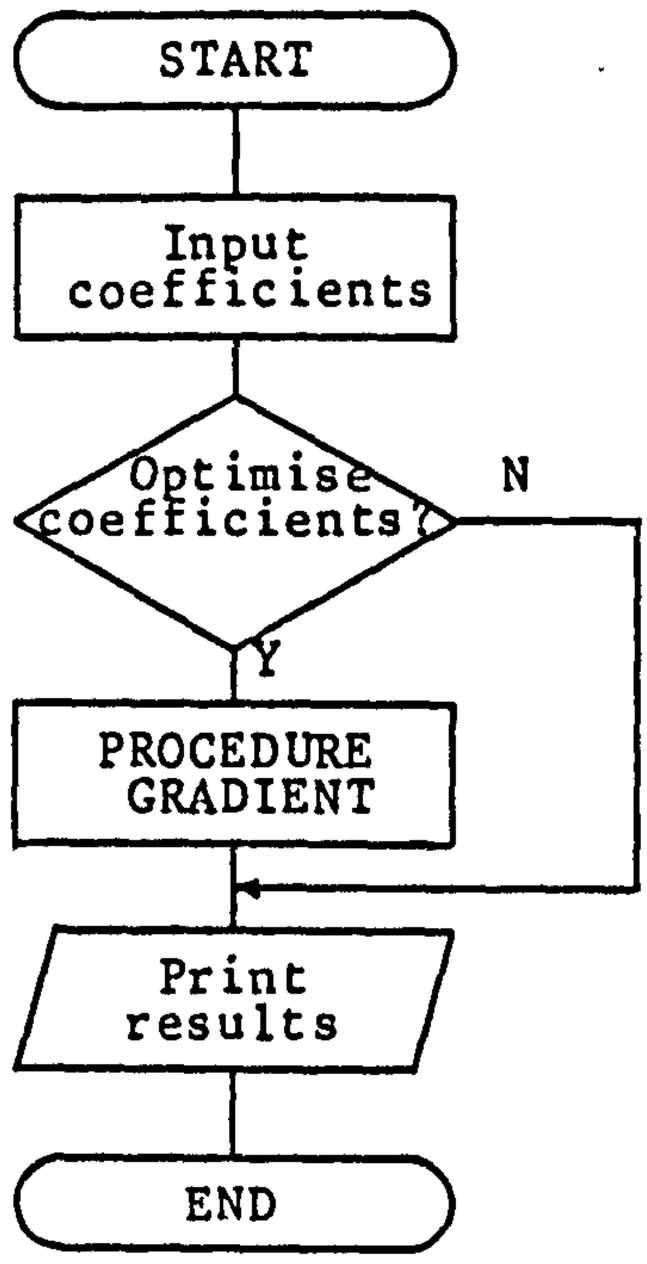

Fig 3. Curve Fitting Main Program

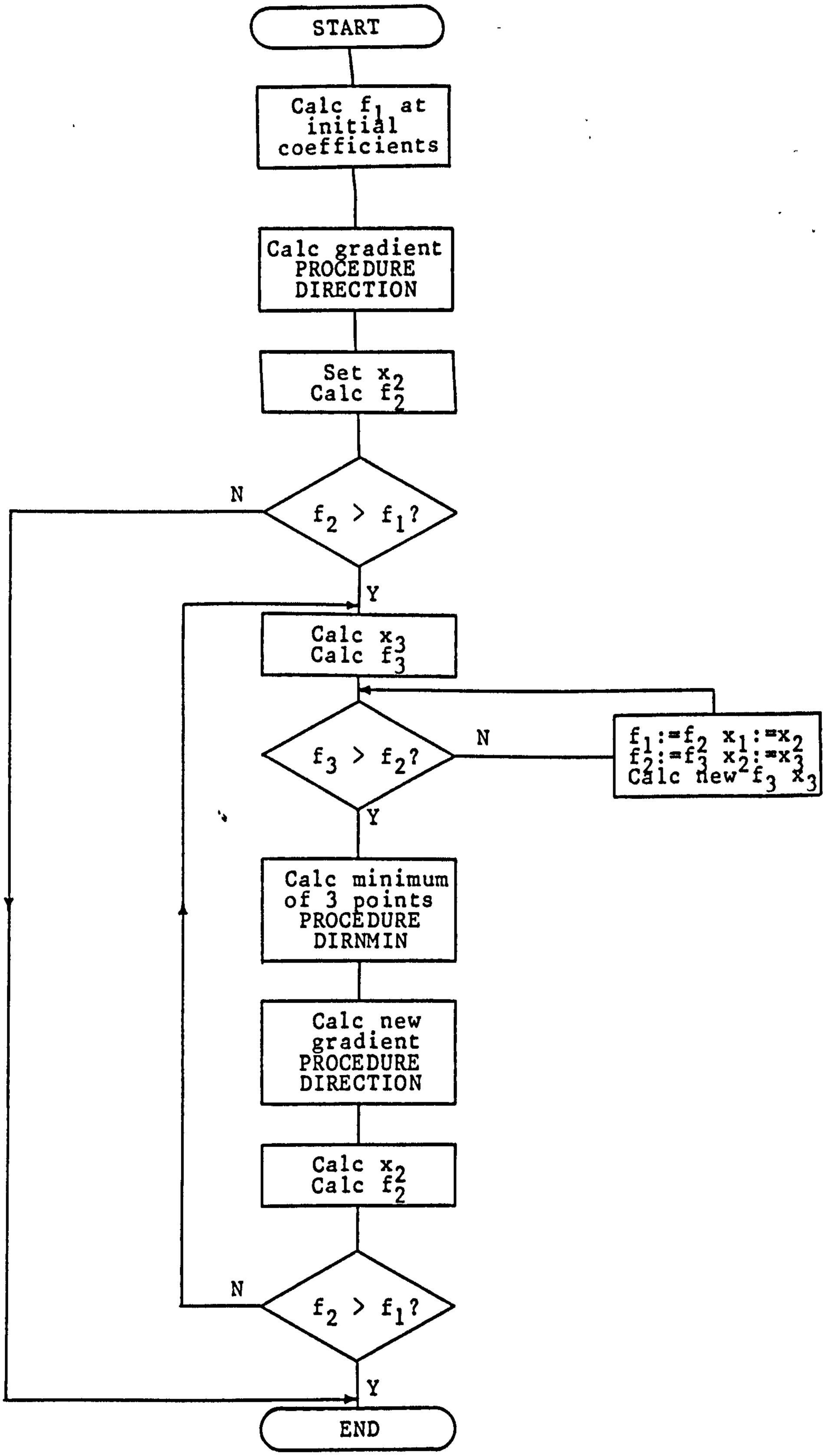

Fig 4. Curve Fitting Procedure GRADIENT

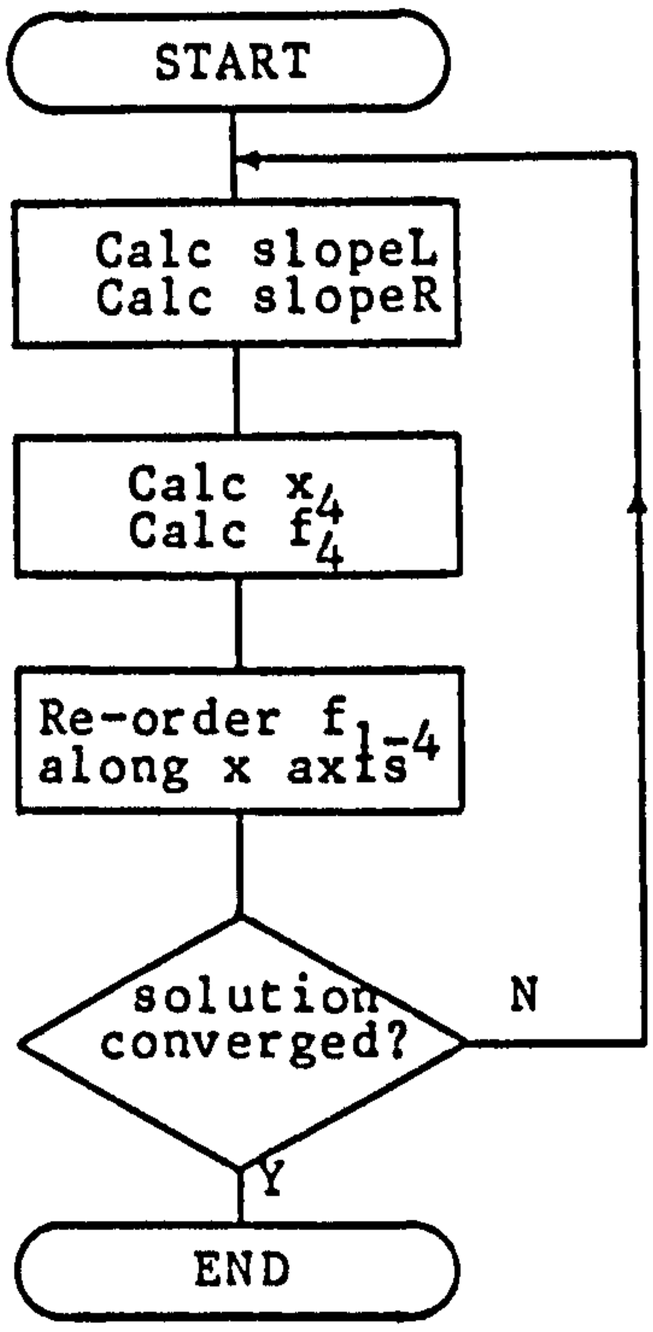

Fig 5. Curve Fitting Procedure DIRNMIN

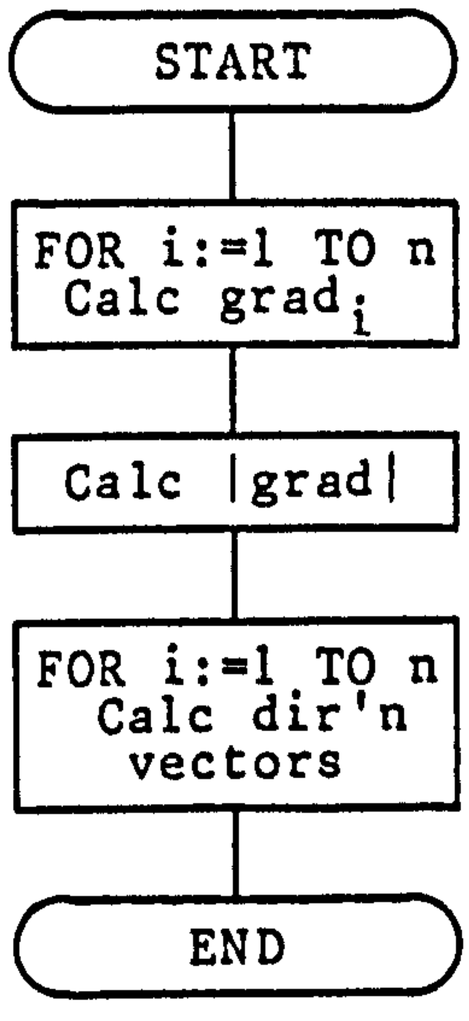

Fig 6. Curve Fitting Procedure DIRECTION

APPENDIX 3.8.4

TEST GEAR TOOTH ROOT STRAIN GAUGE RESULTS AND CALCULATED ROOT STRESSES

Appendix 3.8.4 tabulates the experimental results from the tooth deflection test rig described in chapter 3. The method of calculation of the tooth root stresses is given in detail in section 3.6

*****

Test Gear Strain Gauge Results.

z = 18
x = 0.0 Mn
hao = 1.4 Mn
rao = 0.4 Mn
dy = 18.000 Mn
zF = 7.222 Mn

z [Mn]	Epsa [	Epsb	Epsc 1.0e6 mm/N	Eps1	Eps2]	thta [dg]	sig1 [ ]	sig2 [ ]	sigb [ ]	sigd [ ]
0.556	0.149	0.054	0.000	0.152	-0.003	-37	0.035	0.010	0.019	0.026
1.667	0.257	0.149	0.000	0.259	-0.002	-49	0.059	0.017	0.042	0.035
2.778	0.433	0.324	-0.027	0.463	-0.057	-59	0.102	0.019	0.080	0.041
3.889	0.758	0.582	-0.027	0.814	-0.083	-59	0.181	0.037	0.144	0.074
4.722	1.056	1.053	0.041	1.265	-0.168	-67	0.279	0.049	0.245	0.083
6.111	1.571	2.188	0.325	2.336	-0.440	-77	0.506	0.060	0.482	0.084
7.222	-	2.904	-	-	-	-	-	-	-	-

zF = 2.778 Mn

z [Mn]	Epsa [	Epsb	Epsc 1.0e6 mm/N	Eps1	Eps2]	thta [dg]	sig1 [ ]	sig2 [ ]	sigb [ ]	sigd [ ]
0.556	1.284	1.631	0.203	1.783	-0.296	-74	0.389	0.055	0.365	0.079
1.667	1.649	2.400	0.527	2.515	-0.339	-78	0.554	0.095	0.536	0.114
2.778	1.257	2.993	1.217	2.993	-0.520	-90	0.652	0.087	0.652	0.087
3.889	0.433	2.136	1.595	2.277	-0.250	-14	0.506	0.100	0.122	0.483
4.722	0.135	1.429	1.406	1.686	-0.145	-22	0.377	0.083	0.124	0.336
6.111	0.041	0.620	0.784	0.838	-0.014	-30	0.192	0.055	0.090	0.157
7.222	-	0.297	-	-	-	-	-	-	-	-

zF = 1.667 Mn

z [Mn]	Epsa [	Epsb	Epsc 1.0e6 mm/N	Eps1	Eps2]	thta [dg]	sig1 [ ]	sig2 [ ]	sigb [ ]	sigd [ ]
0.556	1.607	3.254	1.161	3.267	-0.498	-87	0.716	0.111	0.714	0.113
1.667	1.270	3.348	1.621	3.357	-0.466	-3	0.739	0.124	0.125	0.737
2.778	0.432	2.345	1.864	2.543	-0.247	-15	0.567	0.118	0.150	0.535
3.889	0.108	1.351	1.351	1.608	-0.149	-22	0.359	0.076	0.118	0.318
4.722	0.014	0.786	0.986	1.064	-0.065	-30	0.240	0.058	0.103	0.195
6.111	0.014	0.285	0.473	0.476	0.010	-40	0.110	0.035	0.066	0.079
7.222	-	0.136	-	-	-	-	-	-	-	-

zF = 0.556 Mn

z [Mn]	Epsa [	Epsb	Epsc 1.0e6 mm/N	Eps1	Eps2]	thta [dg]	sig1 [ ]	sig2 [ ]	sigb [ ]	sigd [ ]
0.556	1.013	5.712	3.797	5.993	-1.183	-11	1.295	0.141	0.186	1.250
1.667	0.243	3.107	3.040	3.667	-0.384	-22	0.816	0.164	0.255	0.726
2.778	0.000	1.438	1.892	2.012	-0.121	-31	0.454	0.111	0.203	0.362
3.889	-0.054	0.730	1.027	1.079	-0.106	-33	0.241	0.050	0.106	0.184
4.722	-0.041	0.353	0.622	0.627	-0.046	-40	0.141	0.033	0.077	0.097
6.111	0.014	0.136	0.243	0.243	0.013	-43	0.057	0.020	0.037	0.040
7.222	-	0.068	-	-	-	-	-	-	-	-

Test Gear Strain Gauge Results.

z = 18
x = 0.0 Mn
hao = 1.4 Mn
rao = 0.4 Mn
dy = 19.000 Mn
zF = 7.222 Mn

z [Mn]	Epsa [	Epsb	Epsc	Eps1	Eps2]	thta [dg]	sig1 [ ]	sig2 [ ]	sigb [ ]	sigd [ ]
		1.0e6 mm/N								
0.556	0.174	0.135	0.000	0.187	-0.012	-59	0.042	0.010	0.034	0.018
1.667	0.295	0.176	-0.013	0.299	-0.017	-51	0.068	0.017	0.048	0.036
2.778	0.510	0.392	-0.013	0.547	-0.050	-59	0.122	0.026	0.097	0.051
3.889	0.899	0.752	0.000	0.991	-0.092	-62	0.221	0.047	0.183	0.086
4.722	1.262	1.312	0.094	1.540	-0.184	-69	0.341	0.064	0.304	0.100
6.111	1.812	2.570	0.523	2.711	-0.376	-78	0.597	0.100	0.574	0.123
7.222	-	3.166	-	-	-	-	-	-	-	-

zF = 2.778 Mn

z [Mn]	Epsa [	Epsb	Epsc	Eps1	Eps2]	thta [dg]	sig1 [ ]	sig2 [ ]	sigb [ ]	sigd [ ]
		1.0e6 mm/N								
0.556	1.539	2.135	0.297	2.284	-0.448	-76	0.494	0.054	0.470	0.078
1.667	1.890	2.945	0.756	3.042	-0.396	-80	0.671	0.119	0.656	0.134
2.778	1.458	3.337	1.485	3.337	-0.394	0	0.739	0.139	0.139	0.739
3.889	0.648	2.619	1.836	2.742	-0.258	-12	0.612	0.130	0.149	0.592
4.722	0.216	1.770	1.687	2.052	-0.149	-21	0.461	0.107	0.153	0.416
6.111	0.067	0.743	0.945	1.005	0.008	-31	0.231	0.071	0.113	0.189
7.222	-	0.365	-	-	-	-	-	-	-	-

zF = 1.667 Mn

z [Mn]	Epsa [	Epsb	Epsc	Eps1	Eps2]	thta [dg]	sig1 [ ]	sig2 [ ]	sigb [ ]	sigd [ ]
		1.0e6 mm/N								
0.556	1.915	3.942	1.429	3.955	-0.611	-87	0.866	0.132	0.864	0.134
1.667	1.497	3.888	1.942	3.899	-0.461	-3	0.864	0.163	0.165	0.862
2.778	0.647	2.876	2.171	3.062	-0.244	-14	0.686	0.155	0.185	0.656
3.889	0.189	1.726	1.658	2.012	-0.164	-21	0.451	0.101	0.147	0.405
4.722	0.027	1.012	1.213	1.331	-0.091	-28	0.300	0.071	0.122	0.248
6.111	0.013	0.405	0.566	0.589	-0.010	-34	0.135	0.038	0.068	0.105
7.222	-	0.216	-	-	-	-	-	-	-	-

zF = 0.556 Mn

z [Mn]	Epsa [	Epsb	Epsc	Eps1	Eps2]	thta [dg]	sig1 [ ]	sig2 [ ]	sigb [ ]	sigd [ ]
		1.0e6 mm/N								
0.556	1.465	6.243	3.897	6.445	-1.083	-9	1.406	0.195	0.228	1.373
1.667	0.551	3.870	3.427	4.356	-0.379	-19	0.974	0.213	0.291	0.896
2.778	0.081	2.009	2.325	2.584	-0.179	-27	0.581	0.137	0.229	0.489
3.889	-0.027	1.021	1.317	1.415	-0.125	-30	0.316	0.069	0.132	0.253
4.722	-0.040	0.526	0.820	0.841	-0.061	-36	0.189	0.044	0.094	0.138
6.111	0.000	0.202	0.349	0.352	-0.002	-41	0.081	0.024	0.048	0.057
7.222	-	0.094	-	-	-	-	-	-	-	-

Test Gear Strain Gauge Results.

z = 18
x = 0.0 Mn
hao = 1.4 Mn
rao = 0.4 Mn
dy = 19.833 Mn
zF = 7.222 Mn

z [Mn]	Epsa [	Epsb	Epsc 1.0e6 mm/N	Eps1	Eps2]	thta [dg]	sig1 [ ]	sig2 [ ]	sigb [ ]	sigd [ ]
0.556	0.188	0.067	-0.027	0.189	-0.028	-41	0.042	0.007	0.022	0.026
1.667	0.323	0.202	-0.027	0.331	-0.035	-54	0.074	0.015	0.053	0.035
2.778	0.578	0.472	-0.027	0.636	-0.085	-61	0.140	0.024	0.114	0.051
3.889	1.062	0.901	0.000	1.178	-0.116	-62	0.263	0.055	0.218	0.099
4.722	1.465	1.590	0.148	1.830	-0.217	-70	0.405	0.076	0.367	0.115
6.111	2.111	3.099	0.686	3.242	-0.445	-79	0.714	0.121	0.691	0.144
7.222	-	3.813	-	-	-	-	-	-	-	-

zF = 2.778 Mn

z [Mn]	Epsa [	Epsb	Epsc 1.0e6 mm/N	Eps1	Eps2]	thta [dg]	sig1 [ ]	sig2 [ ]	sigb [ ]	sigd [ ]
0.556	1.815	2.513	0.336	2.692	-0.541	-76	0.581	0.061	0.552	0.090
1.667	2.191	3.546	0.941	3.642	-0.510	-81	0.801	0.134	0.786	0.149
2.778	1.761	4.035	1.801	4.035	-0.472	0	0.894	0.170	0.170	0.894
3.889	0.820	3.132	2.164	3.265	-0.280	-11	0.731	0.161	0.182	0.709
4.722	0.296	2.174	1.963	2.465	-0.207	-19	0.552	0.122	0.169	0.505
6.111	0.081	0.924	1.089	1.192	-0.023	-28	0.272	0.077	0.120	0.229
7.222	-	0.448	-	-	-	-	-	-	-	-

zF = 1.667 Mn

z [Mn]	Epsa [	Epsb	Epsc 1.0e6 mm/N	Eps1	Eps2]	thta [dg]	sig1 [ ]	sig2 [ ]	sigb [ ]	sigd [ ]
0.556	2.312	4.726	1.609	4.748	-0.826	-86	1.034	0.137	1.030	0.141
1.667	1.839	4.726	2.299	4.735	-0.598	-2	1.046	0.189	0.191	1.045
2.778	0.838	3.490	2.556	3.685	-0.291	-13	0.826	0.187	0.218	0.795
3.889	0.257	2.082	1.961	2.403	-0.185	-21	0.539	0.123	0.175	0.488
4.722	0.054	1.222	1.433	1.583	-0.096	-28	0.357	0.087	0.145	0.299
6.111	0.027	0.462	0.663	0.683	0.006	-35	0.157	0.049	0.084	0.122
7.222	-	0.217	-	-	-	-	-	-	-	-

zF = 0.556 Mn

z [Mn]	Epsa [	Epsb	Epsc 1.0e6 mm/N	Eps1	Eps2]	thta [dg]	sig1 [ ]	sig2 [ ]	sigb [ ]	sigd [ ]
0.556	1.963	7.128	4.060	7.260	-1.237	-7	1.582	0.216	0.237	1.561
1.667	0.834	4.721	3.791	5.139	-0.514	-16	1.145	0.236	0.303	1.078
2.778	0.188	2.515	2.702	3.096	-0.205	-25	0.697	0.166	0.260	0.604
3.889	0.000	1.291	1.573	1.721	-0.148	-29	0.385	0.085	0.154	0.316
4.722	-0.040	0.686	1.008	1.046	-0.078	-34	0.235	0.054	0.112	0.177
6.111	0.000	0.242	0.430	0.432	-0.002	-41	0.099	0.029	0.060	0.069
7.222	-	0.121	-	-	-	-	-	-	-	-